Turbulent Flow in a Curved Rectangular Channel

Report OF-73

RESEARCH MANAGEMENT DIVISION
UNEDITED
MATERIAL
O.F. 73

THE UNIVERSITY OF ALBERTA

TURBULENT FLOW IN A CURVED RECTANGULAR CHANNEL

BY

PETER M. STEFFLER

A THESIS
SUBMITTED TO THE FACULTY OF GRADUATE STUDIES AND RESEARCH
IN PARTIAL FULFILMENT OF THE REQUIREMENTS FOR THE DEGREE
OF DOCTOR OF PHILOSOPHY

DEPARTMENT OF CIVIL ENGINEERING

EDMONTON, ALBERTA
SPRING 1984

THE UNIVERSITY OF ALBERTA

FACULTY OF GRADUATE STUDIES AND RESEARCH

The undersigned certify that they have read, and recommend to the Faculty of Graduate Studies and Research, for acceptance, a thesis entitled TURBULENT FLOW IN A CURVED RECTANGULAR CHANNEL submitted by PETER M. STEFFLER in partial fulfilment of the requirements for the degree of DOCTOR OF PHILOSOPHY.

....

....

Supervisors

....

K.C. Cheng..............................

....

External Examiner

Date 28 March 84..............................

ABSTRACT

Curvature affects the flow of water in open channels in several ways. These effects include superelevation, secondary (induced) flows, longitudinal velocity redistribution, and bed scour in the case of a mobile boundary such as a natural stream or river. It is important for river engineers to understand and be able to estimate these effects.

This study first presents and discusses the present state of knowledge and understanding of the problem of curved channel flow. The flow mechanics are discussed first with an emphasis on the prediction of specific flow phenomena. The state of the art is found to be adequate with regard to some effects but not others. A body of experimental data obtained under controlled conditions is an important component of the state of knowledge of a field. The existing curved channel experiments are tabulated and evaulated in the second part of this section. A discussion of the relatively recent application of numerical modelling is presented. Aspects of the problem requiring further research and elaboration are also identified.

A theoretical analysis is then performed based on a perturbation of the governing flow equations. This analysis is confined to rectangular channels but may be extended to an arbitrary channel shape. The theoretical predictions of developed and developing longitudinal velocity distributions and maximums are found to agree well with experimental

measurements.

An experimental study comprising two complete runs in a single long (270°) bend was also performed. Use of the Laser Doppler Anaemometer to measure longitudinal and lateral velocity components allowed unprecedented detail and precision. Analysis of the velocity data provided the distributions of bed stress and bed stress angle which are important for scour prediction.

The purpose of this study was to apply recent research to practice and to attempt to fill a few of the gaps in the present state of knowledge of curved channel flows.

Acknowledgements

The write wishes to acknowledge the financial support of the Research Management Division and the River Engineering Branch of Alberta Environment and the Natural Science and Engineering Research Council of Canada.

The writer is also indebted to his supervisors, Dr. N. Rajaratnam, and Professor A.W. Peterson for their support, encouragement and advice. The writer would also like to express his gratitude to Mr. S. Lovell and Mr. J. Gagne for designing, constructing and maintaining the experimental facility; to Mr .R. Gitzel, Mr. D. Lathe, and Mr. A. Dunbar for installing and maintaining the LDA and data aquisition system; to Mr. G. Fonstad for an extensive review of the first part of this thesis; and to Mrs. D. Salvian for her expert production of this document.

Finally, the writer is indebted to his wife, Gail, for her patience and able assistance throughout this study.

TABLE OF CONTENTS

PART ONE: REVIEW OF THE PRESENT KNOWLEDGE....................3

1.1 INTRODUCTION..3

1.2 MECHANICS OF CURVED CHANNEL FLOW.............................4

1.2.1 Introduction...4

1.2.1.1 Co-ordinate System..................................4

1.2.2.1 General Assumptions.................................6

1.2.2 Superelevation...8

1.2.2.1 Derivation..8

1.2.2.2 Superelevation Example.............................12

1.2.2.3 Effect of Varying Longitudinal Velocity.............................13

1.2.2.4 Effect of Bed Friction.............................14

1.2.2.5 Calculation of Superelevation.......................17

1.2.2.6 Developing Flow Considerations......................18

1.2.3 Secondary Flow..20

1.2.3.1 Analysis of Developed Secondary Flow in a Wide Open Channel.......20

1.2.3.2 Bank Effects.......................................28

1.2.3.3 Developing Secondary Flow..........................28

1.2.4 Longitudinal Velocity Redistribution.....................29

1.2.4.1 Inertial Effects....................................30

1.2.4.2 Slope Differential Effect...........................33

1.2.4.2 Depth of Flow (Vertical Friction)....................35

1.2.4.4 Lateral Friction....................................36

1.2.4.5 Lateral Momentum Transport by Secondary Flow.................37
1.2.4.6 Developing Flow......................38
1.2.5 Bed Shear Stress..............................39
1.2.6 Wall Shear Stress.............................41
1.2.7 Friction Coefficient...........................41
1.2.8 Bed Scour and Topography......................43
1.2.8.1 Developed Bed Profile................43
1.3 REVIEW OF EXPERIMENTAL INVESTIGATIONS...........49
1.3.1 Fixed Boundary Channels................57
1.3.2 Mobile Boundary Channels...............58
1.3.3 Natural Stream Observations............58
1.4 MATHEMATICAL MODELS.............................59
1.4.1 Three-Dimensional Models...............59
1.4.2 Two-Dimensional Models.................61
1.4.3 One-Dimensional Models.................62
1.4.4 Summary................................62
1.5 CONCLUSIONS.....................................63
1.5.1 Mechanics of Flow in Curved Channels...63
1.5.2 Experimental Studies...................63
1.5.3 Mathematical Models....................64

2. PART TWO - THEORETICAL ANALYSIS.......................65
2.1 INTRODUCTION.....................................65
2.2 GOVERNING EQUATIONS.............................66
2.2.2 Equations of Motion....................68
2.2.3 Perturbation Expansion.................71

2.4 TURBULENCE CLOSURE....................................80
2.5 VORTICITY EQUATIONS...................................82
2.6 DEVELOPED FLOW..89
  2.6.1 Formulation.......................................89
  2.6.2 Solution..95
2.7 DEVELOPING FLOW.......................................107
  2.7.1 Formulation.......................................107
  2.7.2 Solution..109
  2.7.3 Comparison to Experiment..........................109
2.8 CONCLUSIONS...110

3. PART THREE - EXPERIMENTAL STUDY........................113
3.1 INTRODUCTION..113
3.2 FACILITIES AND PROCEDURES.............................114
  3.2.1 Flume...114
  3.2.2 Laser Doppler Anaemometer.........................116
  3.2.3 Data Reduction....................................119
3.3 EXPERIMENTAL RESULTS..................................123
3.4 ANALYSIS OF RESULTS...................................193
3.5 DISCUSSION..195
3.6 CONCLUSIONS...208

CONCLUSION..213
REFERENCES..216
APPENDIX A - WATER SURFACE AT A CHANGE OF CHANNEL
CURVATURE...220
APPENDIX B - COMPUTER PROGRAMS............................235

LIST OF TABLES

Table 1. Rigid Boundary Curved Channel Experiments.....51

Table 2. Mobile Boundary Curved Channel Experiments....55

Table 3. Natural Stream Bend Measurements..............56

Table 4. Significant Details of the Experiments.......124

LIST OF FIGURES

Figure 1. Definition Sketch - Plan........................5

Figure 2. Definition Sketch - Elevation..................7

Figure 3. Forces Acting on a Water Column................9

Figure 4. Superelevation Versus Curvation Ratio.........15

Figure 5. Secondary Circulation.........................21

Figure 6. Integral Functions............................27

Figure 7. Slope Differential............................34

Figure 8. Particle Equilibrium..........................44

Figure 9. Maximum Scour Versus Curvature Ratio..........47

Figure 10. Calculated Straight Channel Velocity Contours ($\beta = 8.7$, $C_f = 16.0$)................97

Figure 11. Lateral Perturbation Velocity Contours ($\beta = 8.7$, $C_f = 16.0$)..........................98

Figure 12. Vertical Perturbation Velocity Contours $\beta = 8.7$, $C_f = 16.0$)..........................99

Figure 13. Longitudinal Perturbation Velocity Contours ($\beta = 8.7$, $C_f = 16.0$).........................100

Figure 14. Total Longitudinal Velocity Contours ($\beta = 8.7$, $C_f = 16.0$, $\alpha = 0.146$)..............101

Figure 15. Measured Longitudinal Velocity Contours (u/U_0, $\beta = 8.7$, $C_f = 16.0$, $\alpha = 0.146$).......102

Figure 16. Effect of C_b on the Lateral Distribution of Longitudinal Perturbation Velocity ($\nu_R = 3.0$).................................103

Figure 17. Effect of ν_R on the Lateral Distribution of Longitudinal Perturbation Velocity ($C_b = 0.3$).................................104

Figure 18. Depth Averaged Longitudinal Velocity Perturbations at $y/b = 0.9$..................105

Figure 19. Depth Averaged Vertical Velocities at $y/b = 1.0$.................................106

Figure 20. Developing Flow-Comparison of Theory to Experiment...............................111

Figure 21. Flume Layout and Test Locations..............115

Figure 22. Schematic Diagram of LDA Setup...............118

Figure 23. u Velocity Distribution (x = -2.20 m)........128

Figure 24. u Velocity Distribution (x = -0.69 m)........129

Figure 25. u Velocity Distribution (x = 0.05 m).........130

Figure 26. u Velocity Distribution (x = 1.92 m).........131

Figure 27. u Velocity Distribution (x = 3.83 m).........132

Figure 28. u Velocity Distribution (x = 5.75 m).........133

Figure 29. u Velocity Distribution (x = 7.66 m).........134

Figure 30. u Velocity Distribution (x = 9.68 m).........135

Figure 31. u Velocity Distribution (x = 11.49 m)........136

Figure 32. u Velocity Distribution (x = 13.41 m)........137

Figure 33. u Velocity Distribution (x = 16.18 m)........138

Figure 34. u Velocity Distribution (x = 17.43 m)........139

Figure 35. u Velocity Distribution (x = 18.65 m)........140

Figure 36. Expanded u Velocity Distribution (x = -2.20 m)................................141

Figure 37. Expanded u Velocity Distribution (x = 0.69 m).................................142

Figure 38. Expanded u Velocity Distribution (x = 0.05 m).................................143

Figure 39. Expanded u Velocity Distribution (x = 1.92 m).................................144

Figure 40. Expanded u Velocity Distribution (x = 3.83 m).................................145

Figure 41. Expanded u Velocity Distribution (x = 5.75 m).................................146

Figure 42. Expanded u Velocity Distribution (x = 7.66 m).................................147

Figure 43. Expanded u Velocity Distribution (x = 9.68 m).................................148

Figure 44. Expanded u Velocity Distribution (x = 11.49 m)....149

Figure 45. Expanded u Velocity Distribution (x = 13.41 m)....150

Figure 46. Expanded u Velocity Distribution (x = 16.18 m)....151

Figure 47. Expanded u Velocity Distribution (x = 17.43 m)....152

Figure 48. Expanded u Velocity Distribution (x = 18.65 m)....153

Figure 49. v Velocity Distribution (x = -2.20 m)....154

Figure 50. v Velocity Distribution (x = -0.69 m)....155

Figure 51. v Velocity Distribution (x = 0.05 m)....156

Figure 52. v Velocity Distribution (x = 1.92 m)....157

Figure 53. v Velocity Distribution (x = 3.83 m)....158

Figure 54. v Velocity Distribution (x = 5.75 m)....159

Figure 55. v Velocity Distribution (x = 7.66 m)....160

Figure 56. v Velocity Distribution (x = 9.69 m)....161

Figure 57. v Velocity Distribution (x = 11.49 m)....162

Figure 58. v Velocity Distribution (x = 13.41 m)....163

Figure 59. v Velocity Distribution (x = 16.18 m)....164

Figure 60. v Velocity Distribution (x = 17.43 m)....165

Figure 61. v Velocity Distribution (x = 18.65 m)....166

Figure 62. $\overline{u'^2}$ Turbulence Intensity Distribution (x = -2.20 m)....167

Figure 63. $\overline{u'^2}$ Turbulence Intensity Distribution (x = -0.69 m)....168

Figure 64. $\overline{u'^2}$ Turbulence Intensity Distribution (x = 0.05 m)....169

Figure 65. $\overline{u'^2}$ Turbulence Intensity Distribution (x = 1.92 m)....170

Figure 66. $\overline{u'^2}$ Turbulence Intensity Distribution (x = 3.83 m)....171

Figure 67. $\overline{u'^2}$ Turbulence Intensity Distribution (x = 5.75 m)....172

Figure 68. $\overline{u'^2}$ Turbulence Intensity Distribution (x = 7.66 m)....173

Figure 69. $\overline{u'^2}$ Turbulence Intensity Distribution (x = 9.68 x)....174

Figure 70. $\overline{u'^2}$ Turbulence Intensity Distribution (x = 11.49 m)....175

Figure 71. $\overline{u'^2}$ Turbulence Intensity Distribution (x = 13.41 m)....176

Figure 72. $\overline{u'^2}$ Turbulence Intensity Distribution (x = 16.18 m)....177

Figure 73. $\overline{u'^2}$ Turbulence Intensity Distribution (x = 17.43 m)....178

Figure 74. $\overline{u'^2}$ Turbulence Intensity Distribution (x = 18.65 m)....179

Figure 75. $\overline{v'^2}$ Turbulence Intensity Distribution (x = -2.20 m)....180

Figure 76. $\overline{v'^2}$ Turbulence Intensity Distribution (x = -0.69 m)....181

Figure 77. $\overline{v'^2}$ Turbulence Intensity Distribution (x = 0.05 m)....182

Figure 78. $\overline{v'^2}$ Turbulence Intensity Distribution (x = 1.92 m)....183

Figure 79. $\overline{v'^2}$ Turbulence Intensity Distribution (x = 3.83 m)....184

Figure 80. $\overline{v'^2}$ Turbulence Intensity Distribution (x = 5.75 m)....186

Figure 81. $\overline{v'^2}$ Turbulence Intensity Distribution (x = 7.66 m)....187

Figure 82. $\overline{v'^2}$ Turbulence Intensity Distribution (x = 9.68 m)....187

Figure 83. $\overline{v'^2}$ Turbulence Intensity Distribution (x = 11.49 m)....188

Figure 84. $\overline{v'^2}$ Turbulence Intensity Distribution (x = 13.41 m)....................................189

Figure 85. $\overline{v'^2}$ Turbulence Intensity Distribution (x = 16.18 m)....................................190

Figure 86. $\overline{v'^2}$ Turbulence Intensity Distribution (x = 17.43 m)....................................191

Figure 87. $\overline{v'^2}$ Turbulence Intensity Distribution (x = 18.65 m)....................................192

Figure 88. Polar Plot of Velocity Vector (x = 11.49 m)....................................194

Figure 89. Longitudinal Variation of Depth Averaged Longitudinal Velocity - Run 1................196

Figure 90. Longitudinal Variation of Depth Averaged Longitudinal Velocity - Run 2................197

Figure 91. Longitudinal Variation of Longitudinal Shear Velocity - Run 1........................200

Figure 92. Longitudinal Variation of Longitudinal Shear Velocity - Run 2........................201

Figure 93. Longitudinal Variation of Bed Stress Angle - Run 1.................................202

Figure 94. Longitudinal Variation of Bed Stress Angle - Run 2.................................203

Figure 95. Longitudinal Variation of Lateral Bed Stress - Run 1................................204

Figure 96. Longitudinal Variation of Lateral Bed Stress - Run 2................................205

Figure 97. Longitudinal Variation of Depth Averaged Lateral Velocity - Run 1.....................206

Figure 98. Longitudinal Variation of Depth Averaged Lateral Velocity - Run 2.....................207

Figure 99. Longitudinal Variation of Secondary Circulation Intensity - Run 1................209

Figure 100. Longitudinal Variation of Secondary Circulation Intensity - Run 2................210

Figure A1. Definition Sketches..........................222

Figure A2. Water Surface at a Transition to a Curved Channel....232

Figure A3. Water Surface at a Sudden Reversal of Channel Curvature....233

Figure B1. CRVCNL Example Input....239

Figure B2. CRVCNL Example Output....240

Figure B3. CRVCNL Program Listing....241

Figure B4. PERTRB Program Listing....244

Figure B5. DEVFLO Program Listing....251

Figure B6. ANZDAT Program listing....260

LIST OF SYMBOLS

a_i	Constants of integration
b_i	Constants of integration
b	Channel half width
B	Channel width
c_b	Boundary condition constant
C	Chezy coefficient
C_f	Non-dimensional Chezy coefficient
C_{f0}	Average C_f across section
C_i	Constants
d	Depth of flow
d_c	Depth of flow at channel centreline
f	Friction coefficient
f_i	Functions
f_D	Doppler frequency
F	Lateral bed shear force
F_{DL}	Longitudinal drag on particle
F_L	Lift force on particle
F_R	Froude number
g	Acceleration due to gravity
h	Superelevation
h_i	Metrical coefficients
H	Average depth of channel
H'	Non-dimensional depth deviation
H_0	Depth scale
H_s	Depth of scour
I_1, I_2	Integral functions

i	Square root of -1
k	Fourier transform variable
k_s	Equivalent sand grain roughness
L_B	Length scale
L_s	Development length for secondary flow
m	Mass of differential element
n	Refractive index of water
N	Number of accepted samples
N_f	Number of fringes in burst
p	Pieziometric pressure
P_0, P_1	Hydrostatic pressure forces
r	Local radius of curvature
R	Radius of curvature of channel centreline
R_e	Reynolds Number
R_0	Radius of curvature scale
S	Total superelevation across channel
S_0	Longitudinal bed slope
S_{0c}	Longitudinal bed slope of channel centreline
t_p	Particle transit time
u	Longitudinal velocity
u'	Deviation of longitudinal velocity from mean
$\overline{u_i' \, u_j'}$	Reynolds stresses
u_{Bi}	Velocity measured by blue laser beams
u_{Gi}	Velocity measured by green laser beams
u_{0b}	boundary condition constant
u_*	Longitudinal shear velocity
U	Depth averaged longitudinal velocity

U'	Non-dimensional velocity deviation
U_0	Cross-sectionally averaged longitudinal velocity or velocity scale
U_w	Depth averaged longitudinal velocity near side wall
v	Lateral velocity
V	Depth averaged lateral velocity, Fourier transform of v
w	Vertical velocity
W	Weight of sediment particle
x	Longitudinal co-ordinate
y	Lateral co-ordinate
z	Vertical co-ordinate
α	Lateral bed angle, curvature ration
β	Aspect Ratio
γ	Specific wieght of fluid
δ	Angle of total bed stress from longitudinal
ζ	Lateral vorticity
η	Non-dimensional vertical co-ordinate, vertical vorticity
θ	Bend angle
ν	Kinematic viscosity
ν_t	Eddy viscosity
ν_R	Eddy viscosity ratio
ξ	Longitudinal vorticity
ρ	Fluid density
τ_{yz}	Fluid shear stress

τ_{y0}	Lateral bed stress
τ_{x0}	Longitudinal bed stress
τ_0	Total bed stress
$\overline{\tau_0}$	Average total bed stress
τ_w	Wall stress
ϕ	Dynamic friction angle of particle
ψ	Stream function, laser beam intersection angle

INTRODUCTION

Curvature effects in open channels affect many problems in hydraulic engineering such as flow distribution, bank stability, bed topography, resistance, and superelevation. In order to provide more reliable and economical engineering works, these effects must be taken into account. Unfortunately, the three-dimensional nature of the problem makes it very difficult to solve it analytically. Due to the large numbers of variables and geometries inherently possible, a purely empirical approach is not feasible either.

Recently, because of the importance of the problem, much research has been conducted on flow in curved channels. Typically the researchers have attempted to apply an approximate analysis and performed a limited experimental study. The mechanics of the flow have thus been revealed piecemeal as each study pointed to new aspects of the problem. The present knowledge is substantial, but fragmented. The depth of understanding is also uneven with developed secondary flow well documented while main velocity redistribution remains difficult to predict. What knowledge that is available is not of a form useful to the practicing engineer due to the incomplete and fragmentary (and occasionally contradictory) nature of the research.

In this study, it is proposed to first review the present knowledge of curved channel flows. Both the extent and applicability of the results are assessed. Weak areas may thus be identified for further study.

The subsequent parts of this study constitute a contribution to one such relatively weak area; that of the developing flow situation. For simplicity a rectangular channel shape is used. An approximate anaylsis is developed and two detailed experiments are presented.

1. PART ONE - REVIEW OF THE PR

1.1 INTRODUCTION

Almost all rivers and streams are

to some degree. This curvature has a

the flow, bed topography, and stabi

Usually, in practical situations, de

reaches or take account of these ef

overconservative estimates. It is

section to analyse the state-of-the-ar

channel flows and to obtain estimates

that may be used in hydraulic engineer

Generally, the state of prese

divided into the following three areas

1. The flow mechanics which f
   understanding of the problem
2. A body of experimental infor
   validation of theories
   practical situations.
3. Predictive models which may
   design and analysis.

Each of these will be considered separ

Related topics which are very in

the present scope are meander orig

migration as well as dispers

characteristics of curved channels.

1.2. MECHANICS OF CURVED CHANNEL FLOW

1.2.1 Introduction

In order to make engineering judgements and calculations, a reasonable understanding of the physics of the problem is required. At the present time, some aspects of flow in curved open channels are well understood while others are not. The present section will attempt to explain the features of curved channel flow in an engineering manner; that is, to provide a qualitative description which is supported with straight forward formula derivations and pertinent experimental results.

1.2.1.1 Co-ordinate System

The co-ordinate system used will be based on Figure 1, where x and u denote the longitudinal direction and (time-averaged) velocity, y and v the lateral direction and velocity, while z and w denote the vertical direction and velocity. The radius of curvature of the channel centreline is R and the width and average depth of the channel are given by B and H respectively.

The radius of curvature of any point across the channel is given by r which is related to R and y by the relation

$$r = R + y \tag{1}$$

The elevation of the water surface above H (referring to

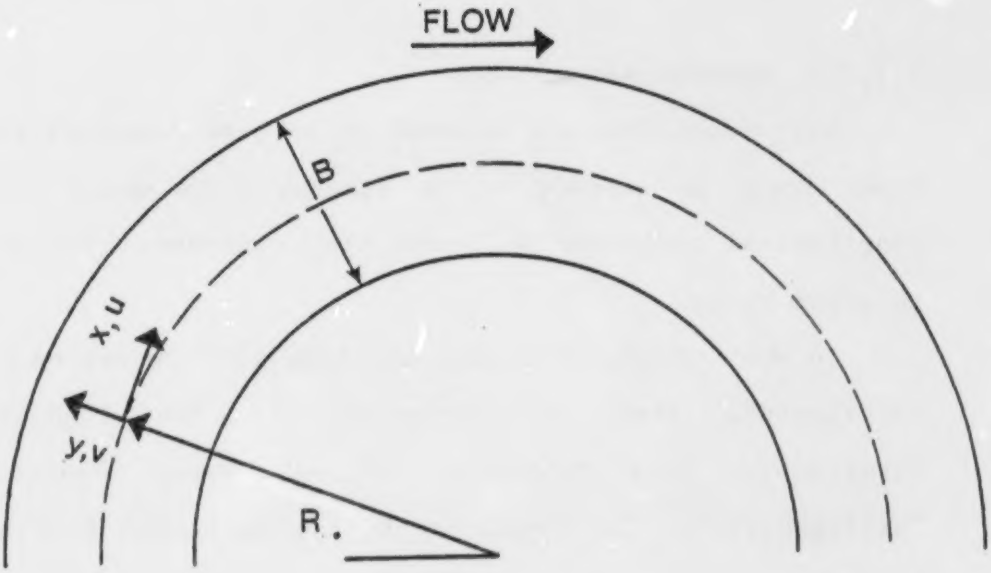
FLOW
B
x,u
y,v
R.

Figure 1. Definition Sketch - Plan

Figure 2) is h while H_s is the scour depth below the mean bed elevation. The actual depth of flow is represented by d and is given by:

$$d = H + H_s + h \qquad (2)$$

1.2.2.1 General Assumptions

All velocities are assumed to be time averaged and the flow itself is assumed to be steady. The depth averaged longitudinal velocity is U and the cross-sectional average is given by U_0.

In much of what follows, the flow will be assumed to be "developed", that is, invariant in the longitudinal direction. This condition has also been described as "axisymmetric". The requirements for developed flow are as follows:

1. The radius of curvature of the channel (R) remains constant (i.e., the bend is circular in plan).
2. The channel is prismatic.
3. The section under consideration is well removed from the entrance and exit (i.e., the bend is long).

These conditions are quite restrictive and are rarely met in a laboratory, much less in the field. The developed flow assumption is useful, however, in isolating some features of the flow for better understanding.

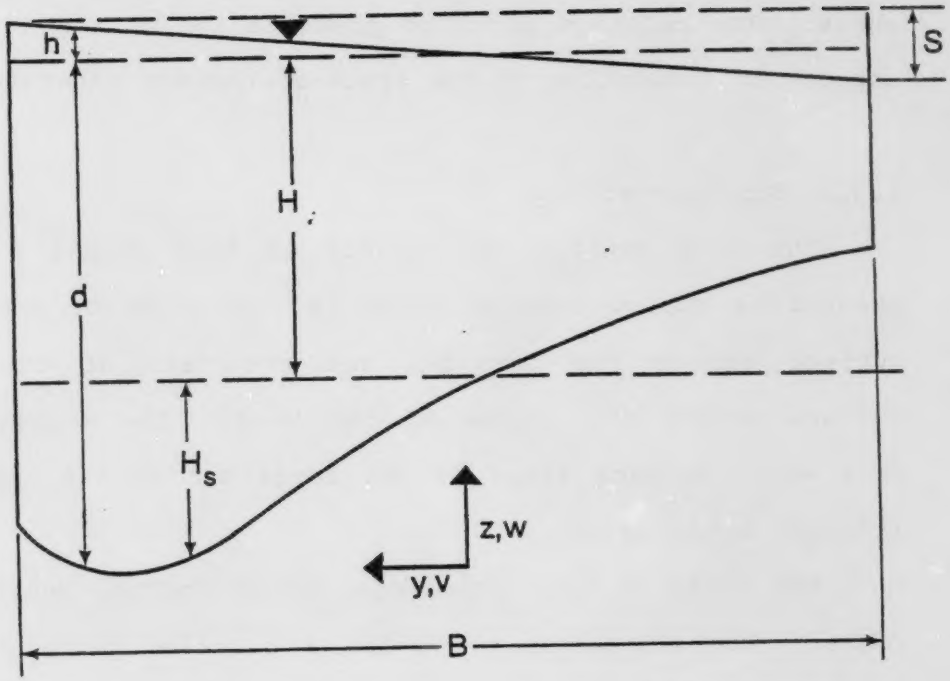
h
S
H_i
d
H_s
z,w
y,v
B

Figure 2. Definition Sketch - Elevation

The procedure in the following will be to attack the individual phenomena separately. This results in the simplest presentation, but it must be remembered that there are significant interactions between them and a proper approach would be to find a solution for the flow as a whole. The relative depth of presentation of the different aspects is indicative of the state-of-the-art understanding.

1.2.2 Superelevation

The most obvious consequence of flow around a curved channel is superelevation, that is, the rise of the water surface around the outside, and the fall of the water surface around the inside of the bend. The magnitude of this water surface slope is not large but it has important indirect consequences.

The cause of this phenomena is, of course, centrifugal force. For the water to follow a circular path, a force must be applied in a direction normal to the flow and directed toward the centre of curvature. This is provided by the excess hydrostatic pressure of an increased depth of water towards the outside of the bend.

1.2.2.1 Derivation

To calculate the water surface profile, consider Figure 3, a free body diagram of a water column of unit thickness flowing concentrically around a bend with depth averaged velocity U. The balance of forces acting on this

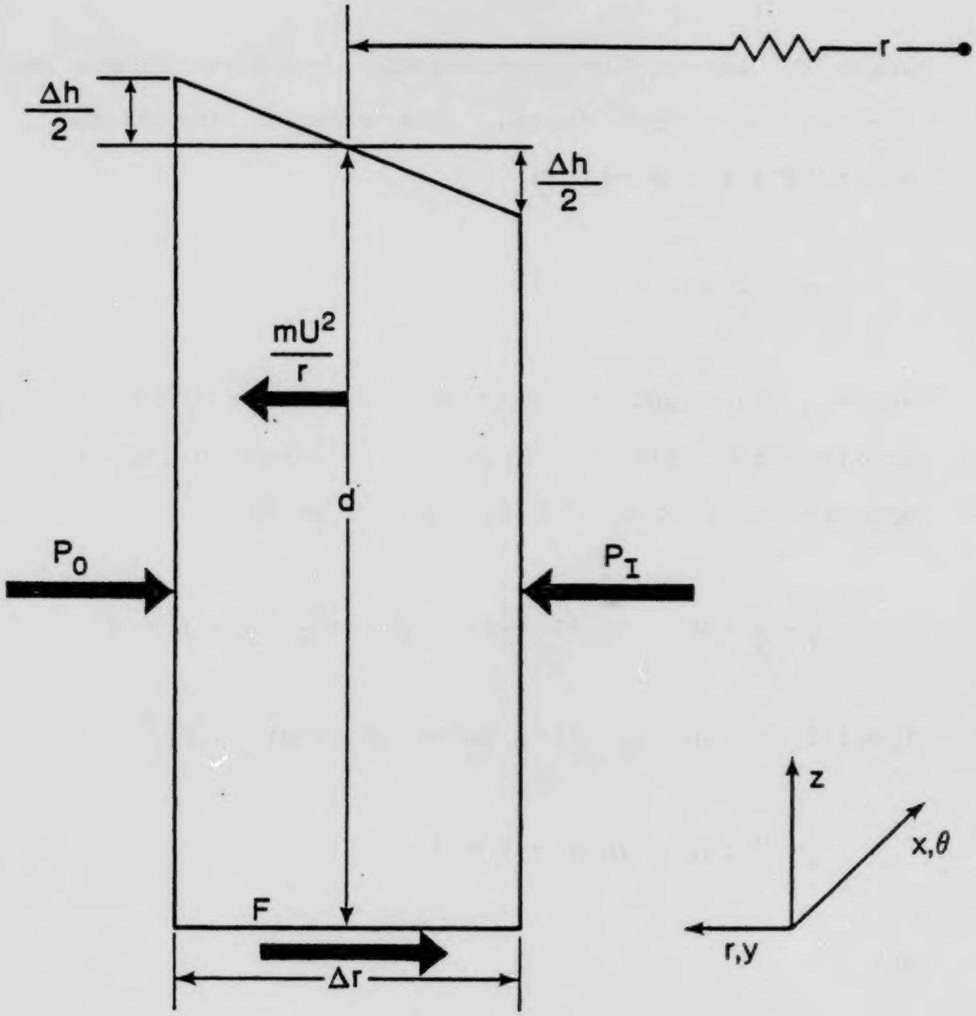
r
Δh/2
Δh/2
mU²/r
d
P_0
P_I
F
Δr
z
x,θ
r,y

Figure 3. Forces Acting on a Water Column

fluid element is:

$$\frac{mU^2}{r} = (P_o - P_1) - F = 0 \tag{3}$$

where P_o and P_1 are hydrostatic pressure forces and F is lateral bed shear force. The mass of the element, m, is given by the expression

$$m = \frac{\gamma}{g} d\Delta r \tag{4}$$

where γ is weight per unit volume of the fluid and g is the acceleration due to gravity. Substituting 4 and the hydrostatic forces into Equation 3 we have:

$$\frac{U^2}{r} \frac{\gamma}{g} d\Delta r - \left(\frac{\gamma}{2} (d+\frac{\Delta h}{2})^2 - \frac{\gamma}{2} (d-\frac{\Delta h}{2})^2\right) - F = 0 \tag{5}$$

Simplifying and ignoring terms of order $(\Delta h)^2$:

$$\frac{U^2}{r} \frac{\gamma}{g} d\Delta r - \gamma d\Delta h - F = 0 \tag{6}$$

or:

$$\frac{\Delta h}{\Delta r} = \frac{U^2}{gr} - \frac{F}{\gamma d\Delta r} \tag{7}$$

or in the limit as $\Delta r \to 0$:

$$\frac{dh}{dr} = \frac{U^2}{gr} - \frac{{}^{\tau}\gamma 0}{dr} \tag{8}$$

where τ_{y0} is the bed shear stress in the lateral direction. In many cases, it is small and may be neglected. As a first approximation we may take U equal to U_0 and r equal to R_0 where R_0 is the radius of curvature of a long circular reach.

$$\frac{dh}{dr} = \frac{U_0^2}{gR_0} \tag{9}$$

Equation 9 may be integrated by noting from Equation 1:

$$dr = dy \tag{10}$$

to give:

$$h = \frac{U_0^2}{gR_0} y \tag{11}$$

At the outside of the bend:

$$h = \frac{U_0^2}{2g} \frac{B}{R_0} \tag{12}$$

and the total superelevation (difference between outside and inside elevations) is:

$$S = 2 \frac{B}{R_0} \frac{U_0^2}{2g} \tag{13}$$

1.2.2.2 Superelevation Example

As an example to illustrate the size of this superelevation, take the North Saskatchewan River bend around the Mayfair golf course in Edmonton (data from Kellerhals, et al., 1972), where:

$$B \approx 140 \text{ m} \tag{14}$$

$$U_0 \approx 1.25 \text{ m/s} \tag{15}$$

$$R_0 \approx 750 \text{ m} \tag{16}$$

Thus:

$$S \approx 30 \text{ mm} \tag{17}$$

This does not seem large, considering that this particular bend is of only moderate curvature, but the cross channel water surface slope:

$$\frac{S}{B} \approx 0.00021 \tag{18}$$

is of the same order of magnitude as the longitudinal bed slope:

$$S_0 \approx 0.00035 \tag{19}$$

The above estimation of superelevation has been found experimentally to be accurate to within about ten percent, although it appears to consistently underestimate the superelevation. In some cases of erodable bed laboratory models, superelevations of up to twice this value have been observed (Yen and Yen, 1971).

1.2.2.3 Effect of Varying Longitudinal Velocity

To improve this estimate, one approach taken is to allow U to vary across the channel. The problem, then, is to specify the variation of U. Ippen and Drinker (1962) tried several variations:

a. the free vortex; $U = U_0 \frac{R_0}{r}$ (20)

Just past the entrance of the bend, the velocity will be distributed according to equation 20. The corresponding expression for superelevation was derived to be:

$$S = 2 \frac{B}{R_0} \frac{U_0^2}{2g} \left(\frac{1}{1 - \left(\frac{B}{2R_0}\right)^2} \right) \qquad (21)$$

b. the forced vortex; $U = U_0 \frac{r}{R_0}$ (22)

The "forced vortex" distribution approximates the flow near the end of the bend where the maximum velocity has shifted to the outside. The superelevation is then:

$$S = 2\,\frac{B}{R_0}\,\frac{U_0^2}{2g}\left(\frac{1}{1 + \frac{1}{3}\left(\frac{B}{2R_0}\right)^2}\right) \qquad (23)$$

Another possibility is to allow r to remain variable. This results (assuming $U = U_0$ again) in:

$$S = 2\,\frac{U_0^2}{2g}\left(\ell n\left(\frac{1 + \frac{B}{2R_0}}{1 - \frac{B}{2R_0}}\right)\right) \qquad (24)$$

Figure 4 is a plot of Equations 19 ,21, 23 and 24. The different formulas diverge widely for large values of B/R_0, but at values typical of natural streams ($B/R_0 < 0.5$) the difference is very small. The free vortex form, Equation 21, is generally preferred since it predicts a superelevation slightly larger than the simple expression given by Equation 19. The actual cross-channel profile is also best fitted by the free vortex form (Ippen and Drinker 1962; Yen and Yen, 1965; Yen, 1971).

1.2.2.4 Effect of Bed Friction

It remains, however, to consider the effect of the bed friction on the superelevation. This bed friction acts as a result of the secondary circulation which is to be considered later. For now, we will borrow two significant results from this later section that will allow us to estimate a correction to the superelevation.

First, the secondary flow near the bed is always towards the inside of the bend. This implies that the bed shear force acts in a negative sense according to the arrow

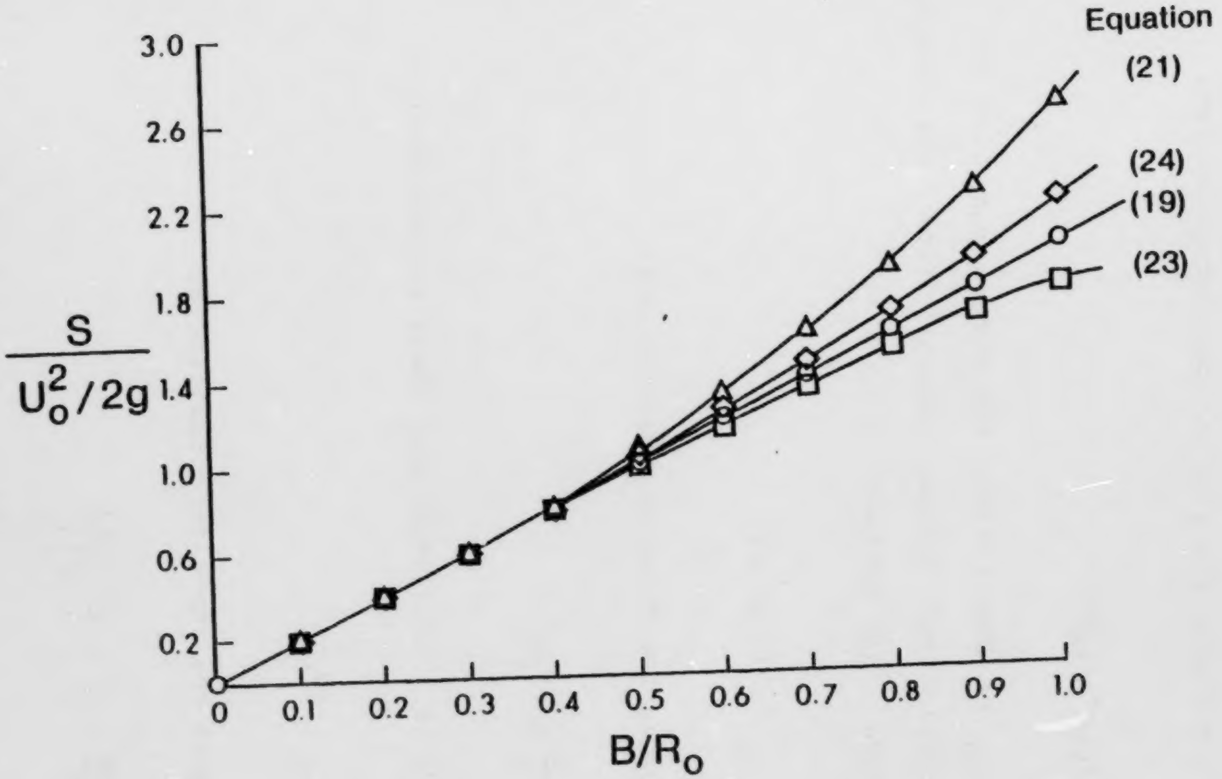

Figure 4. Superelevation Versus Curvation Ratio

on Figure 3. Thus, from Equation 8, the lateral water surface slope is always effectively increased by the bed friction.

To estimate the size of the correction let:

$$\tau_{y0} = \tau_{x0} \tan\delta \tag{25}$$

where τ_{x0} is longitudinal bed stress and δ is the angle of the total bed stress vector from the longitudinal direction. Also define:

$$\tau_{x0} = -(\gamma/g)\ u_*^2 \tag{26}$$

where u_* is the friction velocity and:

$$C_f^2 = U^2/u_*^2 \tag{27}$$

where C_f is a nondimensional Chezy coefficient:

$$C_f = C/\sqrt{g} \tag{28}$$

Substitute the above into Equation 8:

$$\frac{dh}{dr} = \frac{U^2}{gr} + \frac{U^2}{g}\,\frac{\tan\delta}{C_f^2 d} \tag{29}$$

Now make use of the second result to be obtained later, namely:

$$\tan\delta \approx 11 \frac{d}{r} \tag{30}$$

Equation 29 becomes:

$$\frac{dh}{dr} = \frac{U^2}{gr} \left(1 + \frac{11}{C_f^2}\right) \tag{31}$$

Since typical values of C_f range from about 10 (rough) to 20 (smooth), the correction is about 2.5% to 10% and accounts for some of the observed error. This correction applied to any of Equations 19 to 24 will result only in the magnification of the curves by the factor $(1 + 11/C_f^2)$. In practice it is difficult to apply this correction because the constant, taken above as 11, actually is a function of C_f itself and has been quoted as varying from about 7 to 13 (Koch, 1980).

1.2.2.5 Calculation of Superelevation

In practical river situations where it is of interest the superelevation may be calculated by the following method:

1. Obtain the average stage elevation for the desired discharge by standard methods.
2. Obtain a cross-sectional bed profile of the channel (which should be measured but may be estimated using the results of section 2.6). Variation of the resistance coefficient across the channel (e.g. flood plains) should be noted as

well.

3. Calculate U at a number of evenly spaced locations across the channel. At present, the best estimate is given by a resistance equation, such as:

$$U = C_f \sqrt{gdS_0} \qquad (32)$$

Note that the local resistance coefficient may require a minor adjustment to give the same discharge as specified.

4. Integrate Equation 24 numerically across the channel starting at the inside bank. Use the values of U, r (measured from the centre of curvature) and C_f estimated previously at each point. This gives the water surface profile relative to the elevation at the inside bank.

5. The constant of integration is determined by calculating the average elevation increase of the profile from step 4. This value is subtracted from the water surface elevations to give h(y).

6. It may be necessary to repeat the process (starting at step 3) once using the new water surface elevations.

1.2.2.6 Developing Flow Considerations

For the case of developing flow, little is known. At a sudden change in curvature, such as at the beginning or exit of a circular bend, the water surface slope has been noticed to adjust over a length about equal to the width of the stream:

$$L_B \approx B \tag{33}$$

and roughly symmetrical on each side of the point of curvature change. Over a long bend, the magnitude of superelevation decreases slightly as the maximum flow concentration shifts from the inside to the outside of the bend. This corresponds to a gradual shift of superelevation from a value given by Equation 21 to that given by Equation 23.

The lateral inertia of the flow may also have a significant effect on the transverse water surface profile. Yen and Yen (1971) and Kalkwijk and de Vriend (1980) both noticed a large increase in superelevation (up to twice the normal value) in experiments performed in channels with a rigid but "natural" bed. That is, there was a scour hole effect. Both experimenters attributed this effect mainly to lateral inertia. The mechanism is essentially as follows. As the flow proceeds into the bend, it encounters the scour hole on the outside of the bend. Here the flow is faster and, therefore, a large portion of the discharge shifts to the outside. This shifting envolves considerable inertia and, in order to stop the lateral flow, an extra transverse water surface slope is set up.

This effect has been taken into account only in very complex numerical models (Leschziner and Rodi, 1979; de Vriend, 1981). As it is expected that in some cases the effect is significant, especially in natural channels, more research and application is required.

1.2.3 Secondary Flow

Secondary circulation, or helicoidal flow as it is sometimes called, arises from the fact that some of the fluid, specifically near the bed, is moving slower than the average velocity. Since it is moving slower, it lacks the apparent centrifugal force to resist the imposed pressure gradient of the water surface slope. It is, therefore, accelerated inward until friction provides a balancing force. Fluid moving faster than average (near the surface) would experience the opposite effect and be accelerated outward. The net result is a circulation over the flow cross-section, superimposed on the main longitudinal flow (Figure 5). The total streamlines follow a helicoidal path.

The secondary flow is important because it is considered to be the primary cause of river bend scour. It also has significant effects on the lateral diffusion characteristics of a stream.

1.2.3.1 Analysis of Developed Secondary Flow in a Wide Open Channel

The lateral force balance equation for an element of fluid is:

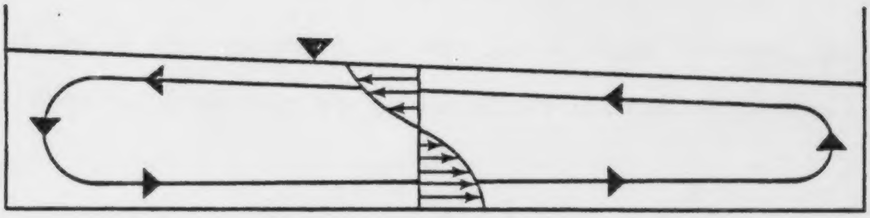

Figure 5. Secondary Circulation

$$-\frac{u^2}{r} = -\frac{\partial(gh)}{\partial r} + \frac{\partial\tau_{yz}}{\partial x}\frac{g}{\gamma} \qquad (34)$$

where τ_{yz} is the lateral shear stress acting on the top and bottom faces of the element. Equation 34 has been derived and used by Rosovskii (1961), Yen (1965) and Engelund (1974). It is directly analagous to Equation 8 except that it has been derived for a fluid element of depth dz instead of for a column of depth equal to the depth of flow d. Alternatively, Equation 34 may be derived from the Reynold's Equation for the radial direction by neglecting the inertial terms and the small stress terms.

To proceed further, substitute Equation 8 into Equation 34 (noting that h is not a function of z so the partial derivative may be replaced by an ordinary derivative):

$$-\frac{u^2}{r} = -\frac{\overline{u^2}}{r} + \frac{g}{\gamma}\frac{\tau_{y0}}{d} + \frac{\partial\tau_{yz}}{\partial z}\frac{g}{\gamma} \qquad (35)$$

A small change has been introduced into Equation 8. The term $\overline{u^2}$, defined by:

$$\overline{u^2} = \frac{1}{d}\int_0^d u^2 dy \qquad (36)$$

(which is the average over the depth of the longitudinal velocity squared) has replaced the depth averaged velocity squared, U^2, which is given by:

$$U^2 = \left(\frac{1}{d}\int_0^d u\, dy\right)^2 \qquad (37)$$

The difference between the two is small, but the former is more correct. Rearranging Equation 35:

$$\frac{g}{\gamma}\frac{\partial \tau_{yz}}{\partial z} = \frac{1}{r}\left(\overline{u^2} - u^2\right) - \frac{g}{\gamma}\frac{\tau_{y0}}{d} \qquad (38)$$

Let

$$u = U + u' \qquad (39)$$

where U is the depth average velocity and u' is the deviation from the average. Substitute into Equation 38:

$$\frac{g}{\gamma}\frac{\partial \tau_{yz}}{\partial z} = \frac{1}{r}\left(U^2 + 2\,\overline{Uu'}\ \overline{+u'^2} - U^2 - 2Uu' - u'^2\right) - \frac{g}{\gamma}\frac{\tau_{y0}}{d} \qquad (40)$$

Simplify Equation 40 to obtain:

$$\frac{g}{\gamma}\frac{\partial \tau_{yz}}{\partial z} = \frac{1}{r}\left(-2Uu' - u'^2 + \overline{u'^2}\right) - \frac{g}{\gamma}\frac{\tau_{y0}}{d} \qquad (41)$$

To proceed further let:

$$\frac{g}{\gamma}\,\tau_{y0} = \nu_t\,\frac{\partial v}{\partial z} \qquad (42)$$

where ν_t is the eddy viscosity and may be a function of z. Also let:

$$\frac{g}{\gamma}\,\tau_{y0} = -u_*^2 \tan\delta \qquad (43)$$

where δ is as defined previously. Assume:

$$u' = u_* f_1 \left(\frac{z}{d}\right) \tag{44}$$

$$\nu_t = u_* d \; f_2\left(\frac{z}{d}\right) \tag{45}$$

$$\eta = z/d \tag{46}$$

Substitute Equations 42 to 46 into Equation 41:

$$\frac{\partial}{\partial \eta} f_2 \frac{\partial v}{\partial \eta} = \frac{Ud}{r} \left(-2f_1 - \frac{1}{C_f}\left(f_1^2 - \overline{f_1^2} - \frac{r}{d} \tan\delta\right)\right) \tag{47}$$

Integrate twice with respect to η to obtain:

$$v = \frac{Ud}{r} \int \frac{1}{f_2} \left[\int\left\{-2f_1 - \frac{1}{C_f}\left(f_1^2 - \overline{f_1^2} - \frac{r}{d}\tan\delta\right)\right\}d\eta + C_1\right]d\eta + C_2 \tag{48}$$

The constants of integration are determined by:

$$f_2 \frac{\partial v}{\partial \eta} = 0 \text{ at } \eta = 1 \tag{49}$$

(shear stress equals zero at water surface) and:

$$\int_0^1 v d\eta = 0 \tag{50}$$

(net lateral discharge equals zero). It remains to evaluate tan δ. This term is clearly of small magnitude as it amounts to a small correction to the lateral water surface slope. Yen (1965) and Rosovskii (1961) ignore it for certain cases. It may be evaluated by application of another boundary condition at the bed. The most obvious is simply:

$$v|_{\eta = 0} = 0 \tag{51}$$

De Vriend (1976) modified this condition slightly to use with logarithimic velocity distributions and stated:

$$v|_{\eta = \eta_0} = 0 \tag{52}$$

where η_0 is the height where the longitudinal velocity given by the logarithmic formula vanishes.

Another possible bed condition is that the angle of the shear stress vector at the bed should coincide with the angle of the velocity vector near the bed:

$$\frac{v}{u} = \frac{\tau_{y0}}{\tau_{x0}} = \tan\delta = \frac{\nu_t \ \partial v/\nabla y}{u_*^2} \tag{53}$$

A difficulty with this condition is that the level of the velocity vector must be specified. Rosovskii (1961) and Engelund (1974) used this condition. De Vriend (1976) reviews these conditions.

In general the results take the form:

$$\tan\delta = K \frac{d}{r} \tag{54}$$

where K is a function of C_f and of the particular velocity and eddy viscosity distributions. Values of K ranging from 7 to 13 have been reported, with K = 11 a reasonable approximation for typical stream conditions (Koch, 1980; Rosovskii, 1961). Equation 54 may be substituted into Equation 48 which may be written as:

$$v = \frac{Ud}{r} [I_1 + \frac{I_2}{C_f}] \qquad (55)$$

where:

$$I_1(\eta) = \eta \frac{1}{f_2} (\int - 2f_1 d_\eta + a_1) \, d\eta + a_2 \qquad (56)$$

and:

$$I_2 (\eta) = \int \frac{1}{f_2} (\int \{-f_1^2 + \overline{f_1^2} + K \} \, d\eta + b_1) \, d\eta + b_2 \qquad (57)$$

The problem is thus solved when the distributions f_1 and f_2 are supplied. Figure 6 is a graph of I_1 and I_2 when the logarithimic distribution of u is chosen for f_1 and a parabolic distribution of eddy viscosity is chosen for f_2. K is assumed to equal 11. Von Karman's constant is taken as 0.4.

In general, increasing roughness (decreasing C_f) leads to smaller secondary velocities, especially near the bed.

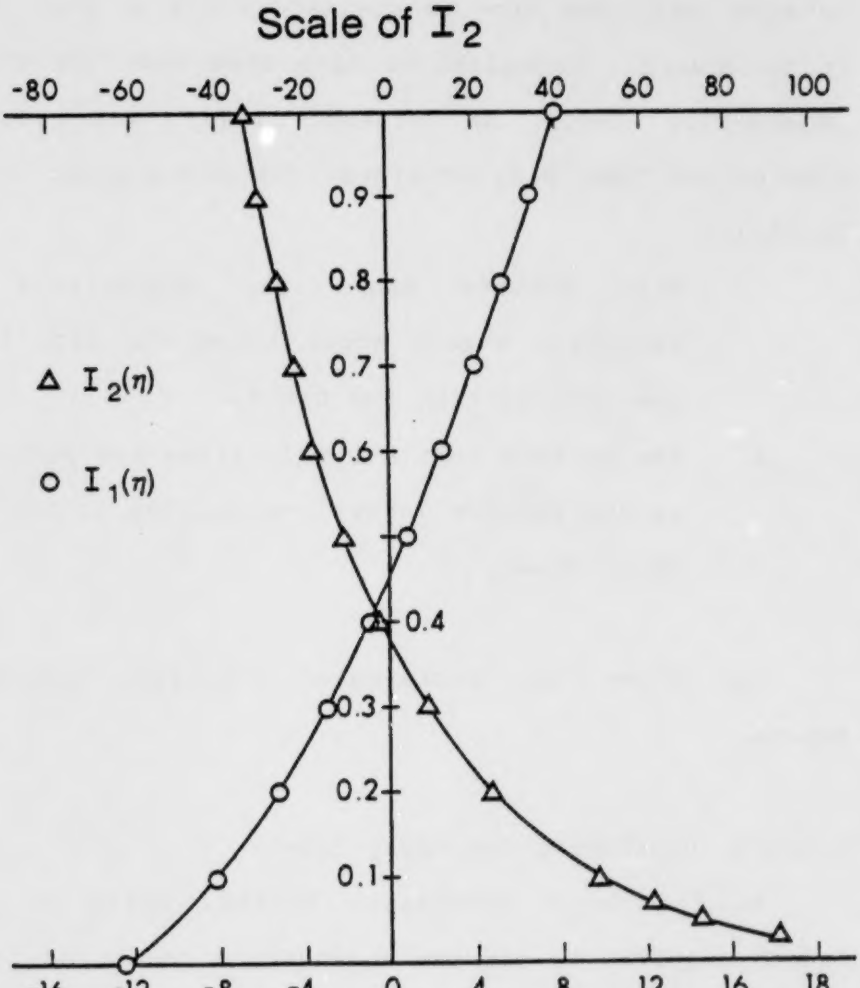

Figure 6. Integral Functions

1.2.3.2 Bank Effects

At the stream banks, the lateral flow is turned vertically to complete the secondary circulation. At the outside bank, the flow is downward while at the inside bank it is upward. Calculations have been made for this region (Rosovskii, 1961; de Vriend, 1973) and some useful conclusions have been obtained (for rectangular channels at least):

1. Wall effects (that is, appreciable vertical velocity) extend about twice the flow depth into the channel from the banks.
2. The maximum vertical velocities are about the same as the maximum lateral velocities in the centre of the channel.

For other than rectangular channels, information is scarce.

1.2.3.3 Developing Secondary Flow

As the fluid possesses inertia, there is a certain length required to set the secondary circulation into motion after the bend entrance. If we assume that the water surface changes abruptly from flat to superelevated, then the development length, or distance to reach 90% of its developed value, has been estimated to be (Rosovskii, 1961; Nouh and Townsend, 1979):

$$L_s = (1.8 \text{ to } 2.3)\ H\ C_f \tag{58}$$

The corresponding development length for superelevation was noted in Equation 33. Thus the ratio is:

$$\frac{L_B}{L_S} = \frac{1}{2C_f}\ \frac{B}{H} \tag{59}$$

For channels with aspect ratios (B/H) of 20 to 40, the two lengths are of similar size. For larger aspect ratios (and rougher channels) the secondary flow development is faster and the overall development is governed by the superelevation development. For smaller aspect ratios or smoother channels (typical of laboratory situations) the secondary flow development governs.

At the bend exit the same situation applies in reverse and the decay lengths are the same as above.

1.2.4 Longitudinal Velocity Redistribution

The longitudinal component of velocity is significantly affected by the curvature of the stream. As the flow enters the bend, the velocity on the inside increases while the velocity on the outside decreases. As the flow proceeds around the bend, the lateral profile becomes uniform again and then begins skewing to the outside. If the bend is long enough, equilibrium may be reached. Near the exit of the bend, a major redistribution toward the outer wall takes place. This exit redistribution is equal but opposite to the entrance redistribution. Thus the largest "skewness" of the lateral velocity profile is actually observed just past the end of the bend.

There are several different mechanisms causing this phenomenon and each will be discussed separately. In the following, the longitudinal velocity referred to is taken to be the depth averaged velocity, U, defined previously.

1.2.4.1 Inertial Effects

Over a short distance near a change in curvature, a velocity redistribution takes place that is essentially independant of friction. This results in the free vortex velocity distribution and may be considered simply a conservation of vorticity from the first curvature to the second.

To calculate this effect, consider the specific energy along a streamline:

$$E = h_1 + \frac{U_1^2}{2g} = h_2 + \frac{U_2^2}{2g} \qquad (60)$$

Point 1 is in the straight reach upstream of the bend and point 2 is in the bend. Differentiating Equation 60 with respect to r:

$$\frac{d}{dr}\left(h_1 + \frac{U_1^2}{2g}\right) = 0 = \frac{d}{dr}\left(h_2 + \frac{U_2^2}{2g}\right) \qquad (61)$$

But we know already from Equation 8 that:

$$\frac{dh_2}{dr} = \frac{U_2^2}{rg} \tag{62}$$

Thus:

$$\frac{dU_2}{dr} = -\frac{U_2}{r} \tag{63}$$

Integrating (noting that $U_2 = U_0$ at $r = R_0$):

$$U_2 = \frac{U_0 R_0}{r} \tag{64}$$

as expected.

At a bend exit, we may apply the same analysis. Point 3 is before the end and point 4 is after the end:

$$\frac{d}{dr}\left(h_3 + \frac{U_3^2}{2g}\right) = \frac{d}{dr}\left(h_4 + \frac{U_4^2}{2g}\right) \tag{65}$$

For simplicity U_3 is assumed to be uniformly distributed. Thus:

$$\frac{dh_3}{dr} = \frac{d}{dr}\left(\frac{U_4^2}{2g}\right) \tag{66}$$

Again:

$$\frac{dh_3}{dr} = \frac{U_0^2}{gr} = \frac{U_4^2}{gr} \tag{67}$$

then:

$$\frac{dU_4}{dr} = \frac{U_4}{r} \qquad (68)$$

and finally:

$$U_4 = \frac{U_0 r}{R_0} \qquad (69)$$

From the point of view of vorticity, the phenomenon may be explained as follows. Initially the flow is uniform across the channel (neglecting the sidewall regions). Its vertical vorticity is therefore zero. After entering the bend, the flow is constrained to move basically concentrically. This may be achieved without altering the vorticity only if the lateral profile assumes the form of an irrotational (free) vortex.

Friction, of course, acts to change the vorticity but it requires a significant length to cause an appreciable change. In this case it would act to make the profile more uniform. Since the flow is moving concentrically, a uniform distribution implies that the flow contains vorticity. This is evident after the end of the bend, where the velocity profile skews outward.

As is obvious from the above, the inertial velocity redistribution is closely associated with the superelevation. We expect, and in fact notice, that the development lengths for velocity redistribution and superelevation are about the same. This applies to both the entrance and exit of the bend.

1.2.4.2 Slope Differential Effect

Referring to Figure 7, we observe that for a given arc θ, flow on the outside must travel further than on the inside. Presumably, however, the change in the bed elevation will be the same from A to B. Or:

$$S_0 = \frac{\Delta z_b}{\Delta x} = \frac{\Delta z_b}{r\theta} \tag{70}$$

For the channel centreline:

$$S_{0c} = \frac{\Delta z_b}{R_0\theta} \tag{71}$$

Therefore:

$$S_0 r = S_{0c} R_0 \tag{72}$$

Thus the slope is steeper on the inside of the channel. To estimate the effect on the lateral distribution of longitudinal velocity, consider the uniform flow approximation:

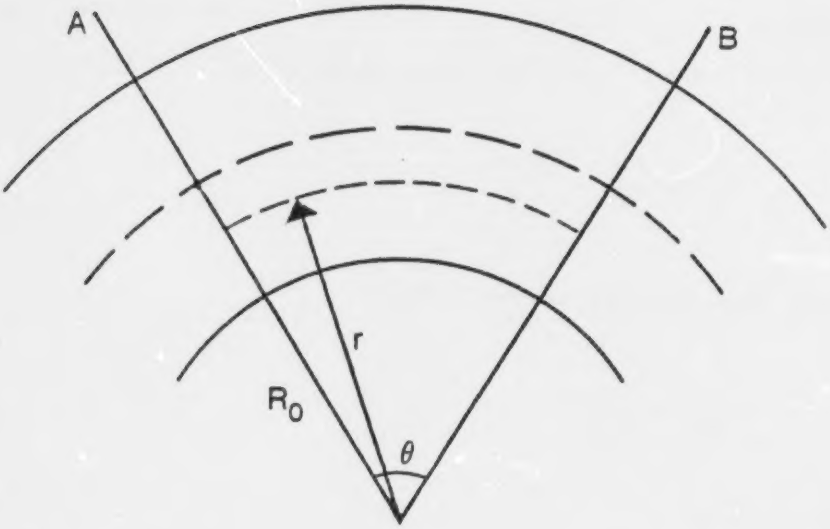
A
B
r
R_0
θ

Figure 7. Slope Differential

$$U = C_f u = C_f \sqrt{gdS_0} \tag{73}$$

Substituting Equation 72:

$$U = C_f \frac{\sqrt{gdS_{0c}R_0}}{\sqrt{r}} \tag{74}$$

But:

$$U_C = C_f \sqrt{gdS_{0c}} \tag{75}$$

Thus:

$$\frac{U}{U_C} = \sqrt{\frac{R_0}{r}} \tag{76}$$

assuming d is constant.

Equation 76 indicates that, if the slope differential were the only important factor, then, after some distance, the flow would still be faster on the inside but the variation across the channel would be reduced. This implies that the flow gains vorticity.

1.2.4.2 Depth of Flow (Vertical Friction)

In a similar manner to the above, we may include the effect of a non-uniform bed profile. In Equation 74, let d be a function of r to obtain:

$$\frac{U}{U_C} = \sqrt{\frac{R_0}{r}} \; \sqrt{\frac{d}{d_C}} \tag{77}$$

Thus the flow is faster where the water is deeper. In natural bends, it is almost invariably observed that the outside of the bend is scoured deeper than the normal depth while deposition occurs on the inside of the bend. Therefore, in natural channels a strong skewing of velocity toward the outside wall may take place.

1.2.4.4 Lateral Friction

The ultimate effect of lateral friction would be to cause the flow to move as a rigid body around the bend. This would require that the lateral profile be given by the forced vortex equation:

$$\frac{U}{U_C} = \frac{r}{R_0} \tag{78}$$

This effect, however, is not very strong as may be shown by consideration of the magnitude of the lateral stress gradient compared to the vertical stress gradient. The vertical stress gradient may be estimated by:

$$\nu_t \frac{\partial^2 u}{\partial z^2} \sim \nu_t \frac{U_0}{H^2} \tag{79}$$

while the lateral gradient is:

$$\nu_t \frac{\partial^2 u}{\partial y^2} \sim n_t \frac{U_0}{B^2} \qquad (80)$$

Thus the lateral stress gradient over the vertical stress gradient is proportional to $(d/b)^2$ and, since aspect ratios of natural channels are of the order 10 to far greater, the lateral friction cannot have much effect.

Near the banks, lateral friction becomes much more important, especially in slowing down the initial fast flow on the inside bank. Otherwise it has little but local effect, although it is useful to note that it does act in such a way as to shift the location of maximum velocity away from the inside of the bend.

1.2.4.5 Lateral Momentum Transport by Secondary Flow

The secondary circulation effect on the longitudinal flow is the least understood, but in some cases the most important mechanism of flow redistribution. Essentially the secondary flow convects the faster moving upper layer flow toward the outside while moving the slower bed layer flows toward the inside. Of itself, it accomplishes nothing since the fluid is merely replacing other fluid of similar momentum. If there is a velocity gradient across the channel, then the lower transport will act to partially counteract the upper transport.

When the fluid nears the walls, however, the vertical transport becomes important and the effects are significant. At the outer wall, fast fluid (continuously replenished from the centre of the channel) is convected downward causing an increase in mean velocity, while the opposite occurs on the inside. The effect, first noticed near the walls, would be convected again by the secondary flow towards the centre. Kalkwijk and de Vriend (1980) took this effect partially into account while only the numerical analyses of varying complexity by Rosovskii (1961), Leschziner and Rodi (1979) and de Vriend (1981) take full account.

At present, the only results are qualitative and suggest that this effect is more important for channels of small aspect ratio (narrow channels) and also more important for smooth channels simply because frictional effects are smaller by comparison. Therefore, this effect would be much more important in a laboratory flume than in a natural stream.

1.2.4.6 Developing Flow

As may be observed from the above, there remains much that is not quantified regarding the problem of longitudinal velocity redistribution. This makes the situation of developing flow very difficult to handle in a practical manner. It has been observed that a large portion of every bend, even in the laboratory, is in a developing situation with regard to the longitudinal velocity distribution. The superelevation and secondary flow develop quickly and remain fairly stable but the longitudinal flow develops slowly.

Further, it is the rare natural bend that maintains a constant curvature. For these reasons, a model of developing flow is desired. Short of using a three-dimensional numerical model, a reasonable approximation is (Engelund, 1974):

$$\frac{\partial U'}{\partial x} = - y \frac{d}{dx} \left(\frac{1}{R}\right) - \frac{1}{C_f^2 H} (2U' - H') \tag{81}$$

where:

$$U' = \frac{U - U_0}{U_0} \tag{82}$$

$$H' = \frac{d - H}{H} \tag{83}$$

This model takes account of some inertial and bed friction effects for channels with a lateral bed slope. It is, therefore, a good approximation for wide natural streams. Momentum transfer by the secondary flow is not included.

1.2.5 Bed Shear Stress

Another important area of concern is the bed shear stress distribution. Ippen and Drinker (1962) and various others have studied this problem, experimentally at least.

As a first approximation, we may take:

$$\frac{\tau_{x0}}{\rho} = u_*^2 + \frac{U^2}{C_f^2} \tag{84}$$

and assume C_f to be a constant or a function of the relative roughness (k_s/d).

From Equation 84 and what we know from the previous section about the behaviour of U, we can qualitatively predict the bed shear stress distribution. The shear stress would be maximum near the inside wall at the beginning of the bend, then shift to the outside wall, and finally reach a peak near the outside wall just past the end of the bend. This is in fact what is observed (Ippen and Drinker, 1962).

The correlation is reasonable, but consistent discrepancies do occur. For example, the stress near the inside wall is usually somewhat lower than predicted while the stress near the outside wall is somewhat larger. Clearly, this is an effect of the secondary flow on the velocity distributions themselves. Only in the complex numerical models has this been accounted for.

The lateral bed stress arising from the secondary flow itself was evaluated previously as:

$$\tau_{y0} = \tau_{x0} \, K \frac{d}{r} \tag{85}$$

The total shear stress (magnitude) is therefore:

$$\tau_0 = \sqrt{\tau_{y0}^2 + \tau_{x0}^2} = \tau_{x0} \sqrt{1 + \left(K\frac{d}{r}\right)^2} \tag{86}$$

Even if we take K to be 11, as suggested previously, for any natural stream:

$$\tau_0 \simeq \tau_{x0} \tag{87}$$

1.2.6 Wall Shear Stress

Wall shear stresses are even less well understood, despite their importance in bank protection works. The only approach available seems to be:

$$\frac{\tau_w}{\rho} \propto U_w^2 \tag{88}$$

where U_w is the velocity extrapolated (by eye) to the wall (as if there were no boundary layer). For cases of natural or non-rectangular channels even this approach becomes doubtful.

1.2.7 Friction Coefficient

The average shear stress across the bed in relation to the overall friction coefficient is as follows:

$$\frac{\overline{\tau_0}}{\rho} = \frac{1}{C_{f0}^2} U_0^2 \tag{89}$$

If we average Equation 84 across the channel we obtain (assuming C_f is constant):

$$\frac{\overline{\tau_0}}{\rho} = \frac{1}{C_f^2} (\overline{U^2}) \tag{90}$$

Let (as in Equation 82):

$$U = U_0 + U_0 U' \tag{91}$$

Substitute Equation 91 into 90:

$$\frac{\overline{\tau_0}}{\rho} = \frac{U_0^2}{C_f^2} (1 + \overline{U'^2}) \tag{92}$$

Simplify to obtain:

$$\frac{C_{f0}^{\ 2}}{C_f^2} = \frac{1}{(1 + \overline{U'^2})} \tag{93}$$

indicating that the overall friction coefficient will decrease (apparently increasing roughness), depending upon the skewness of the velocity. Equation 93 may be approximated by:

$$C_{f0}^{\ 2} = C_f^2 \ (1 - \overline{U'^2}) \tag{94}$$

which may be used to evaluate the overall friction coefficient if the distribution of U is known. Many studies, both analytic and experimental have been performed to determine the excess friction loss of a curved reach. The results are not conclusive and in some cases are contradictory. A better understanding of the mechanics of the bed stress distributions is important for this purpose.

1.2.8 Bed Scour and Topography

Since we now have at least a reasonable idea of the flow field in a bend, the next step is to attempt to predict the stable bed topography or scour pattern. Since, of course, the bed topography affects the flow field which in turn affects the bed topography, we expect that a successive approximation technique will be required. The method outlined below, which follows Engelund (1974), will be to first estimate the bed profile in a developed section, and then estimate developing effects to apply a correction.

1.2.8.1 Developed Bed Profile

Under developed conditions, the net rate of sediment transport across the channel is zero. Thus the forces acting on a sediment particle must balance. Figure 8 shows the lateral forces acting on a sediment particle on the bed of a curved stream. The simplest force balance will be:

$$(W - F_L) \sin \alpha = F_{DR} \tag{95}$$

where W is particle weight, F_L is lift force, α is lateral bed angle and F_{DR} is lateral drag force. F_{DR} is assumed to be proportional to bed shear stress:

$$F_{DR} = F_{DL} \tan\delta \tag{96}$$

where F_{DL} is longitudinal drag force, F_{DL} may be estimated,

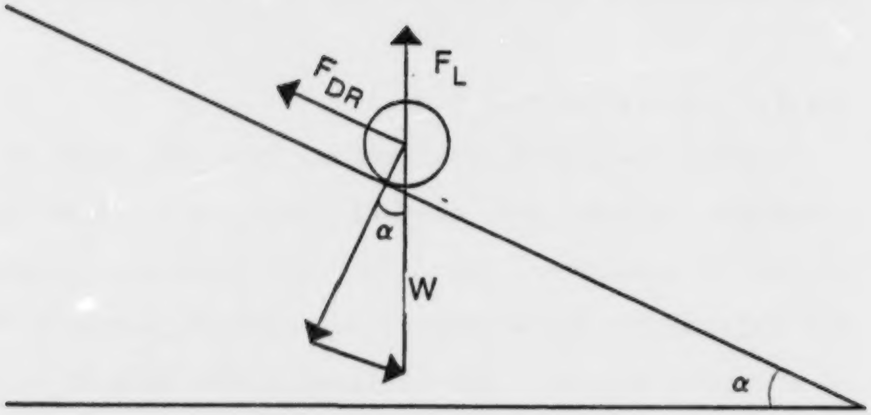
F_{DR}
F_L
α
W
α

Figure 8. Particle Equilibrium

if the particle is moving longitudinally at a constant speed, as:

$$F_{DL} = (W - F_L)\cos\alpha\tan\phi \qquad (97)$$

where ϕ is the dynamic friction angle (about 25°). Substitute Equation 97 into Equation 96 to obtain:

$$(W - F_L)\sin\alpha = (W - F_L)\cos\alpha\tan\phi\tan\delta \qquad (98)$$

or:

$$\tan\alpha = \tan\phi\tan\delta \qquad (99)$$

Since:

$$\tan\alpha = \frac{dd}{dr} \qquad (100)$$

Equation 99 becomes:

$$\frac{dd}{dr} = K\tan\phi\frac{d}{r} \qquad (101)$$

Solve the differential equation:

$$d = C\,r^{(K\tan\phi)} \qquad (102)$$

Substitute y for r and solve for C to obtain:

$$\frac{d}{H} = \left(1 + \frac{y}{R}\right)^{K \tan\Phi} \tag{103}$$

The maximum depth including scour is:

$$\frac{d_m}{H} = \left(1 + \frac{B}{2R}\right)^{K \tan\Phi} \tag{104}$$

For moderate curvature ratios ($B/R_0 < 0.5$) Equation 104 may be approximated as:

$$\frac{d_m}{H} = 1 + \frac{K}{2} \tan\Phi \frac{B}{R} \tag{105}$$

Taking K as 11 and Φ as 25°, the above becomes:

$$\frac{d_m}{H} = 1 + 2.5 \frac{B}{R} \tag{106}$$

This was derived assuming vertical sides and has been found to be an overestimate. An average of field observations (Suga, 1963, cited by Ikeda et al., 1981) gives a constant of approximately 1.5. Figure 9 shows a plot of Equations 104 and 106 with the modified constant against observed values for the North Saskatchewan River (data from Nwachukwu and Neill, 1972). The average depth and width were evaluated at a stage corresponding to a discharge of 100,000 cfs.

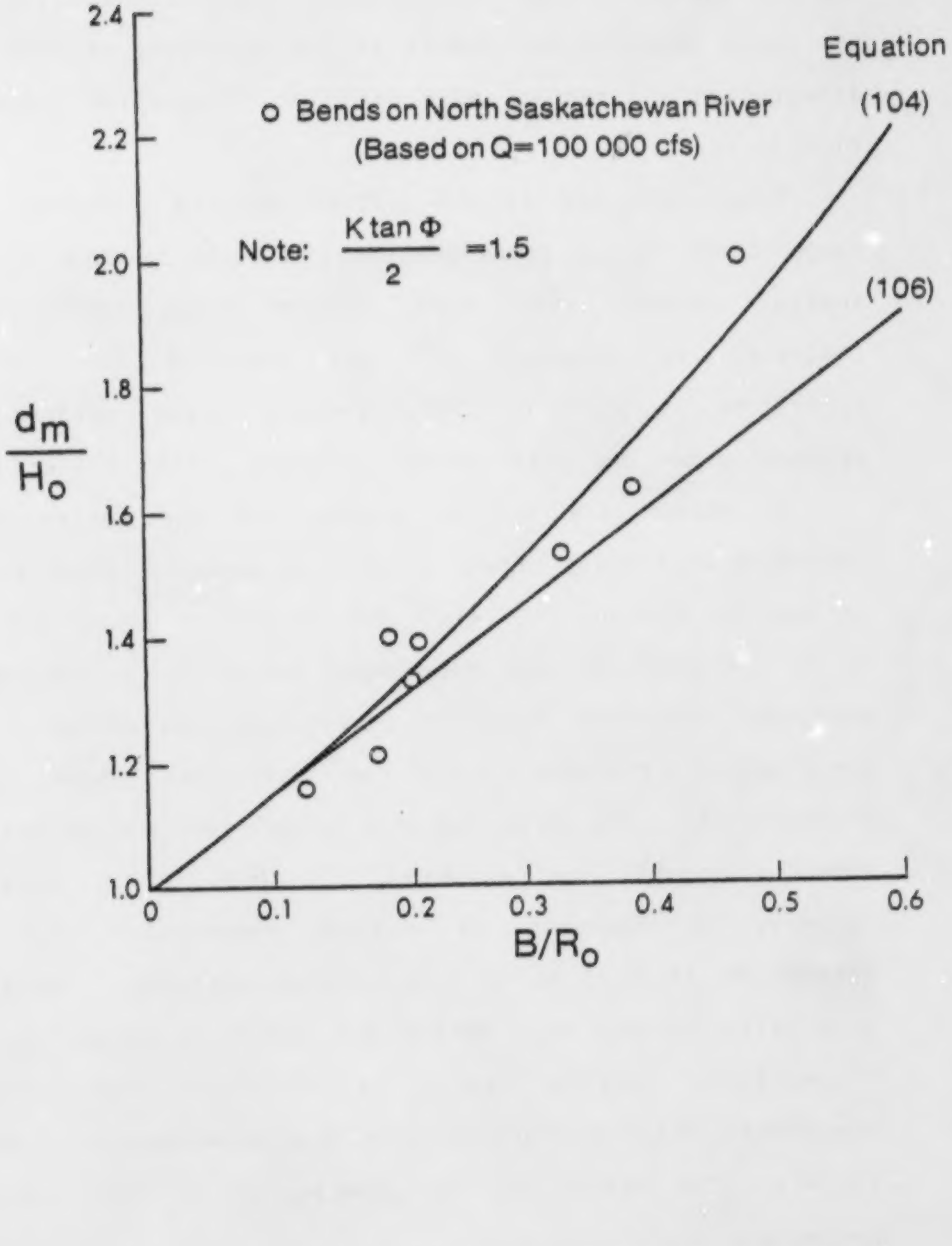

Figure 9. Maximum Scour Versus Curvature Ratio

Other attempts at predicting stable developed bend scour have been made by Kikkawa, et al, (1976), Koch (1980 and Yen (1970). These involve more complete evaluations of the force balances but result in the necessity of numerical integration and require more detailed information about the flow field.

Zimmermann and Kennedy (1978) derived a lateral bed slope based on a cross-sectional torque balance. This analysis showed that much steeper slopes than those indicated by Equation 101 are possible for certain conditions. Odgaard (1981) reviews these methods and proposes a new one based on an incipient motion criteria.

To obtain the bed topography for the entire bend, including developing effects, the only approach taken so far is due to Engelund (1974). The procedure is to set the first estimate of bed topography equal to a series of developed profiles depending on local curvature. The longitudinal velocity field is then calculated using equation 81. The mean lateral velocities are calculated from a continuity equation. Finally, a sediment conservation equation is solved numerically and the correction is applied to the initial estimate. Engelund originally derived this method for use on a channel with a sinusoidally varying radius of curvature and obtained reasonable results compared with the experiments of Hooke (1974). The method may be generalized to other meander patterns.

Generally, the results for sinusoidal channels indicate the following:

1. The deepest scour is usually somewhat downstream of the point of maximum curvature.
2. The tip of the point bar (deposition) is usually even further downstream.

Both the theoretical and experimental work supports these conclusions. A more detailed evaluation of this method is included in section 1.4.3.

1.3. REVIEW OF EXPERIMENTAL INVESTIGATIONS

Many researchers have undertaken studies on various aspects of curved open channel flow. Due to the complexity of the problem, and its many manifestations, the experimental purposes and designs are as diverse as the number of experimenters. Broadly, the experiments may be classified into three categories:

1. Fixed boundary channels;
2. Mobile boundary channels; and
3. Natural streams.

Yen (1965) gives a review of experimental work prior to his own. Included in this report is an update to that review containing the important experiments published up to 1980. Table 1 summarizes rigid boundary experiments. Table 2 is concerned with mobile bed results and Table 3 presents field observations of natural streams. An overall evaluation of the experiments is also included.

Table 1. Rigid boundary curved channel experiments.

Investigator	Channel Plan	Cross Section	#exps	R_0/B	B/H_0	R_0/H_0	F_R	$R_e(x10^{-4})$	Notes
Raja[a]	1 90° bend	rectangular	nd	1. to 3.	1.6 to 4.3	nd	<1	1.5 to 4.5	loss coefficient
Boss[a]	1 90° bend	rectangular	2	2.16	3.33, 2.72	6.1 5.9	0.64,	3.6, 3.4 0.48	superelevation
Yarnell and Woodward[a]	1 180°bend	rectangular	nd	1.0 to 2.5	0.67 to 1.33	1.07 to 1.67	0.6 to 0.7	4.2 to 6.8	u vel, superelevation
Mockmore[a]	2 180° bend	rectangular	2	1.17	3.2,4.0	3.75, 4.6	0.15, 0.14	1.7, 1.3	u vel, superelevation
Shukry[a]	1 bend of variable angle	rectangular	nd	0.5 to 3.0	0.83 to 1.67	0.42 to 5.0	0.1 to 0.9	0.10 to 0.79	u,v vel, superelevation
Prus-Chacinski[a]	5 45° bends	rectangular	1	6.5	4.4	6.5	nd	0.55	spiral motion
Einstein & Harder[a]	1 120° bend	rectangular	nd	7.5	4.9 to 12.2	37. to 91.	0.2 to 0.4	0.5 to 1.3	u vel distribution
Leopold, Bagnold, Wolman and Brush[a]	sinusoidal	trapezoidal 1:1 side slopes	nd	nd	2.9 to 4.3	nd	0.2 to 0.9	1.4 to 2.4	resistance
Ippen, Drinker, Jobin, and Shemdin[a]	1 60° bend	trapezoidal 2:1 side slopes	nd	2.5,5.8	3.0 to 8.0	9.9 to 34.7	0.32 to 0.55	1.1 to 7.5	u vel, superelevation, boundary shear
Milovich[a]	1 180° bend	rectangular	nd	1.16	1.7 to 5.3	2.0 to 6.2	<1.0	0.016 to 0.12	bottom velocity, surface velocity

Investigator	Channel Plan	Cross Section	#exps	R_0/B	B/H_0	R_0/H_0	F_R	$R_e(x10^{-4})$	Notes
Danelia[a]	1 180° bend	rectangular	1	1.5	3.33	5.0	0.28	2.1	u, v vel, distributions
Kozhevnikov[a]	1 to 3 180° bends	rectangular, trapezoidal, triangular	nd	2.0	6.7 to 40.0	13.3 to 90.0	0.2 to 0.7	0.23 to 1.5	bottom velocity, surface velocity, superelevation
Ter-Asvatsatryan[a]	1 bend 67.5° 180°	rectangular	nd	1.5 to 5.5	2.5 to 3.5	3.85 to 19.0	0.3 to 0.4	1.8 to 3.2	u, v vel, distributions
Konovalov, Makkaveev Romonenko[a]	sinusoidal	trapezoidal	nd	nd	3.8 to 8.3	nd	0.2 to 0.3	0.7 to 1.4	bottom and surface velocities
Makkaveev and Romanenko[a]	sinusoidal	rectangular	nd	>2.0	2.0 to 10.0	>4.17	<1.0	0.4 to 4.0	bottom and surface velocities
Fidman[a]	3 117.5° bends	rectangular	nd	2.25	6.25 to 8.33	14.0 to 19.5	0.07 to 0.3	0.9 to 3.8	superelevation
Ananyan[a]	2 180° bends	rectangular	nd	5.0	4.8 to 5.3	2.8 to 3.3	0.21 to 0.28	2.4 to 3.1	u, v vel, distribution
Rozovskii[a]	1 bend 29° to 180°	rectangular triangular	nd	1.0 to 2.5	4.3 to 27	5.3 to 45.0	0.2 to 0.5	0.028 to 2.7	u, v vel, superelevation
Siebert and Gotz	3 180° bends	rectangular	2	4.6, 20.	18.2, 80.	0.23	2.5,20.		long. dist. of u and v vel.
Yen and Yen (1971)	2 90° bends	trapezoidal	1	4.7	nd	nd	nd	nd	water surface configuration

Investigator	Channel Plan	Cross Section	#exps	R_0/B	B/H_0	R_0/H_0	F_R	$R_e(\times10^{-4})$	Notes
Fox and Ball (1968)	1 180° bend	rectangular	1	3.5	2.0	7.0	0.25	5	u, v distributions
Kikkawa, Ikeda, Kitagawa (1976)	1 330° bend	rectangular	3	4.5	15.9 to 20	71.4 to 90	0.56 to 0.63	2 to 3	u,v at 180° meas. bed stress at 6 sections
Yen (1965)	2 90° bends	trapezoidal 1:1 side slopes	5	4.67	8.0 to 17.0	41.5 to 83.8	0.36 to 0.82	6.3 to 13.8	u, v velocities, superelevation, bed stress
Varshney and Garde (1975)	1 60° bend	rectangular	84	1.5 to 6.0	2.06 to 11.95	3.09 to 83.70	0.11 to 0.78	2.27 to 10.9	various roughness, bed stress only
Choudhary and Narasimhan (1977)	1 180° bend	rectangular	6	0.833	5, 10	4.2 to 8.3	0.2 to 0.6	4.10	u,v,h and bed stress
Soliman and Tinney (1968)	1 180° bend	rectangular	6	0.625	1.2 to 1.5	0.75 to 0.94	0.35 to 0.58	nd	h, used guide vanes
Zimmerman (1977)	1 330° bend	rectangular	6	5.5	2.10 to 36.7	3.8 to 6.7	0.22 to 0.35	6.7 to 16.0	measured only at 0.2 cm above bed for various roughness
Zimmerman (1977)	1 330° bend	rectangular	6	4.25	27.5 to 55.0	5.0 to 10.0	0.21 to 0.39	3.6 to 9.2	same as above but 1 roughness only
Kalkwijk and de Vriend (1980)	1 90° bend	"natural"	2	8.2	250.0	30.0	0.14 to 0.28	nd	depth averaged velocities & water surface elevations

Investigator	Channel Plan	Cross Section	#exps	R_0/B	B/H_0	R_0/H_0	F_R	$R_e(x10^{-4})$	Notes
Francis and Asfari	1 180° bend	rectangular	2	3 to 7.9	4 to 8	24	0.11 to 0.17	.55 to .66	long. vel. distributions

---

[a] Adapted from original table in Yen (1965).

Table 2. Mobile boundary curved channel experiments

Investigator	Channel Plan	#exps	R_0/B	R_0/H_0	B/H_0	F_R	$R_e(\times 10^{-4})$	D_{50}(mm)	Notes
Zimmerman (1977)	1 300° bend	12	3.0 to	21.1 to	5.6 to	0.23 to	4.1 to	0.21	angle of ripples to obtain bed stress angle
Hooke (1974)	sinusoidal	5	2.46 (using min radius)	20.2 to 48.4	8.2 to 19.6	0.27 to 0.40	nd	0.30	bed topopgraphy, shear stress, sediment discharge
Yen (1970)	2 90° bends	5	4.7	nd	18.0 to 30.0	0.30 to 0.70	7.0 to 14.0	0.25	topography, velocities, shear stress
Zimmerman and Kennedy (1978)	1 330° bend	49	3.0 to	16.7 to	5.4 to	nd	nd	0.21, 0.55	transverse bed slopes and sediment discharge
Onishi, Jain and Kennedy (1976)	2 90° bends	26	3.6 to 7.3	62.5 to 110.3	8.63 to 30.2	0.28 to 0.56	10.3 to 266	0.25	friction factor and sediment discharge
Kikkawa, Ikeda Kitagawa (1976)	1 330° bend	2	4.5	71.4 to 81.8	15.9 to 18.2	0.61 to 0.63	nd	0.90	bed profiles (time variation)

Table 3. Natural stream bend measurements.

Investigator	River	$Q(m^3/s)$	Notes
Bridge and Jarvis (1977)	South Esk (Scotland)	3.0 to 22.0	Measured velocity profiles and bed stresses in a gently curving stream.
Bathurst, Thorne and Hey (1979)	Severn (Wales)	1.0 to 15.5	Measured velocity (longitudinal and transverse) and shear stress at four locations.
de Vriend and Geldof (1983)	Dommel (Netherlands)	1.27	Measured longitudinal velocity profiles over two complete bends to compare transverse redistribution of longitudinal velocity with model.
Odgaard (1981)	Scaramento	220-810	Average velocity and bed topography

1.3.1 Fixed Boundary Channels

Most fixed boundary channels were constructed for one of two reasons. First, as general experiments to understand curved channel flows, and second to evaluate the bed stress distribution for a particular situation. Thus some experiments include detailed information on many aspects of the flow while others are very limited. Therefore the diversity in the important geometrical and flow parameters is not as large as it appears. Additionally, some of the experiments have unrealistic values of some parameters. A low aspect ratio ($B/H < 5$) is the most obvious example, although a low ratio R_0/H is unrealistic as well.

Secondary velocities have not often been measured due to their relatively small size. When measured, the lateral velocities have universally been determined by measuring the total horizontal velocity and the angle of deviation from the longitudinal direction. Usually the angle is measured by lining up a protractor-like device with a short thread in the flow. The error in these measurements is relatively large. Vertical velocity measurements are practically nonexistent.

The only turbulence measurements reported are those of Yen (1965), but these were taken in a closed air duct model. Some measurements, especially of the turbulent Reynold's stresses, would be very useful.

An interesting result of these experiments is that only in the configuration of Kikkawa et al. (1976) was a convincing demonstration of a fully developed situation achieved. The total angle turned by their flume was over 300 degrees.

1.3.2 Mobile Boundary Channels

Most mobile boundary curved channel experiments were set up to investigate the bed topography. Typically the bed is initially flat and then the experiment run until an equilibrium bed topopgraphy is reached. The bed elevations, and in some cases various flow variables, are then measured.

Many of the same criticisms applied to the rigid boundary channels may also be applied to the mobile channel. Additionally it should be noted that all these experiments utilizied rigid vertical walls. Also, to measure mean bed topography, it was often necessary to smooth local bedforms, which may introduce further distortions.

1.3.3 Natural Stream Observations

Detailed studies of natural stream bends are notable by their relative scarcity. The complexity and uncontrolled nature of the situation limit the utility of the results. Measurements of this kind are very important in validation of theoretical or experimental conclusions. It is, however, difficult to obtain general results from them.

1.4. MATHEMATICAL MODELS

To calculate maximum scour, superelevation, and secondary flow, the developed flow assumption appears to be adequate, provided that a representative curvature can be obtained. For more detailed studies requiring bed topography and flow distribution over a reach of a natural or artificial channel, this simple approach is inadequate. A more complex physical or mathematical model is required. As curvature presents no special difficulties to a properly scaled and constructed physical model, we will focus our attention on mathematical models.

At present, no complete mathematical model is available, but some attempts have been made at solving various aspects of the problem. This section will briefly consider these approaches in order of decreasing complexity.

1.4.1 Three-Dimensional Models

A fully three-dimensional model based on the full Reynold's equations and appropriate boundary conditions would be the most complete possible. Difficulties arise, however, in the modelling of the turbulent stresses. Rodi (1980) gives a review of the possibilities, ranging from simple constant eddy viscosity assumptions to full two parameter turbulence transport models. Based on some consideration of the developed flow analysis we conclude that the actual turbulence model chosen is not that significant. For example, the secondary circulation profile obtained by assuming a mixing length model (Rosovskii, 1961) does not differ greatly from that obtained using an average eddy viscosity model (Engelund, 1974). Rodi (1980) points out this observation as well when considering a developing strongly curved flow.

The three-dimensional model of Leschizner and Rodi (1979) uses the $\kappa - \varepsilon$ turbulence transport model. This model, although the most complete yet attempted, contains some simplifications. First, the variable water surface location is ignored in the calculation. That is, an imaginary frictionless lid is placed over the flow. The water elevations are calculated later from the pressure distributions. The effect of this simplification is to limit the model to situations where the Froude number is small.

A second simplification was made with regard to longitudinal derivatives of the turbulent stresses. These were neglected, leaving only the pressure as an effective downstream-to-upstream mechanism. This allows a storage efficient calculation procedure, where the pressure field is first assumed, and then the calculation is performed starting at the beginning and proceeding downstream. The scheme requires the storage of only cross-sectional velocity and turbulence values, reducing computer memory requirements considerably.

This model achieved good agreement with an experiment of Rosovskii (1961) where the relative curvature was large

$(B/R_0 = 1)$ and the Froude number was small $(F = 0.1)$. The channel shape was rectangular with rigid sides and bed. As yet, no three-dimensional model includes sediment transport features.

1.4.2 Two-Dimensional Models

A two-dimensional curved open channel flow model could be formed by assuming a hydrostatic pressure distribution, and depth averaging the equations of motion. Assumed vertical profiles could be used to calculate integral transfer coefficients. Such a model has been proposed by Kalkwijk and de Vriend (1980). The flow is assumed to be wide and shallow. The depth is allowed to vary gradually across the channel, and the channel need not be prismatic. The effect of secondary flow convection on the main flow distribution is included in an approximate way.

The inertia of the lateral mean flow and circulation are neglected, which restricts the model to gentle transitions of curvature and bed topography. This model was used to give a good prediction of the longitudinal flow field and superelevation in a rigid boundary flume of natural bed topography. Prediction of some natural channels bends was generally successful with some discrepancies (de Vriend and Geldof, 1983).

Koch and Flockstra (1981) have introduced a model which also predicts bed topography.

1.4.3 One-Dimensional Models

If lateral distributions may be approximated by linear functions, the problem may be simplified to a one-dimensional form. An example is the model proposed by Engelund (1974) which was partially discussed previously in Section 1.2.4.6. The restrictions on this model are at least as severe as those on either of the more complex models. Additionally, the restriction of gentle curvature ($B/R_0 <1$) is required.

In the original paper, Engelund (1974) provided a solution for the case of sinusoidal variation of channel curvature. This may be easily generalized to an arbitrary alignment by solving Equation 69 numerically. As an example of such implementation, the program CRVCNL is presented in the appendix (Section 1.7). As of this writing, the Engelund model is the only one that will calculate bed topography as well. The main limitation of this calculation is that it applies to vertical rigid walls requiring some judgement to evaluate the scour depths if applied to natural streams. The bed topography calculation has been included in CRVCNL as well.

1.4.4 Summary

Mathematical modelling of curved open channels has only recently been attempted with some positive results. None of the models presented are truly of a general purpose nature, and indeed most are quite restrictive.

1.5. CONCLUSIONS

This section has covered three aspects of the present knowledge concerning the subject of flow in curved open channels. The following is a brief evaluation of the state of the art in each of these aspects.

1.5.1 Mechanics of Flow in Curved Channels

Over the past twenty years or so, much effort has been expended attempting to understand the mechanics of flow in curved open channels. The phenomena of superelevation and secondary flow are well understood for the idealized situation of developed flow in a wide channel. Developing flow and the associated redistribution of longitudinal velocity are not well understood, and no simple predictive tools are available. Bed and wall stresses are likewise poorly understood. Equalibrium bed scour is more successfully predicted, due mainly to its dependence more upon the secondary flow than on the longitudinal flow and shear stress. Even here, the success is due to the calibration of the friction coefficient Φ, since the constant K and its variation with C_f are still the subject of considerable debate.

1.5.2 Experimental Studies

Many experiments have been performed, but most are faulted by a lack of scope. The nature of the problem is such that there is an enormous range of geometrical and flow variations. With a few notable exceptions, the present body of experimental data provides many geometrical variations, but with only a few aspects of the flow actually measured.

As far as the measurements themselves are concerned, there is a need for accurate lateral velocity, turbulence, and vertical velocity measurements, all of which are practically nonexistent.

1.5.3 Mathematical Models

Mathematical modelling of curved channel flows is only a relatively recent development. At present there have been some promising approaches taken. Much more effort is required, however, to extend these models to practical situations where arbitrary geometries, flow conditions and sediment transport are important.

2. PART TWO - THEORETICAL ANALYSIS

2.1 INTRODUCTION

Developing flow in a curved open channel is clearly a complex three-dimensional problem. The review of the present state of knowledge indicated that this problem is however, important and not well understood. It is the purpose of the present theoretical investigation to develop analyses which will shed some light on this difficult but fascinating problem.

The procedure to be followed will be to first develop a general-purpose co-ordinate system appropriate for a meandering stream. The equations of motions are then written in this system and non-dimensionalized using typical scales for the channel geometry and flow. Assuming relatively mild curvature, a perturbation analysis is performed which results in most of the essential features of the developing flow being represented in the first order approximation. An analysis is performed by forming vorticity-like equations to predict secondary flow, longitudinal velocity redistribution for developed flow in a bend. A simplified analysis of developing flow is also done. Preliminary comparison with experiment is also made.

2.2 GOVERNING EQUATIONS

2.2.1 Co-ordinate System

The nomenclature and co-ordinate system to be used in the following is the same as was utilized in the review section. The co-ordinate system will, however, be generalized and formalized in a form appropriate for an arbitrarily specified meandering channel. The co-ordinate directions are specified as follows.

1. The x co-ordinate and associated velocity u are in a direction tangential to the channel centreline. The x axis is, in fact, the channel centreline. The origin may be established arbitrarily. The positive x-direction is downstream.
2. The y co-ordinate and velocity v are perpendicular to the x axis in plan. The y coordinate is defined to be positive to the left of an observer standing on the channel centreline facing downstream.
3. The z co-ordinate and w velocity originate at the bed of the channel and are positive upwards. Strictly, the z direction is perpendicular to the bed but may be taken as vertical in most cases.

For this co-ordinate system the metrical coefficients (Nash and Patel, 1972) are:

$$h_1 = \frac{R(x) + y}{R(x)} \qquad (108)$$

$$h_2 = 1 \qquad (109)$$

$$h_3 = 1 \qquad (110)$$

R(x) is positive if the center of curvature at that value of x is to the right of an observer facing downstream.

This system may be shown to be triply orthogonal by the application of the Lame conditions (Nash and Patel, 1972). As it stands, however, the above system does not establish a unique relation between these co-ordinates and for example, Cartesian co-ordinates. In other words, a given point in space may be described by more than one set of co-ordinates in this system. In such cases, the extra condition required for uniqueness will be to choose that set for which the absolute value of the y co-ordinate is the smallest.

For use in practical situations this system requires the measurement of longitudinal distances along the channel centerline which is the normal procedure. The variation of radius of curvature must be evaluated by analytical, numerical or graphical means. An example of a numerical procedure is given as part of the demonstration program in the review section.

2.2.2 Equations of Motion

In terms of the above coordinate system, the Reynold's Equations of motion for the steady flow case with negligable viscous effects may be written as:

$$\frac{R\bar{u}}{R+y}\frac{\partial\bar{u}}{\partial x} + \bar{v}\frac{\partial\bar{u}}{\partial y} + \bar{w}\frac{\partial\bar{u}}{\partial z} + \frac{\overline{uv}}{R+y} = \frac{1}{\rho}\frac{R}{R+y}\frac{\partial p}{\partial x}$$

$$- \left(\frac{R}{R+y}\frac{\partial\overline{u'^{2}}}{\partial x} + \frac{\partial\overline{u'v'}}{\partial y} + \frac{\partial\overline{u'w'}}{\partial z} + \frac{\overline{u'v'}}{R+y}\right) \qquad (111)$$

$$\frac{R\bar{u}}{R+y}\frac{\partial\bar{v}}{\partial x} + \bar{v}\frac{\partial\bar{v}}{\partial y} + \bar{w}\frac{\partial\bar{v}}{\partial z} - \frac{\bar{u}^{2}}{R+y} = -\frac{1}{\rho}\frac{\partial p}{\partial y}$$

$$- \left(\frac{R}{R+y}\frac{\partial\overline{u'v'}}{\partial x} + \frac{\partial\overline{v'^{2}}}{\partial y} + \frac{\partial\overline{v'w'}}{\partial z} + \frac{\overline{v'^{2}}}{R+y} - \frac{\overline{u'^{2}}}{R+y}\right) \qquad (112)$$

$$\frac{R\bar{u}}{R+y}\frac{\partial\bar{w}}{\partial z} + \bar{v}\frac{\partial\bar{w}}{\partial y} + \bar{w}\frac{\partial\bar{w}}{\partial z} = -\frac{1}{\rho}\frac{\partial p}{\partial z}$$

$$- \left(\frac{R}{R+y}\frac{\partial u'w'}{\partial x} + \frac{\partial v'w'}{\partial y} + \frac{\partial\overline{w'^{2}}}{\partial z} + \frac{\overline{v'w'}}{R+y}\right) \qquad (113)$$

where p is the pieziometric pressure. The overbars indicate time averaged quantities and the primes indicate fluctuating velocity components.

The corresponding continuity equation is:

$$\frac{R}{R+y}\frac{\partial \overline{u}}{\partial x} + \frac{\partial \overline{v}}{\partial y} + \frac{\partial \overline{w}}{\partial z} + \frac{\overline{v}}{R+y} = 0 \tag{114}$$

Before proceeding further it is desirable to non-dimensionalize Equations 111 - 114. Let:

$$x_* = x/b \tag{115}$$

$$y_* = y/b \tag{116}$$

$$z_* = z/d_0 \tag{117}$$

$$u_* = u/U_0 \tag{118}$$

$$v_* = v/U_0 \tag{119}$$

$$w_* = w/U_0 \tag{120}$$

$$p_* = p/\gamma d_0 \tag{121}$$

$$R_* = R/R_0 \tag{122}$$

where b, d_0, U_0 and R_0 are representative values (average or maximum (minimum in the case of R_0)). The following non-dimensional groupings may be formed from these scales:

$$\alpha = b/R_0 \tag{123}$$

$$\beta = b/d_0 \tag{124}$$

$$F_R{}^2 = V_0{}^2/gd_0 \tag{125}$$

Equations 115-125 may be substituted into Equations 111-114 to give:

$$\left(\frac{1}{1+\alpha\frac{y_*}{R_*}}\right)\bar{u}_*\frac{\partial\bar{u}_*}{\partial x_*} + \bar{v}_*\frac{\partial\bar{u}_*}{\partial y_*} + \beta\bar{w}_*\frac{\partial\bar{u}_*}{\partial z_*} + \frac{\alpha\bar{u}_*\bar{v}_*}{R_*(1+\alpha\frac{y_*}{R_*})}$$

$$= \left(\frac{-1}{1+\alpha\frac{y_*}{R_*}}\right)\frac{1}{F_R^{2}}\frac{\partial p_*}{\partial x_*} - \left[\left(\frac{1}{1+\alpha\frac{y_*}{R_*}}\right)\frac{\partial\overline{u_*'^{2}}}{\partial x_*} + \frac{\partial\overline{u'_*\,v'_*}}{\partial y_*} + \beta\frac{\partial\overline{u'_*w'_*}}{\partial z_*}\right.$$

$$\left. + \frac{2\alpha}{R_*}\frac{\overline{u'_*v'_*}}{(1+\alpha\frac{y_*}{R_*})}\right] \qquad (126)$$

$$\left(\frac{1}{1+\alpha\frac{y_*}{R_*}}\right)\bar{u}_*\frac{\partial\bar{v}_*}{\partial x_*} + \bar{v}_*\frac{\partial\bar{v}_*}{\partial y_*} + \beta\bar{w}_*\frac{\partial\bar{u}_*}{\partial z_*} - \frac{\alpha\bar{u}_*^{2}}{R_8(1+\frac{y_*}{R_*})} = -\frac{1}{F_R^{2}}\frac{\partial p_*}{\partial y_*}$$

$$- \left[\left(\frac{1}{1+\alpha\frac{y_*}{R_*}}\right)\frac{\partial\overline{u'_*v'_*}}{\partial x_*} + \frac{\partial\overline{v'^{2}_*}}{\partial y_*} + \beta\frac{\partial v'_*w'_*}{\partial z_*} + \frac{\alpha\overline{v'^{2}_*}}{R_*(1+\alpha\frac{y_*}{R_*})}\right. .$$

$$- \frac{\alpha\overline{u'^{2}_*}}{R_*(1+\alpha\frac{y_*}{R_*})} \qquad (127)$$

$$\left(\frac{1}{1+\alpha\frac{y_*}{R_*}}\right)\bar{u}_*\frac{\partial\bar{w}_*}{\partial x_*} + \bar{v}_*\frac{\partial\bar{w}_*}{\partial y_*} + \beta\bar{w}_*\frac{\partial\bar{w}_*}{\partial z_*} = -\frac{1}{F_R^{2}}\frac{\partial p_*}{\partial z_*}$$

$$- \left[\left(\frac{1}{1+\alpha\frac{y_*}{R_*}}\right)\frac{\partial\overline{u'_*w'_*}}{\partial x_*} + \frac{\partial\overline{v'_*w'_*}}{\partial y_*} + \beta\frac{\partial\overline{w'^{2}_*}}{\partial z_*} + \frac{\alpha\overline{v'_*w'_*}}{R_*(1+\alpha\frac{y_*}{R_*})}\right] \qquad (128)$$

$$\left(\frac{1}{1+\alpha\frac{y_*}{R_*}}\right)\frac{\partial\bar{u}_*}{\partial x_*}+\frac{\partial\bar{v}_*}{\partial y_*}+\beta\frac{\partial\bar{w}_*}{\partial z_*}+\frac{\alpha\bar{v}_*}{R_*(1+\alpha\frac{y_*}{R_*})}=0 \qquad (129)$$

For convenience, from this point on, all starred quantities will be represented by their unstarred equivalents.

The flow equations have now been scaled such that all variable terms are of order of magnitude one or less. A preliminary estimation of the size of each term is indicated by the size of it's coefficient. The three parameters involved are α, β, and $F_R{}^2$. $F_R{}^2$ is a typical Froude number and may vary from near zero to above one. The parameter β is usually referred to as the channel aspect ratio. For natural channels it is usually vary large (~50), while for laboratory channels it may be an order of magnitude less (~10). Some experiments have been performed with values of β about 1. Finally, α is a measure of the relative curvature of the channel. From a maximum possible value of one to a minimum of zero it may be the best indication of curvature effects. Typical channel bends would have α less than 0.5. Average bends (Yen, 1965) are typically about 0.1.

2.2.3 Perturbation Expansion

The system of Equations 125-129 is not solvable by present methods. In order to derive useful results, it is necessary to utilize approximate analysis methods. A productive technique is that of perturbation analysis (Lin and Segal, 1972). This method has been applied to the curved channel flow problem in the past to predict secondary flow (Rosovskii, 1961; Yen, 1965: de Vriend, 1976 for example). The parameter most often chosen for the expansion is α/β which certainly is very small. Since the horizontal dimensions were scaled with R_0, this resulted in drastic simplification of the equations and postponement of any consideration of developing flow to the second order approximation at least.

In the present study, a different approach is followed. The horizontal dimensions are scaled with the channel half-width which increases the relative importance of the differential terms involved. The perturbation expansion parameter is chosen to be α which is larger than β but allows more information to be gained from a first order approximation. Still α is small enough to allow reasonably accurate calculations for all but the sharpest of bends.

The procedure is to expand all of the unknown variables in a power series of α, which is taken to be the entire dependance of the variable on α. For example:

$$\bar{u}\ (x,y,z,\alpha,\beta,F_R^2\ ) = \bar{u}_0\ (x,y,z,\beta,F_R^2) + \alpha\bar{u}_1(x,y,z,\beta,F_R^2)$$

$$+\ \alpha^2\ \bar{u}_2\ (x,y,z,\beta,F_R^2) + \ldots \tag{130}$$

Such series may be formed for $\bar{u}$, $\bar{v}$, $\bar{w}$, p, $\overline{u'^2}$, $\overline{v'^2}$,

$\overline{w'^2}$, $\overline{u'w'}$, and $\overline{v'w'}$ and substituted into Equations 126-129. In addition, the following approximation is used.

$$\left(\frac{1}{1+\alpha\frac{y}{R}}\right) = 1 - \alpha\,\frac{y}{R} + \left(\alpha\,\frac{y}{R}\right)^2 - \ldots \qquad (131)$$

After substitution, straightforward but considerable algebra yields sets of equations for each power of α. The first set, the zero order set, is:

$$\bar{u}_0\,\frac{\partial\bar{u}_0}{\partial x} + v_0\,\frac{\partial\bar{u}_0}{\partial y} + \beta\bar{w}_0\,\frac{\partial\bar{u}_0}{\partial z} = -\frac{1}{F_R^2}\,\frac{\partial p_0}{\partial x} - \frac{\partial(\overline{u'^2})}{\partial x}$$

$$-\frac{\partial(\overline{u'v'})_0}{\partial y} - \beta\,\frac{\partial(\overline{u'w'})_0}{\partial z} \qquad (132)$$

$$\bar{u}_0\,\frac{\partial\bar{v}_0}{\partial x} + \bar{v}_0\,\frac{\partial\bar{v}_0}{\partial y} + \beta\bar{w}_0\,\frac{\partial\bar{v}_0}{\partial z} = -\frac{1}{F_R^2}\,\frac{\partial p_0}{\partial y} - \frac{\partial(\overline{u'v'})_0}{\partial x}$$

$$-\frac{\partial(\overline{v'^2})_0}{\partial y} - \beta\,\frac{\partial(\overline{v'w'})_0}{\partial z} \qquad (133)$$

$$\bar{u}_0 \frac{\partial \bar{w}_0}{\partial x} + \bar{v}_0 \frac{\partial \bar{w}_0}{\partial y} + \beta \bar{w}_0 \frac{\partial \bar{w}_0}{\partial z} = - \frac{1}{F_R^2} \frac{\partial p_0}{\partial z} - \frac{\partial (\overline{u'w'})_0}{\partial x}$$

$$- \frac{\partial (\overline{v'w'})_0}{\partial y} - \beta \frac{\partial (\overline{w'^2})}{\partial z} \tag{134}$$

$$\frac{\partial \bar{u}_0}{\partial x} + \frac{\partial \bar{v}_0}{\partial y} + \beta \frac{\partial \bar{w}_0}{\partial z} = 0 \tag{135}$$

The first order (α^1) set is:

$$\bar{u}_0 \frac{\partial \bar{u}_1}{\partial x} + \bar{u}_1 \frac{\partial \bar{u}_0}{\partial x} - \frac{y}{R} \bar{u}_0 \frac{\partial \bar{u}_0}{\partial x} + \bar{v}_0 \frac{\partial \bar{u}_0}{\partial y} + \beta \bar{w}_0 \frac{\partial \bar{u}_1}{\partial z}$$

$$+ \beta \bar{w}_0 \frac{\partial \bar{u}_1}{\partial z} + \beta \bar{w}_0 \frac{\partial \bar{u}_1}{\partial z} + \frac{\bar{u}_0 \bar{v}_0}{R} = \frac{1}{F_R^2} \left(\frac{y}{R} \frac{\partial p_0}{\partial x} - \frac{\partial p_1}{\partial x}\right)$$

$$- \frac{\partial (\overline{u'^2})_1}{\partial x} + \frac{y}{R} \frac{\partial (\overline{u'^2})_0}{\partial y} - \frac{\partial (\overline{u'v'})_1}{\partial y} - \beta \frac{\partial (\overline{u'w'})_1}{\partial z} - \frac{2(\overline{u'v'})_0}{R} \tag{136}$$

$$\bar{u}_0 \frac{\partial \bar{v}_1}{\partial x} + \bar{u}_1 \frac{\partial \bar{v}_0}{\partial x} - \frac{y}{R} \bar{u}_0 \frac{\partial \bar{v}_0}{\partial x} + \bar{v}_0 \frac{\partial \bar{v}_1}{\partial y} + \bar{v}_1 \frac{\partial \bar{v}_0}{\partial y}$$

$$+ \beta \bar{w}_0 \frac{\partial \bar{v}_1}{\partial z} + \beta \bar{w}_1 \frac{\partial \bar{v}_0}{\partial z} - \frac{\bar{u}_0{}^2}{R} = \frac{-1}{F_R^2} \frac{\partial p_1}{\partial y} - \frac{\partial (\overline{u'w'})_1}{\partial x}$$

$$+ \frac{y}{R} \frac{\partial (\overline{u'v'})_0}{\partial x} - \frac{\partial (\overline{v'^2})_1}{\partial y} - \beta \frac{\partial (\overline{v'w'})_1}{\partial x} - \frac{(v'^2)_0 - (u'^2)_0}{R} \qquad (137)$$

$$\bar{u}_0 \frac{\partial \bar{w}_1}{\partial x} + \bar{u}_1 \frac{\partial \bar{w}_0}{\partial x} - \frac{y}{R} \bar{u}_0 \frac{\partial \bar{w}_0}{\partial x} + \bar{v}_0 \frac{\partial \bar{w}_1}{\partial y} + \bar{v}_1 \frac{\partial \bar{w}_0}{\partial y} + \beta \bar{w}_0 \frac{\partial \bar{w}_1}{\partial z}$$

$$+ \beta \bar{w}_1 \frac{\partial \bar{w}_0}{\partial z} = - \frac{1}{F_R^2} \frac{\partial p_1}{\partial z} - \frac{\partial (\overline{u'w'})_0}{\partial x} + \frac{y}{R} \frac{\partial (\overline{u'w'})_1}{\partial y}$$

$$- \beta \frac{\partial (\overline{w'^2})_1}{\partial z} - \frac{(v'w')_0}{R} \qquad (138)$$

$$\frac{\partial u_1}{\partial x} + \frac{\partial v_1}{\partial y} + \beta \frac{\partial w_1}{\partial z} + \frac{V_0}{R} + \frac{y}{R} \frac{\partial u_0}{\partial x} = 0 \qquad (139)$$

The zero order set may be recognized as the Reynold's

Equations in Cartesian co-ordinates. This indicates that to zero order in α, curvature has no effect on channel flow. The zero order quantities may be calculated as for straight channel flow. This may be very difficult but for the present assume that it can be done.

The first order set of equations look longer and more difficult but in fact are more tractable than the zero order set because this set is linear in the unknown first order variables. The zero order functions appear here as known functions.

A particular simple situation of practical interest is that of uniform flow in a prismatic channel. If secondary flows due to turbulence are neglected, the solution to the zero order set is:

$$u_0 = u_0\,(y,\ z) \tag{140}$$

$$w_0 = v_0 = 0 \tag{141}$$

$$\frac{dp_0}{dx} = -\,\frac{b}{d_o}\,S_0 \tag{142}$$

where

S_0 is channel bed slope (143)

and all longitudinal derivatives of the zero order turbulence terms vanish. For such a case Equations 136 to 139 reduce to:

$$\bar{u}_0 \frac{\partial \bar{u}_1}{\partial x} + \bar{v}_1 \frac{\partial \bar{u}_0}{\partial y} + \beta \bar{w}_1 \frac{\partial \bar{u}_0}{\partial z} = \frac{1}{F_R^2}\left(\beta \frac{yS_0}{R} + \frac{\partial p_1}{\partial x}\right)$$

$$- \frac{\partial(\overline{u'^2})_1}{\partial x} - \frac{\partial(\overline{u'w'})_1}{\partial y} - \beta \frac{\partial(\overline{u'w'})_1}{\partial z} - \frac{2(\overline{u'w'})_0}{R} \qquad (144)$$

$$\bar{u}_0 \frac{\partial \bar{v}_1}{\partial x} - \frac{\bar{u}_0^2}{R} = - \frac{1}{F_R^2} \frac{\partial p_1}{\partial y} - \frac{\partial(\overline{u'v'})_1}{\partial x} - \frac{\partial(\overline{v'^2})_1}{\partial y}$$

$$- \beta \frac{\partial(\overline{v'w'})_1}{\partial z} - \frac{(\overline{v'^2})_0 - (\overline{u'^2})_0}{R} \qquad (145)$$

$$\bar{u}_0 \frac{\partial \bar{w}_1}{\partial x} = - \frac{\beta}{F_R^2} \frac{\partial p_1}{\partial z} - \frac{\partial(u'w')_1}{\partial x} - \beta \frac{\partial(\overline{w'^2})_1}{\partial z} - \frac{(\overline{v'w'})_0}{R} \qquad (146)$$

$$\frac{\partial u_1}{\partial x} + \frac{\partial v_1}{\partial y} + \beta \frac{\partial w_1}{\partial z} = 0 \qquad (147)$$

It may be argued further that Equations 144 to 147 would also apply to situations of gradually varied nonuniform flow and even to rapidly varied flow where the changes are of the order of α or less. The reason is that these situations may be constructed as a power expansion in two or more variables, for example:

$$u = u_{00} + \alpha_1 u_{10} + \alpha_2 u_{01} + \alpha_1 \alpha_2 u_{11} + \alpha_1^2 u_{20} + \alpha_2^2 u_{02} + \ldots \quad (148)$$

Keeping only linear order terms will give the same two sets of equations as above plus an additional set for each additional variable. The different effects may then be superimposed to give the final approximate result.

There are, of course, other ways of performing the perturbation expansions which will result in slightly or greatly different sets of equations. In such a large and complex set of equations assumptions and approximations can have unforeseen consequences.

Such a situation arises in this particular set of first order equations. No assumption was made about the size of the Froude number but the analysis is already restricted to situations where it is small. To see this, consider the situation in the immediate vicinity of a sharp change in channel curvature. In such a short location, friction may be ignored, the channel may be considered horizontal, the pressure distribution hydrostatic and zero order quantities equal to a constant. Equations 144 to 147 reduce to:

$$\frac{\partial \bar{u}_1}{\partial_x} = -\frac{1}{F_R^2}\frac{\partial h_1}{\partial x} \qquad (149)$$

$$\frac{\partial \bar{v}_1}{\partial x} - \frac{1}{R} = -\frac{1}{F_R^2}\frac{\partial h_1}{\partial y} \qquad (150)$$

$$\frac{\partial u_1}{\partial x} + \frac{\partial \bar{v}_1}{\partial y} = 0 \qquad (151)$$

where $\bar{u}_1$ and $\bar{v}_1$ are now depth averaged quantities. These three equations may [illegible] solved for h_1 to give:

$$\frac{\partial^2 h_1}{\partial x^2} + \frac{\partial^2 h_1}{\partial y^2} = 0 \qquad (152)$$

Treating the problem a little differently and depth averaging before carrying out the perturbation expansion (applying the same set of assumptions; see Appendix A) results in:

$$\frac{\partial^2 h_1}{\partial x^2} + \frac{1}{(1-F_R^2)}\frac{\partial^2 h_1}{\partial y^2} = 0 \qquad (153)$$

Equation 152 is ellipitic for all Froude numbers while Equation 153 becomes hyperbolic for supercritical flow. Equation 153 correctly predicts (to a linear approximation) the standing cross-channel waves that occur at a bend entrance for supercritical flow. For small Froude numbers the two equations are almost equivalent. Thus the set 144 to 147 is limited to small Froude numbers.

The derivation and solution of Equation 152 is given in

Appendix A. The results indicate that unless the Froude number is very close to one, the effects are small. The solution itself is useful as it also shows that appropriate length scale is the channel half width as was assumed in this derivation.

2.4 TURBULENCE CLOSURE

To proceed with calculations based on the approximate set of Equations 144 to 147 it is necessary to relate the turbulence terms to the mean flow quantities. This problem is universal to turbulent flow calculations. For the curved channel flow situation, there are no measurements available to guide our approximation. In the review section, however, it was noted that the precise form of the turbulence model used was not very important in the calculation of the 'developed' secondary flow. Rodi (1980) indicated the same is true for developing flow calculations.

For simplicity the closure used will simply be a constant but nonisotropic eddy viscosity model using a straight wide rectangular channel value. In comparsion to other approximations made to this point this assumption should prove reasonable. The form for this model is:

$$- \overline{u'_i u'_j} = \nu_t \left(\frac{\partial \bar{u}_i}{\partial x_j} + \frac{\partial \bar{u}_j}{\partial x_i}\right) \qquad (154)$$

written in tensor notation (dimensional quantities). A proper non-dimensionalization of ν_t is:

$$\nu_{t*} = \frac{\nu_t}{u_* d_0} \tag{155}$$

Equation 154 takes the following non-dimensional form:

$$-\overline{u'_i u'_j} = \frac{\nu_{t*}}{\beta C_f} \left(\frac{\partial \bar{u}_{i*}}{\partial x_{j*}} + \frac{\partial \bar{u}_{j*}}{\partial x_{i*}}\right) \tag{156}$$

This formulation assumes that the effective turbulent eddy viscosity is isotropic. Studies of mixing (Fischer, et al, 1978) have shown however that the lateral eddy diffusivity (as distinct from eddy viscosity) is at least two to three times the vertical depth averaged value. For the following a value of three is applied to the lateral direction in the form of a constant, ν_R.

Equation 156 may be substituted into Equations 144 to 147 (stars dropped) to give:

$$\bar{u}_0 \frac{\partial \bar{u}_1}{\partial x} + \bar{v}_1 \frac{\partial \bar{u}_0}{\partial y} + \beta \bar{w}_1 \frac{\partial \bar{u}_0}{\partial z} = -\frac{1}{F_R^2}\left(\frac{\beta y S_0}{R} + \frac{\partial p_1}{\partial x}\right)$$

$$+ \frac{\nu_t}{\beta C_f}\left(\frac{\partial^2 \bar{u}_1}{\partial x^2} + \nu_R \frac{\partial^2 \bar{u}_1}{\partial y^2} + \beta^2 \frac{\partial^2 \bar{u}_1}{\partial z^2}\right) + \frac{\nu_t}{\beta C_f}\frac{1}{R}\frac{\partial \bar{u}_0}{\partial y} \tag{157}$$

$$\overline{u}_0 \frac{\partial \overline{v}_1}{\partial x} - \frac{\overline{u}_0^{\,2}}{R} = - \frac{1}{F_R^2} \frac{\partial p_1}{\partial y} + \frac{\nu_t}{\beta C_f} \nabla^2 \overline{v}_1 \tag{158}$$

$$\overline{u}_0 \frac{\partial \overline{w}_1}{\partial x} = - \frac{\beta}{F_R^2} \frac{\partial p_1}{\partial z} + \frac{\nu_t}{\beta C_f} \nabla^2 \overline{w}_1 \tag{159}$$

where the operator:

$$\nabla^2 = \frac{\partial^2}{\partial x^2} + \nu_R \frac{\partial^2}{\partial y^2} + \beta^2 \frac{\partial^2}{\partial z^2} \tag{160}$$

For the presant purpose:

$$\nu_t \approx 0.077 \tag{161}$$

From this point on the overbars will be dropped.

2.5 VORTICITY EQUATIONS

The set of perturbation Equations, Equations 158 to 160 and 147 can be further reduced by eliminating the pressure by cross-differentiation. This results in equations for a vorticity-like combination. The first is derived by differentiating Equation 157 with respect to y and Equation

158 with respect to x and then taking the difference. After some algebra the following equation is obtained:

$$u_0 \frac{\partial}{\partial x}\left(\frac{\partial u_1}{\partial y} - \frac{\partial v_1}{\partial x}\right) + v_1 \frac{\partial^2 u_0}{\partial y^2} + u_0^2 \frac{d}{dx}\left(\frac{1}{R}\right) + \beta \left(\frac{\partial w_1}{\partial y}\frac{\partial u_0}{\partial z} - \frac{\partial u_0}{\partial y}\frac{\partial w_1}{\partial z}\right.$$

$$\left. + w_1 \frac{\partial^2 u_0}{\partial y \partial z}\right) = - \frac{\beta}{F_R^2}\frac{S_0}{R} + \frac{\nu_t}{\beta C_f} \nabla^2 \left(\frac{\partial u_1}{\partial y} - \frac{\partial v_1}{\partial x}\right)$$

$$+ \frac{\nu_t}{\beta C_f R}\frac{\partial^2 u_0}{\partial y^2} \qquad (162)$$

The term:

$$\eta = \left(\frac{\partial v_1}{\partial x} - \frac{\partial u_1}{\partial y}\right) \qquad (163)$$

has the appearance of vorticity although in this co-ordinate system it is not equal to the vorticity. The form is convenient however and will be utilized. Equation 162 becomes:

$$u_0 \frac{\partial \eta}{\partial x} - v_1 \frac{\partial^2 u_0}{\partial y^2} - \beta \left(\frac{\partial w_1}{\partial y}\frac{\partial u_0}{\partial z} - \frac{\partial u_0}{\partial y}\frac{\partial w_1}{\partial z} + w_1 \frac{\partial^2 u_0}{\partial y \partial z}\right)$$

$$= + \frac{\beta S_0}{F_R^2 R} + \frac{\nu_t}{\beta C_f}\left(\nabla^2 \eta - \frac{1}{R}\frac{\partial^2 u_0}{\partial y^2}\right) + u_0^2 \frac{d}{dx}\left(\frac{1}{R}\right) \qquad (164)$$

The other two "vorticity" equations are:

$$u_0 \frac{\partial \xi}{\partial x} + \beta\left(\frac{2u_0}{R} - \frac{\partial v_1}{\partial x}\right) \frac{\partial u_0}{\partial z} + \frac{\partial w_1}{\partial x} \frac{\partial u_0}{\partial y} = \frac{\nu_t}{\beta Cf} \nabla^2 \xi \tag{165}$$

where:

$$\xi = \left(\frac{\partial w_1}{\partial y} - \beta \frac{\partial v_1}{\partial z}\right) \tag{166}$$

and:

$$u_0 \frac{\partial \zeta}{\partial x} + \beta\left(\frac{\partial v_1}{\partial z} \frac{\partial u_0}{\partial y} - \frac{\partial u_0}{\partial z} \frac{\partial v_1}{\partial y} + v_1 \frac{\partial^2 u_0}{\partial y \partial z} + \beta w_1 \frac{\partial^2 u_0}{\partial z^2}\right)$$

$$= \frac{\nu_t}{\beta C_f} \left(\nabla^2 \zeta + \frac{1}{R} \frac{\partial^2 u_0}{\partial y \partial z}\right) \tag{167}$$

where:

$$\zeta = \left(\beta \frac{\partial u_1}{\partial z} - \frac{\partial w_1}{\partial x}\right) \tag{168}$$

These equations describe the transport of perturbation "vorticities". The vorticities have direct physical interpretations if the major components are studied. The longitudinal vorticity ξ is clearly related to the secondary circulation through the $\beta \frac{\partial v_1}{\partial z}$ term.

The lateral vorticity ζ, through it's dependance on $\beta \frac{\partial u_1}{\partial z}$, will give information on the distribution of bed stress. Finally, the vertical vorticity η is related to the skewing of the longitudinal velocity distriubtion because it contains a $\frac{\partial u_1}{\partial y}$ term.

To facilitate discussion and highlight the important features of these vorticity transport equations consider a situation where u_0 is a function of z only. This would apply in the central portion of a wide channel. For this situation Equations 164, 165 and 167 reduce to:

$$u_0 \frac{\partial \eta}{\partial x} = \frac{\nu_t}{\beta C_f} \nabla^2 \eta + \beta \frac{\partial w_1}{\partial y} \frac{\partial u_0}{\partial z} + \frac{\beta S_o}{F_R^2 R} + u_0^2 \frac{d}{dx} \left(\frac{1}{R}\right) \tag{169}$$

$$u_0 \frac{\partial \xi}{\partial x} = \frac{\nu_t}{\beta C_f} \nabla^2 \xi = \beta \left(\frac{\partial v_1}{\partial x} - \frac{2u_0}{R}\right) \frac{\partial u_0}{\partial z} \tag{170}$$

$$u_0 \frac{\partial \zeta}{\partial x} = \frac{\nu_t}{\beta C_f} \nabla^2 \zeta + \beta \frac{\partial u_0}{\partial z} \frac{\partial v_1}{\partial y} - \beta^2 w_1 \frac{\partial^2 u_0}{\partial z^2} \tag{171}$$

Equation 169 describes the transport of vertical vorticity which is related to the lateral distribtuion of longitudinal velocity. The rate of change of this quantity along the channel is equal to the four terms on the right-hand-side of Equation 169. The first is a turbulent diffusion term which would tend to reduce η to 0. The third term accounts for the slope differential effect (shorter path around inside of bend). The second term provides the secondary flow effect on the longitudinal velocity. It is interesting that this effect is accounted for by the vertical velocity distribution. The lateral component effect depends on the lateral distribution of u_0 whereas the vertical component effect depends on the vertical distribution of u_0. The relative size of this term may be estimated from previous studies. Typically (Yen, 1965):

$$w_1 \approx \frac{v_1}{\beta} \tag{172}$$

and:

$$\alpha\, v_1 \approx K\, \frac{d_0}{R} \tag{173}$$

where K ≈ 4.

Equation 173 can be written as:

$$v_1 \approx \frac{K}{\beta} \tag{174}$$

Therefore:

$$w_1 \approx \frac{K}{\beta^2} \tag{175}$$

All other terms are of order one so t

$\beta = 8$, $\alpha = 0.15$ (as in the experim

later):

$$\beta \frac{\partial w_1}{\partial y} \frac{\partial u_0}{\partial z} \approx 0.5$$

The slope differential effect on the

$S_0 \approx 0.001$):

$$\frac{\beta S_0}{F_R^2 R} \approx 0.03$$

And the largest of the diffusion terms

$$\frac{\beta \nu_t}{C_f} \frac{\partial u^{3}_{1}}{\partial z^{2} \partial y} \approx 0.05$$

This secondary flow effect may thus

the velocity profile toward the

rectangular channels.

The second vorticity transport e

concerns the longitudinal component

associated with the secondary flow

longitudinal derivatives, taking th

ratio to be one, and using the c

provide a stream function, Equation 1

$$\nabla^4 \psi = \frac{\beta^4 C_f}{\nu_t} \frac{2u_0}{R} \frac{\partial u_0}{\partial z} \tag{179}$$

where:

$$\nabla^4 = \frac{\partial^4}{\partial y^4} + 2\beta^2 \frac{\partial^4}{\partial y^2 \partial z^2} + \beta^4 \frac{\partial^4}{\partial z^4} \tag{180}$$

This relation has been derived and used by Rosovskii (1961) and others to calculate secondary flow. The forcing term is related to the radius of curvature and the vertical gradient of longitudinal velocity. The term including $\partial v_1/\partial x$ in Equation 170 can be shown to represent the local streamline curvature, which is especially important when the boundary curvature changes suddenly.

The last vorticity transport equation, Equation 171, characterizes the bed stress distribution. The last term represents a convection effect. The second last term is clearly a vortex stretching effect. ζ will be increased at the outer bank by this term and decreased near the inner bank.

The other terms involving $\partial u_0/\partial y$ may be shown to have similar interpretations. Overall, it appears that the secondary flow currents interacting with the main flow gradients have many interesting effects and seem to account for many observed phenomena.

2.6 DEVELOPED FLOW

2.6.1 Formulation

Although the emphasis of this study is on developing flow, it is useful to evaluate the model for an asymtotic, developed condition. In particular, the prediction of longitudinal velocity distribution is of interest. The relevant equations may be formed from Equations 163 to 168 by ignoring any terms involving a longitudinal derivative. R may be taken as 1.0. These are:

$$\nu_R \frac{\partial^2 \eta}{\partial y^2} + \beta^2 \frac{\partial^2 \eta}{\partial z^2} = -\left(\frac{v_1 \beta C_f}{\nu_t} + \frac{1}{R}\right) \frac{\partial^2 u_0}{\partial y^2}$$

$$- \frac{\beta^2 C_f}{\nu_t} \left(\frac{\partial w_1}{\partial y} \frac{\partial u_0}{\partial z} - \frac{\partial w_1}{\partial z} \frac{\partial u_0}{\partial y} + w_1 \frac{\partial^2 u_0}{\partial y \partial z} + \frac{1}{{C_f}^2}\right) \tag{181}$$

$$\nu_R \frac{\partial^2 \xi}{\partial y^2} + \beta^2 \frac{\partial^2 \xi}{\partial z^2} = \frac{\beta^2 C_f}{\nu_t} \left(2u_0 \frac{\partial u_0}{\partial z}\right) \tag{182}$$

$$\nu_R \frac{\partial^2 \zeta}{\partial y^2} + \beta^2 \frac{\partial^2 \zeta}{\partial z^2} = \left(\frac{v_1 \beta C_f}{\nu_t} + 1\right) \frac{\partial^2 u_0}{\partial y^2}$$

$$- \frac{\beta^2 C_f}{\nu_t} \left(\frac{\partial v_1}{\partial z} \frac{\partial u_0}{\partial y} - \frac{\partial v_1}{\partial y} \frac{\partial u_0}{\partial z} + v_1 \frac{\partial^2 u_0}{\partial y \partial z} + \beta w_1 \frac{\partial^2 u_0}{\partial z^2}\right) \tag{183}$$

$$\frac{\partial v_1}{\partial y} + \frac{\partial w_1}{\partial z} = 0 \tag{184}$$

$$\eta = -\frac{\partial u_1}{\partial y} \qquad (185)$$

$$\xi = \frac{\partial w_1}{\partial y} - \beta\frac{\partial v_1}{\partial z} \qquad (186)$$

$$\zeta = \frac{\partial u_1}{\partial z} \qquad (187)$$

Two of these equations are redundant so Equations 183 and 187 will not be considered further.

The calculation procedure will be to solve for ξ from Equation 182. The secondary circulation velocities may then be solved by using Equations 184 and 186 as follows. Define a stream function ψ, such that:

$$\beta\frac{\partial \psi}{\partial z} = v_1 \qquad (188)$$

$$\frac{\partial \psi}{\partial y} = -w_1 \qquad (189)$$

This stream function automatically satisfies Equation 184 and may be introduced into Equation 186 to produce:

$$\frac{\partial^2 \psi}{\partial y} + \beta^2 \frac{\partial^2 \psi}{\partial z^2} = -\xi \qquad (190)$$

Given ξ from Equation 182, Equation 190 may be solved for ψ and then Equations 188 and 189 give v_1 and w_1. Equation 181 then gives η and u_1 may then be obtained by integrating Equation 185.

Boundary conditions, especially at the solid boundaries, are complex and controversial. Some simplification may be obtained by considering the symmetries of the problem. If u_0 is symmetric about $y = 0$ then ξ and ψ will also be symmetric. The vertical vorticity η will also be symmetric. The calculations may be done then only for $0 < y < 1.0$. On the virtual boundary created at $y = 0$, the normal derivative of these quantities is zero. In addition, u_1 is zero here. On the other boundaries ψ may be set arbitrarily to zero, completing this particular boundary value problem.

At the free surface, the shear stress is approximately zero resulting in ξ and $\partial\eta/\partial z$ being equal to zero at $z = 1$. Finally, boundary conditions for ξ and η are required at $z = 0$ and $y = 1$. As was discussed in the review section this condition is somewhat dependent on the particular form assumed for u_0. Rosovskii (1961) and Ikeda (1978) have suggested a particularly simple form for ξ, namely that it will be zero at the solid boundaries. This implies that the shear stress is also zero at these boundaries. It was argued however, that this approximation only affected the secondary flow distribution in the immediate vicinity of the boundary. This assumption makes analytical solutions, at least for the secondary circulation (v_1 and w_1) possible.

For the present study, however, a numerical approach was chosen. This allowed the most flexibility with regard to distributions of u_0 as well as inclusion of more realistic boundary conditions. Once a program is written, numerical "experiments" could be performed to show the dependence of the perturbation velocities on the various parameters.

It is still necessary to provide an initial velocity (u_0) distribution and the remaining boundary conditions. In the interest of simplicity, the slip velocity formulation of Engelund (1974) is a reasonable approximation. Any other prescribed distribution could be used but this method is consistent with the constant eddy viscosity approximation and leads to reasonably simple boundary conditions.

The initial velocity distribution may be calculated from:

$$\nu_R \frac{\partial^2 u_0}{\partial y^2} + \beta^2 \frac{\partial^2 u_0}{\partial z^2} = -\frac{1}{\nu_t C_f} \qquad (191)$$

with boundary conditions:

$$\frac{\partial u_0}{\partial y} = 0 \qquad y = 0; \qquad (192)$$

$$\frac{\partial u_0}{\partial z} = 0 \qquad z = 1; \qquad (193)$$

$$\frac{\partial u_0}{\partial z} = \frac{u_0}{\nu_t C_f u_{0b}} \qquad \text{at } z = 0 \tag{194}$$

and:

$$\frac{\partial u_0}{\partial y} = \frac{C_b \beta\, u_0}{\nu_R \nu_t C_f u_{0b}} \qquad \text{at } y = 1 \tag{195}$$

where C_b is a constant to allow the distribution to be tuned to fit measured distributions. The constant u_{0b} is given by:

$$u_{0b} = \left(1 - \frac{1}{3\nu_t C_f}\right) \tag{196}$$

This formulation has the advantage that the same method may be used to solve for the initial velocity distribution as for the perturbation velocities. The velocities calculated by Equations 191-196 must however be normalized such that the mean value is 1.0.

The boundary conditions for the perturbation velocities may be formulated (Engelund, 1974) by the requirement that the ratio of boundary perturbation velocity to boundary perturbation stress be the same as the u_0 boundary velocity (slip velocity) to stress ratio. In dimensional terms (for the lateral velocity):

$$\frac{v_1}{\nu_t \frac{\partial v}{\partial z}} = \frac{u_{0b}}{u_*^2} \tag{197}$$

In nondimensional form:

$$\nu_t C_f u_{0b} \frac{\partial v_1}{\partial z} = v_1 \qquad (198)$$

which may be written as:

$$\xi = \frac{-\beta v_1}{\nu_t C_f u_{0b}} \qquad \text{on } z = 0 \qquad (199)$$

Similarily:

$$\xi = \frac{-\beta w_1}{\nu_t C_f u_{0b}} \qquad \text{on } y = 1 \qquad (200)$$

For u_1 the same condition gives:

$$\frac{\partial u_1}{\partial z} = \frac{u_1}{\nu_t C_f u_{0b}} \qquad \text{on } z = 0 \qquad (201)$$

which may be converted into a boundary condition in η by differentiation:

$$\frac{\partial \eta}{\partial z} = \frac{\eta}{\nu_t C_f u_{0b}} \qquad \text{on } z = 0 \qquad (202)$$

The remaining condition is:

$$\eta = \nu_R \frac{C_b\, u_1}{\nu_t C_f u_{0b}} \qquad \text{on } y = 1 \qquad (203)$$

consistent with Equation 195 for the main velocity.

Boundary condition 202 may be used directly but the other three require advance knowledge of u_1, v_1 and w_1. An iterative procedure must then be used. As indicated previously the effect of assuming zero boundary values does not have a large effect on the overall solution so convergence is very rapid.

2.6.2 Solution

As indicated previously the above problem was solved numerically for a range of the independent parameters β, C_f and η. A successive-over-relaxation iterative procedure was used to solve the Poisson-like equations. This procedure is very simple to code, is the most economical of storage space, provides rapid convergence and works well with the iterative boundary conditions imposed. The last point is due to the fact that the latest approximation is used as an initial guess for the iteration. Thus as the boundary value approaches it's final value, fewer and fewer iterations are required to obtain a new value.

The FORTRAN source code for this problem is included in Appendix B. Typically, a run took about three minutes to complete on the University of Alberta Computing Services AP164 processor using a fifty by fifty finite difference grid. Figures 10 to 14 display the output of the various stages of the calculations. Figure 15 shows a measured final velocity profile for similar conditions (from part 3 of this study).

The effect of ν_R and C_b on the output was investigated and it was found that $C_b \approx 0.3$ gave a reasonable approximation for u_0 while $\nu_R = 3.0$ gave reasonable results. Increasing C_b caused the final perturbation longitudinal velocity profile to be more evenly distributed in the y direction as is shown in Figure 16. Decreasing ν_R results in much smaller longitudinal velocity perturbations as shown in Figure 17.

Using the values quoted above the model was run a number of times to investigate the effect of the friction coefficient and the channel aspect ratio. The results are sumarized in Figure 18 where the depth averaged longitudinal perturbation velocities at $y = 0.9$ are plotted. This graph shows a strong dependence on aspect ratio and a weaker dependence on friction coefficient.

Also investigated was the importance of the various forcing terms in Equation 181. The overriding term was the one involving $\frac{\partial w_1}{\partial z}$. The rest of the terms had the effect of smoothing the lateral distribution of longitudinal perturbation velocity. Figure 19 shows the depth averaged vertical velocity at $y = 1.0$ and while the magnitudes are not large, the correspondence with Figure 18 is remarkable.

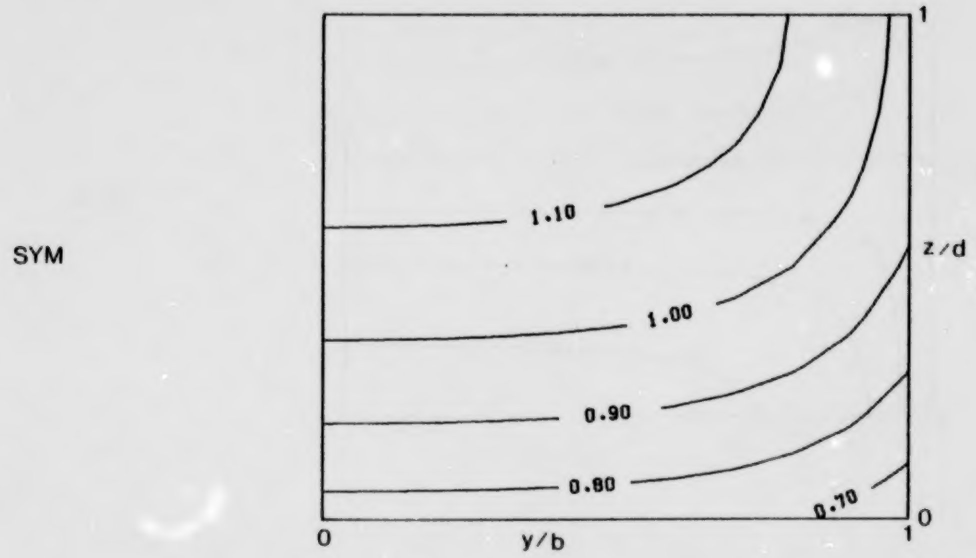

Figure 10. Calculated Straight Channel Velocity Contours ($\beta = 8.7$, $C_f = 16.0$)

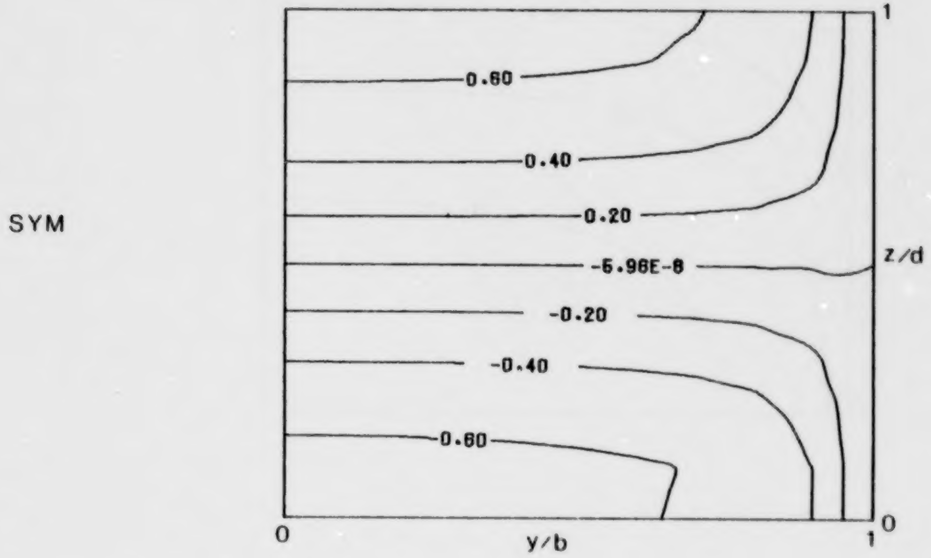

Figure 11. Lateral Perturbation Velocity Contours ($\beta = 8.7$, $C_f = 16.0$)

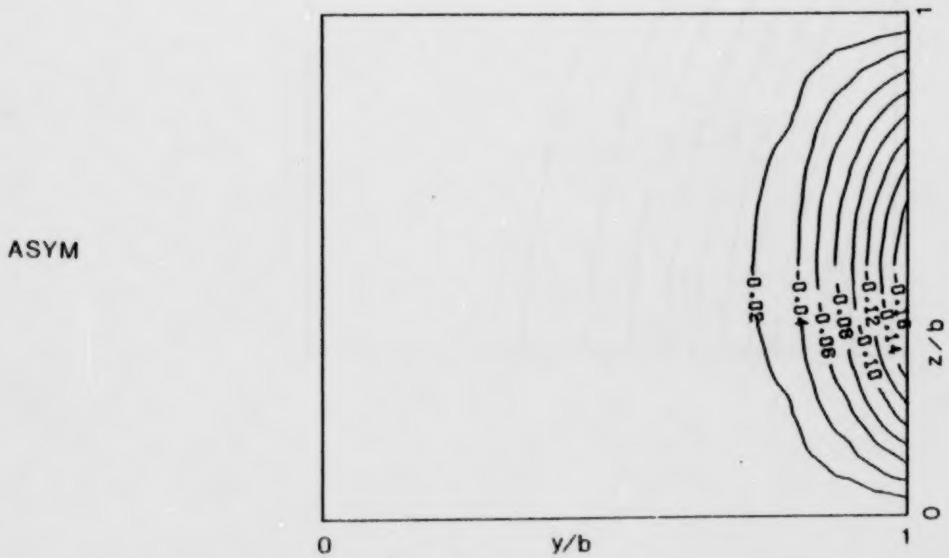

Figure 12. Vertical Perturbation Velocity Contours $\beta = 8.7$, $C_f = 16.0$)

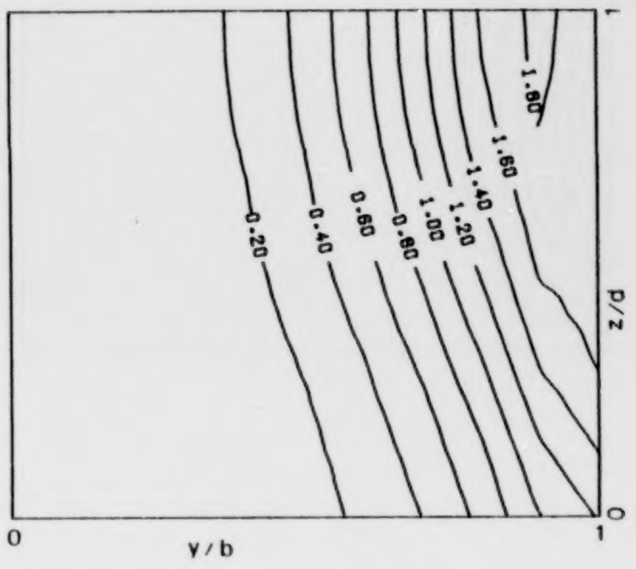

Figure 13. Longitudinal Perturbation Velocity Contours ($\beta = 8.7$, $C_f = 16.0$)

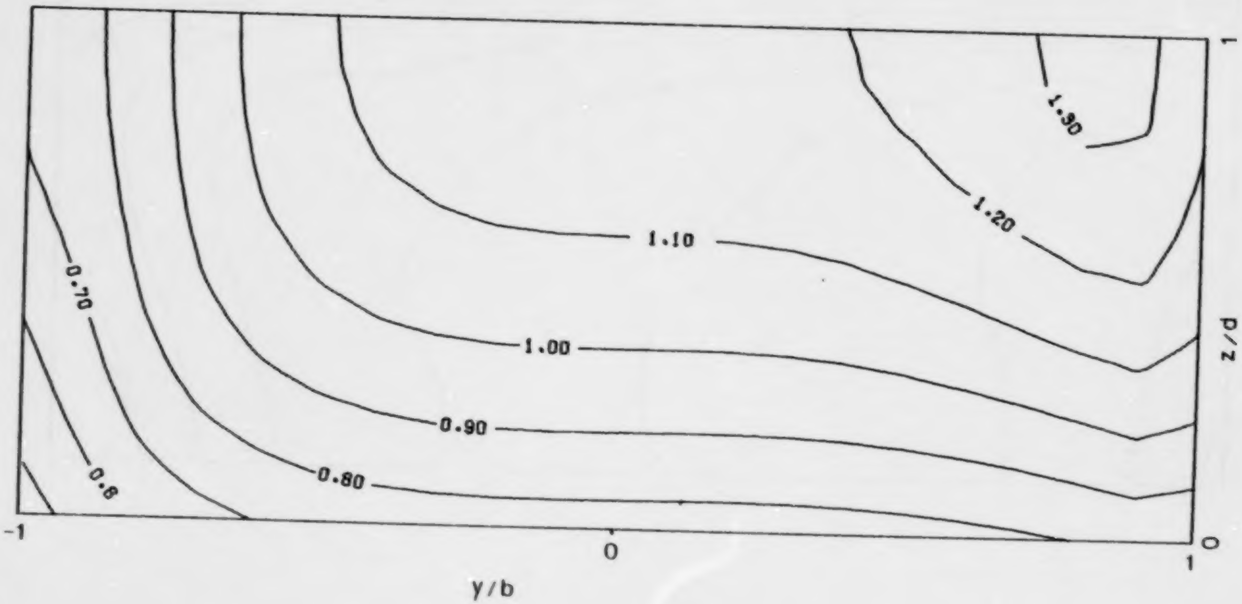

Figure 14. Total Longitudinal Velocity Contours ($\beta = 8.7$, $C_f = 16.0$, $\alpha = 0.146$)

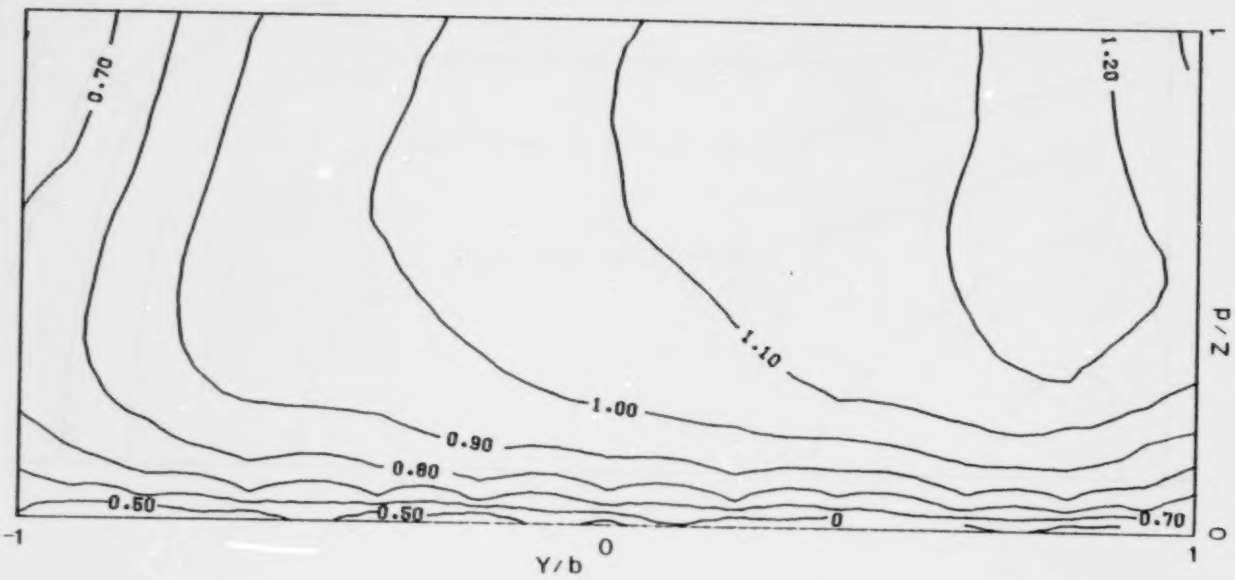

Figure 15. Measured Longitudinal Velocity Contours (u/U_0, $\beta = 8.7$, $C_f = 16.0$, $\alpha = 0.146$)

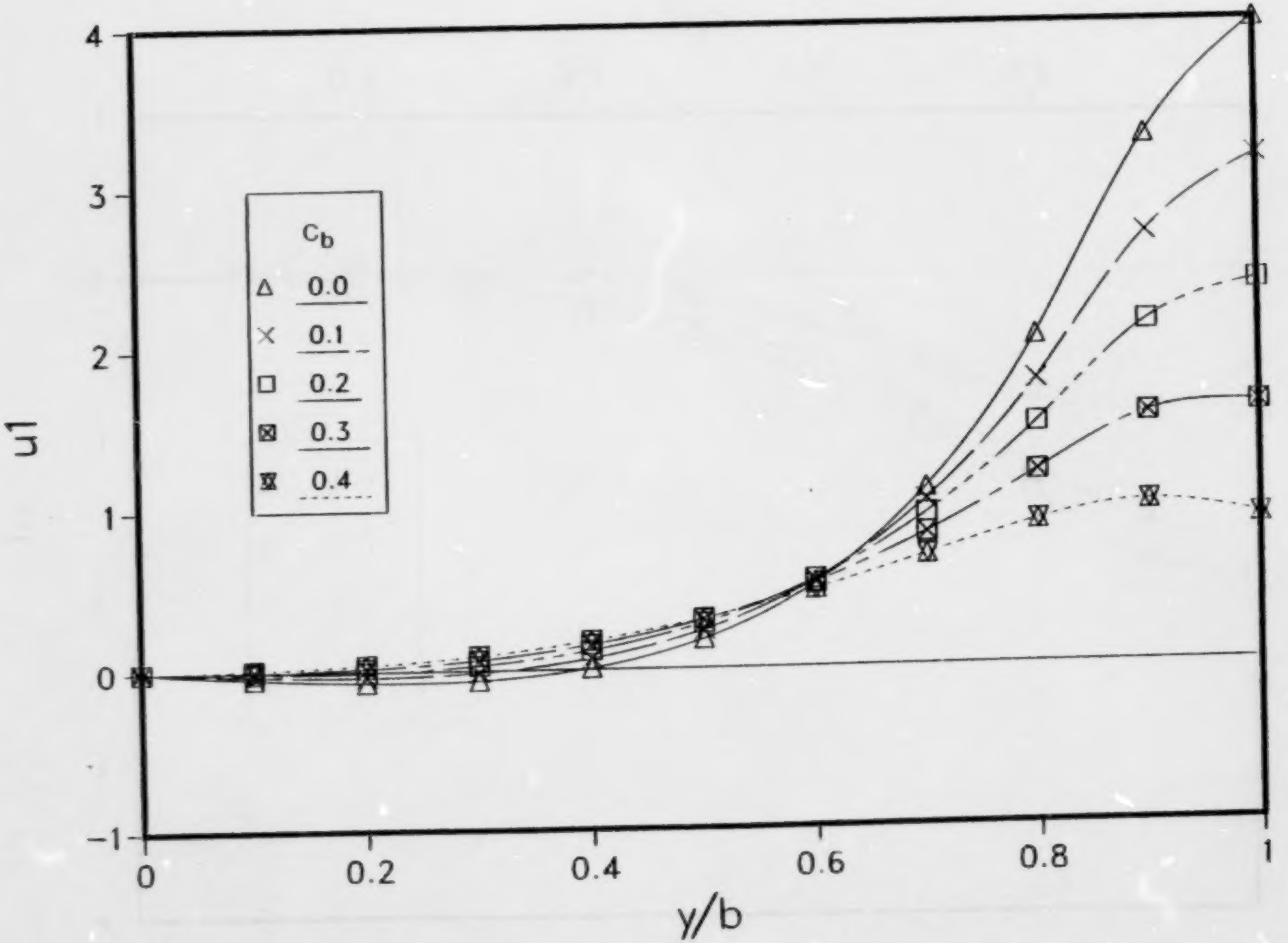

Figure 16. Effect of C_b on the Lateral Distribution of Longitudinal Perturbation Velocity ($\nu_R = 3.0$)

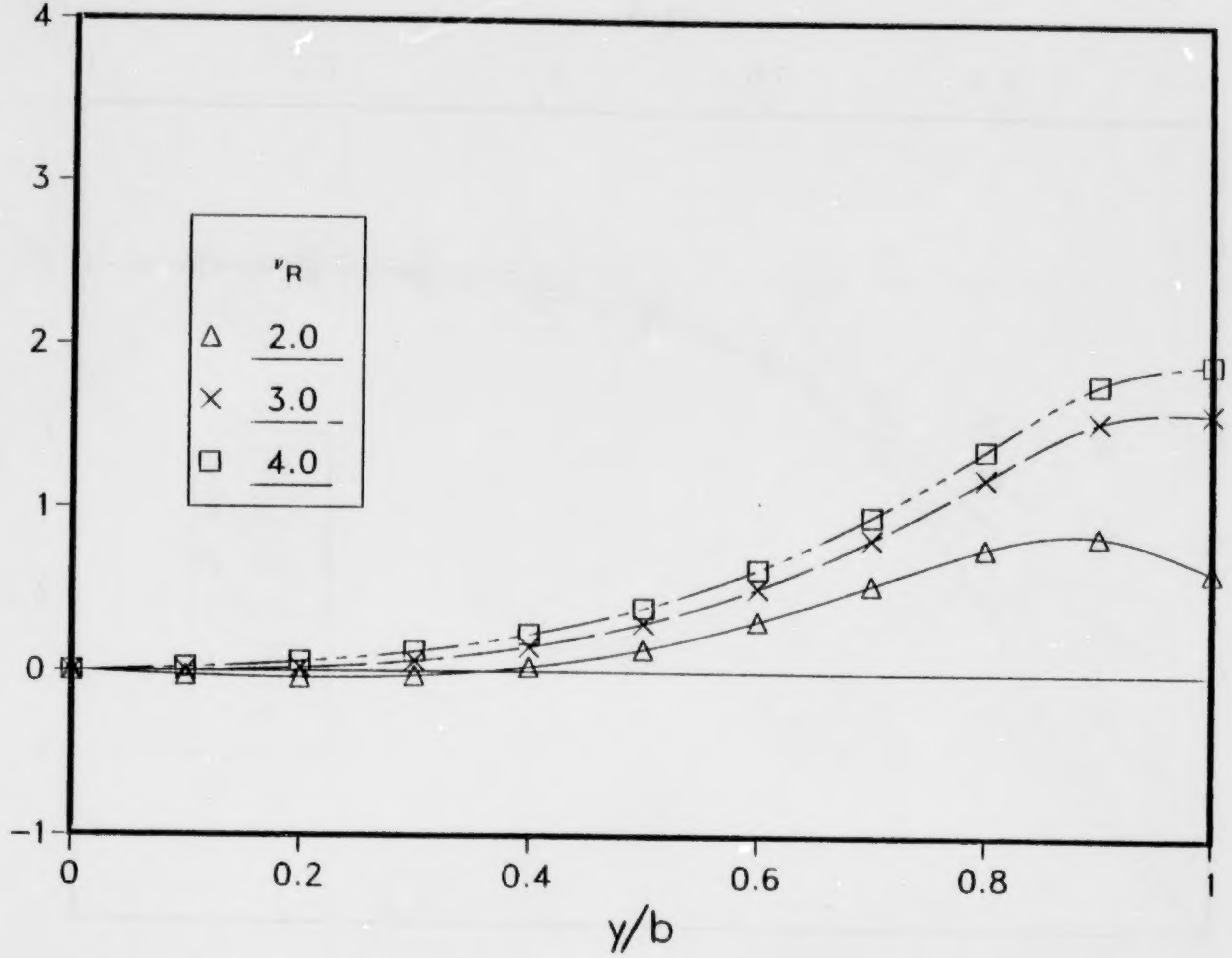

Figure 17. Effect of ν_R on the Lateral Distribution of Longitudinal Perturbation Velocity ($C_b = 0.3$)

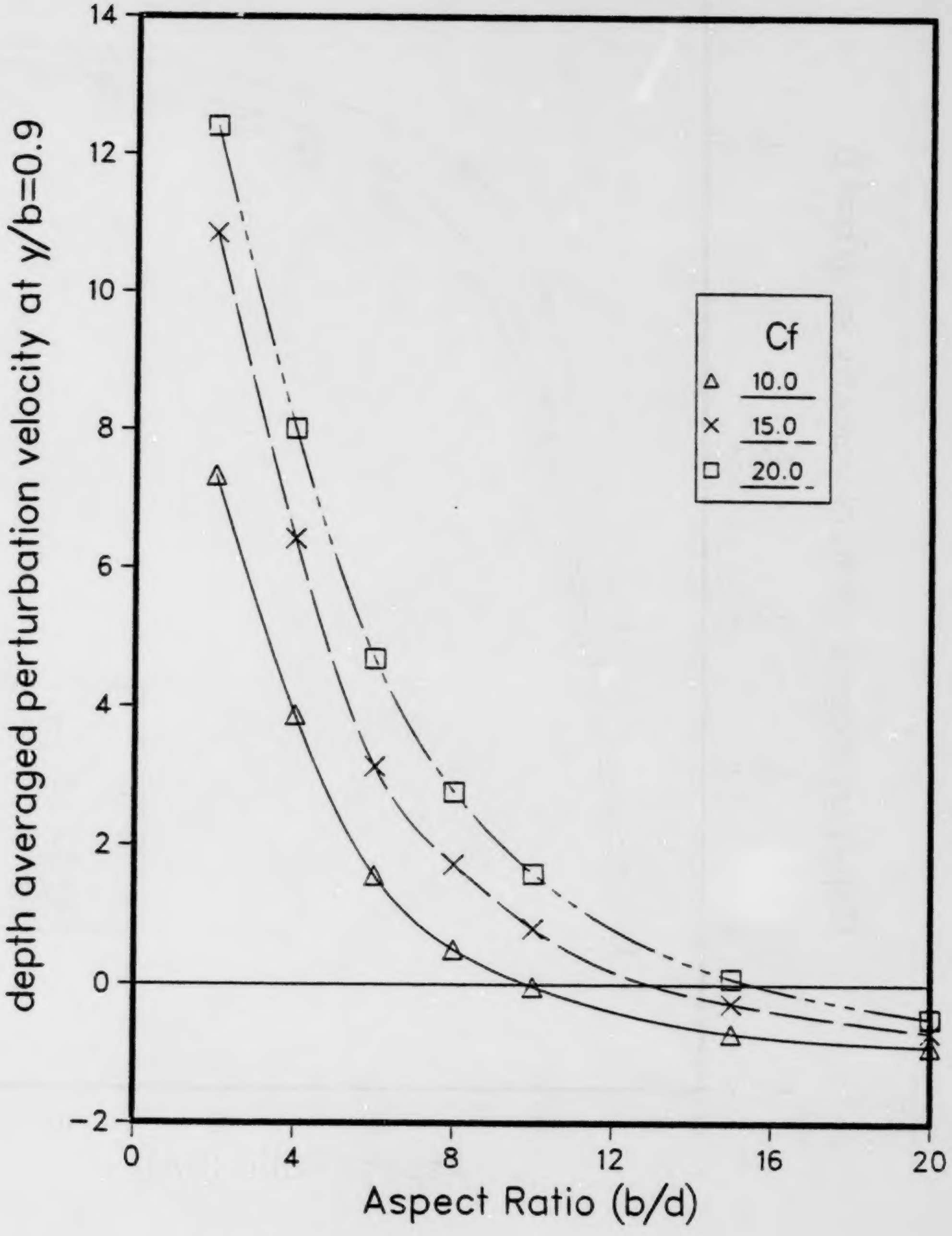

Figure 18. Depth Averaged Longitudinal Velocity Perturbations at y/b = 0.9

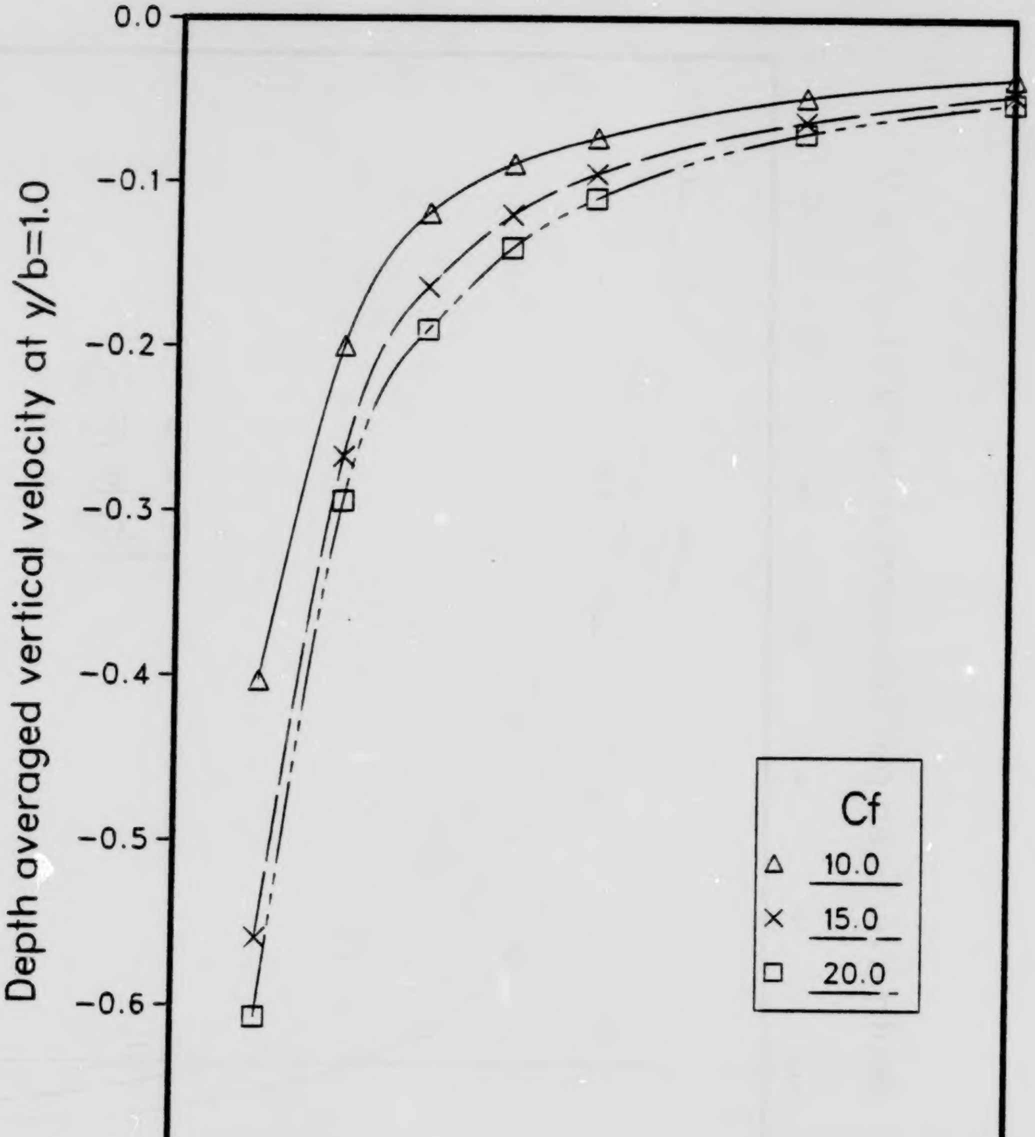

Figure 19. Depth Averaged Vertical Velocities at y/b = 1.0

2.7 DEVELOPING FLOW

2.7.1 Formulation

To predict longitudinal variations of the perturbation velocity components, the full set of Equations 163 to 168 should be considered. The most important difference from developed flow is the inclusion of terms involving derivatives with respect to the x direction. The solution of this set of linear equations would be a formidable but not impossible task.

A simplified solution procedure is suggested by the following. The development of the superelevation and associated inertial effects is very rapid ($L \approx b$) and is centered about a change of curvature (see Appendix A). Secondary circulation development occurs somewhat more slowly (Rosovskii, 1961) but is still very rapid compared to the shifting of the longitudinal velocity profiles. The behaviour of the first two aspects of developing flow is also somewhat better understood. While all three interact and affect each other, it appears that the first two reach developed values very quickly and are not strongly affected by the developing longitudinal velocity distribution.

This analysis of developing flow, then, considers only Equation 163, the equation for the vertical vorticity with the following simplifications:

1. The terms involving v_1 and w_1 are to be evaluated using the fully developed solution with the short

developing region represented by a linear variation of the term from zero to fully developed between $x = 0$ and $x = 0.1C_f/\beta$.

2. The term involving the rate of change of curvature $(1/R)$ is to be represented as a triangular function about $x = 0$ with a maximum value of one and a base extending from $x = -1$ to $x = 1$.
3. The u_0 multiplying the first term and the rate of change of curvature term are taken as 1.0 for simplicity.
4. The 'vorticity' η is taken as

   $$\eta = -\frac{\partial u_1}{\partial y}$$

   neglecting the variation of v_1 with x as being small.
5. The second derivative of η with respect to x in $\nabla^2\eta$ is neglected compared to the vertical derivative. This simplification reduces the equation to parabolic form which will be easier to solve.

The equation for developing longitudinal velocity is then:

$$\frac{\partial \eta}{\partial x} = \frac{\beta \nu_t}{C_f}\left(\frac{\nu_R}{\beta^2}\frac{\partial^2 \eta}{\partial y^2} + \frac{\partial^2 \eta}{\partial z^2}\right) + v_1\frac{\partial^2 u_0}{\partial y^2} + \beta\left(\frac{\partial w_1}{\partial y}\frac{\partial u_0}{\partial y}\right.$$

$$\left. - \frac{\partial u_0}{\partial y}\frac{\partial w_1}{\partial z} + w_1\frac{\partial^2 u_0}{\partial y \partial z}\right) + \frac{\beta}{{C_f}^2} + u_0^2\frac{d}{dx}\left(\frac{1}{R}\right) \qquad (204)$$

The boundary conditions in y and z are the same as for developed flow except that η is taken simply as zero at $y = 1$ to avoid having to iterate for a solution. The velocity u_1 is then derived by integrating η with respect to y.

2.7.2 Solution

Equation 204 may be solved numerically by an explicit technique very similar to the successive-over-relaxation technique used to solve for the developed flow distribution. In fact, since the developed values of v_1 and w_1 are required, it is only necessary to modify slightly the program used for developed flow and to save the longitudinal velocity distribution at periodic distance steps.

This method, however, limits the maximum distance step for a stable solution. The (conservative) distance step used was:

$$\Delta x = 0.25 \frac{C_f}{\beta \nu_t} (\Delta y)^2 \qquad (205)$$

where $\Delta z = \Delta y$.

2.7.3 Comparison to Experiment

This problem was solved for parameters corresponding to Run 1 of the experimental study and the results are compared in Figure 20. This plot shows the variation of the depth averaged longitudinal perturbation velocity at y = 0.9 with experimental values at y = 0.8 where the peak occurred. The graph shows a negative dip at the beginning of the bend and then an exponential climb toward the fully developed value and a jump at the end of the bend followed by an exponential decay toward zero. The agreement with measured values is seen to be reasonable.

2.8 CONCLUSIONS

A theoretical model based on a perturbation of the Reynold's equations for a moderate curvature ratio is presented. The first set of perturbation equations (linear in curvature ratio) appear to predict many aspects observed in curved channel flows. In particular it is possible to calculate an approximate redistribution of longitudinal velocity. The equations derived are complex but linear and are solved by a standard numerical technique for both developed and developing flow. Comparison with experiment indicates reasonable agreement.

The vertical velocity appears to have an important effect on the redistribution of longitudinal velocity. The lateral velocity appears only to smooth the distribution out and transfer what is essentially a wall effect towards the center of the channel. A constant, but anisotropic, eddy viscosity was used to model the turbulent momentum transport which had a similar effect. It is felt that higher order approximations if calculated would further smooth out the

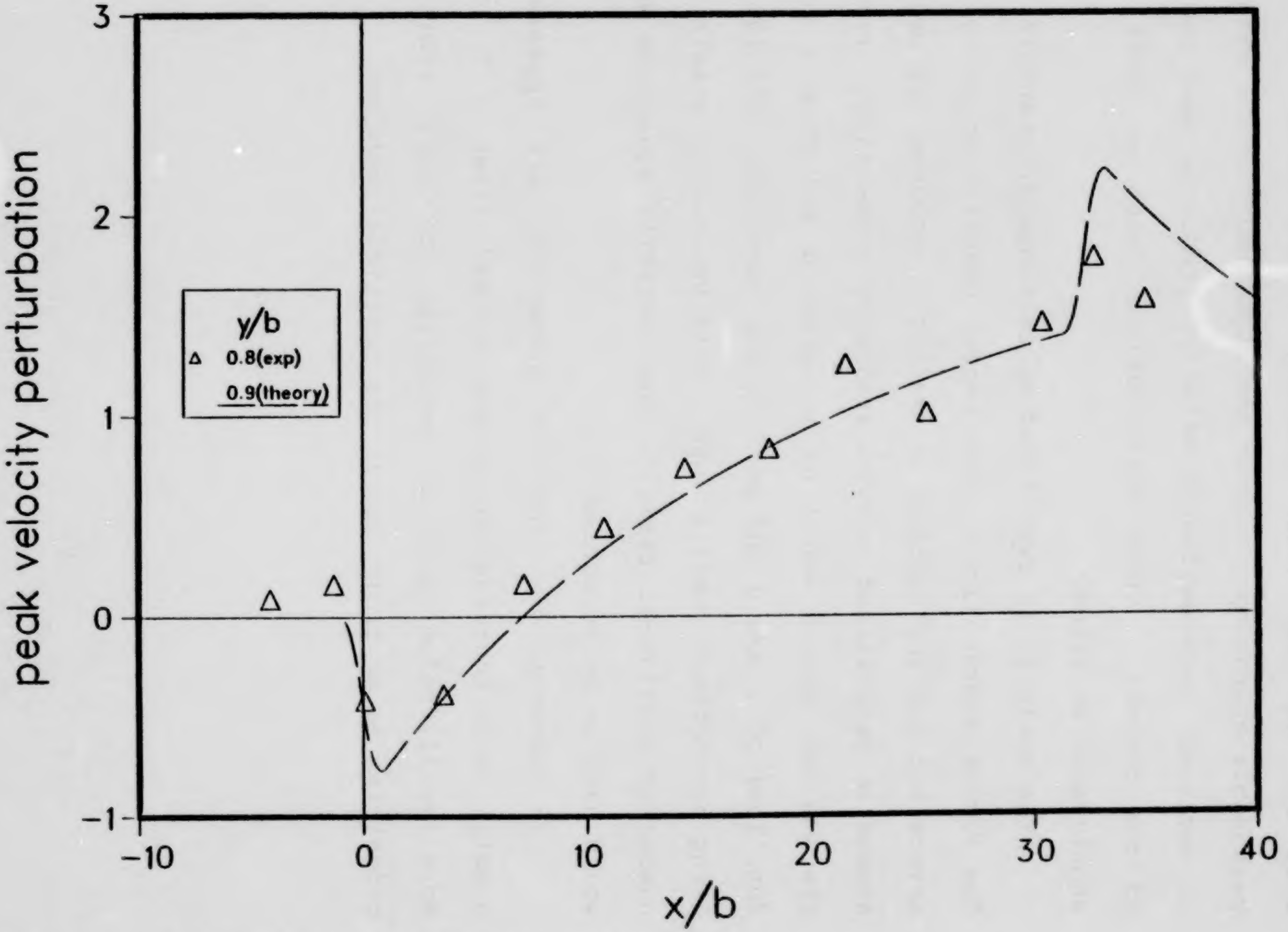

Figure 20. Developing Flow-Comparison of Theory to Experiment

longitudinal velocity distribution.

The weakest part of the analysis is likely the assumed form for the zero order velocity distribution. While a reasonable approximation over the upper half of the channel, it seriously underestimates velocity gradients near the bed of the channel. Other distributions, such as power law, should also be tried.

The analysis is restricted to rectangular channels with low Froude Number flows. The second restriction is not too severe but for application to practical problems the problem should be generalized to more arbitrary geometries. Perhaps the easiest method would be to allow d and thus β to be functions of x and y and perform the numerical calculations using nonconstant coefficients. This would also result in a number of additional terms in the vorticity equations which would have to be accounted for.

In summary, the analysis presented here appears to predict many features of curved channel flows. It needs more verification and an extension to more arbitrary geometries to be truly useful for practical problems.

3. PART THREE - EXPERIMENTAL STUDY

3.1 INTRODUCTION

An experimental study was performed to provide physical insights into the problem of flow in curved channels, validation for the assumptions and results of the theoretical analysis and to add significantly to the body of existing experimental data. The Laser Doppler Anaemometer (LDA) provides unprecedented accuracy and resolution in liquid flow measurements and the experimental facility was designed specifically for the DISA LDA system in the University of Alberta's T. Blench Graduate Hydraulics Laboratory.

The objectives of the experimental study were as follows:

1. The physical dimensions of the flume should be of realistic proportions and the channel should be as large as space permits.
2. The total angle turned by the bend should be as large as possible so that the full extent of developing flow would be observed, if possible.
3. The experiment should be designed to take full advantage of the LDA's unique capabilities for velocity and turbulence measurements including:
    (a) detailed longitudinal velocity measurements which would also provide longitudinal bed stresses

(b) detailed lateral mean velocity measurements which would be measured directly and which in combination with the longitudinal velocity measurements near the bed would provide the angle of the shear stress vector at the bed.

(c) detailed measurements of longitudinal and lateral turbulence intensities.

Due to the detail of each experiment, only two experiments were performed and only the depth of flow and the discharge were different between the two runs. Measurements were made at over 5,600 locations, each involving 10,000 individual velocity resolutions in each direction, for a total of over one hundred million velocity realizations.

3.2 FACILITIES AND PROCEDURES

3.2.1 Flume

The layout of the flume designed and used for these experiments is shown in Figure 21. Also included in the figure are the locations of the measurement stations. It is comprised of a straight section 13.4 m long and a single bend of 3.66 m centreline radius over an arc of 270° (distance of 17.2 m) followed by a 2.4 m straight exit section. The channel was 1.07 m wide and 0.20 m deep. The slope was adjustable but was set at 1/1,200 for both experiments. At this slope (necessarily small to allow a

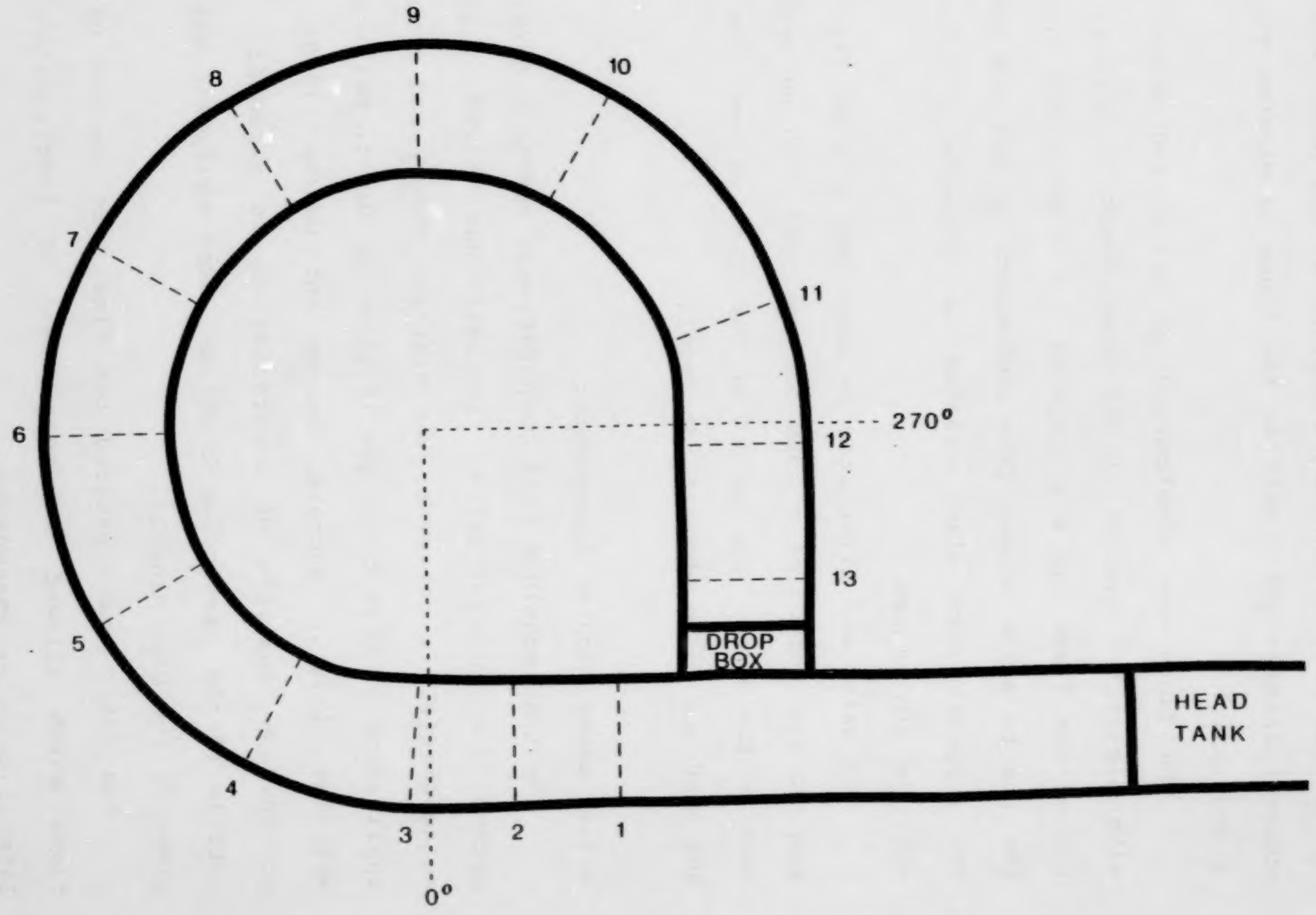
9
8
10
7
11
6
270°
12
13
5
DROP BOX
HEAD TANK
4
3
2
1
0°

Figure 21. Flume Layout and Test Locations

reasonable Froude number), there was only a few centimetres difference between the bed elevation at the point where the channel intersected itself so the flume terminated there in a drop box.

The flume was constructed of galvanized sheet metal with plexiglass inserts at the measurement locations. The bed of the flume was a minimum of 1.5 m above the floor of the lab to allow access from underneath by the LDA system. The supports were also arranged to minimize interference with the LDA system.

The water was circulated by pump from a level regulated sump to the bottom of a head box equipped with an overflow back to the sump. The height of the flume allowed the sump and head box to be above floor level.

3.2.2 Laser Doppler Anaemometer

The LDA technique is a comparatively recently developed method for non-intrusive, instantaneous fluid velocity measurements. A review of the history, theory and range of application of this technique is given by Durst, Melling and Whitelaw (1978). Buchave, George and Lumley (1979) have provided an analysis of accuracies to be expected. The details of the particular 2 colour laser equipment used is given in the DISA Manuals.

The laser beams entered the flow from the bed of the flume which allowed the measurement of longitudinal and lateral velocity components.

Figure 22 is a schematic diagram showing the main components of the LDA measurement system as well as the control, data aquisition and analysis systems. The laser was a 4W Argon-Ion laser with special optics to enhance the blue (488 nm) line and an etalon to improve coherence. Actual power used was about 500 mW.

The LDA optics performed the dual function of laser beam manipulation and scattered light collection. The single beam from the laser was split into three: one blue (488 nm), one green (514.5 nm) and one mixed with an approximate power distribution of 25%/25%/50%. The two single colour beams were frequency shifted 40 MHz by means of a Bragg cell to enhance signal quality and insure flow direction information. To further enhance signal quality and to reduce the size of the measuring volume, a beam expander (1.9:1) was used.

The three beams exited the optics parallel to and concentric about the optical axis. The optics were rotated so that the blue and mixed beams were perpendicular to the longitudinal direction while the green and mixed beams were parallel to the longitudinal direction.

The traversing system consisted of a plane mirror and the focusing lens mounted on threaded tracks. The position of the mirror and lens was controlled by computer. The nominal position accuracy was ±0.01 mm. Focal lengths of the lenses used were 80 mm and 160 mm. A benefit of this system was that the laser and optics remained stationary during traversing.

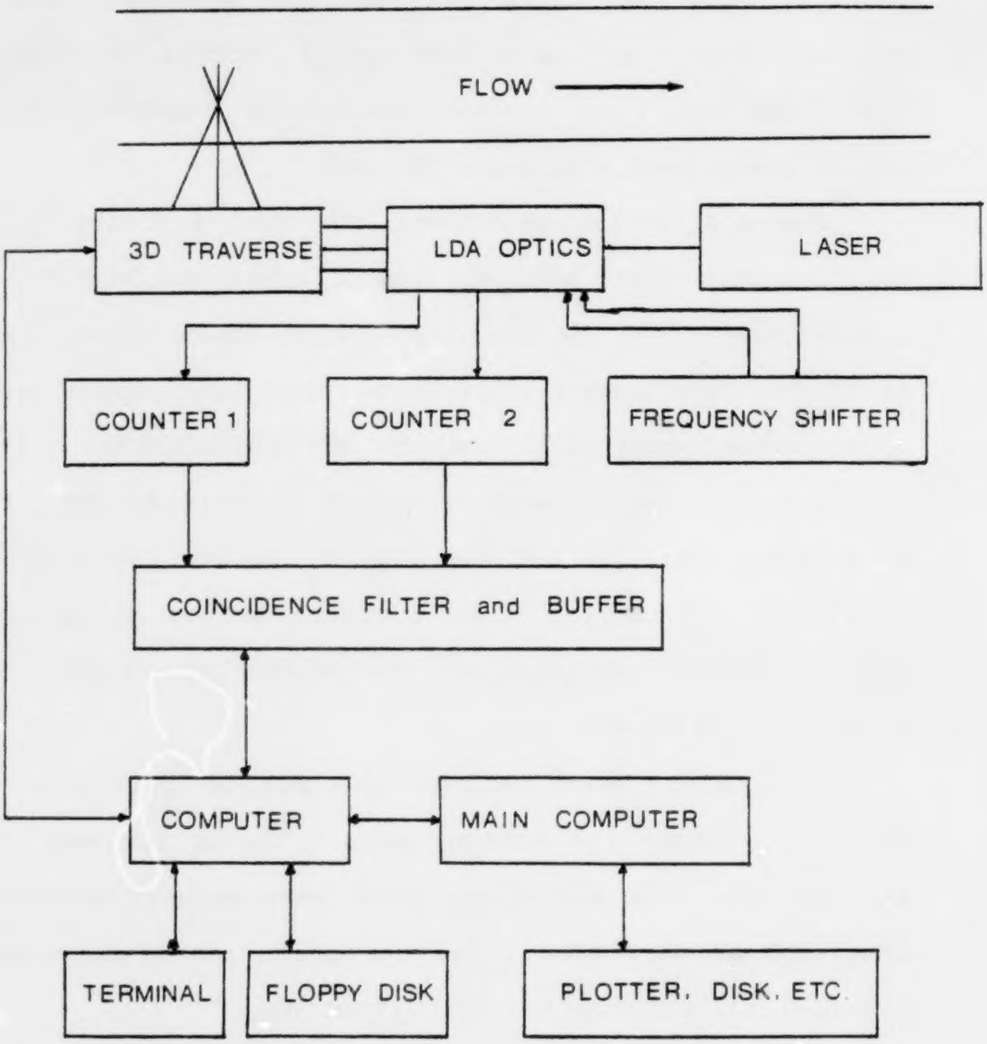
FLOW
3D TRAVERSE
LDA OPTICS
LASER
COUNTER 1
COUNTER 2
FREQUENCY SHIFTER
COINCIDENCE FILTER and BUFFER
COMPUTER
MAIN COMPUTER
TERMINAL
FLOPPY DISK
PLOTTER, DISK, ETC.

Figure 22. Schematic Diagram of LDA Setup

The traversing mechanisms were limited to 0.6 m total travel which was more than adequate in the vertical direction but covered only about half the width of the channel. The entire LDA system was mounted on a trolley which was manually positioned twice at each measurement section. A string through the centre of channel curvature was used to align the traverse in a radial direction.

The flow was seeded with latex paint in concentrations of less than 2 ppm. This material was found to be very effective at a minimum cost. Seeding was essential for measurements with the very short focal length lenses where the measuring volume was very small.

The scattered light was collected by the same optics and separated by colour sensitive mirrors. The light was converted to electrical signals by photomultipliers and passed through the dual channel channel frequency shifter to two identical counters. The counters evaluated the Doppler frequency for each burst and this value was transmitted to a computer for analysis. A coincidence filter was used to assure approximately simultaneous information on each channel. One of the counters also provided the total number of fringes in the burst. This assured only one reading per burst and was also useful in the analysis of the data.

3.2.3 Data Reduction

The coincident pairs of Doppler frequencies were stored as they arrived in the computer memory. Due to the limited memory capacity, only 2,000 pairs could be stored at one time. These were then reduced and successive sets of data taken until the desired sample size was obtained. For these experiments a sample size of 10,000 was used. The average data rate was about 200 samples per second.

The flow statistics obtained were: $\overline{u_G}$, the mean velocity measured by the green set of beams; $\overline{u_B}$, the mean velocity in the blue direction; $\overline{u'_G{}^2}$, the mean square turbulence intensity in the green direction; $\overline{u'_B{}^2}$, the mean square turbulence intensity in the blue direction; and $\overline{u'_B u'_G}$, the covariance of the velocity fluctuations. These values were calculated for Run 1 using a two-dimensional bias correction method (Buchave, George & Lumley, 1979). The formulas used were:

$$\overline{u_G} = \frac{\sum_{i=1}^{N} \frac{u_{G_i}}{|U_i|}}{\sum_{i=1}^{N} \frac{1}{|U_i|}} \qquad (206)$$

$$\overline{u_B} = \frac{\sum_{i=1}^{N} \frac{u_{G_i}}{|U_i|}}{\sum_{i=1}^{N} \frac{1}{|U_i|}} \qquad (207)$$

$$\overline{u'^{2}_{G}} = \frac{\sum\limits_{i=1}^{N} \frac{u_{G_i}^{2}}{|U_i|}}{\sum\limits_{i=1}^{N} \frac{1}{|U_i|}} - (\overline{u_G})^2 \qquad (208)$$

$$\overline{u'^{2}_{B}} = \frac{\sum\limits_{i=1}^{N} \frac{u_{G_i}^{2}}{|u_i|}}{\sum\limits_{1=i}^{N} \frac{1}{|U_i|}} - (\overline{u_B})^2 \qquad (209)$$

$$\overline{u'_B u'_G} = \frac{\sum\limits_{i=1}^{N} \frac{u_{B_i} u_{G_i}}{|U_i|}}{\sum\limits_{1=1}^{N} \frac{1}{|U_i|}} \qquad (210)$$

where:

u_{B_i} = velocity reading from blue beams

u_{G_i} = velocity reading from green beams

$$U_i = \sqrt{u_{B_i}^{2} + u_{G_i}^{2}} \qquad (211)$$

N = number of accepted samples

The data from the second run was analyzed using the total number of fringes in a burst which is related to the particle transit time by:

$$t_p = \frac{N_f}{f_D} \qquad (211)$$

where

t_p = particle transit time

N_f = number of fringes observed (zero crossings)

f_D = doppler frequency

The averages were then computed using t_p as a weighting coefficient. For example:

$$\bar{u}_G = \frac{\sum_{i=1}^{N} u_{Gi}\, t_{Pi}}{\sum_{i=1}^{N} t_{P_i}} \qquad (212)$$

The two methods gave almost identical results for the same profiles but the second method allowed much faster computation.

The procedure used a two pass method to eliminate extreme outlying values. Preliminary statistics were calculated using a sample size of 300 points. The calculation then proceeded on the full sample with any points more than 4 standard deviations from the mean being excluded. If more than 2.5% of the points were thus excluded the calculation was repeated once more using the new mean and standard deviation. Generally, less than 1.0% of the readings were excluded.

It was also necessary to correct the vertical coordinate for refraction. The following formula was used:

$$z = (z' - z'_I)\,\frac{n}{\cos(\phi/2)}\,\sqrt{\left(1 - \frac{\sin^2(\phi/2)}{n^2}\right)} \qquad (213)$$

where:

z = distance from the inside of the bed to measuring point.

z' = traverse reading.

z'_I = is traverse reading when measuring point is focused on the inside of the wall.

n = refractive index of water (1.33)

ψ = beam intersection angle

For each location the coordinates and the 5 statistics were recorded on floppy disk for later retrieval and analysis.

The data was taken in the form of vertical profiles starting as close to the bed as possible and proceeding upward to the surface. Eleven profiles were taken at each section with about twenty points on each profile. The spacing of the points was about 0.1 mm near the bed to about 6-10 mm through the upper part of the flow. The approximate bed location was noted at the start of each profile. It was not possible to make measurements near the water surface because of reflections from the undulating free surface.

3.3 EXPERIMENTAL RESULTS

The significant details of the two experiments performed are given in Table 4.

Table 4. Significant details of the experiments

Run	R_0 (m)	b (m)	H_0 (m)	U_0 (m/s)	S_0	b/R_0	b/H_0	H_0/R_0	F_R	R_e (x 10^{-4})	C_f
1	3.66	.533	.061	0.36	.00083	0.146	8.74	0.0167	.491	2.3	16.0
2	3.66	.533	.085	0.42	.00083	0.146	6.27	0.0232	.460	3.6	16.0

The entire set of data for Run 1 is reproduced in Figures 23 to 87. The information of u velocity, v velocity, $\overline{u'^2}$ fluctuation intensity, $\overline{v'^2}$ fluctuation intensity for each of thirteen sections are shown on separate plots. An additional plot for each section shows the u velocity with the vertical scale magnified focussing on the region very close to the bed. All dimensions are in millimetres.

The figures are organized to show the variation of the quantity around the bend so the u profiles are shown in sequence followed by expanded u profiles, lateral velocity profiles and turbulence profiles. The second run is not shown since the parameter differences from the first run are not large enough to result in any significant qualitative difference. All of the data for both runs is available from the writer in the form of tables or on computer tape.

The u velocity profiles in particular show an interesting variation. The first two sections, before the start of the bend, have an almost uniform lateral distribution with only the two outermost profiles being noticeably different. The next profile, just past the start of the bend and the one after it show the velocity larger on the inside of the channel than on the outside. The furthest outside profile is already catching up to the rest by the fourth section, however. The fifth and sixth sections show the two inside profiles falling off while the rest become almost uniform again (the sixth section is 90° into the bend). Subsequent profiles, up to the eleventh show a consistent spreading out of the profiles with the velocity increasing at the outside and decreasing at the inside of the bend. The twelfth section, just past 270° (the end of the bend) shows a sudden increase of velocity skewness from the eleventh section and the thirteenth shows an even larger variation. The shape of the velocity profiles in the latter sections of the bend are also significantly different from the corresponding straight channel profiles. They are almost uniform and in some cases receding through the greater part of the channel whereas in the straight channel the profiles increase throughout the depth.

The expanded u velocity profiles indicate much the same variation over the bend as the full profiles, although the slopes of the velocity profiles near the bed may be taken as indicative of the bed stress at that location. Many of these profiles appear not to pass through the origin, indicating a small error in fixing the bed location. This error is less than a few tenths of a millimetre.

The lateral velocity (v) profiles show the development of the secondary circulation around the bend. The profiles in the straight channel, especially the second one, also show evidence of the much smaller secondary flow expected in a straight channel. The maximum magnitude, near the surface at the furthest outside profiles, directed toward the centre of the channel and approximately symmetrical is about two per cent of the channel mean velocity.

At the third section, relatively large, inward corrected, lateral velocities are observed. This corresponds to the shifting of the longitudinal velocity maximum towards the inside here. At the fourth section the circulation profile is much more developed but now there is clearly a large mean outward component. Again this corresponds to a shifting longitudinal velocity profile. By the fifth section, the secondary circulation is fully developed and in fact appears to actually decline in magnitude through the rest of the bend. The furthest outside profile also shows evidence of a counterrotating circulation cell. The twelfth section also shows a net outward discharge and the thirteenth section, in the straight reach following the end of the bend shows the secondary circulation decaying.

The turbulence intensity profiles, first $\overline{u'^2}$ and then $\overline{v'^2}$ are also presented although interpretation is not simple. The measurements of $\overline{u'w'}$ turned out to be too small to show any systematic variation at all. Since this correlation corresponds to the turbulent stress that would act on the side walls it was expected to be very small through the main central part of the channel. In fact, it was smaller than the experimental scatter.

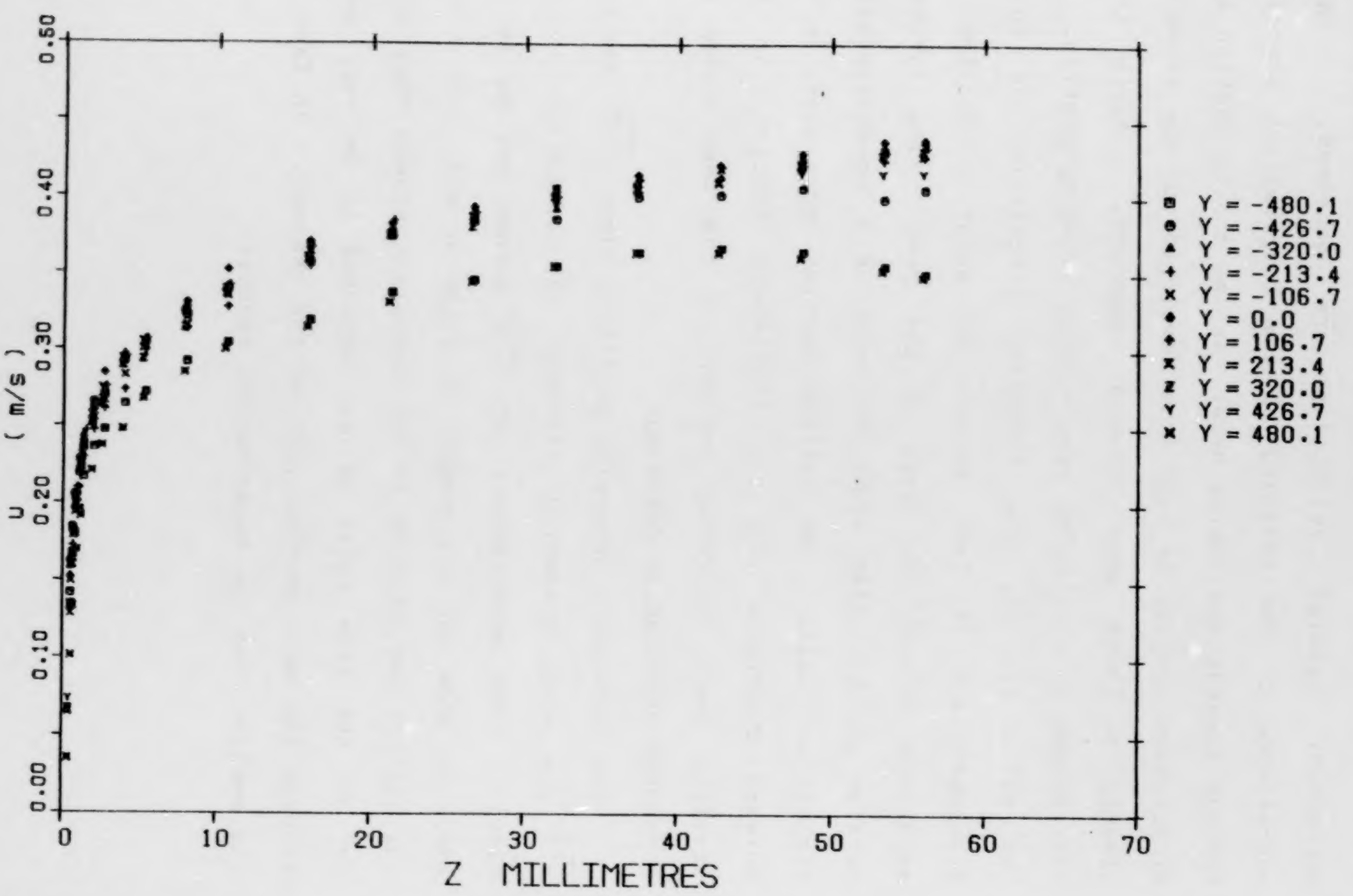

Figure 23. u Velocity Distribution (x = -2.20 m)

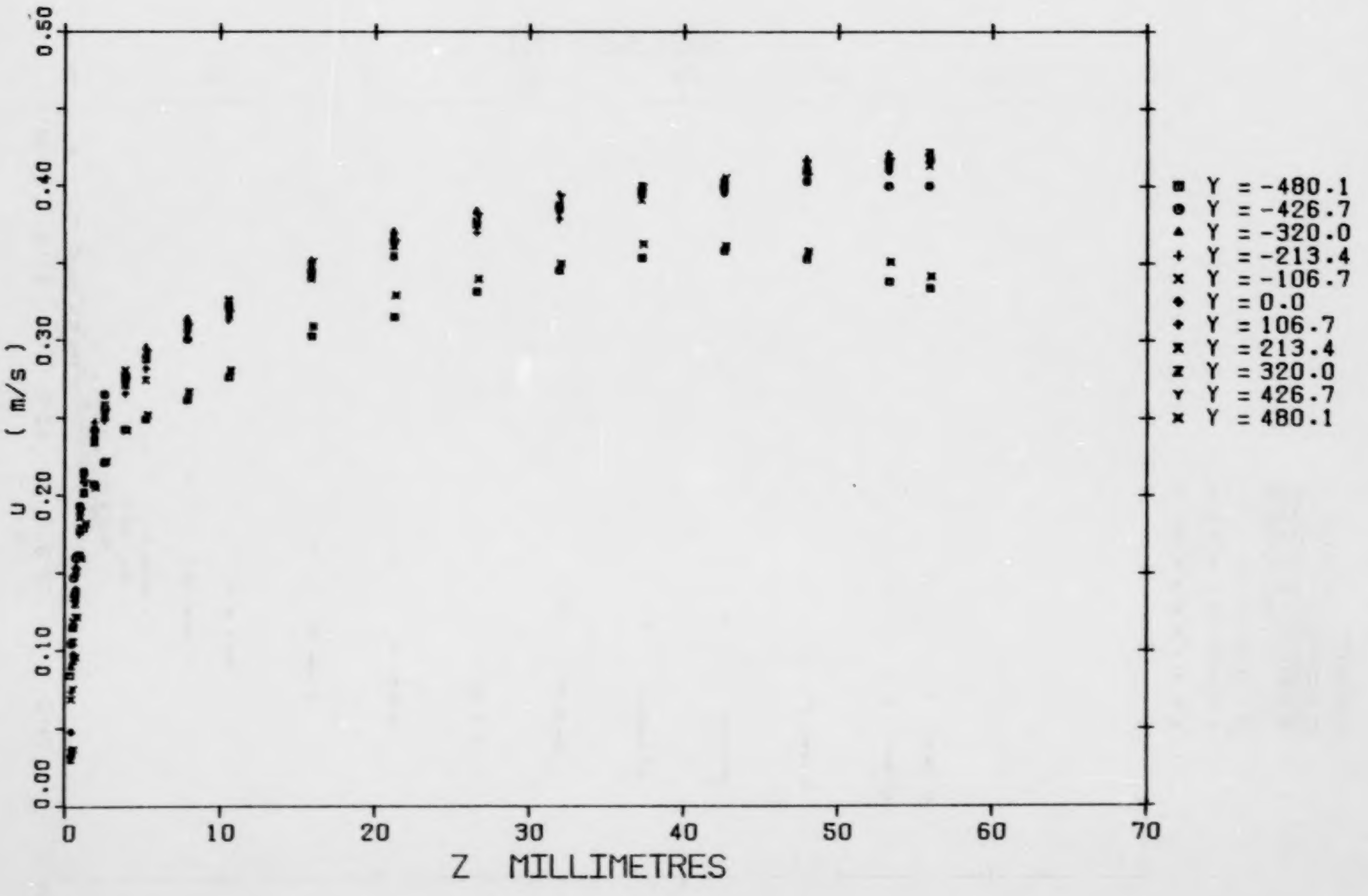

Figure 24. u Velocity Distribution (x = -0.69 m)

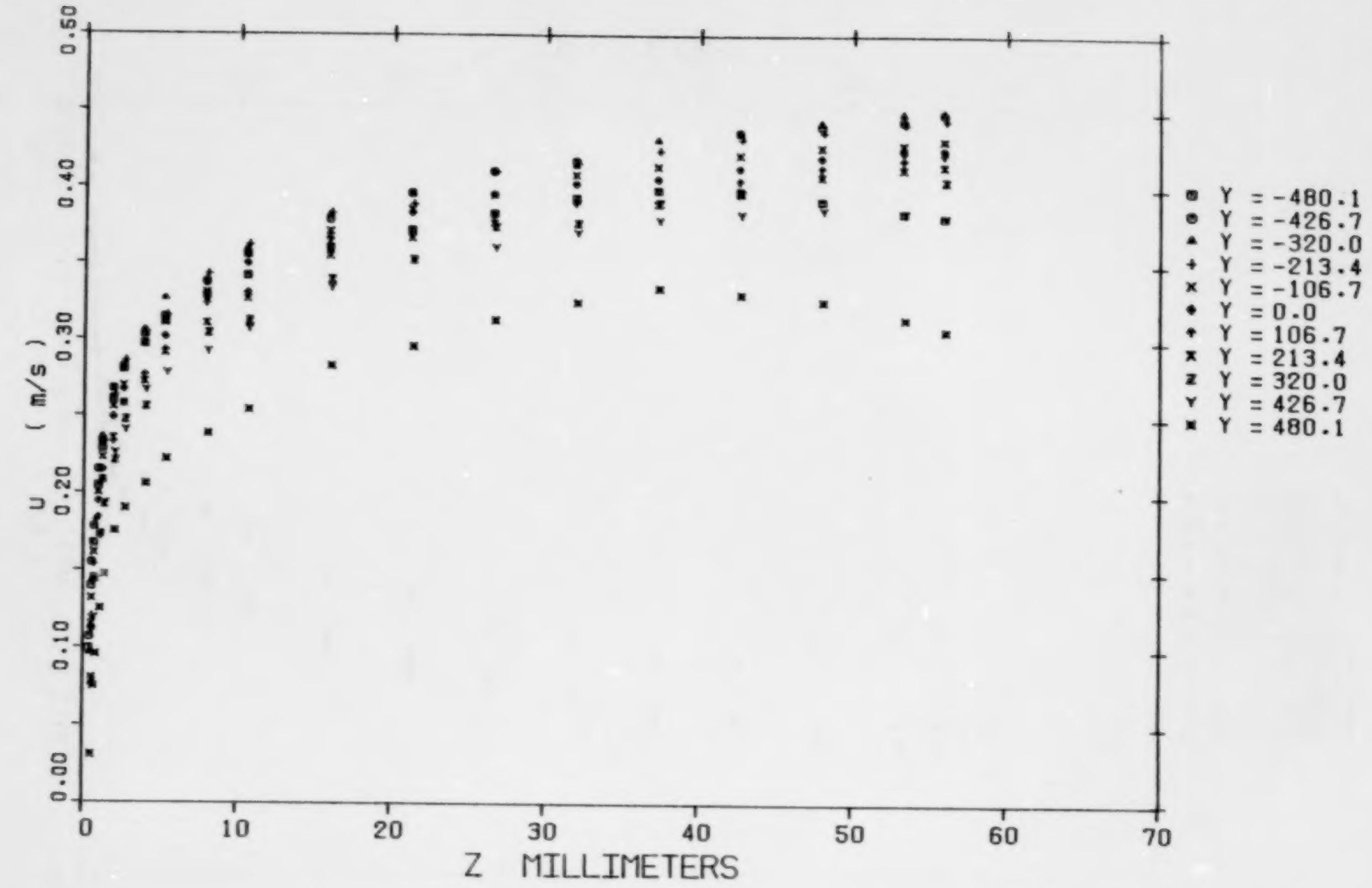

Figure 25. u Velocity Distribution (x = 0.05 m)

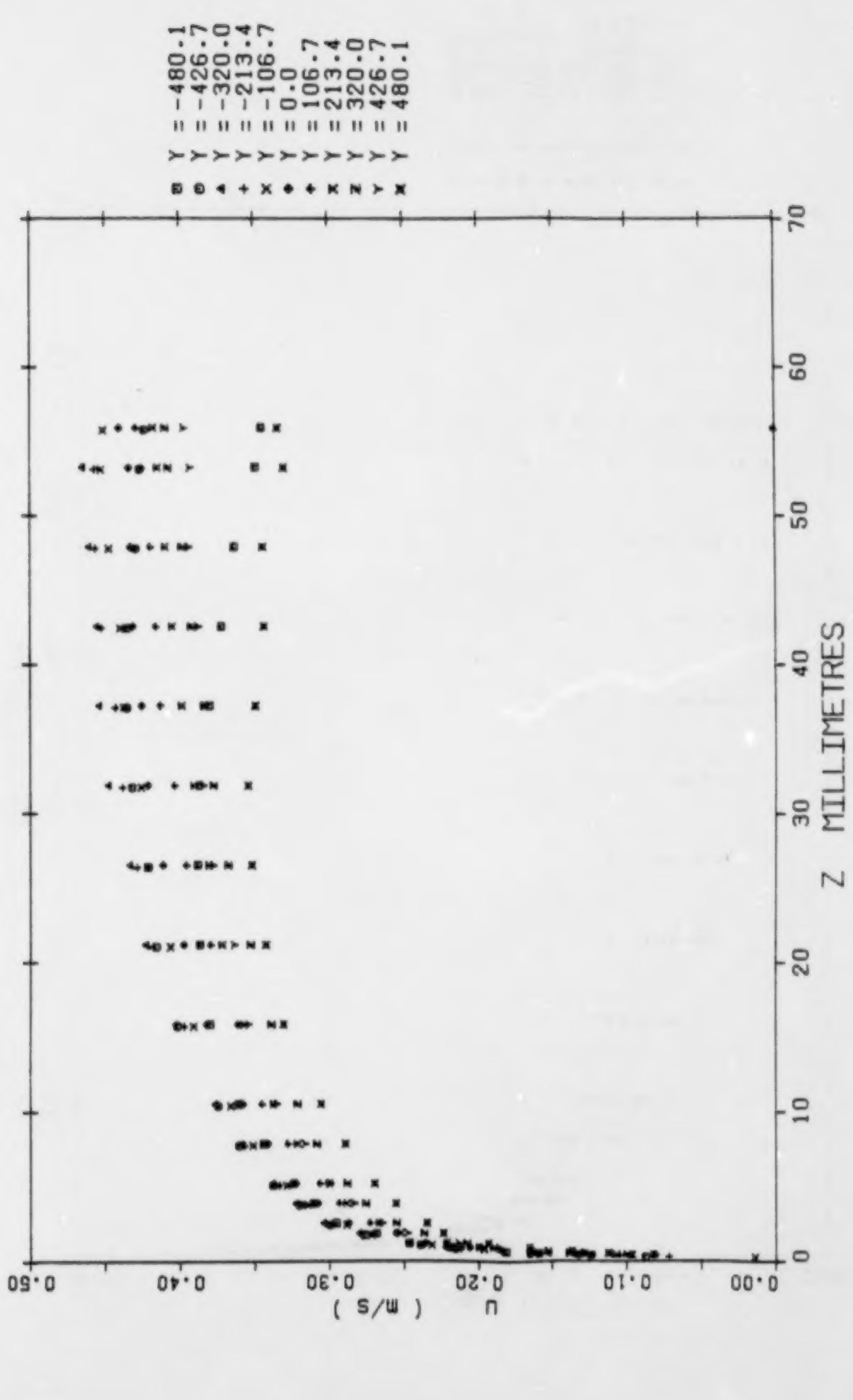

Figure 26. u Velocity Distribution (x = 1.92 m)

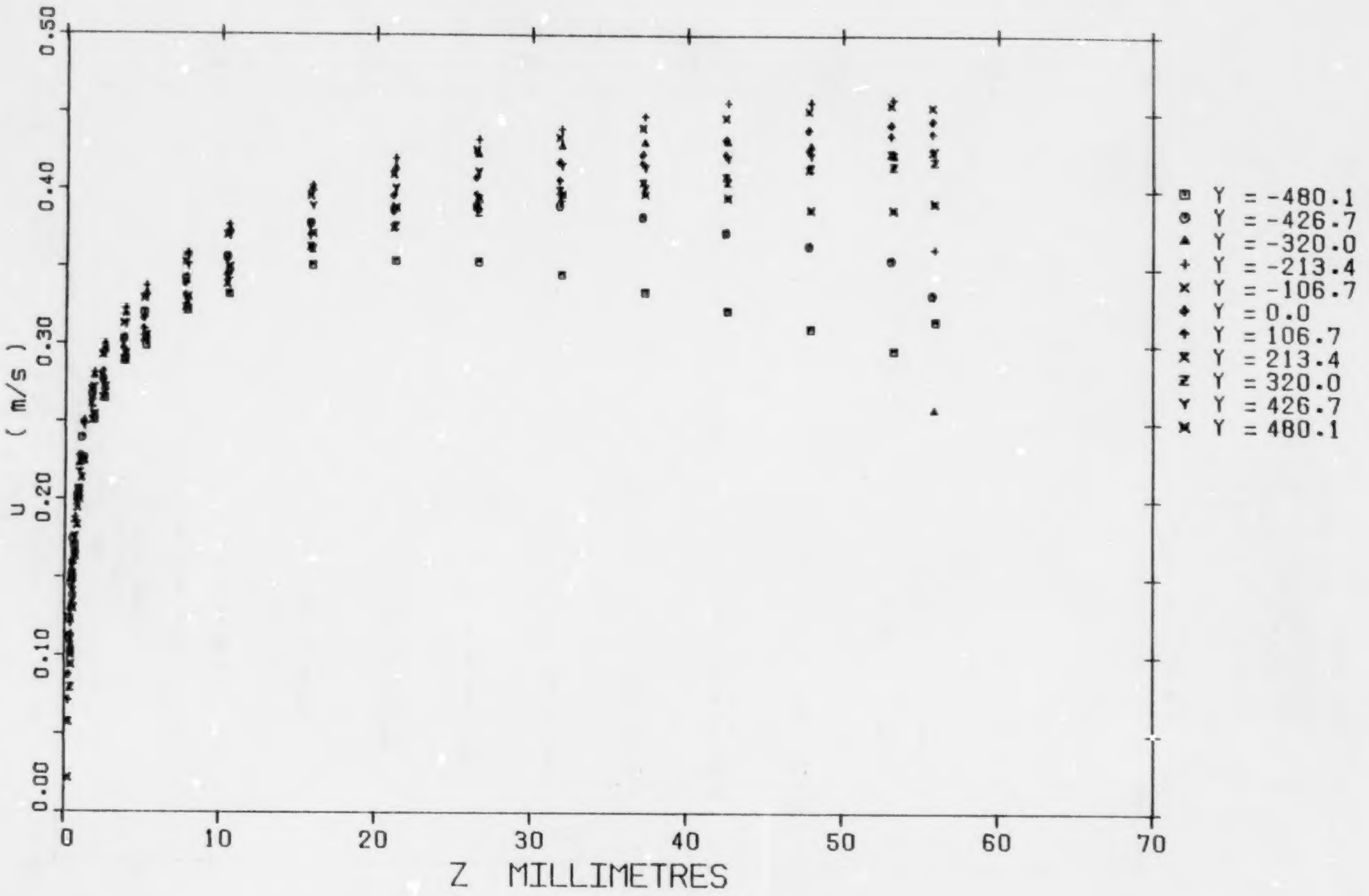

Figure 27. u Velocity Distribution (x = 3.83 m)

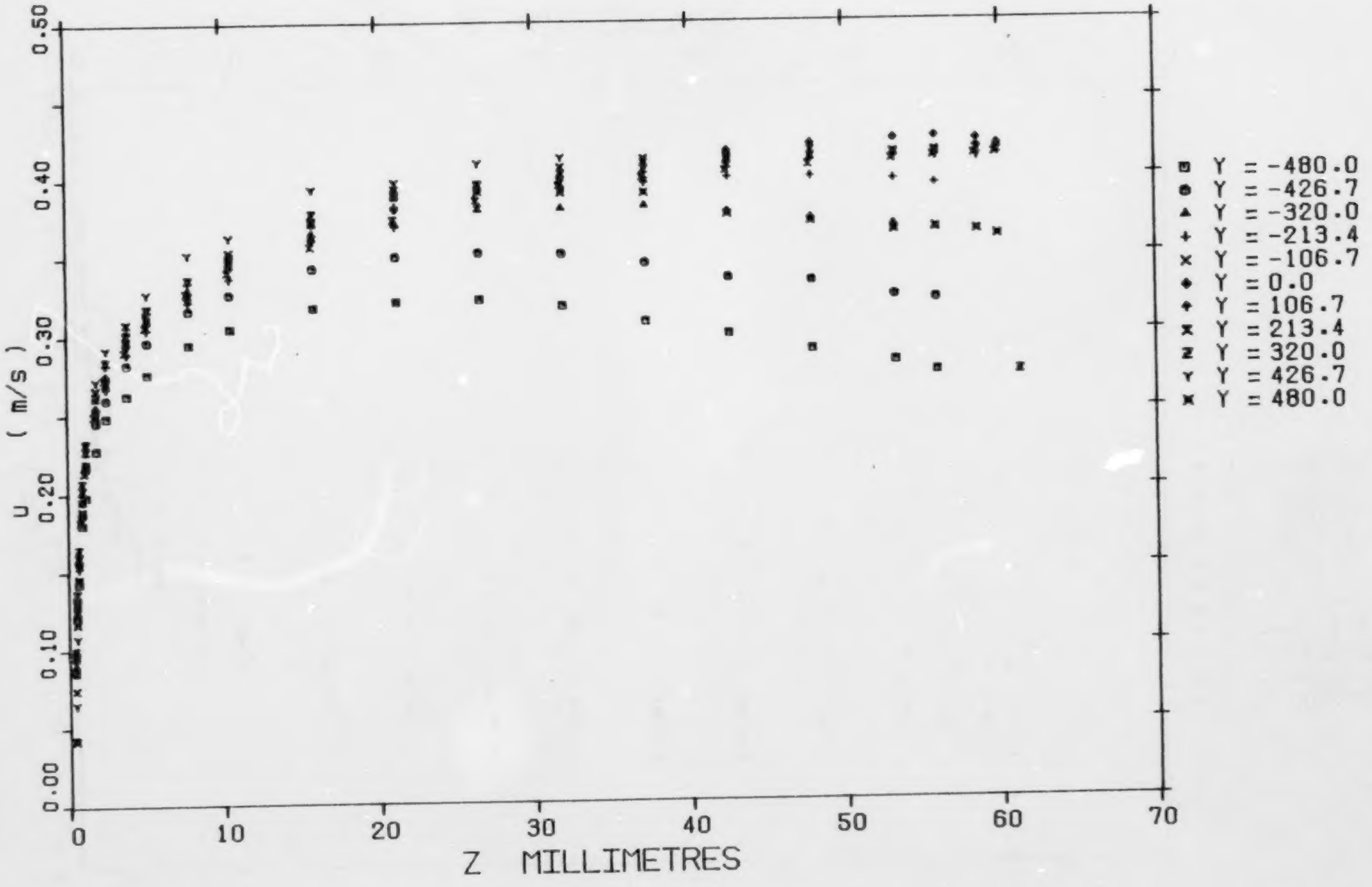

Figure 28. u Velocity Distribution (x = 5.75 m)

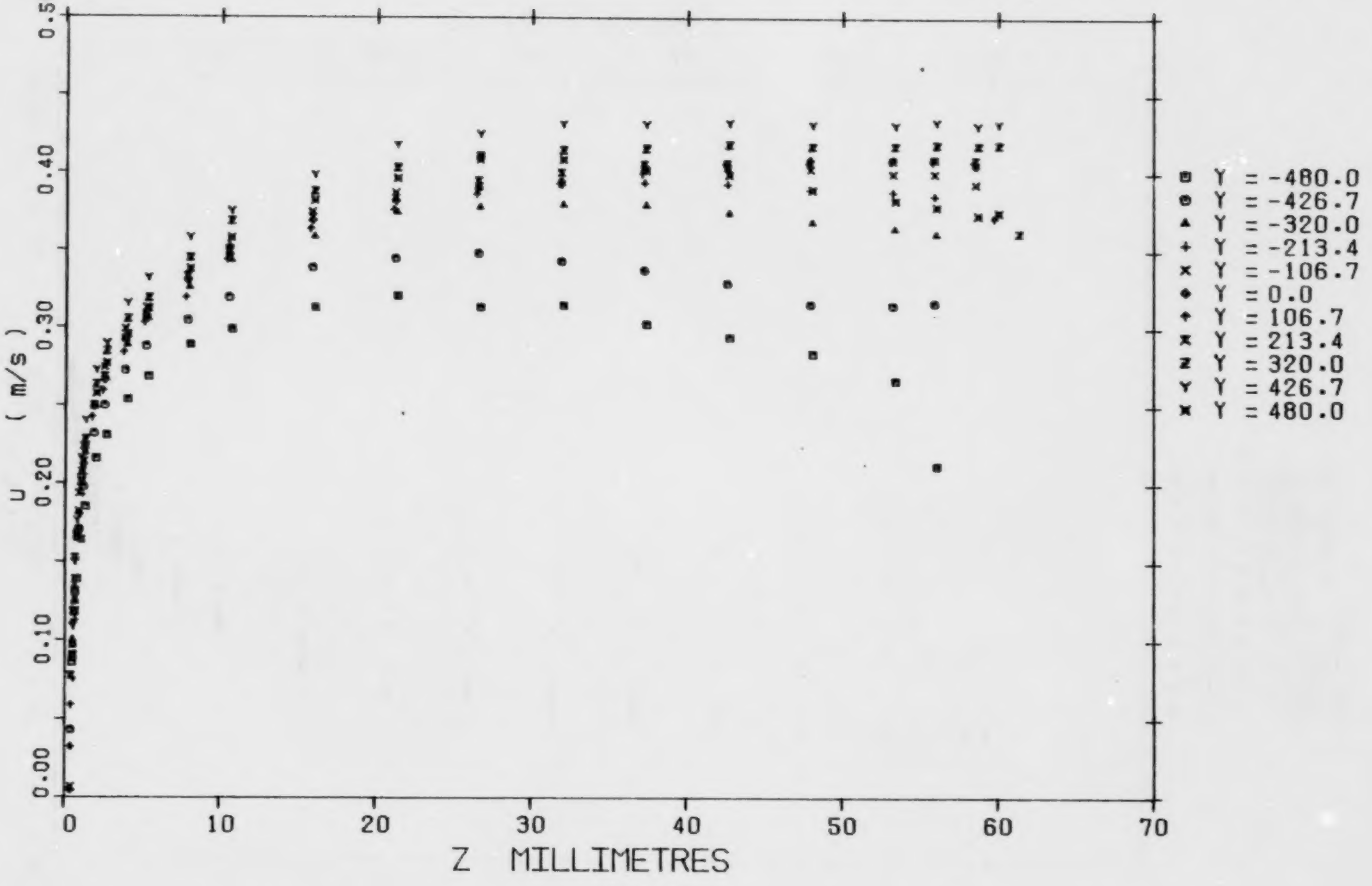

Figure 29. u Velocity Distribution (x = 7.66 m)

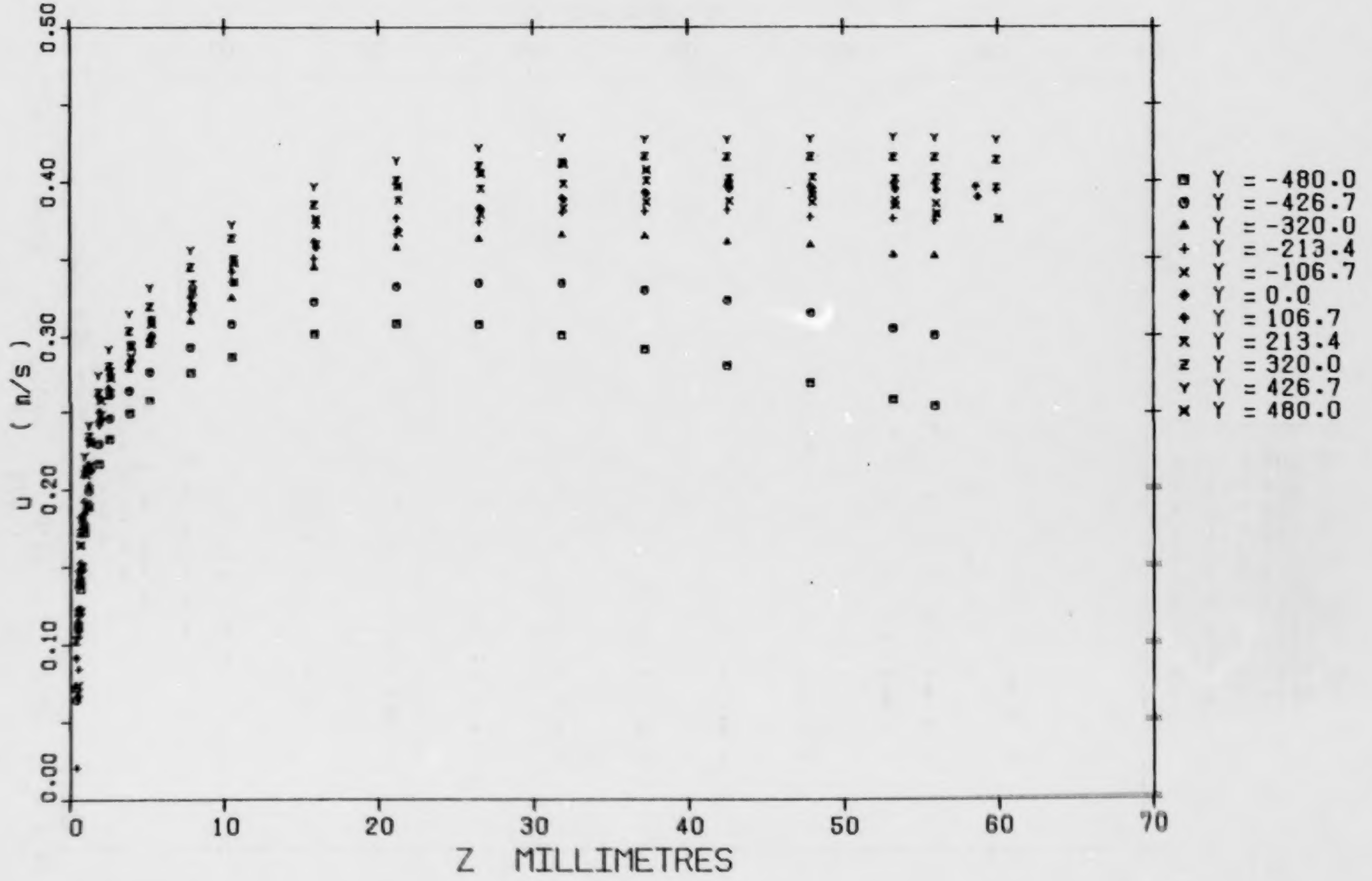

Figure 30. u Velocity Distribution (x = 9.68 m)

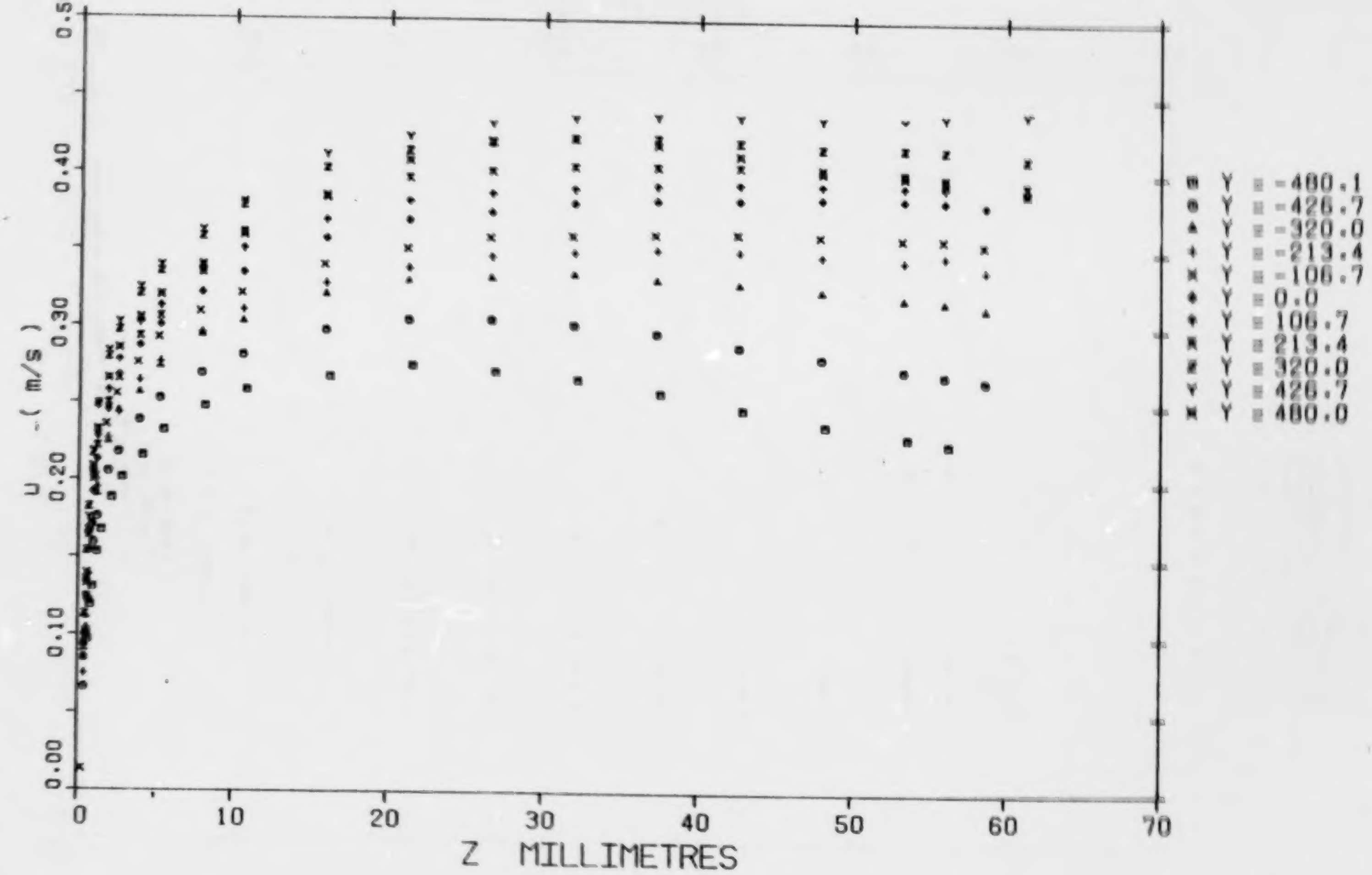

Figure 31. u Velocity Distribution (x = 11.49 m)

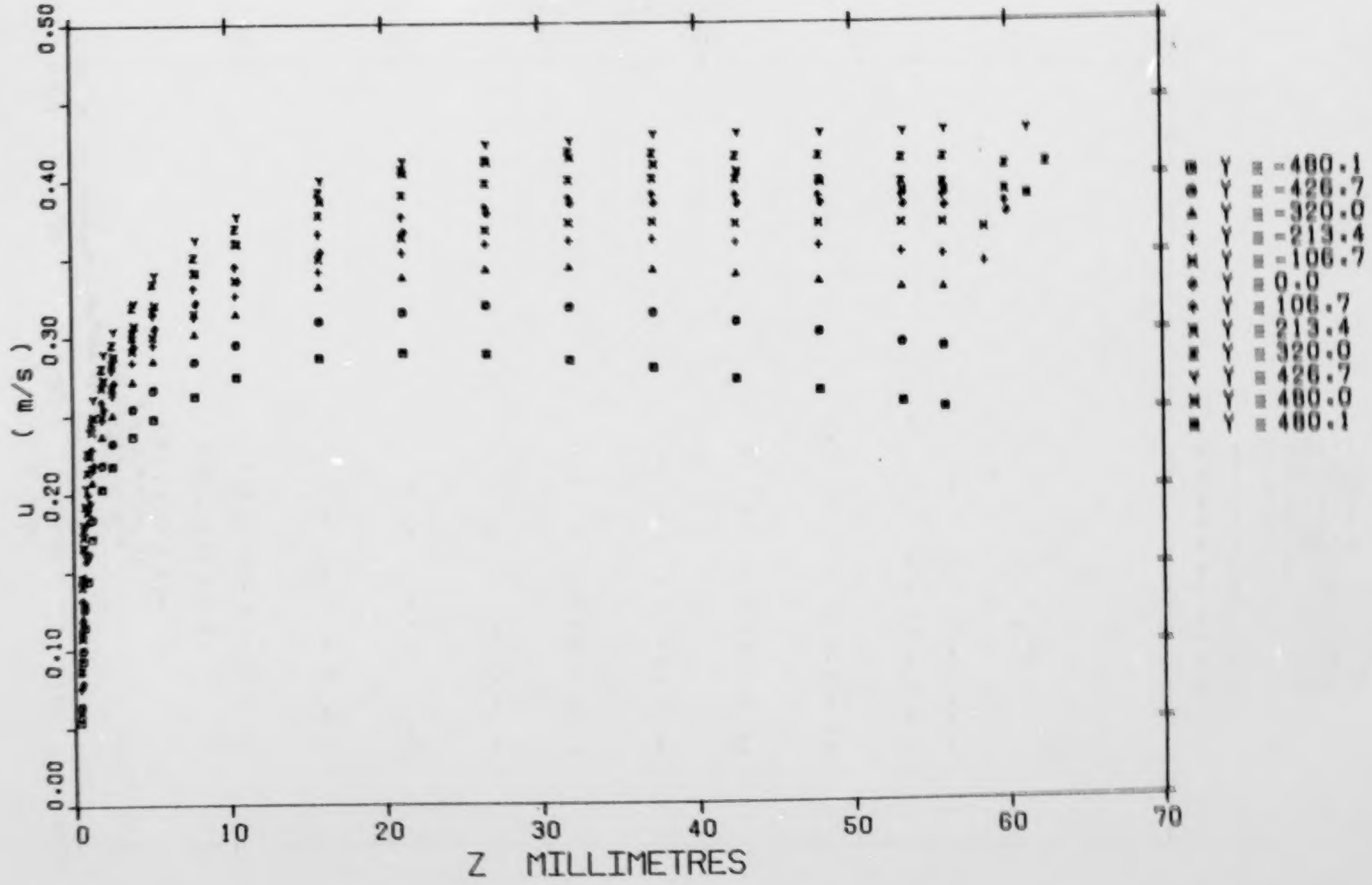

Figure 32. u Velocity Distribution (x = 13.41 m)

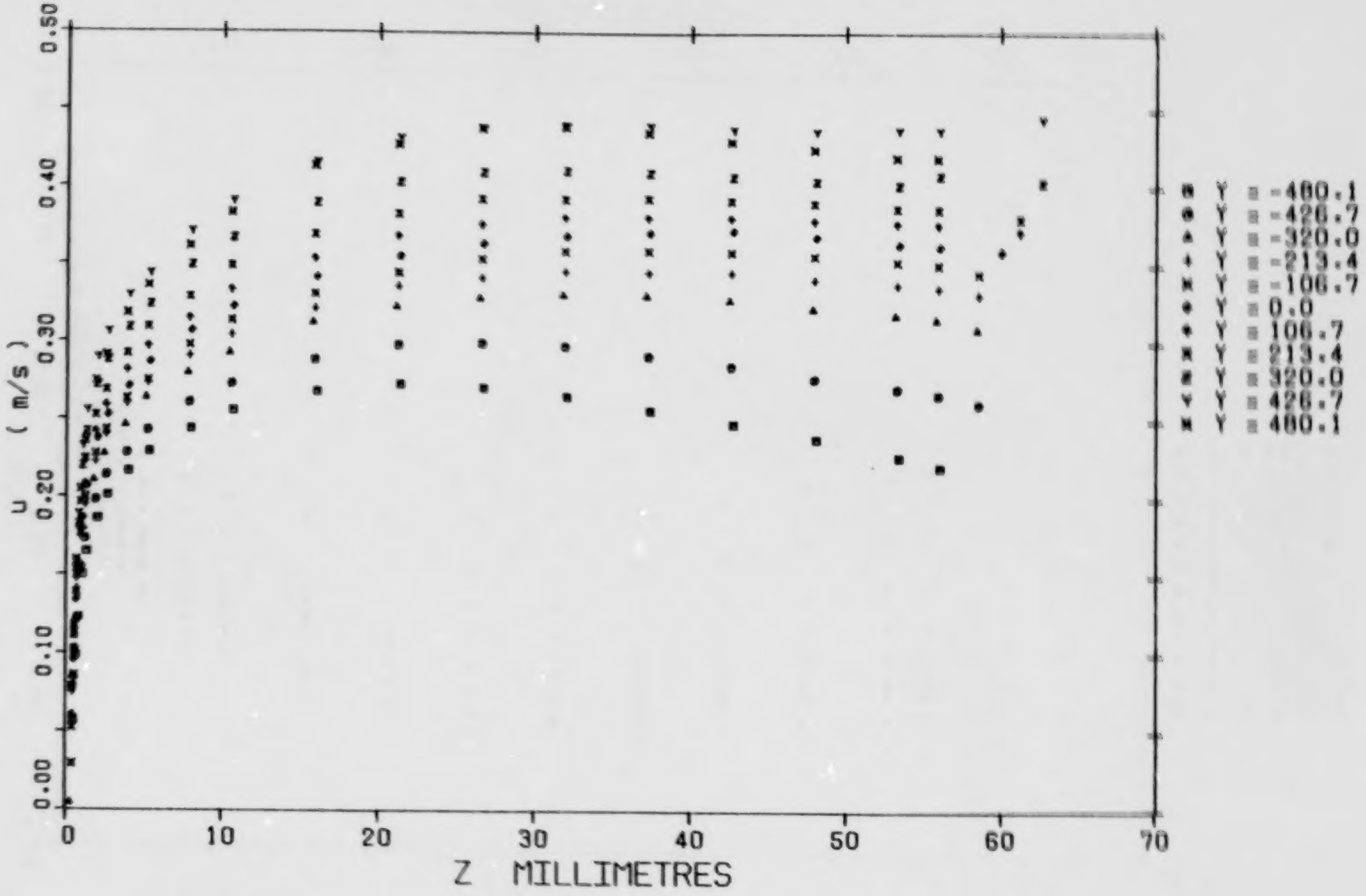

Figure 33. u Velocity Distribution (x = 16.18 m)

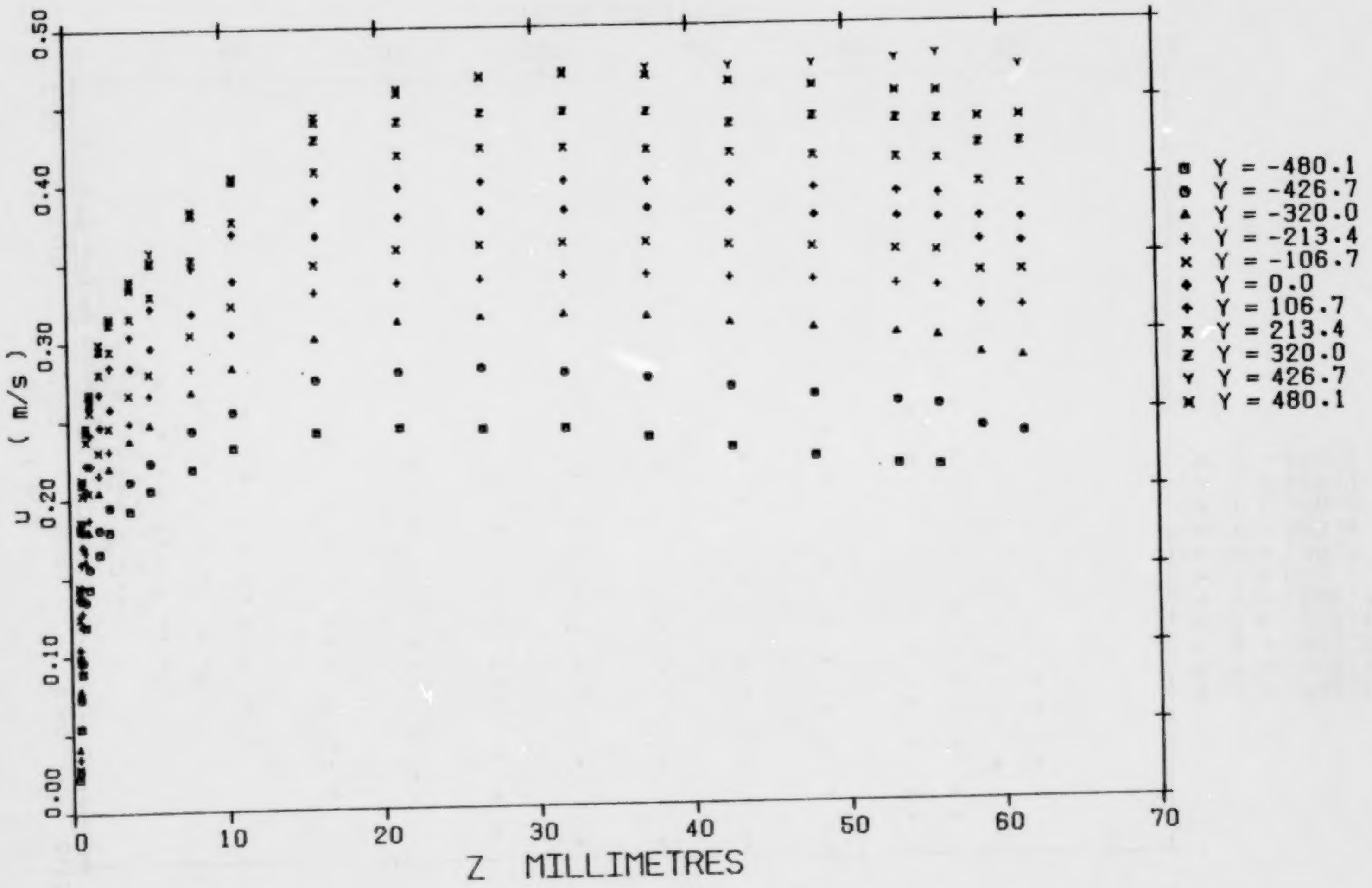

Figure 34. u Velocity Distribution (x = 17.43 m)

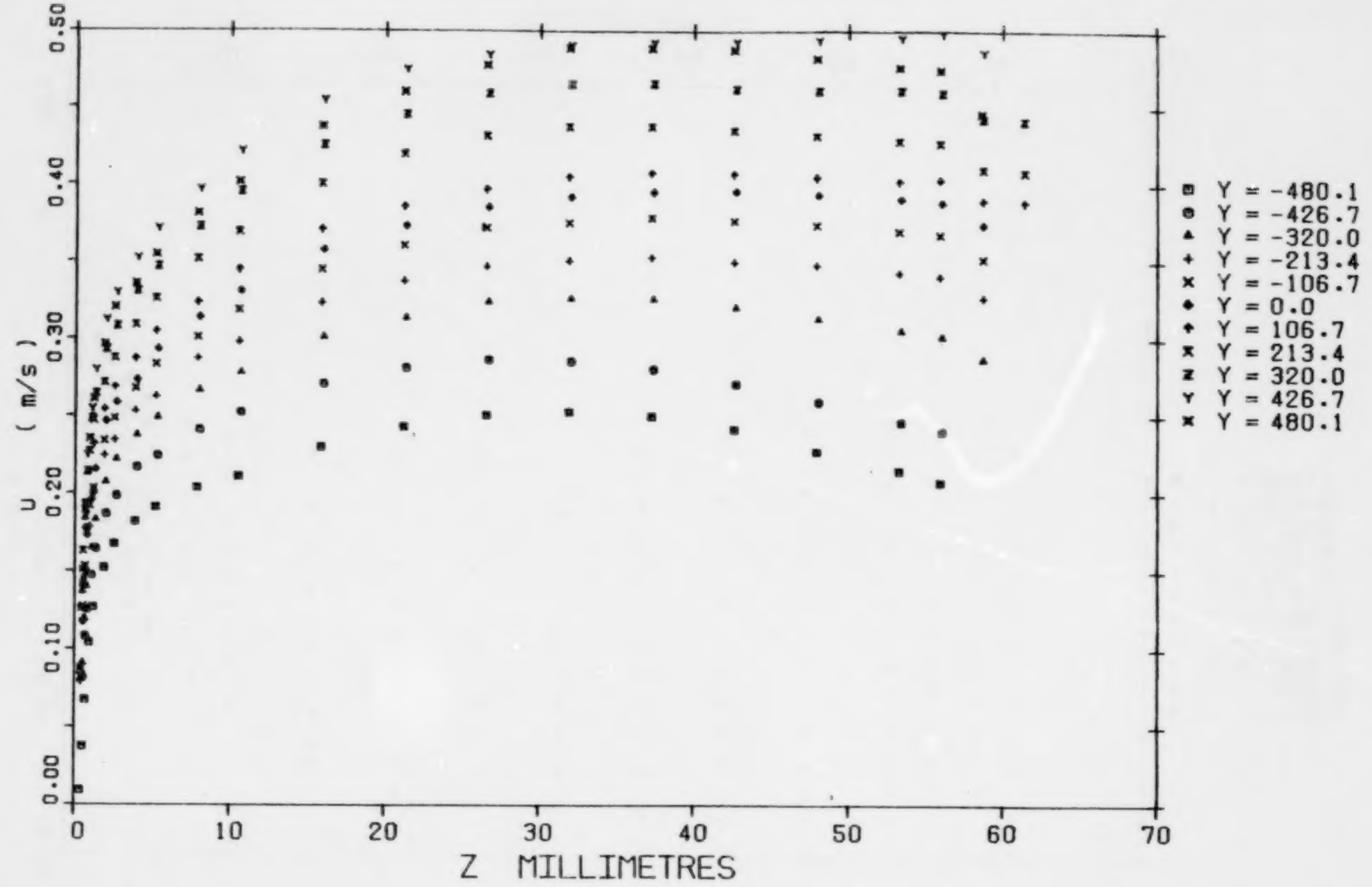

Figure 35. u Velocity Distribution (x = 18.65 m)

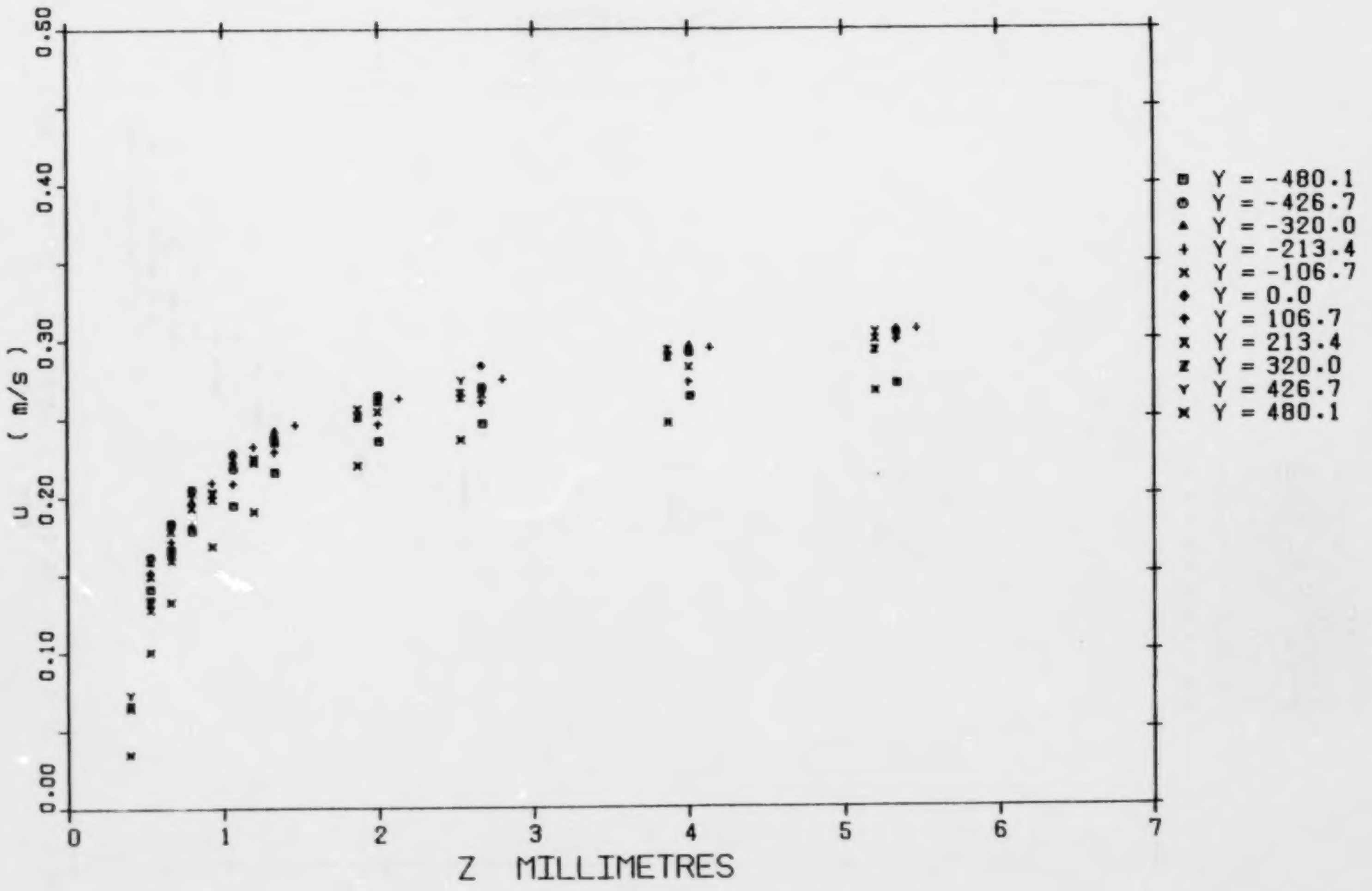

Figure 36. Expanded u Velocity Distribution (x = -2.20 m)

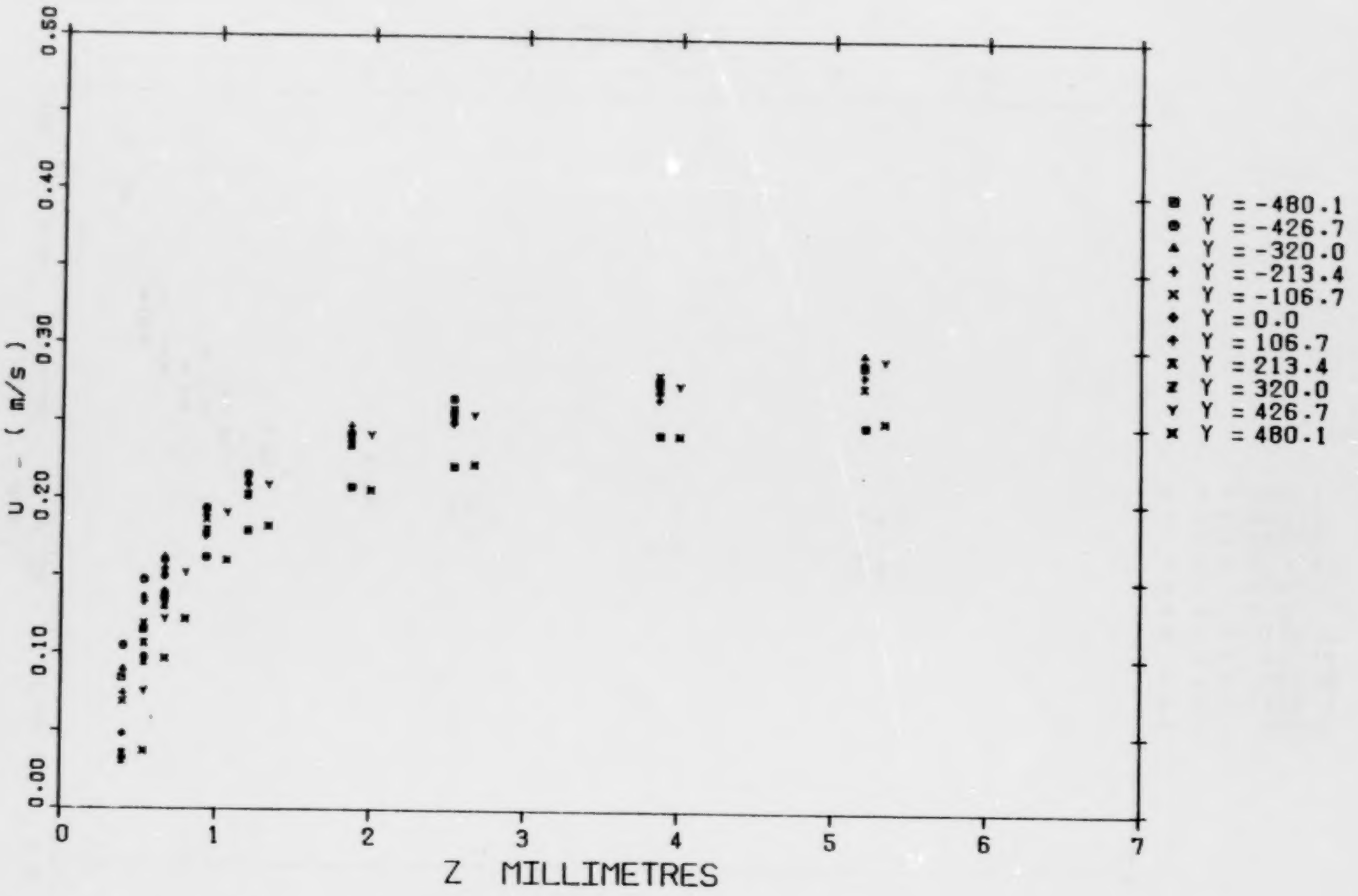

Figure 37. Expanded u Velocity Distribution
(x = 0.69 m)

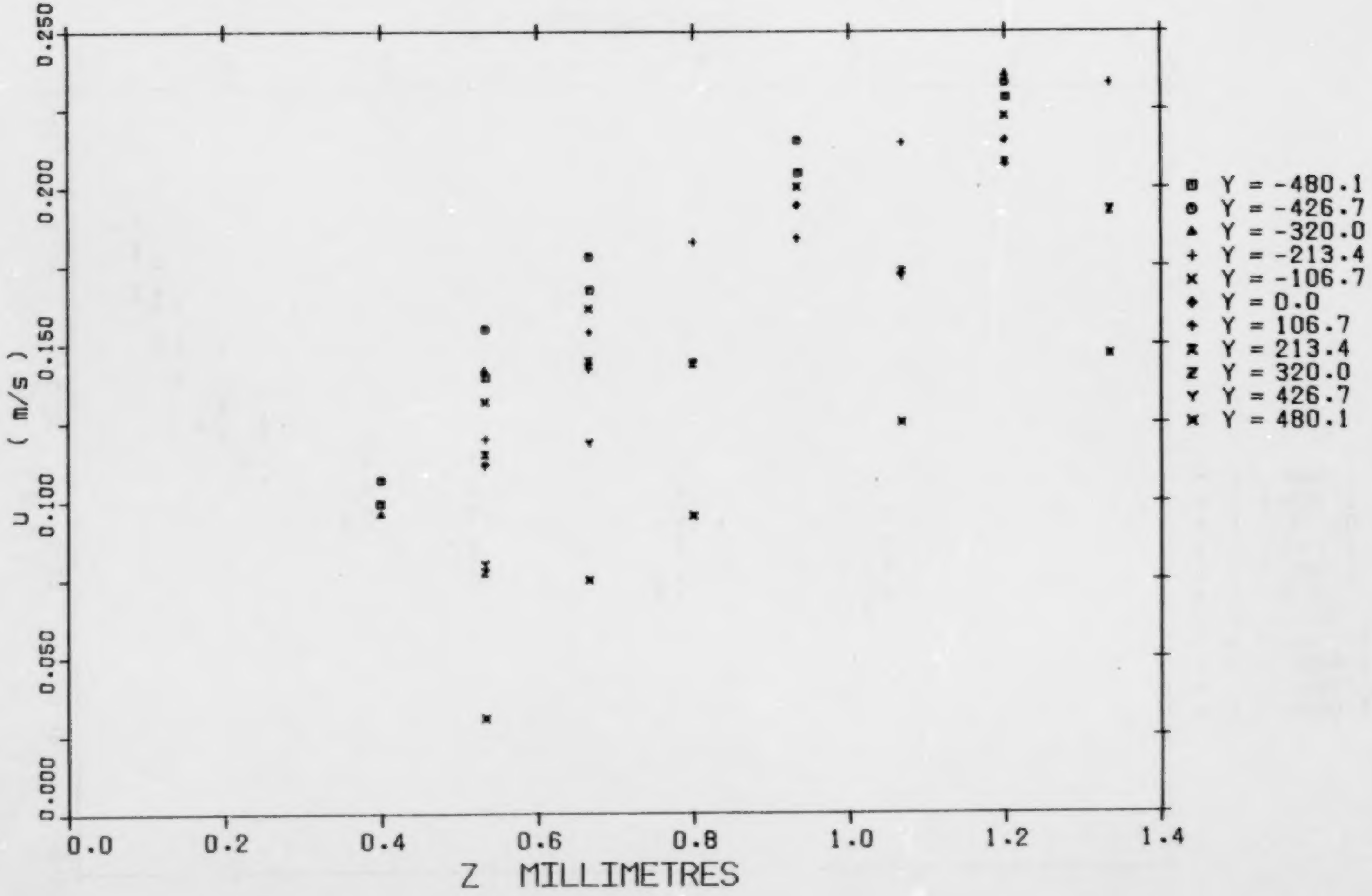

Figure 38. Expanded u Velocity Distribution
(x = 0.05 m)

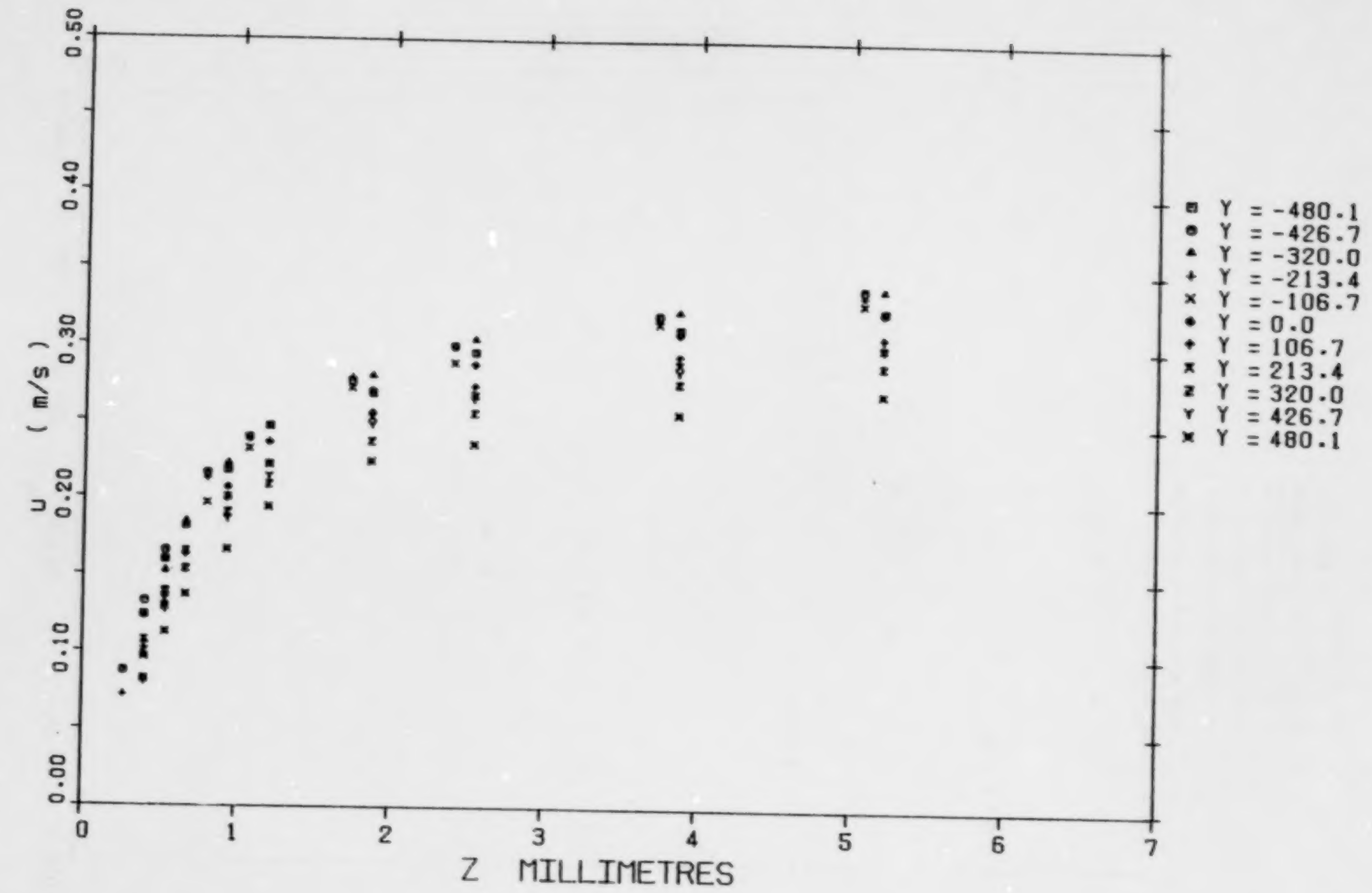

Figure 39. Expanded u Velocity Distribution
(x = 1.92 m)

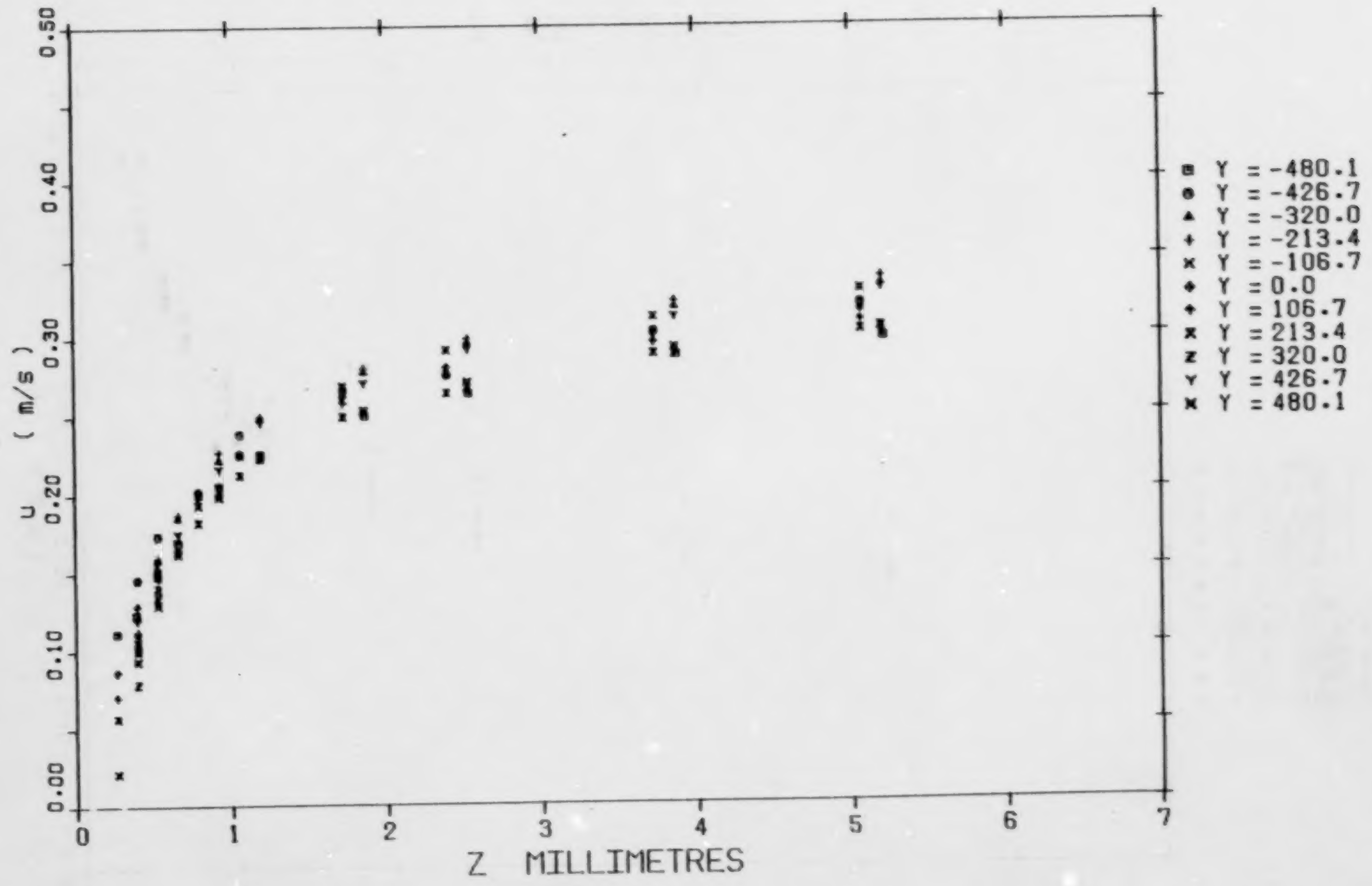

Figure 40. Expanded u Velocity Distribution (x = 3.83 m)

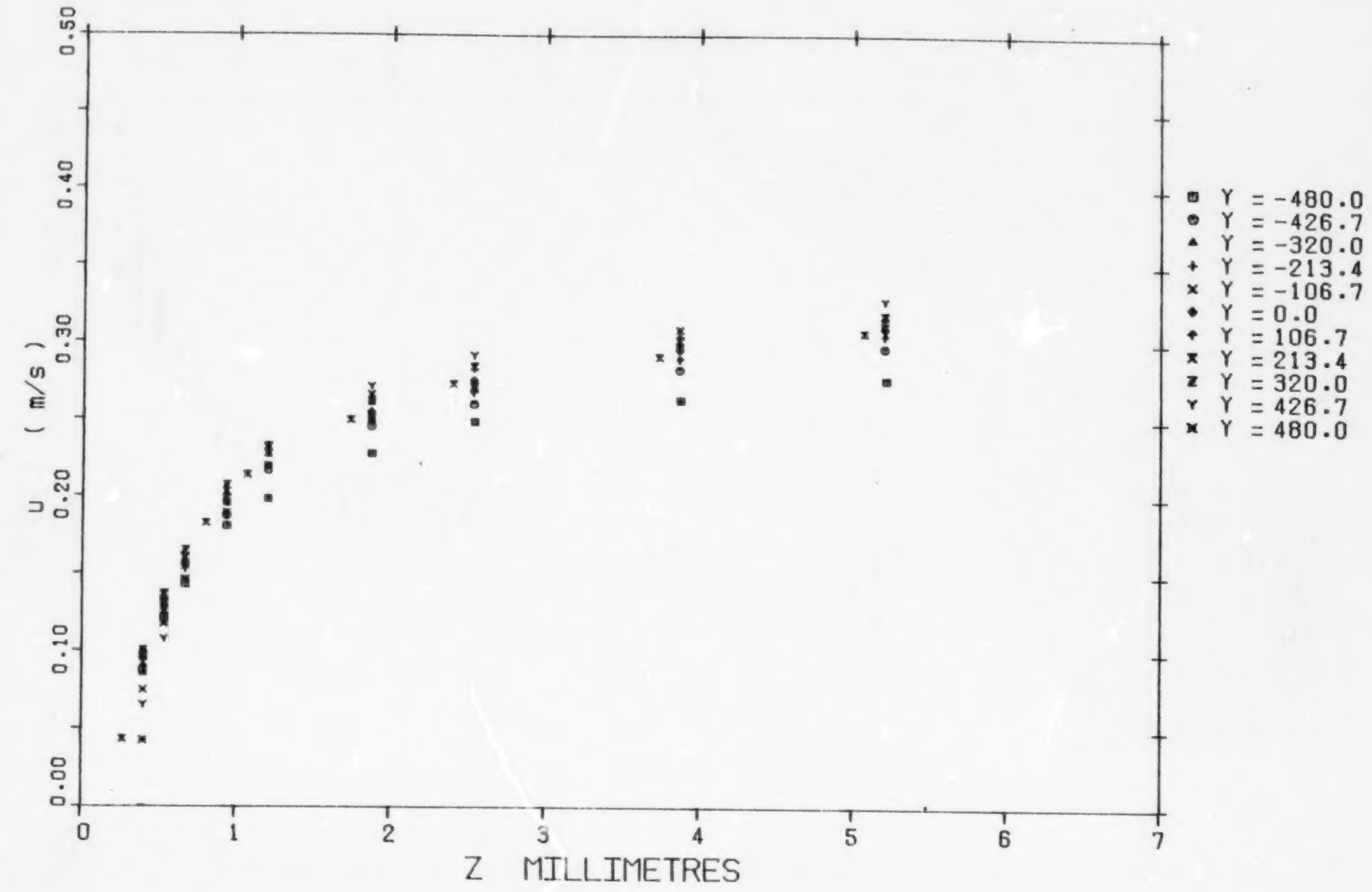

Figure 41. Expanded u Velocity Distribution (x = 5.75 m)

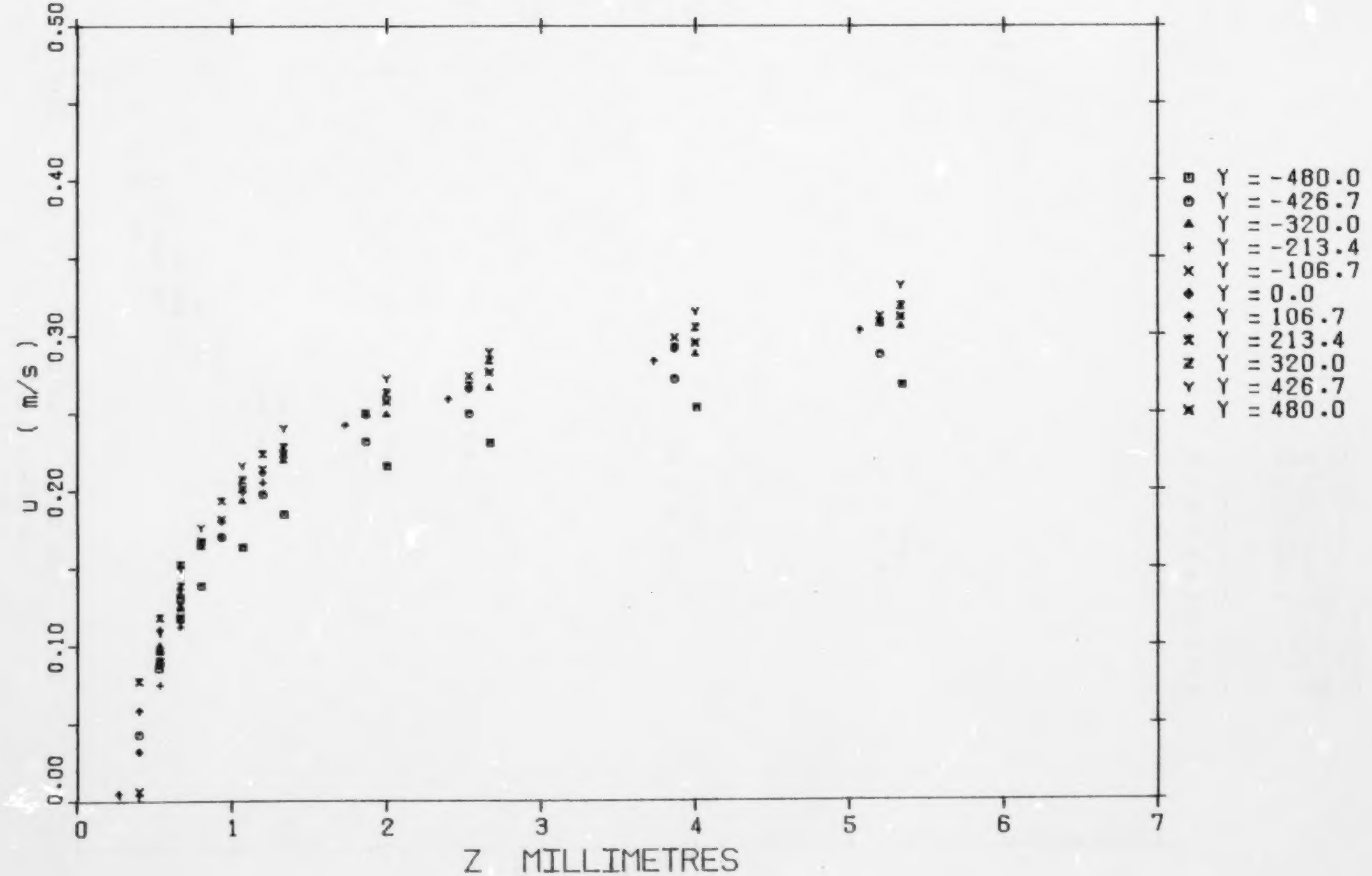

Figure 42. Expanded u Velocity Distribution (x = 7.66 m)

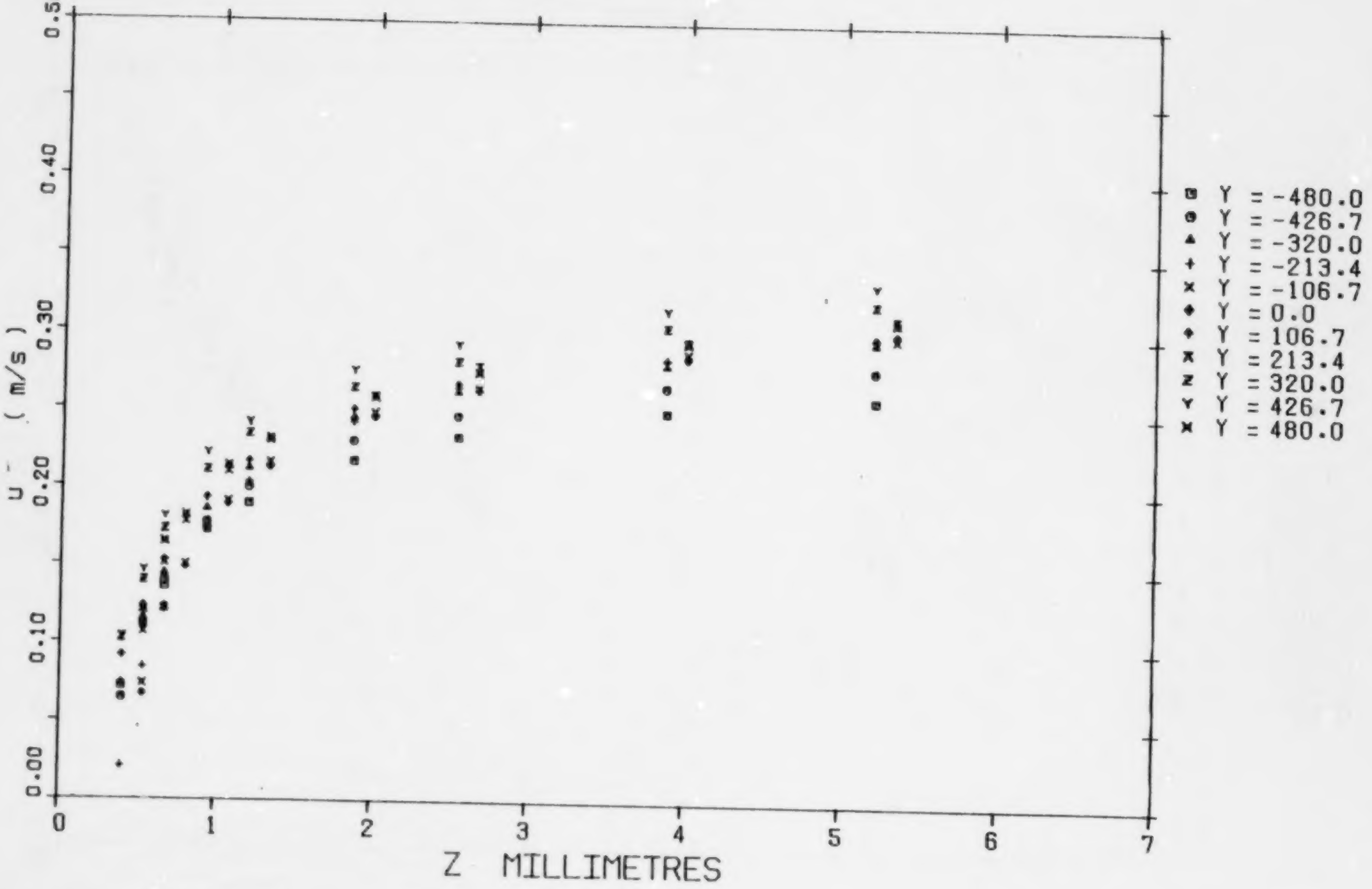

Figure 43. Expanded u Velocity Distribution
(x = 9.68 m)

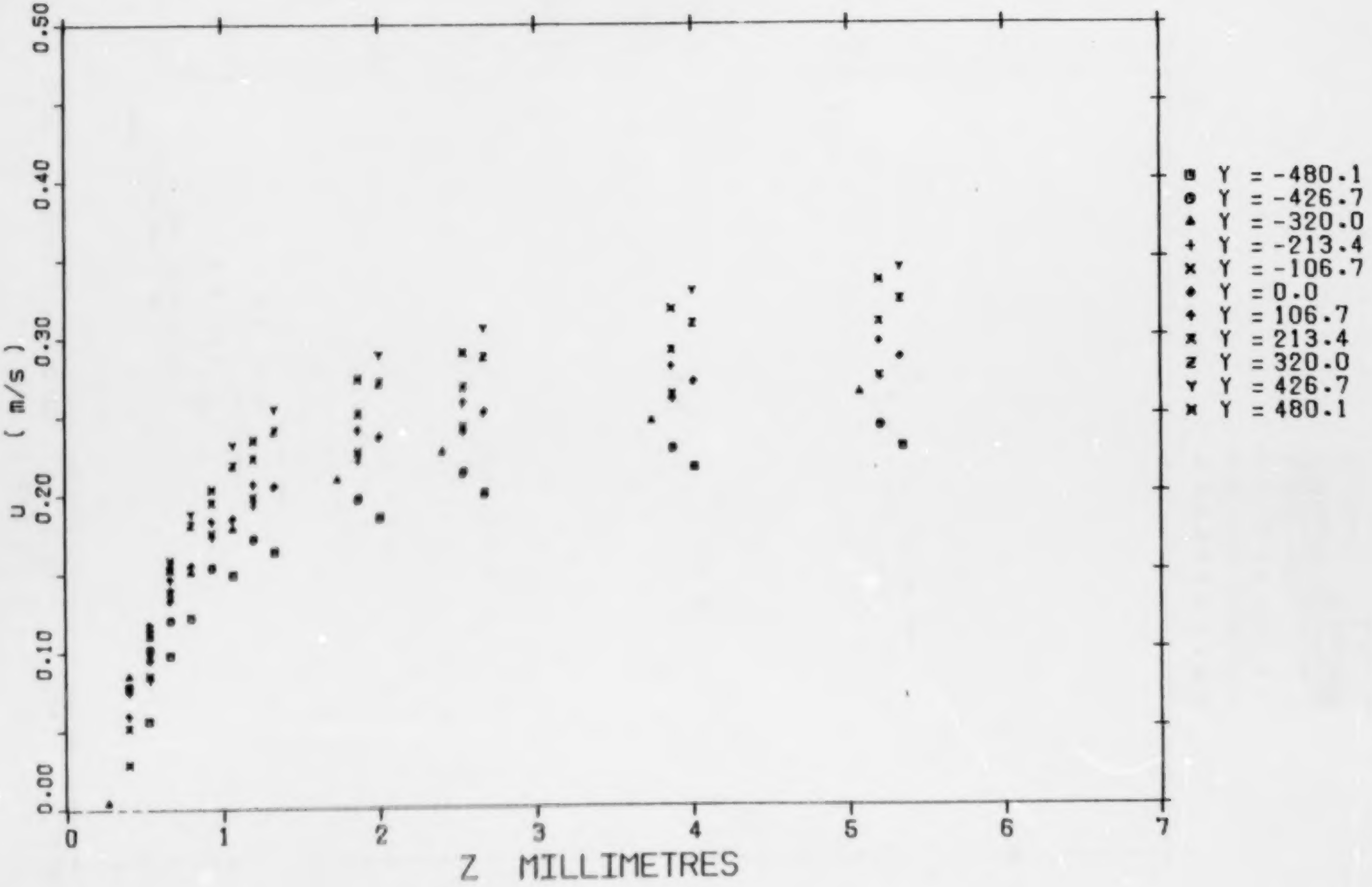

Figure 46. Expanded u Velocity Distribution
(x = 16.18 m)

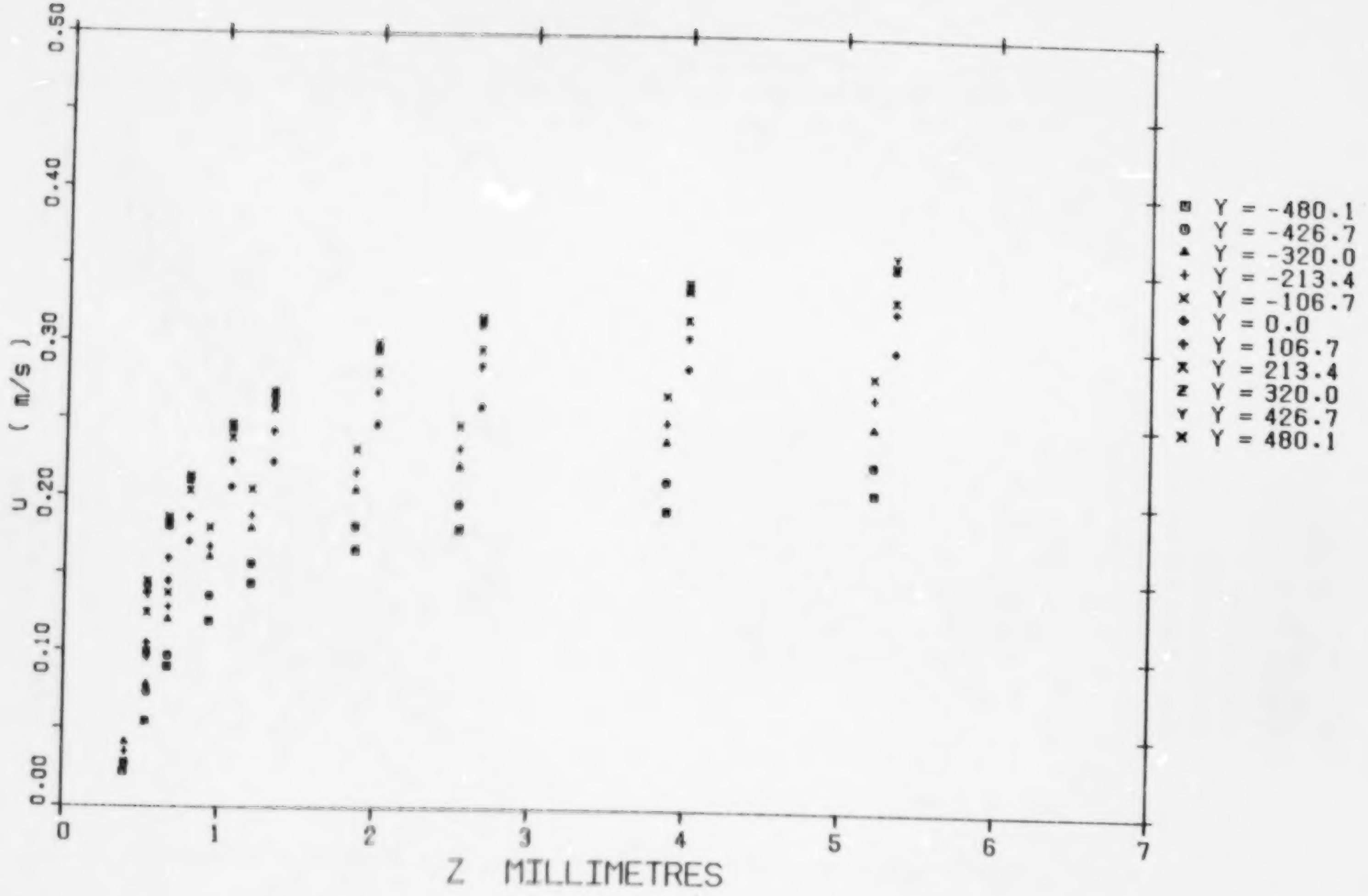

Figure 47. Expanded u Velocity Distribution
(x = 17.43 m)

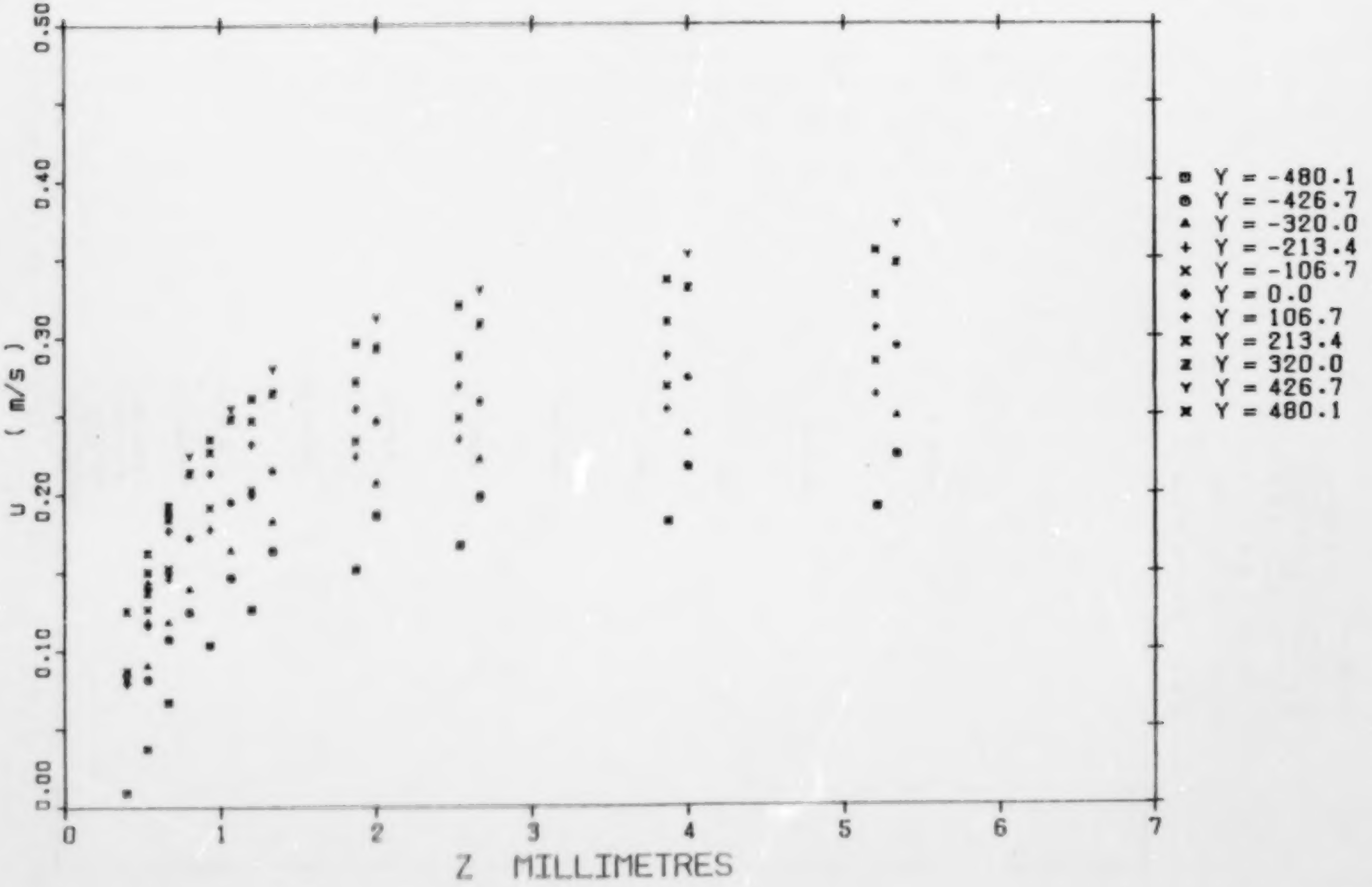

Figure 48. Expanded u Velocity Distribution (x = 18.65 m)

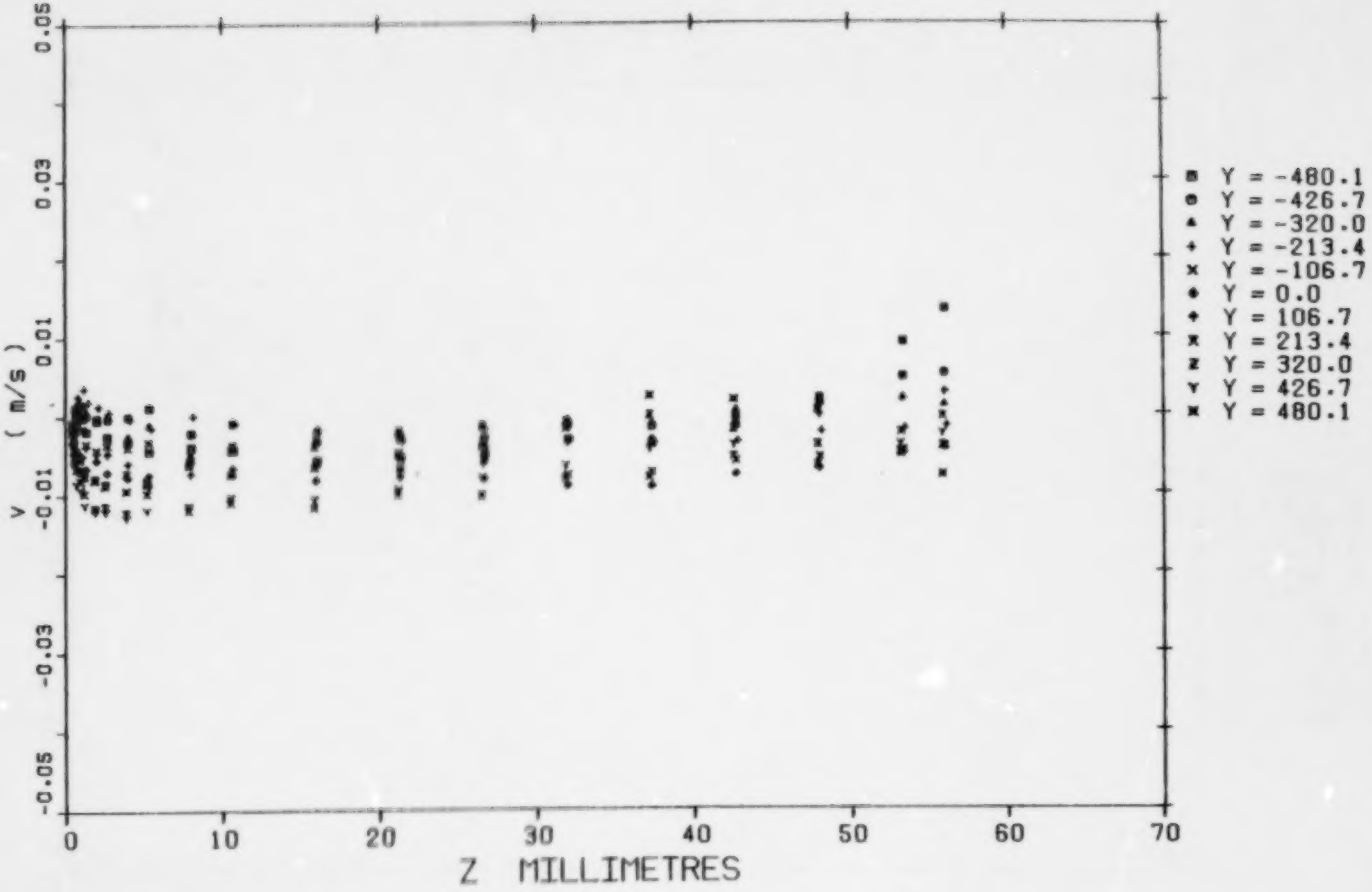

Figure 49. v Velocity Distribution (x = -2.20 m)

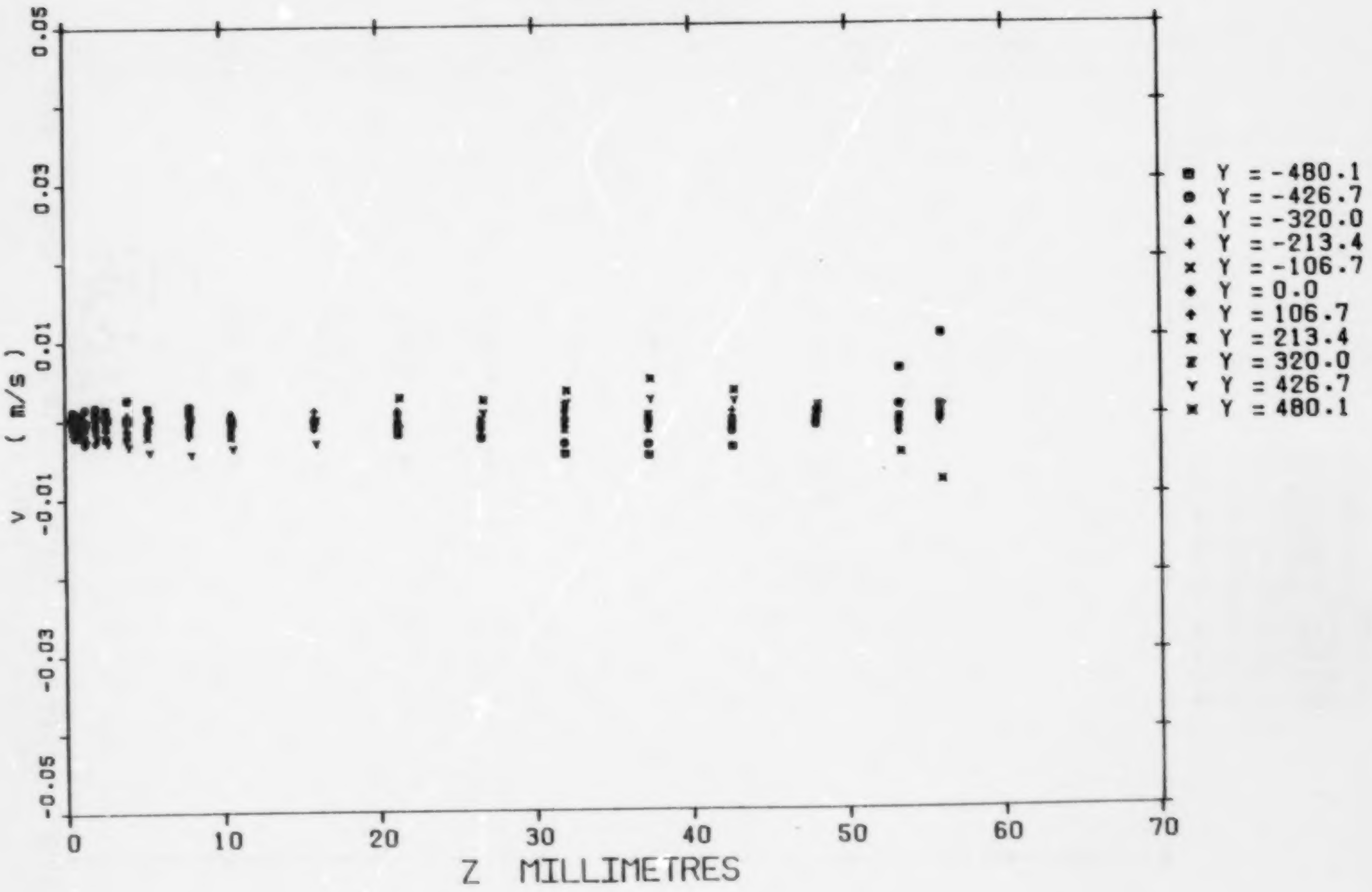

Figure 50. v Velocity Distribution (x = -0.69 m)

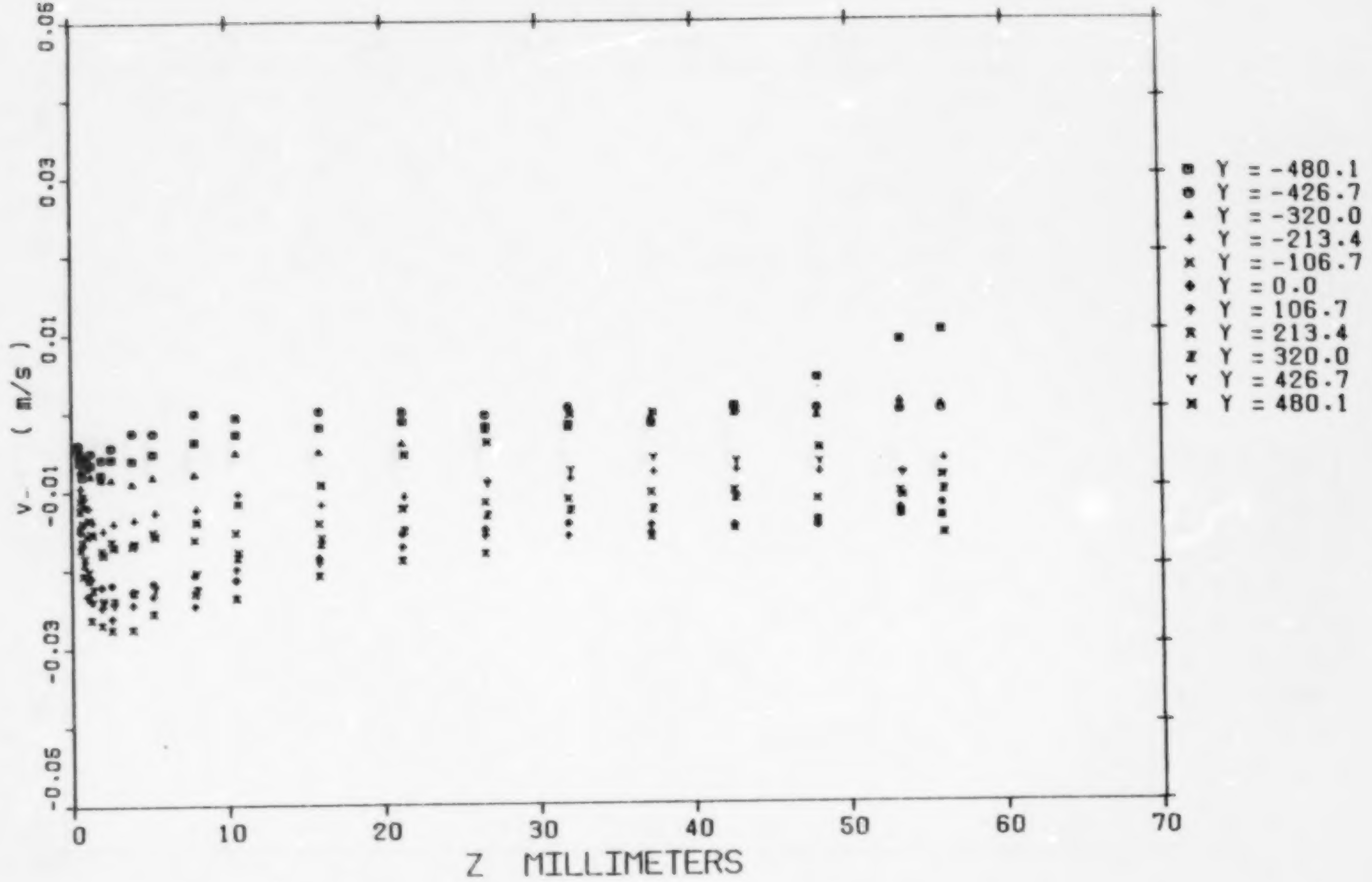

Figure 51. v Velocity Distribution (x = 0.05 m)

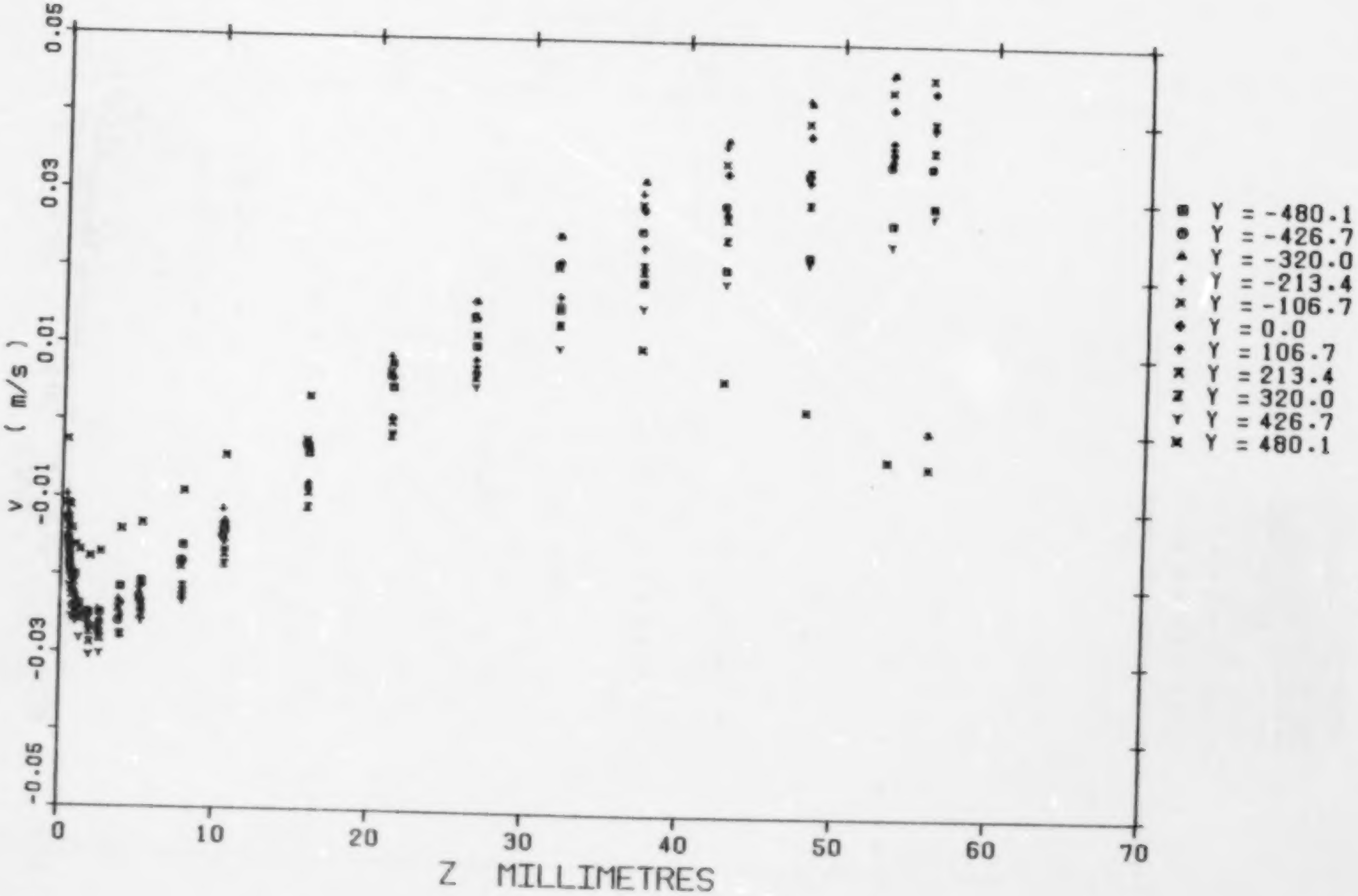

Figure 52. v Velocity Distribution (x = 1.92 m)

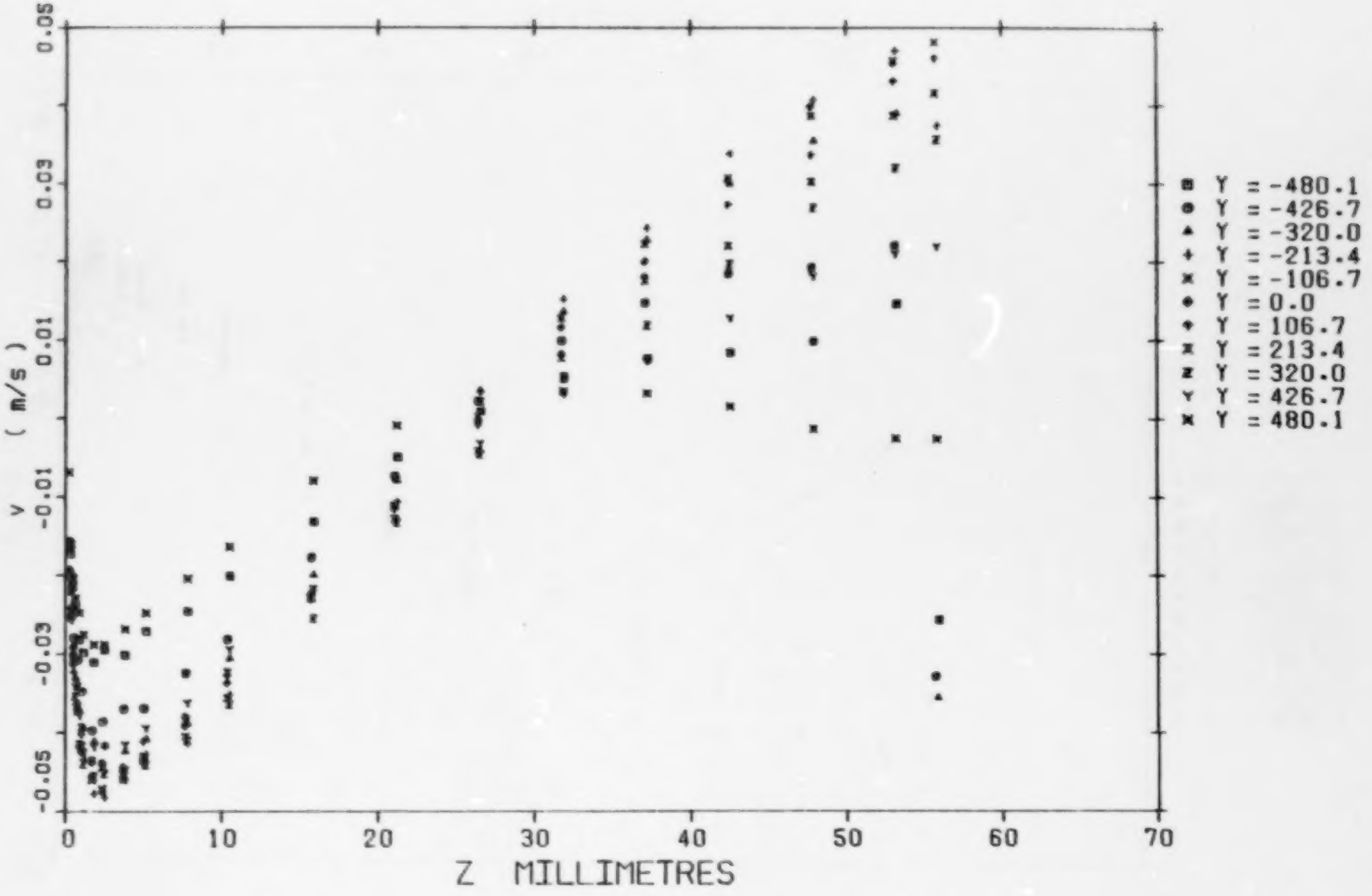

Figure 53. v Velocity Distribution (x = 3.83 m)

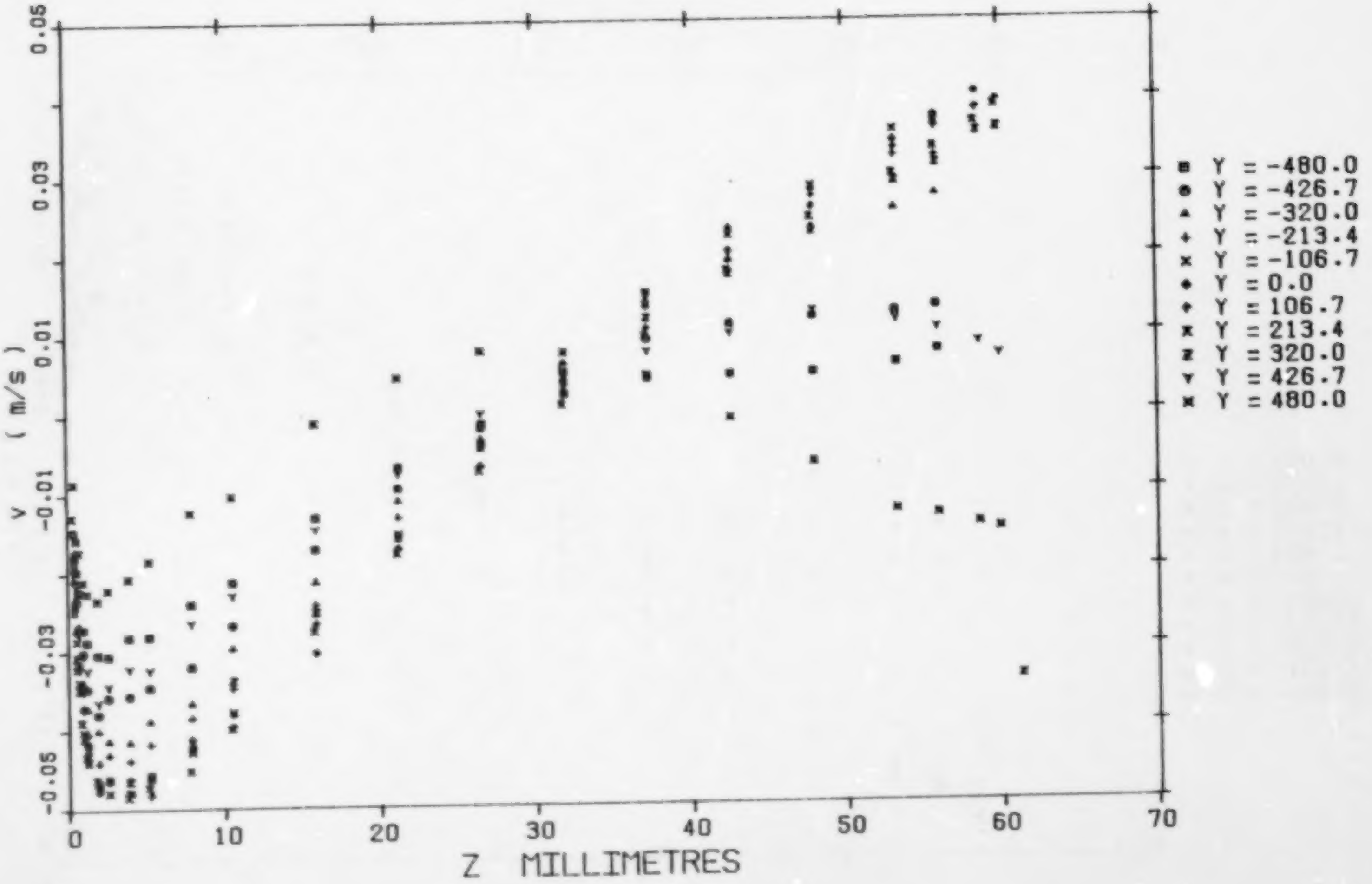

Figure 54. v Velocity Distribution (x = 5.75 m)

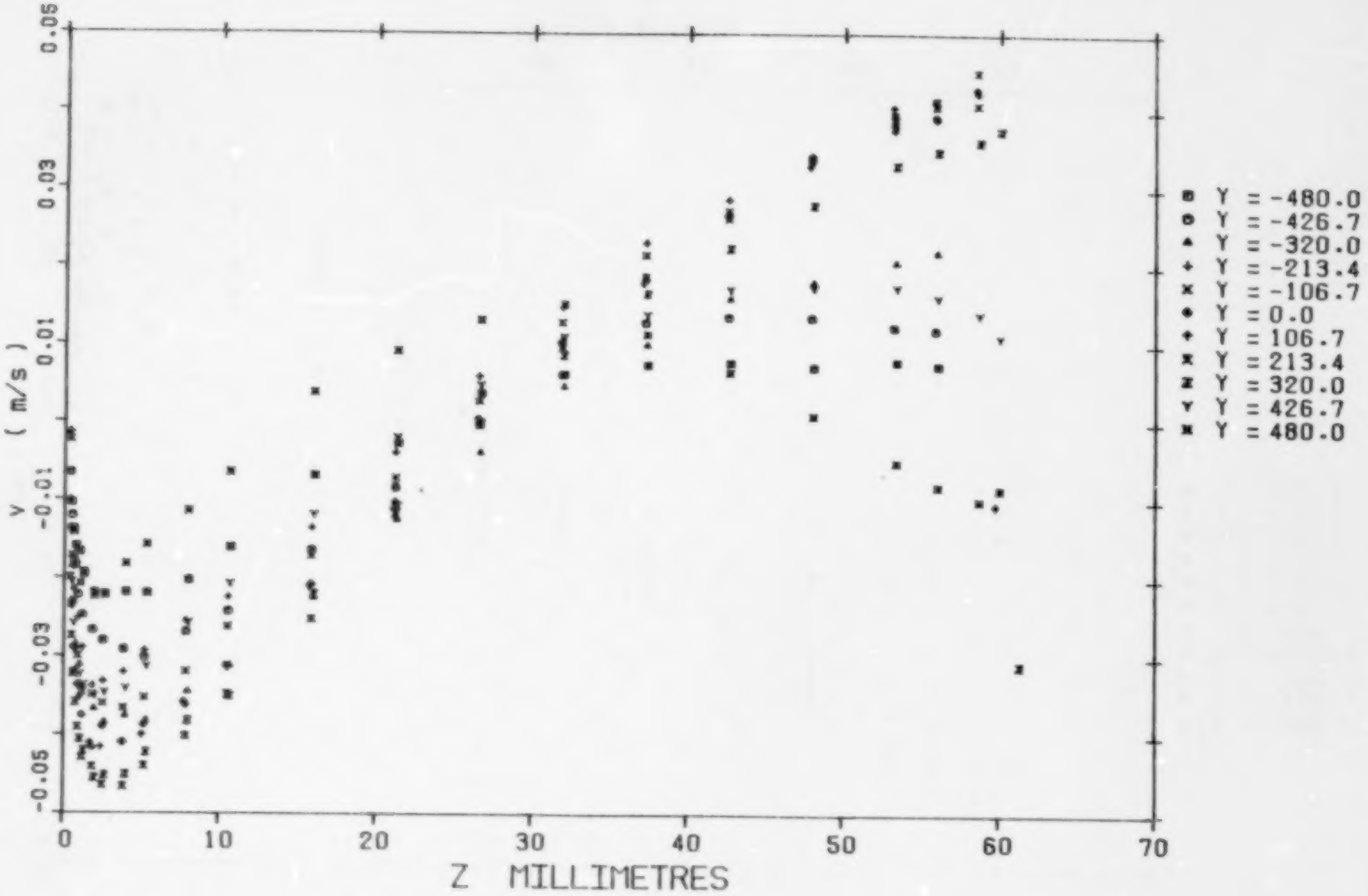

Figure 55. v Velocity Distribution (x = 7.66 m)

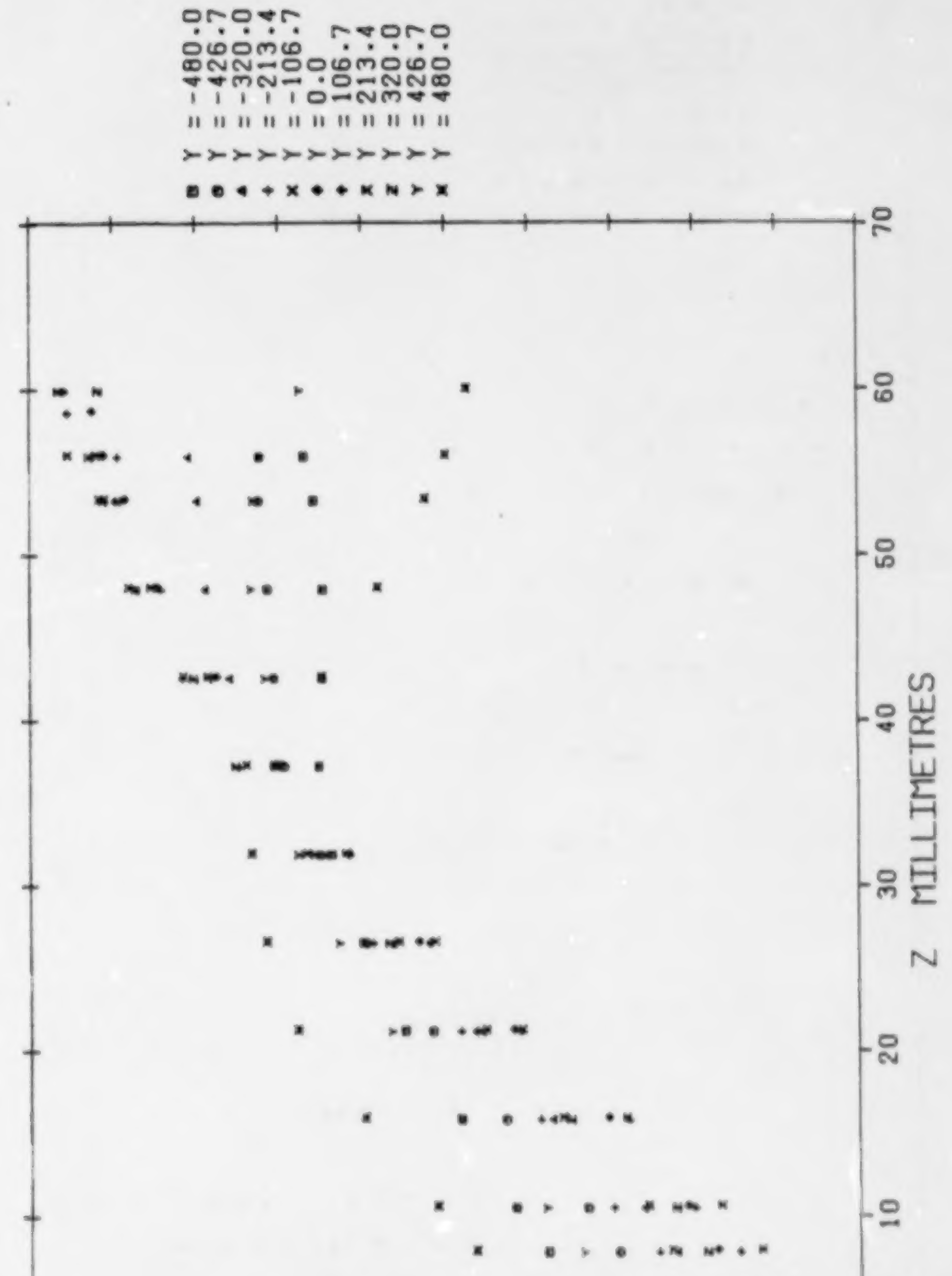

Figure 56. v Velocity Distribution (x = 9.69 m)

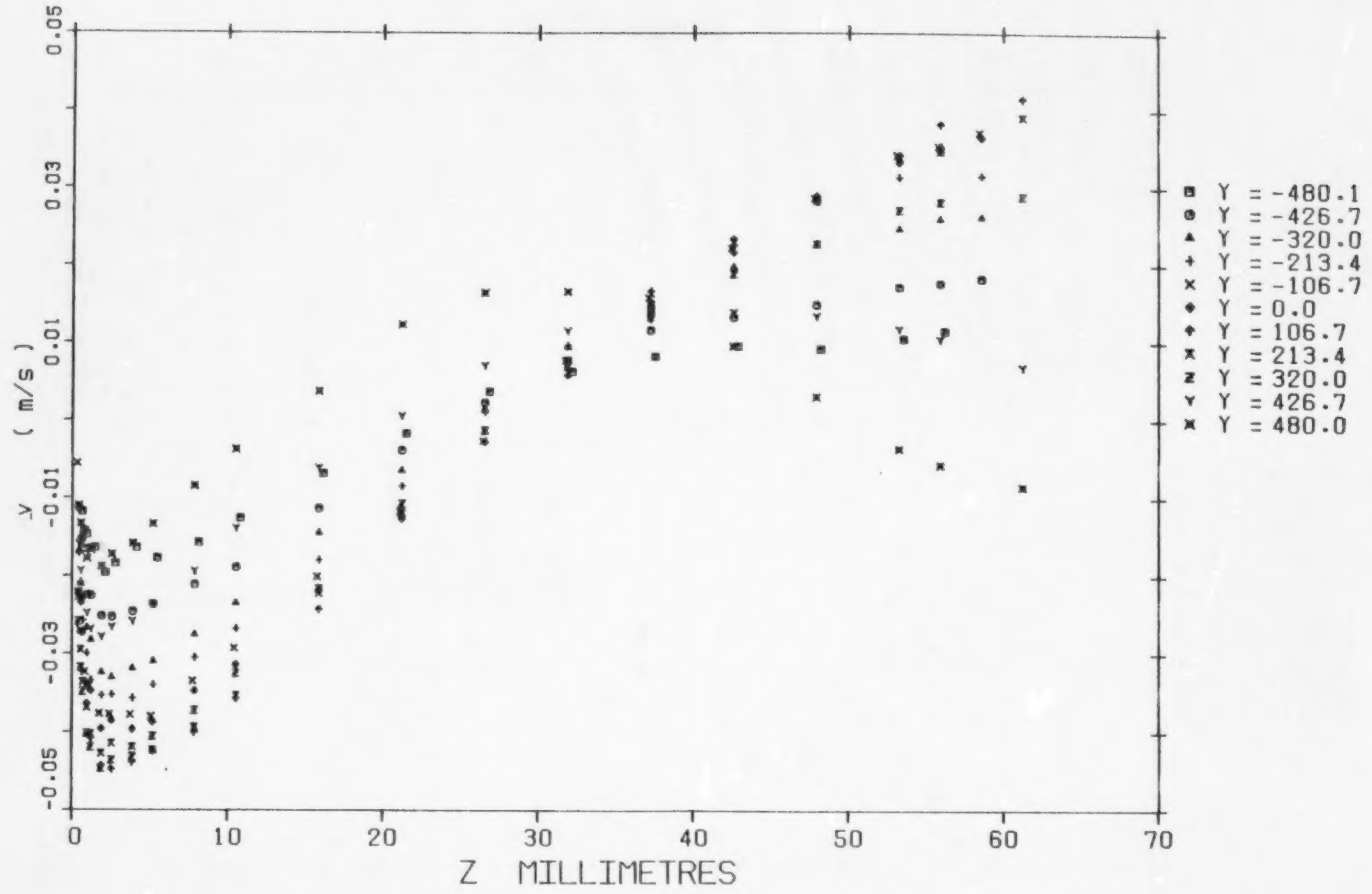

Figure 57. v Velocity Distribution (x = 11.49 m)

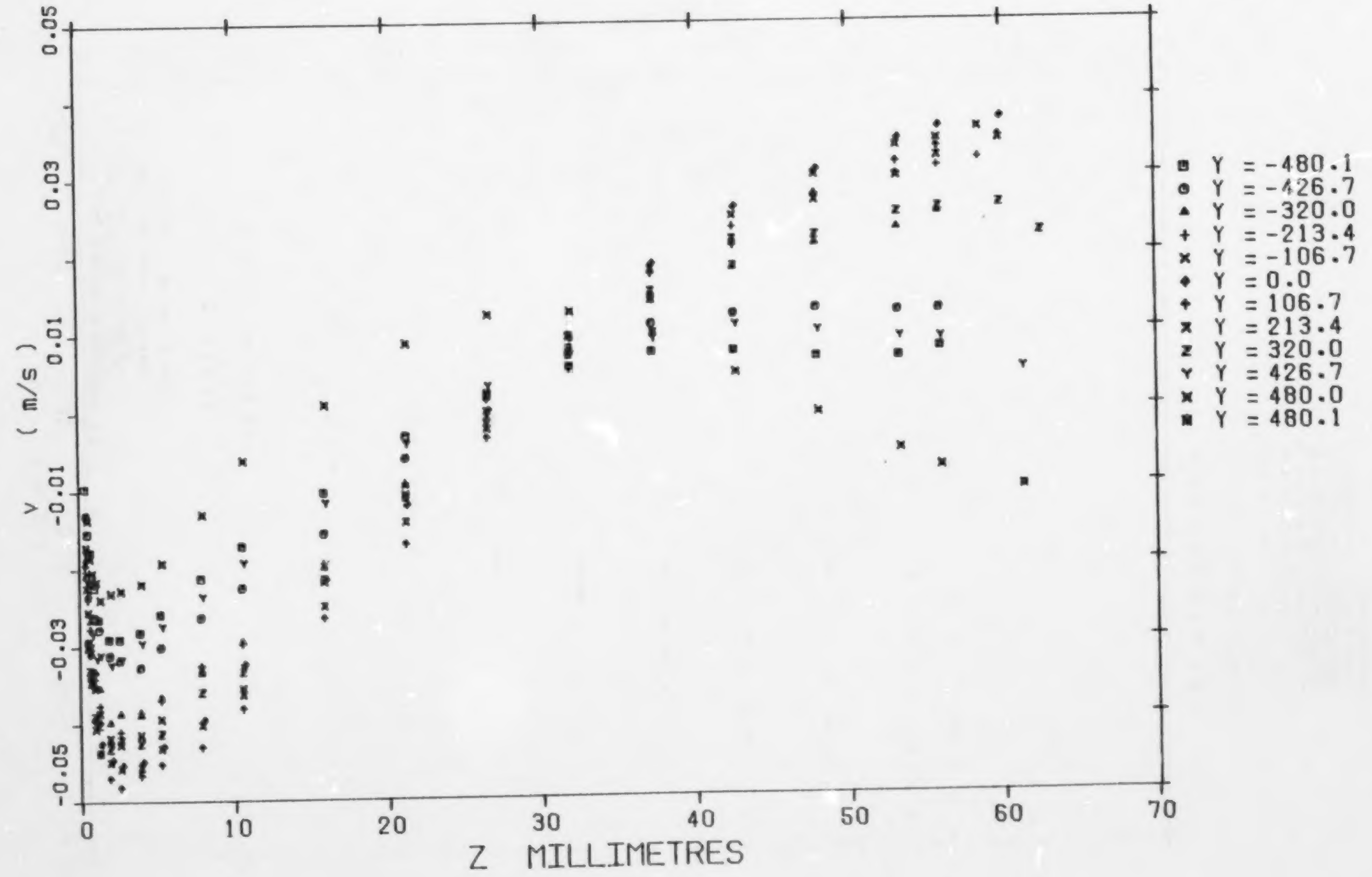

Figure 58. v Velocity Distribution (x = 13.41 m)

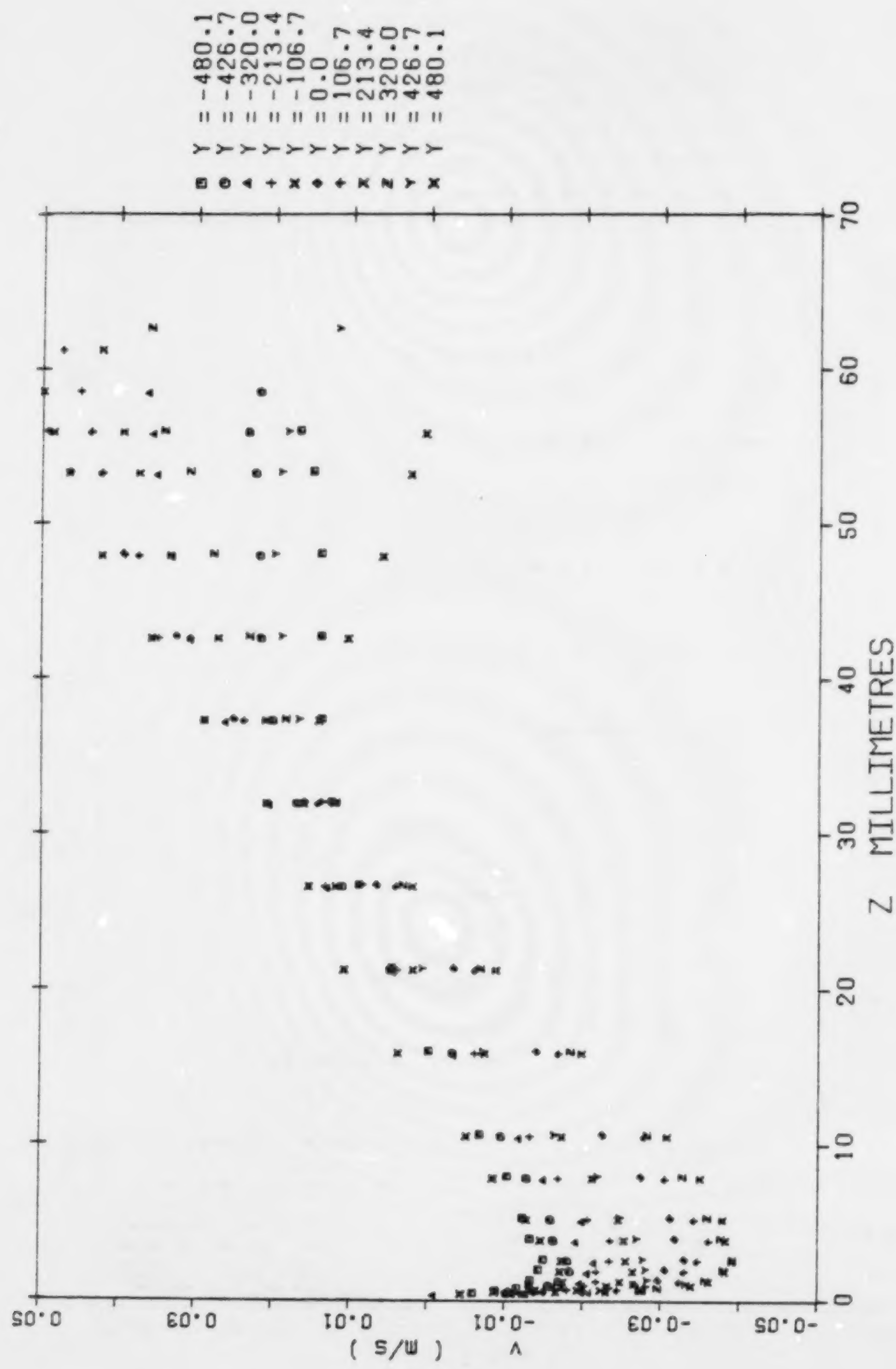

Figure 59. v Velocity Distribution (x = 16.18 m)

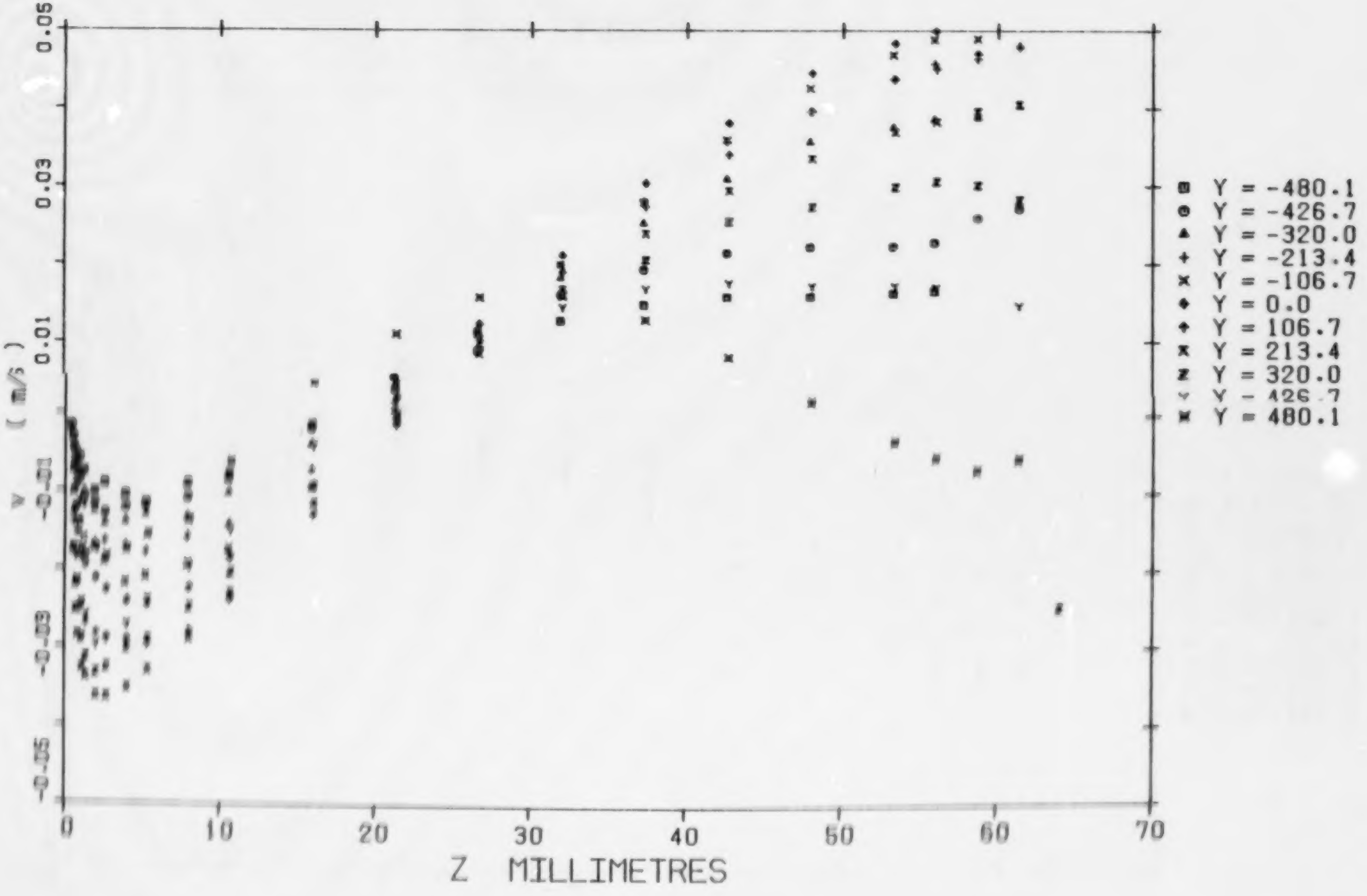

Figure 60. v Velocity Distribution (x = 17.43 m)

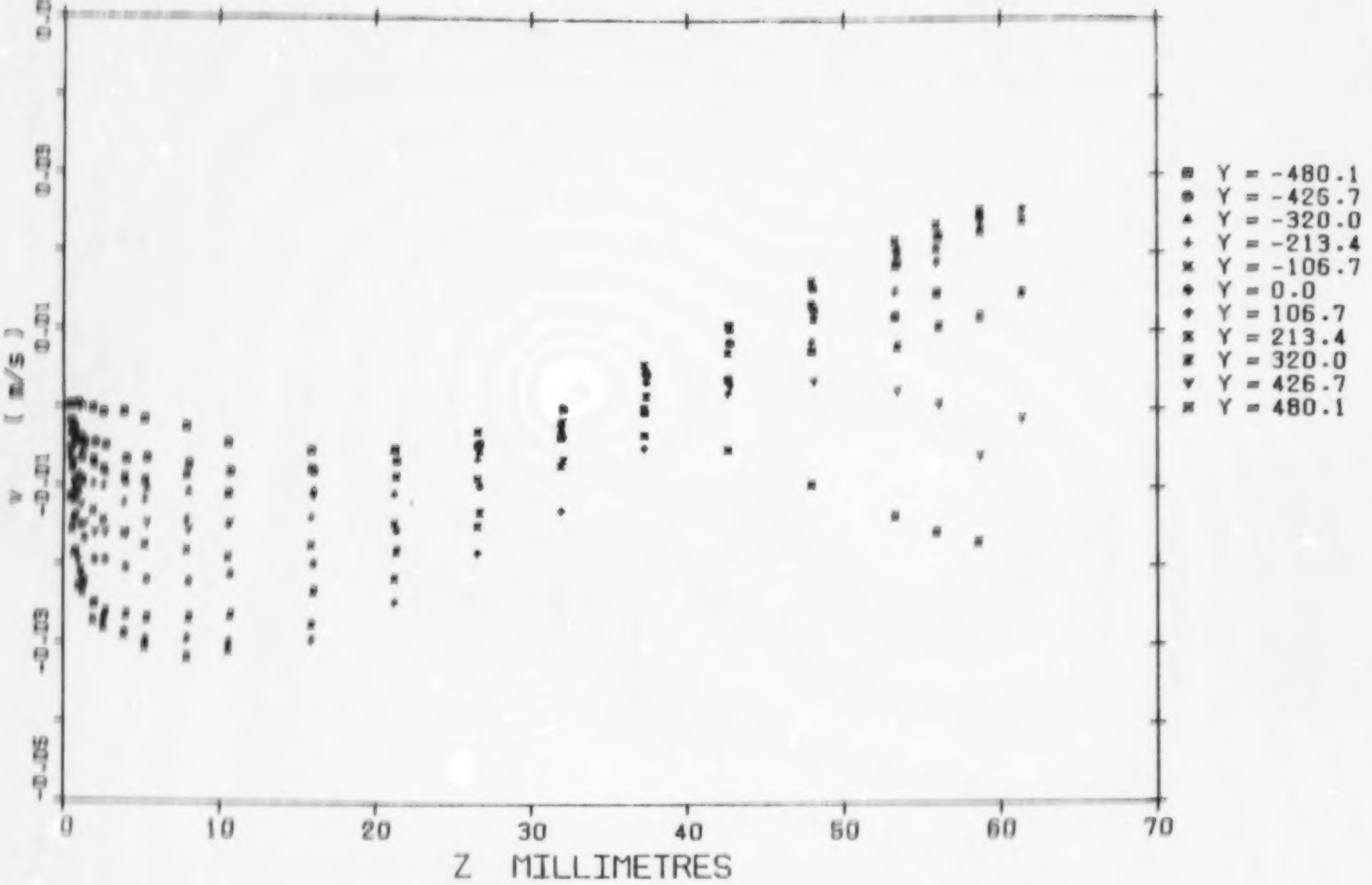

Figure 61, v Velocity Distribution (x = 18.65 m)

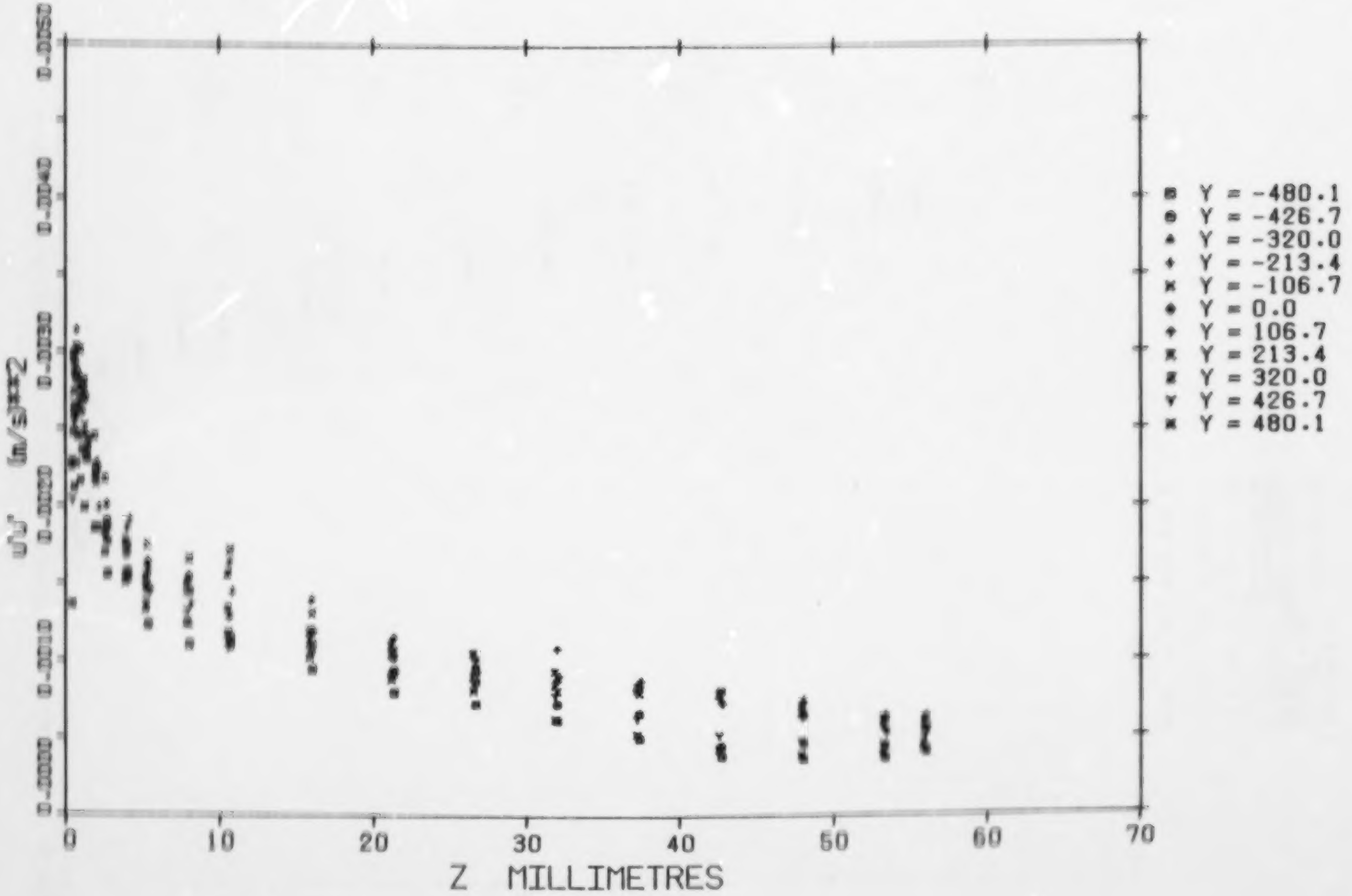

Figure 62. $\overline{u'^2}$ Turbulence Intensity Distribution
(x = -2.20 m)

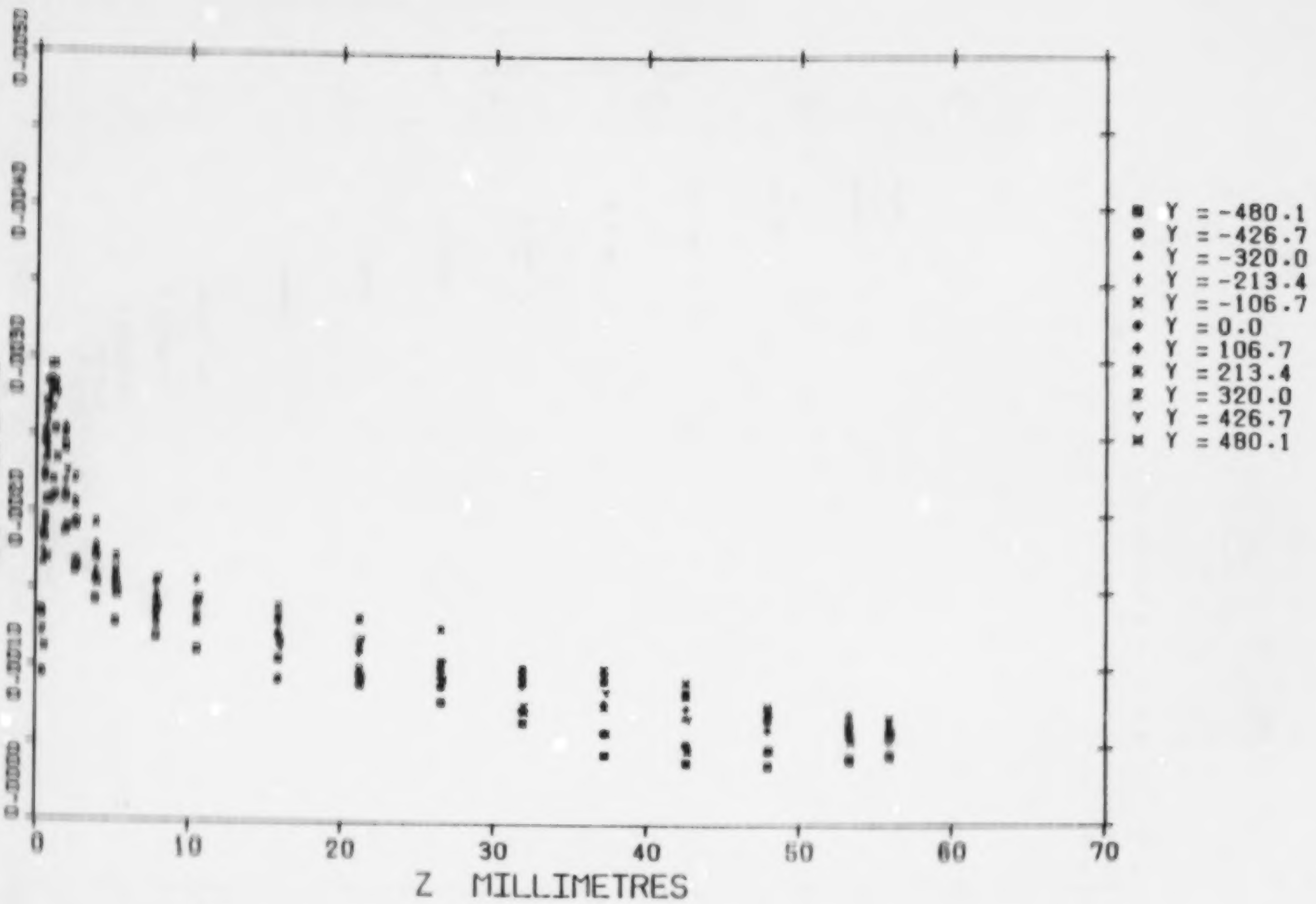

Figure 61. $\overline{u'^2}$ Turbulence Intensity Distribution
(x = -0.69 m)

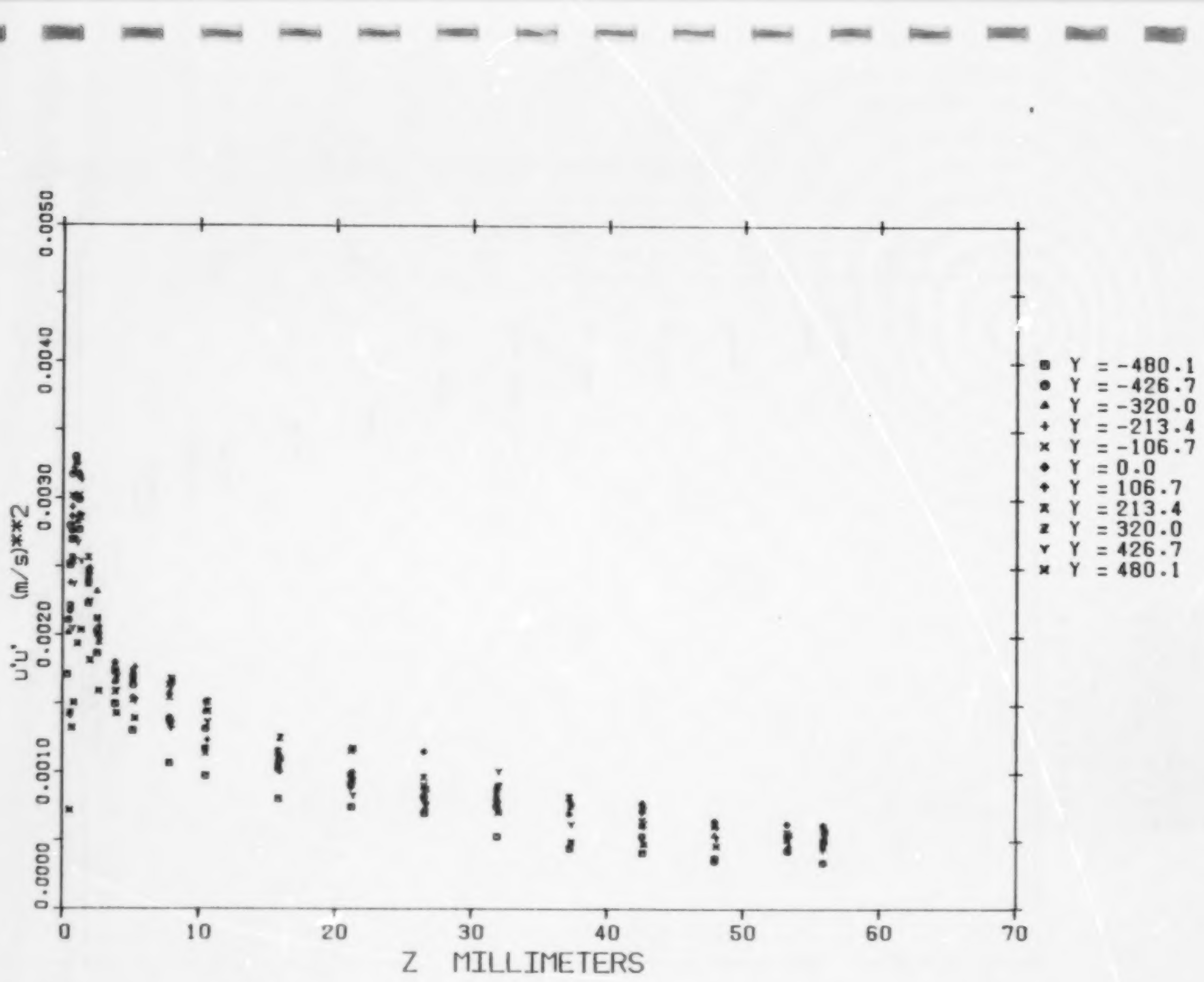

Figure 64. $\overline{u'^2}$ Turbulence Intensity Distribution (x = 0.05 m)

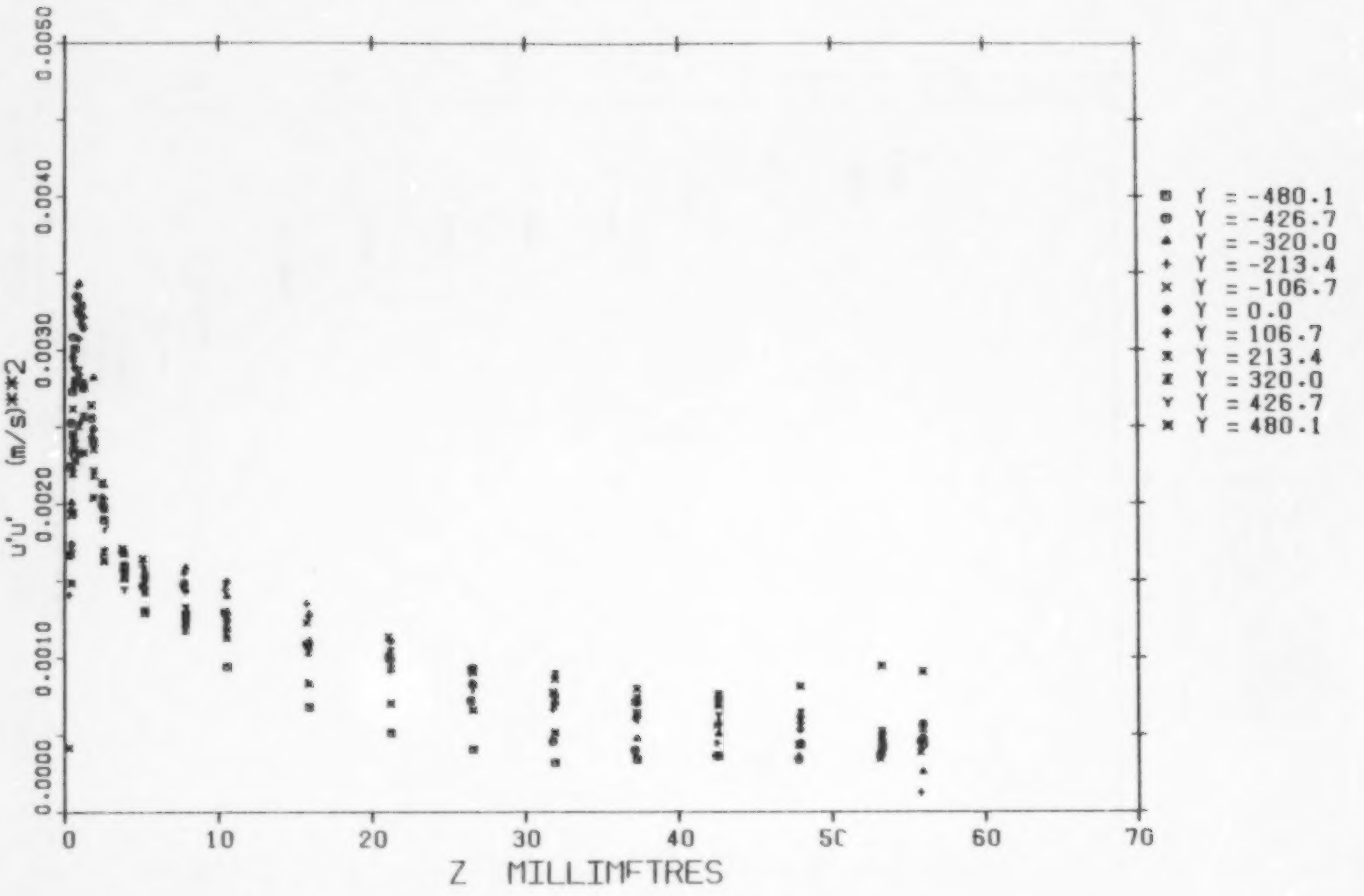

Figure 65. $\overline{u'^2}$ Turbulence Intensity Distribution
(x = 1.92 m)

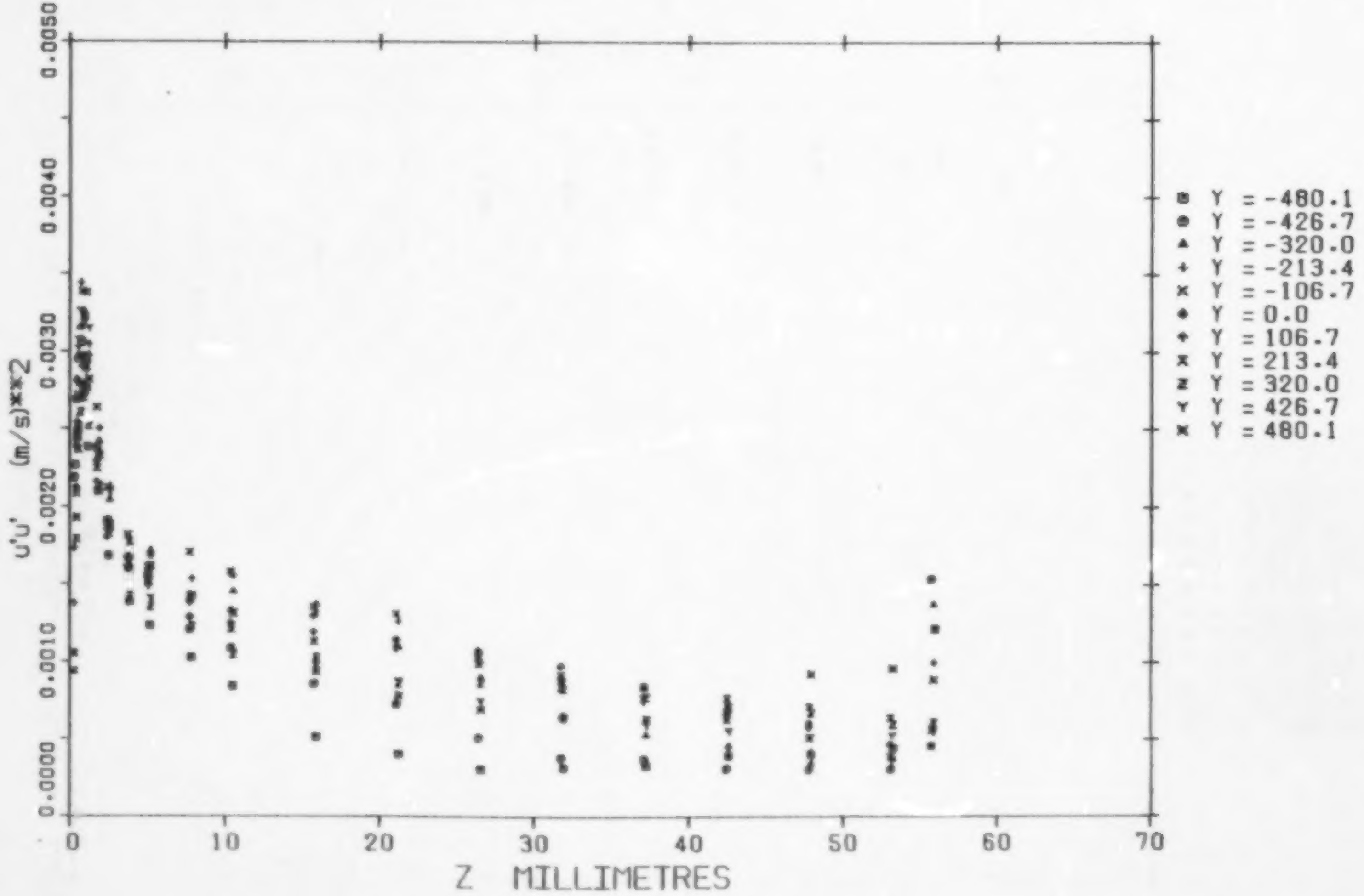

Figure 66. $\overline{u'^2}$ Turbulence Intensity Distribution (x = 3.83 m)

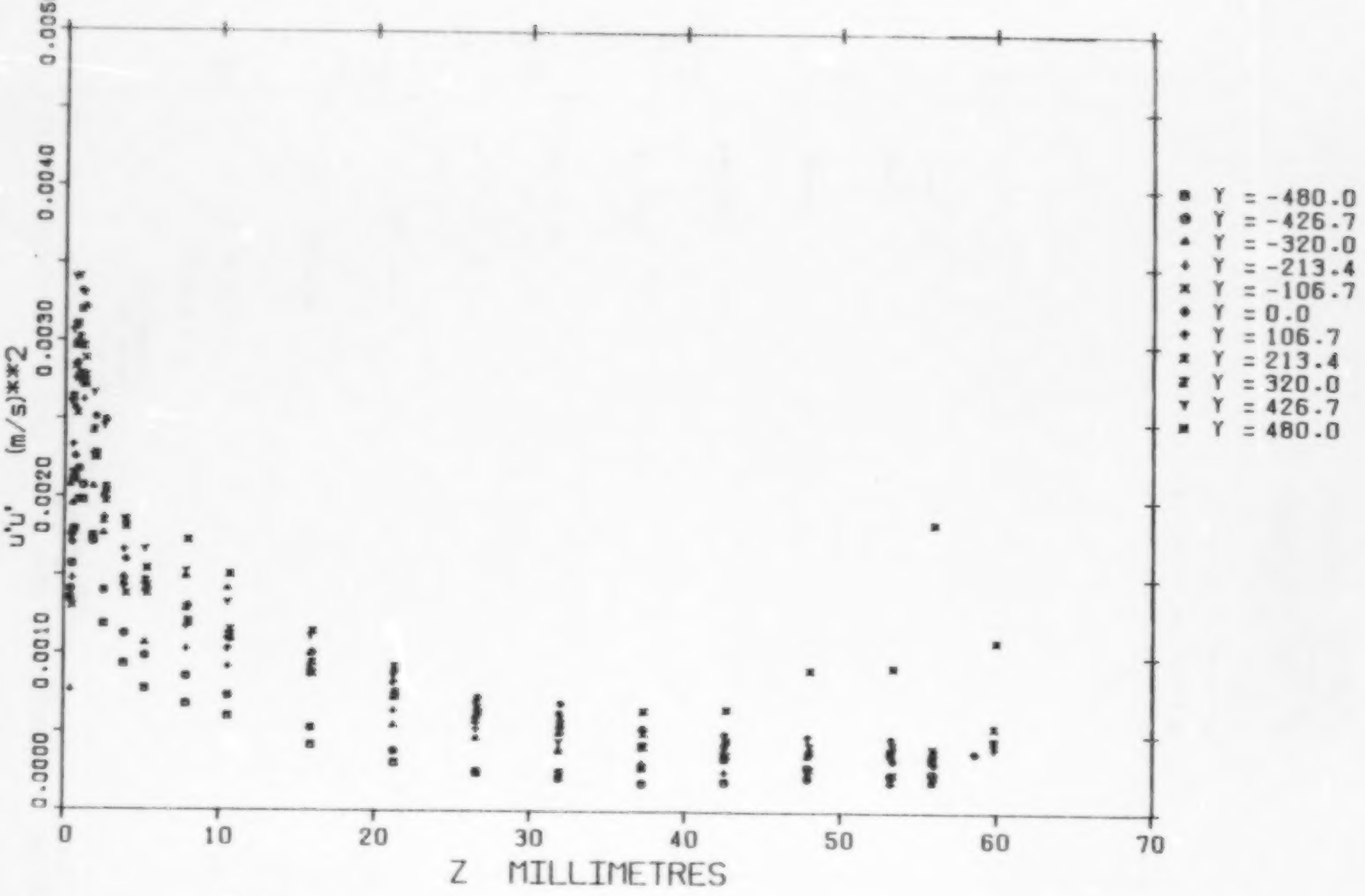

Figure 67. $\overline{u'^2}$ Turbulence Intensity Distribution (x = 5.75 m)

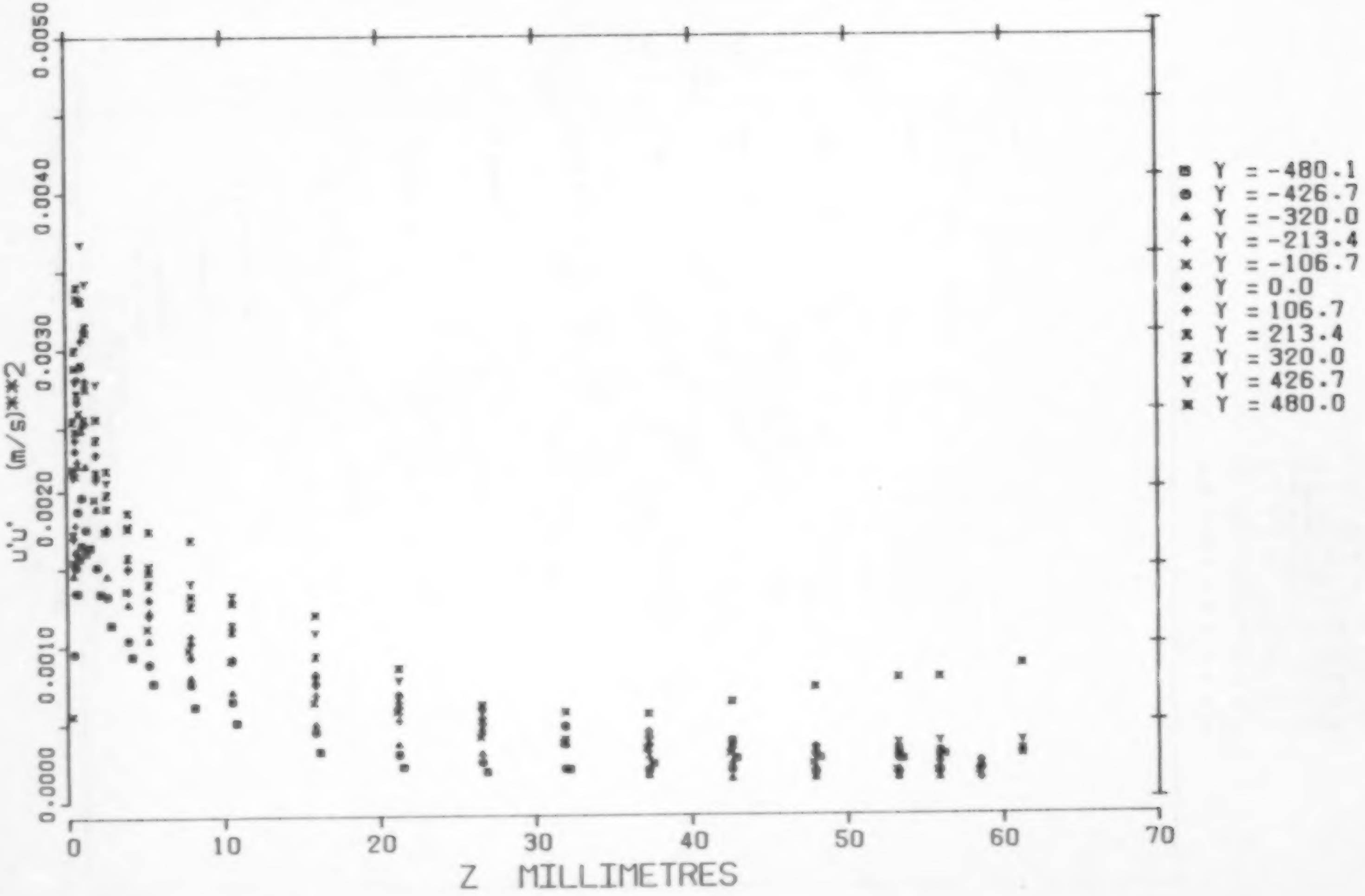

Figure 68. $\overline{u'^2}$ Turbulence Intensity Distribution
(x = 7.66 m)

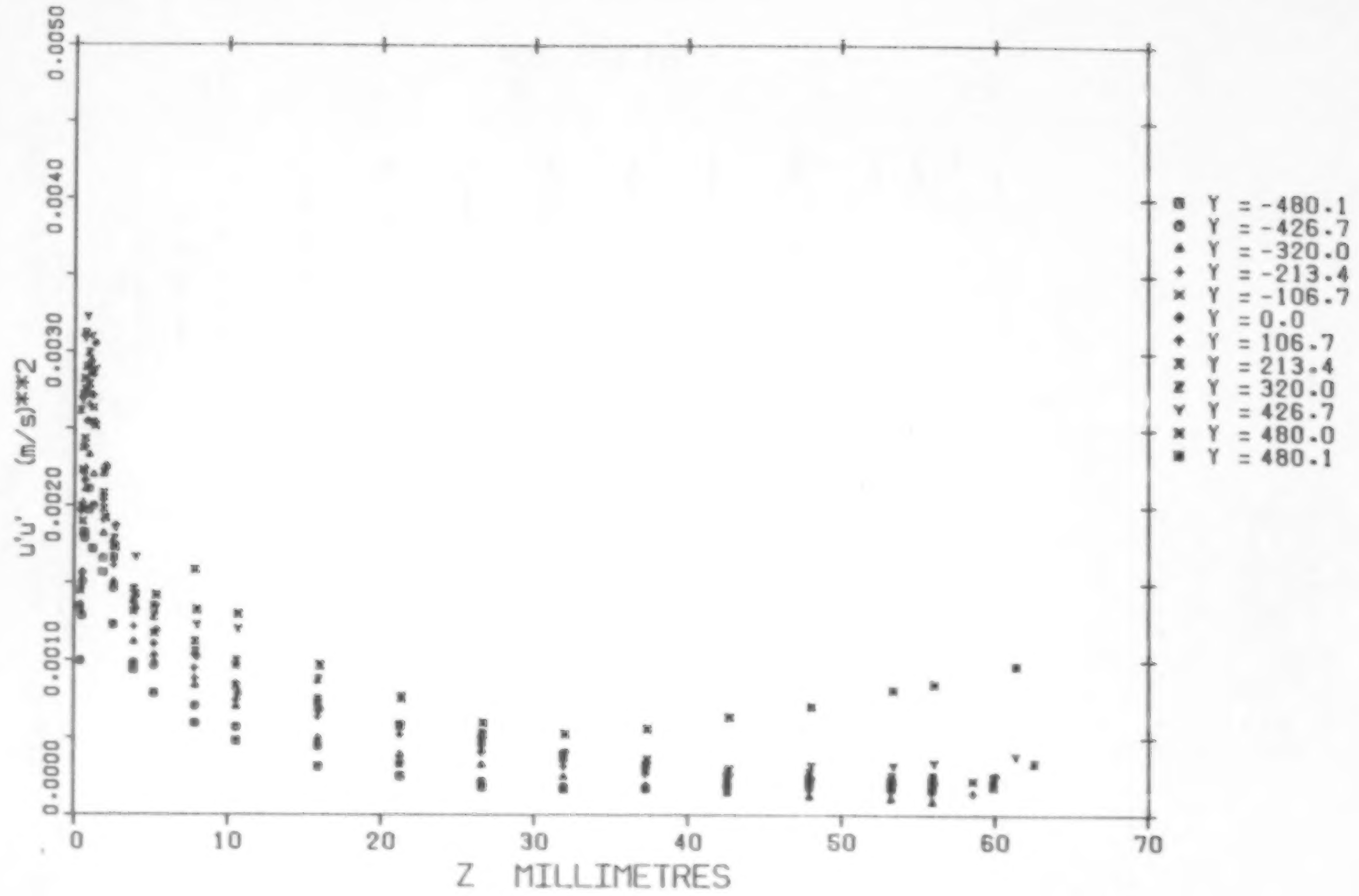

Figure 69. $\overline{u'^2}$ Turbulence Intensity Distribution
(x = 9.68 x)

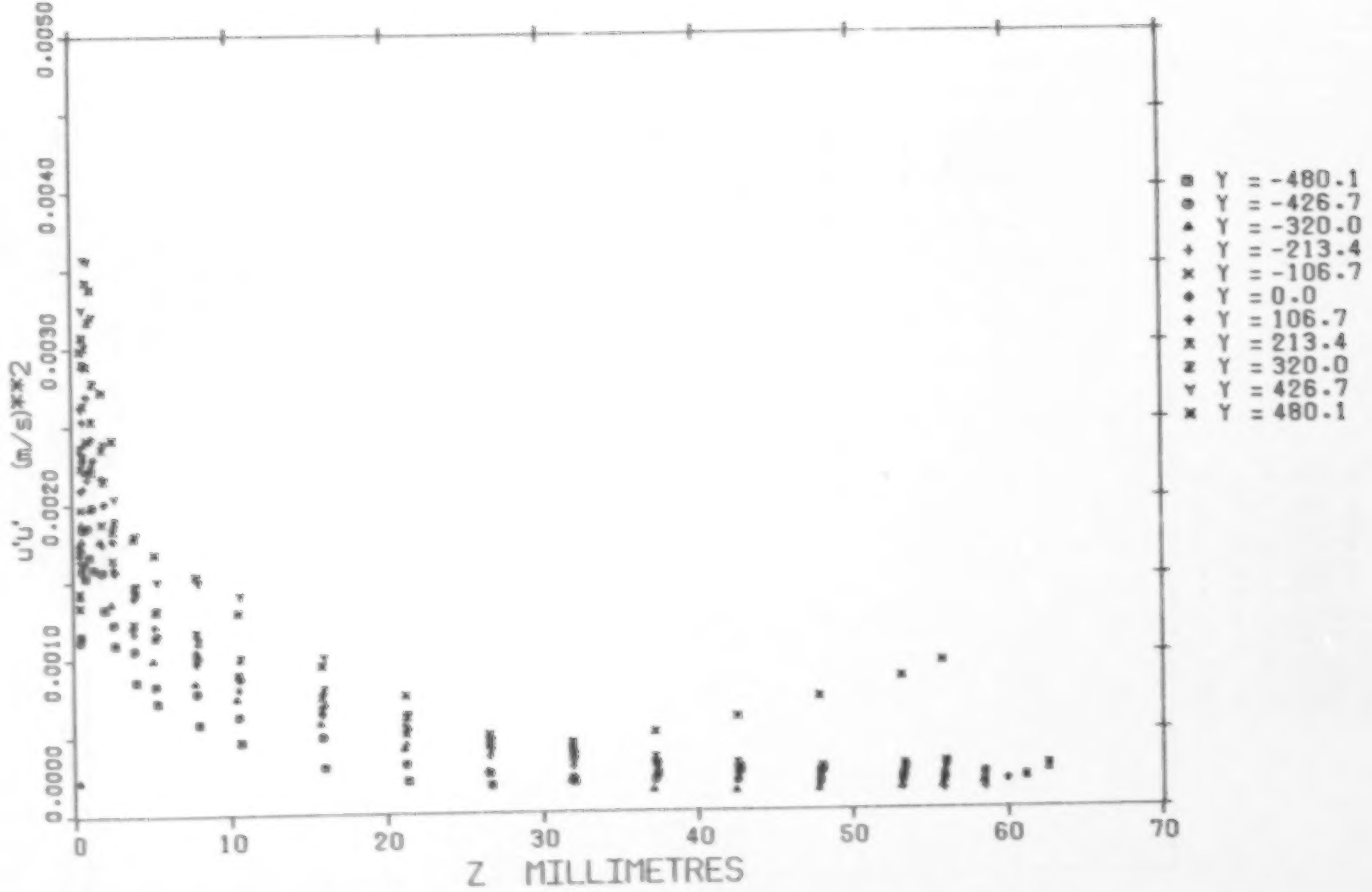

Figure 70. $\overline{u'^2}$ Turbulence Intensity Distribution
(x = 11.49 m)

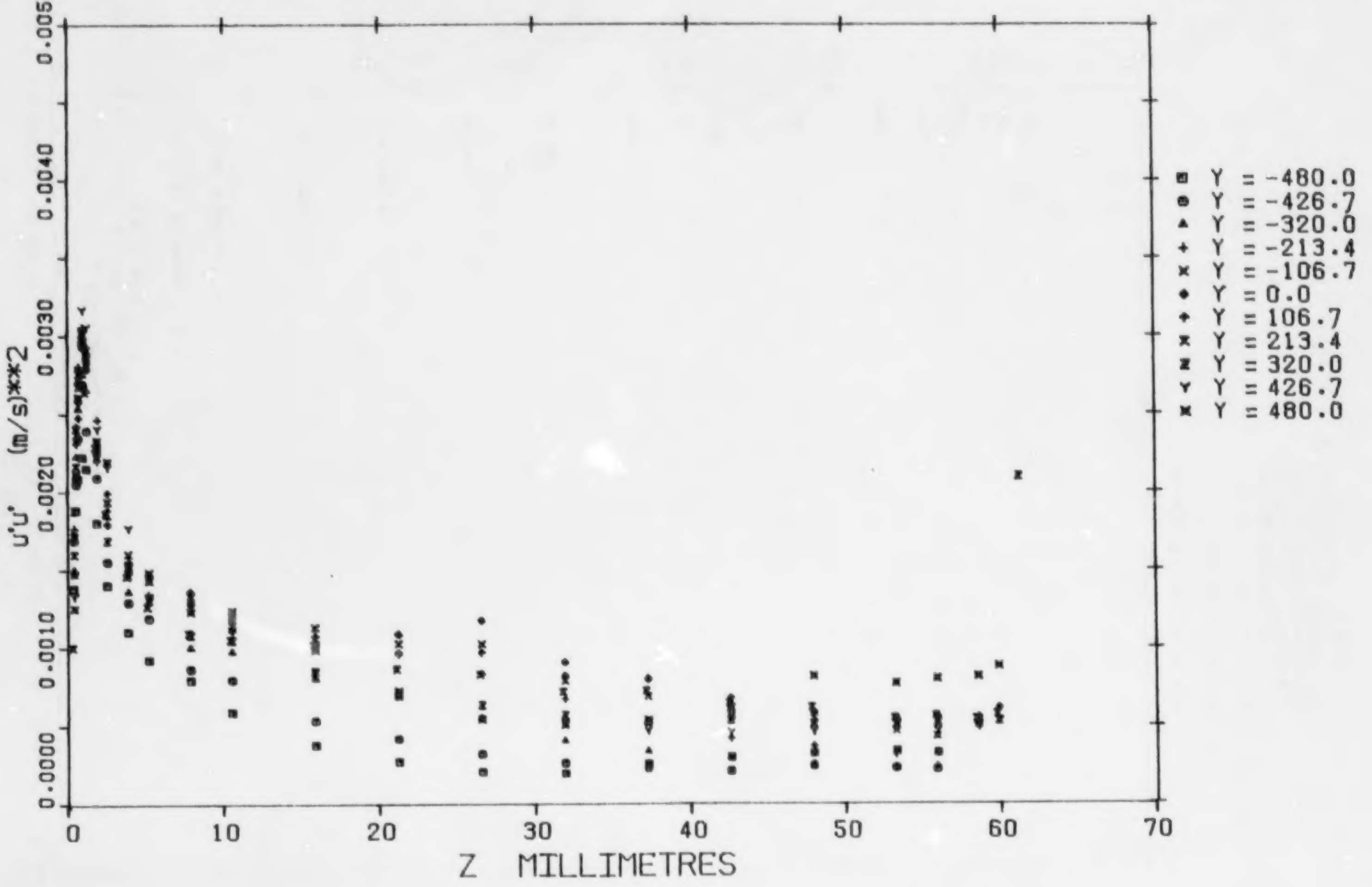

Figure 71. $\overline{u'^2}$ Turbulence Intensity Distribution (x = 13.41 m)

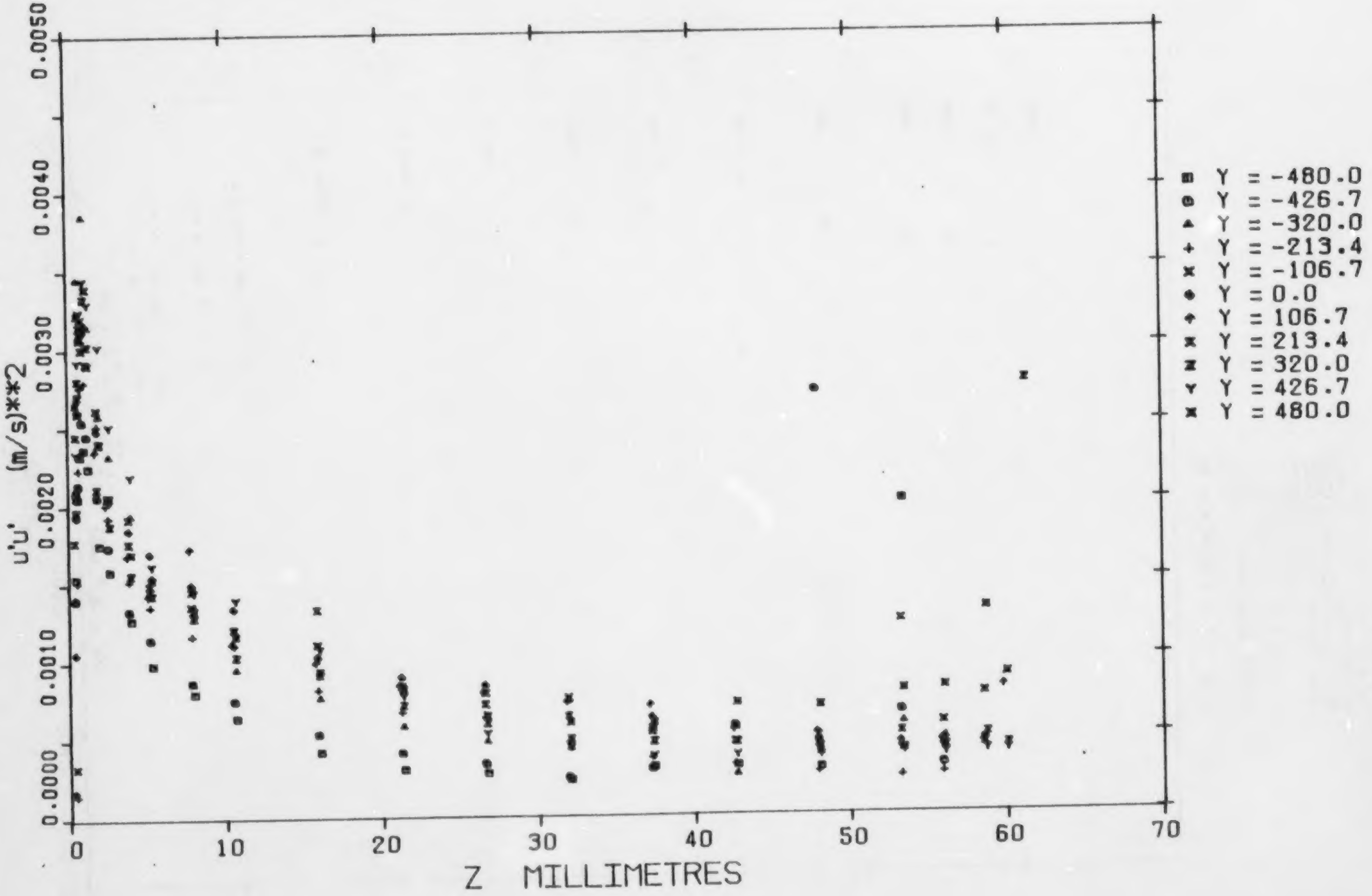

Figure 72. $\overline{u'^2}$ Turbulence Intensity Distribution (x = 16.18 m)

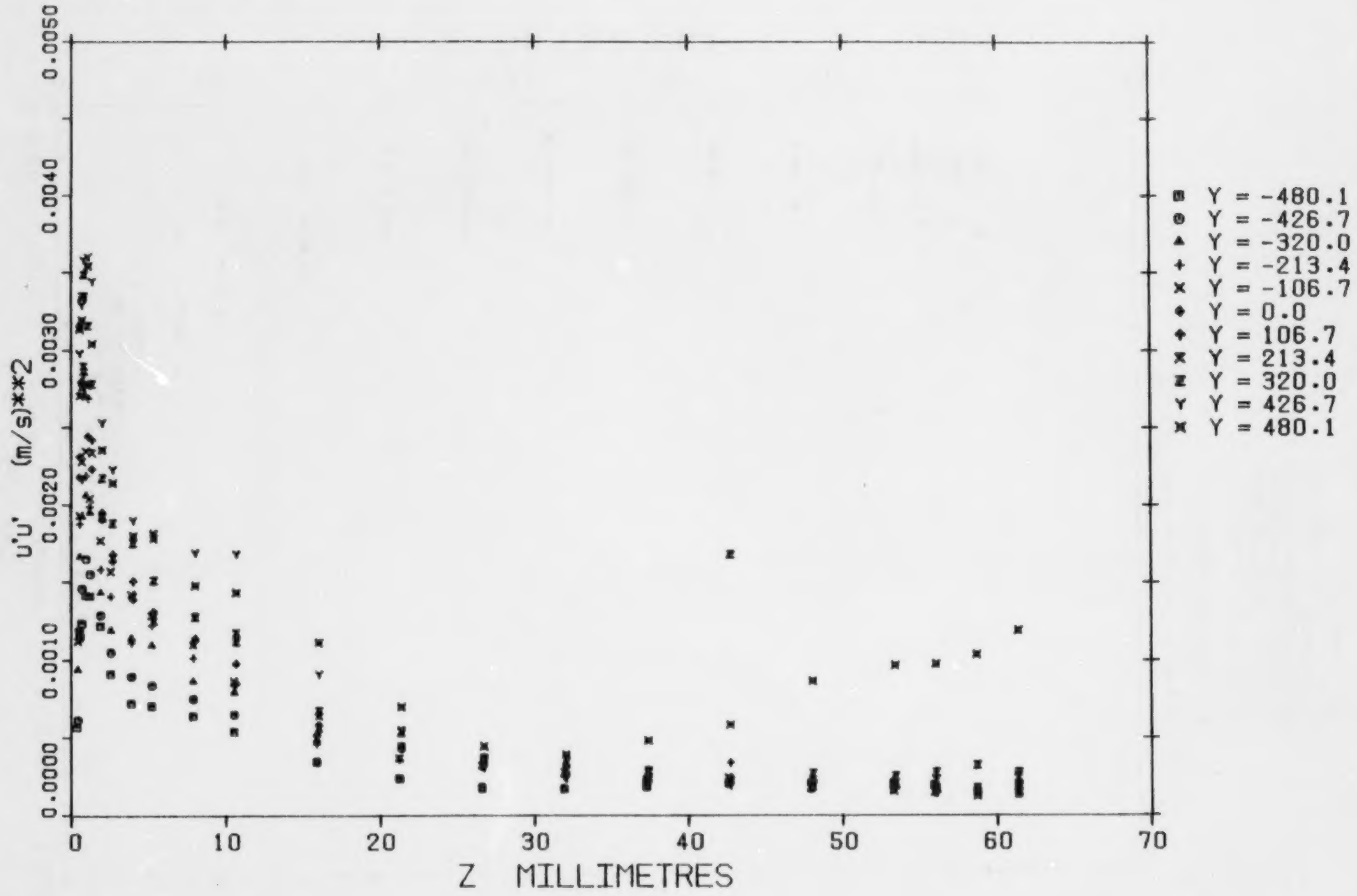

Figure 73. $\overline{u'^2}$ Turbulence Intensity Distribution
(x = 17.43 m)

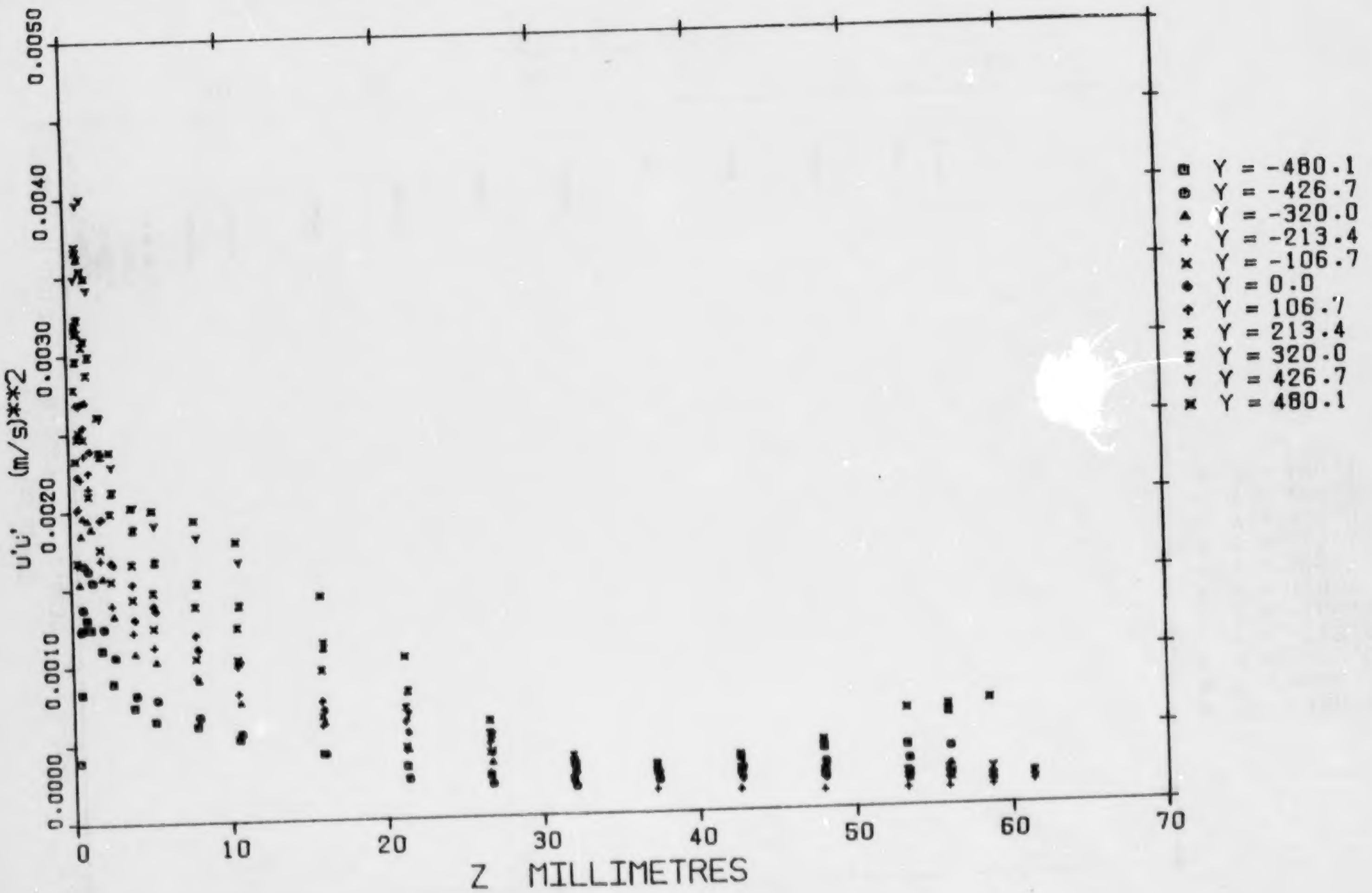

Figure 74. $\overline{u'^2}$ Turbulence Intensity Distribution (x = 18.65 m)

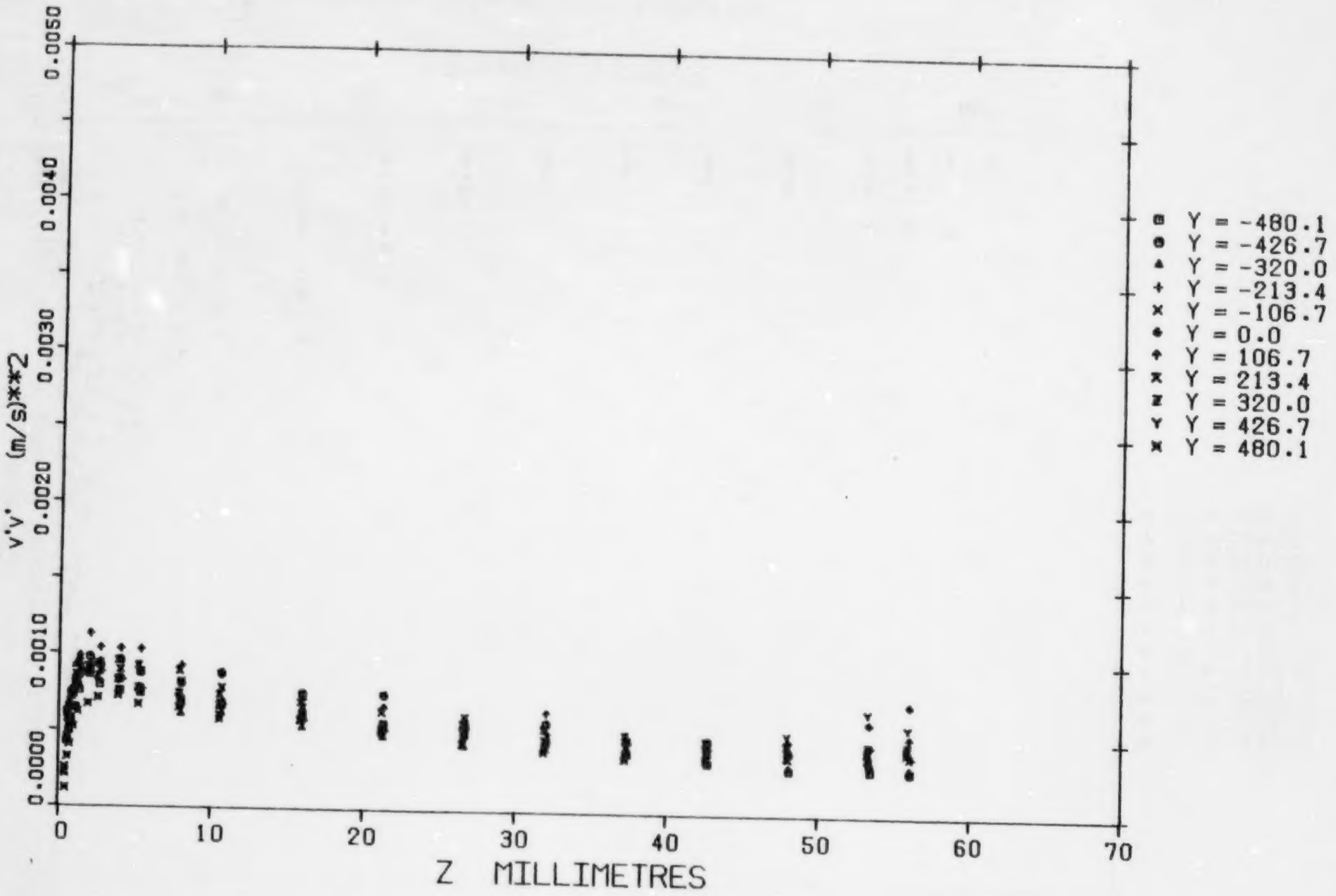

Figure 75. $\overline{v'^2}$ Turbulence Intensity Distribution (x = -2.20 m)

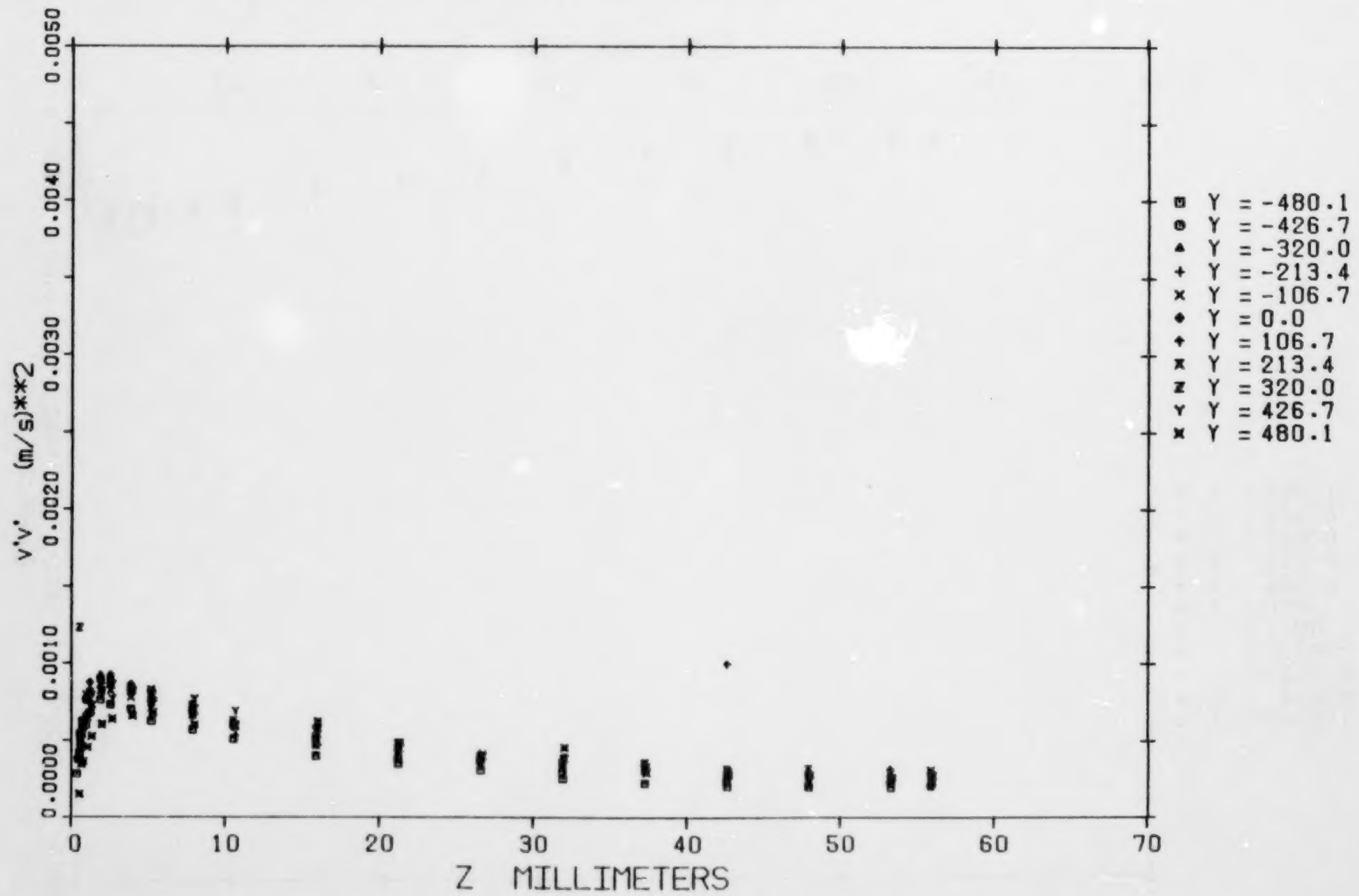

Figure 76. $\overline{v'^2}$ Turbulence Intensity Distribution (x = -0.69 m)

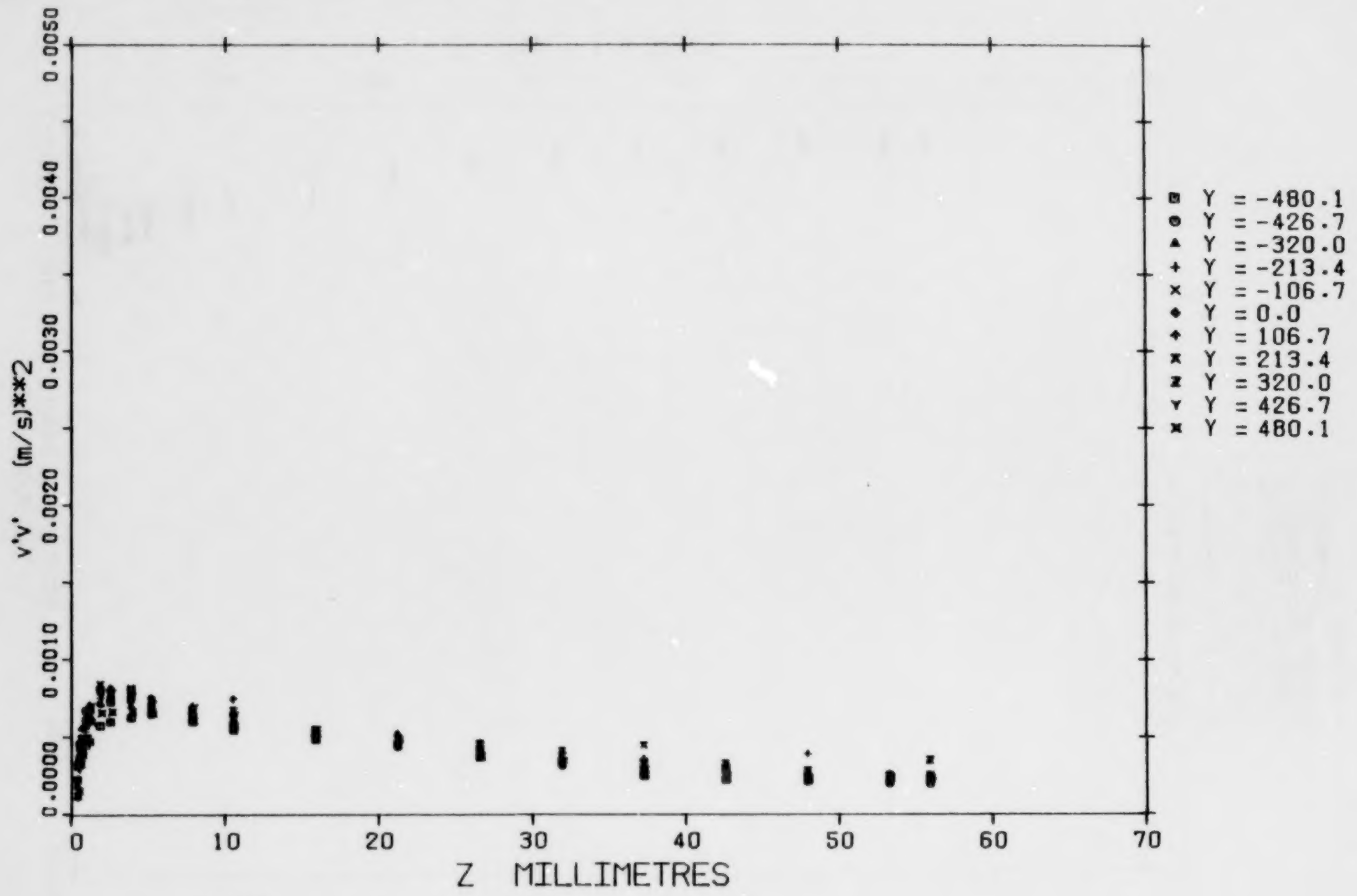

Figure 77. $\overline{v'^2}$ Turbulence Intensity Distribution
(x = 0.05 m)

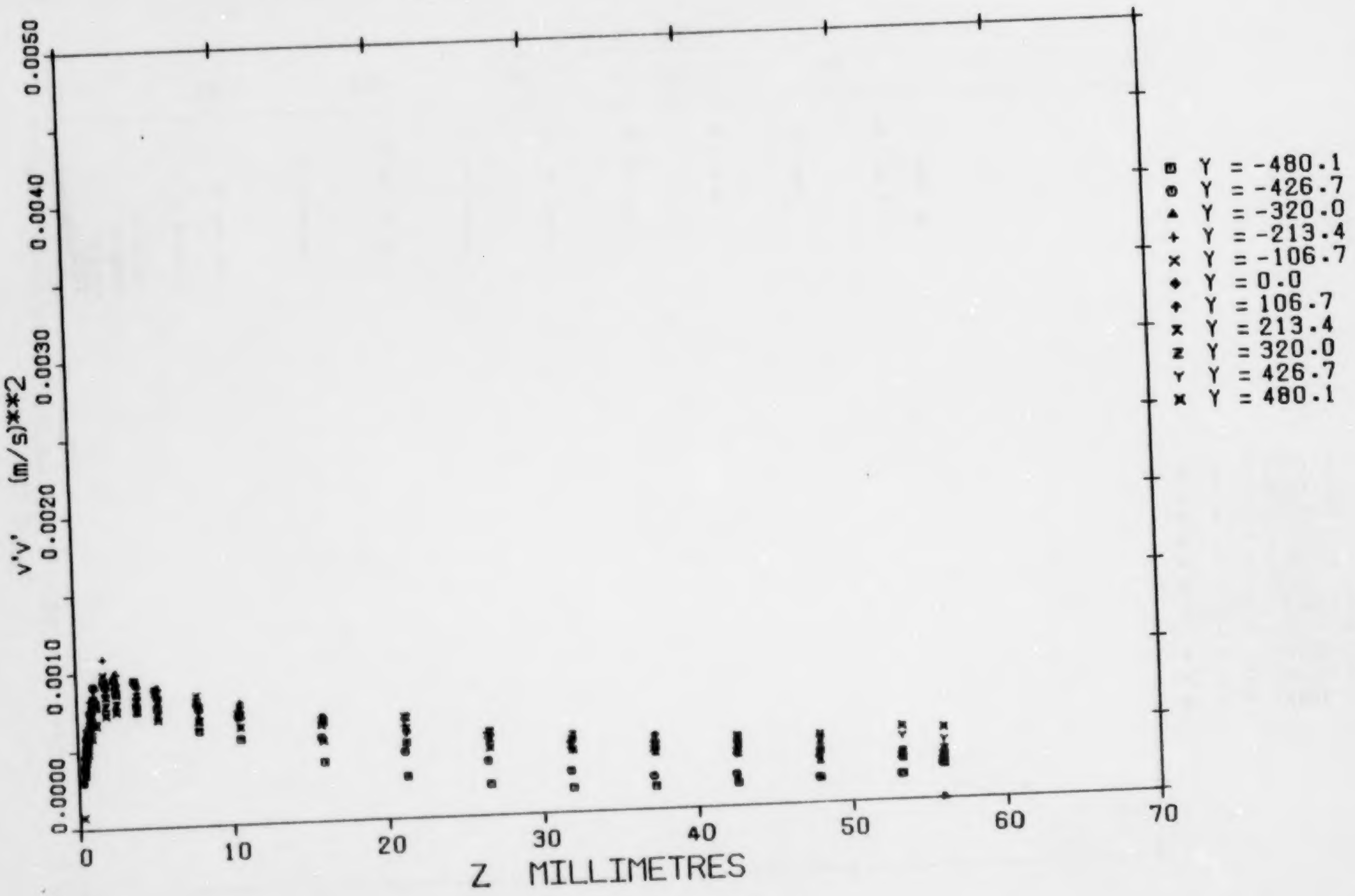

Figure 78. $\overline{v'^2}$ Turbulence Intensity Distribution
(x = 1.92 m)

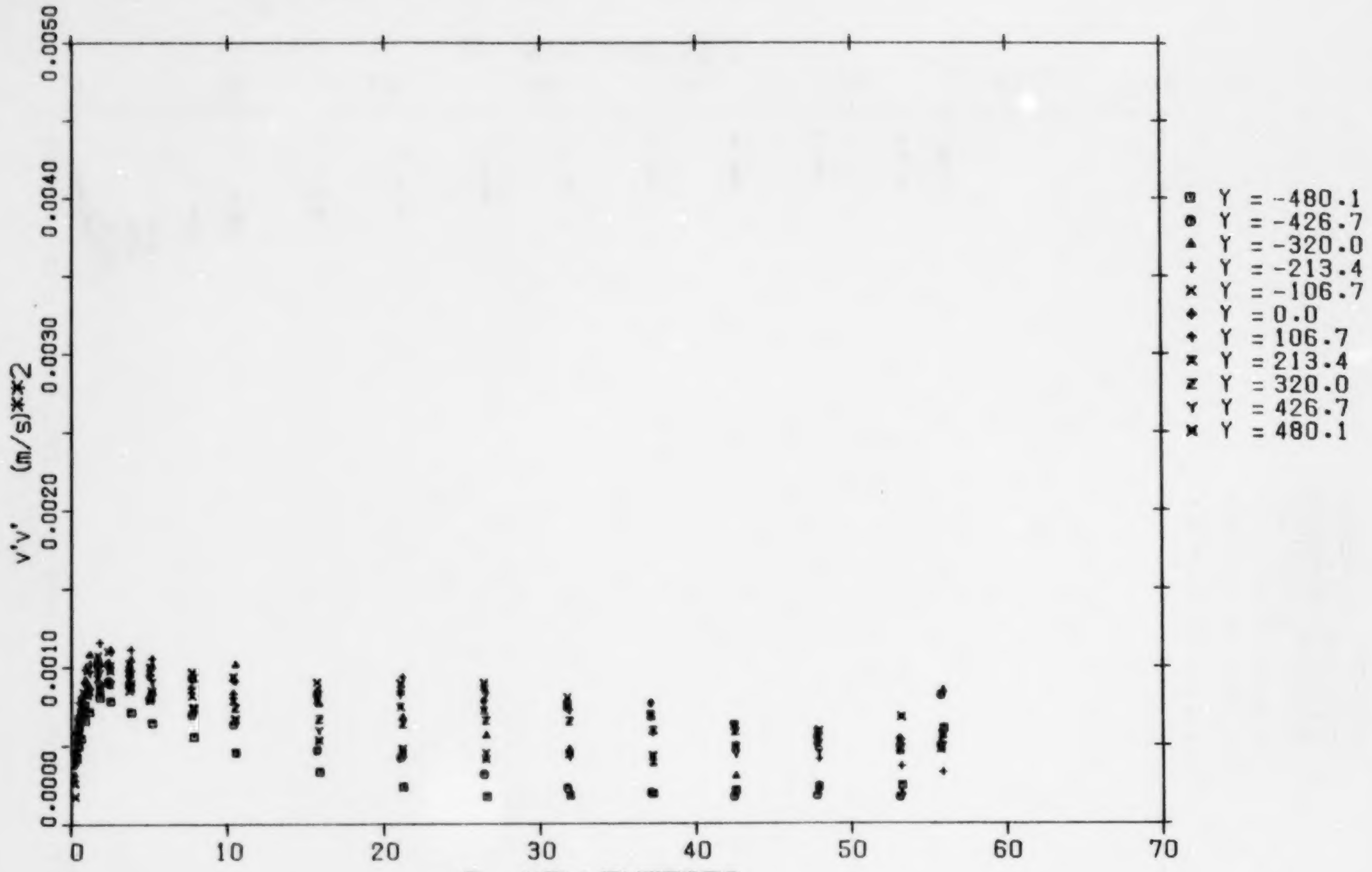

Figure 79. $\overline{v'^2}$ Turbulence Intensity Distribution
(x = 3.83 m)

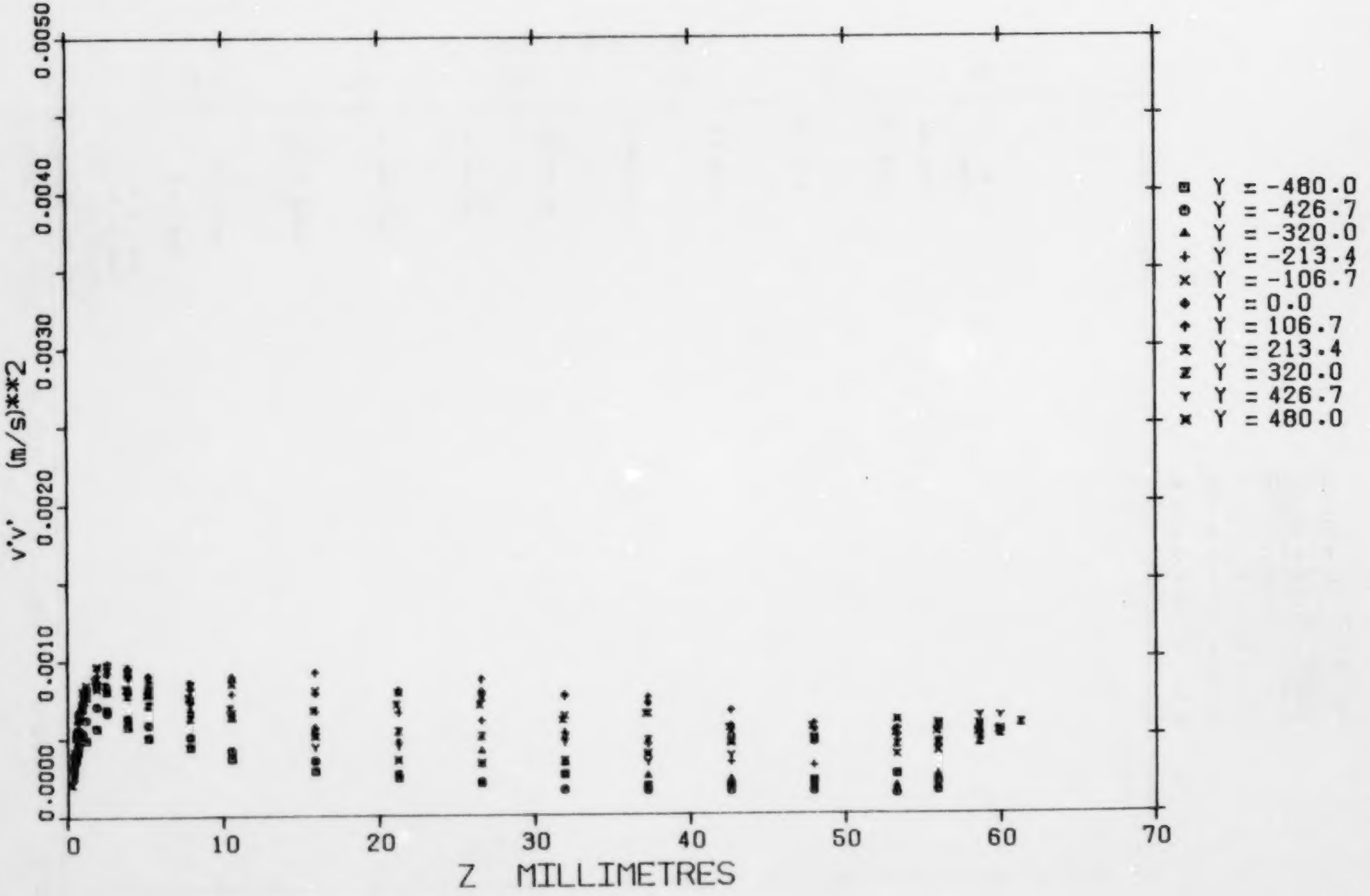

Figure 80. $\overline{v'^2}$ Turbulence Intensity Distribution
(x = 5.75 m)

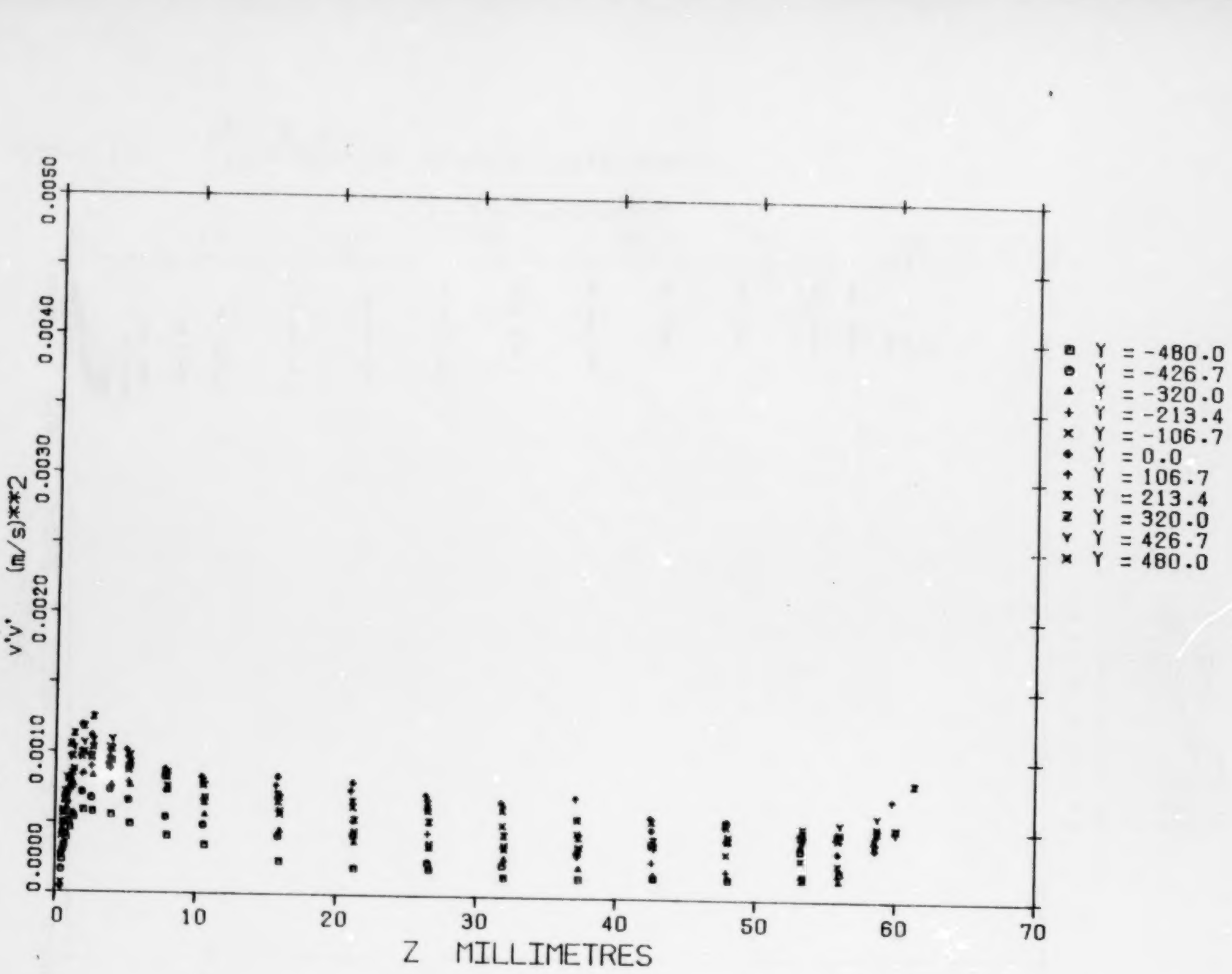

Figure 81. $\overline{v'^2}$ Turbulence Intensity Distribution
(x = 7.66 m)

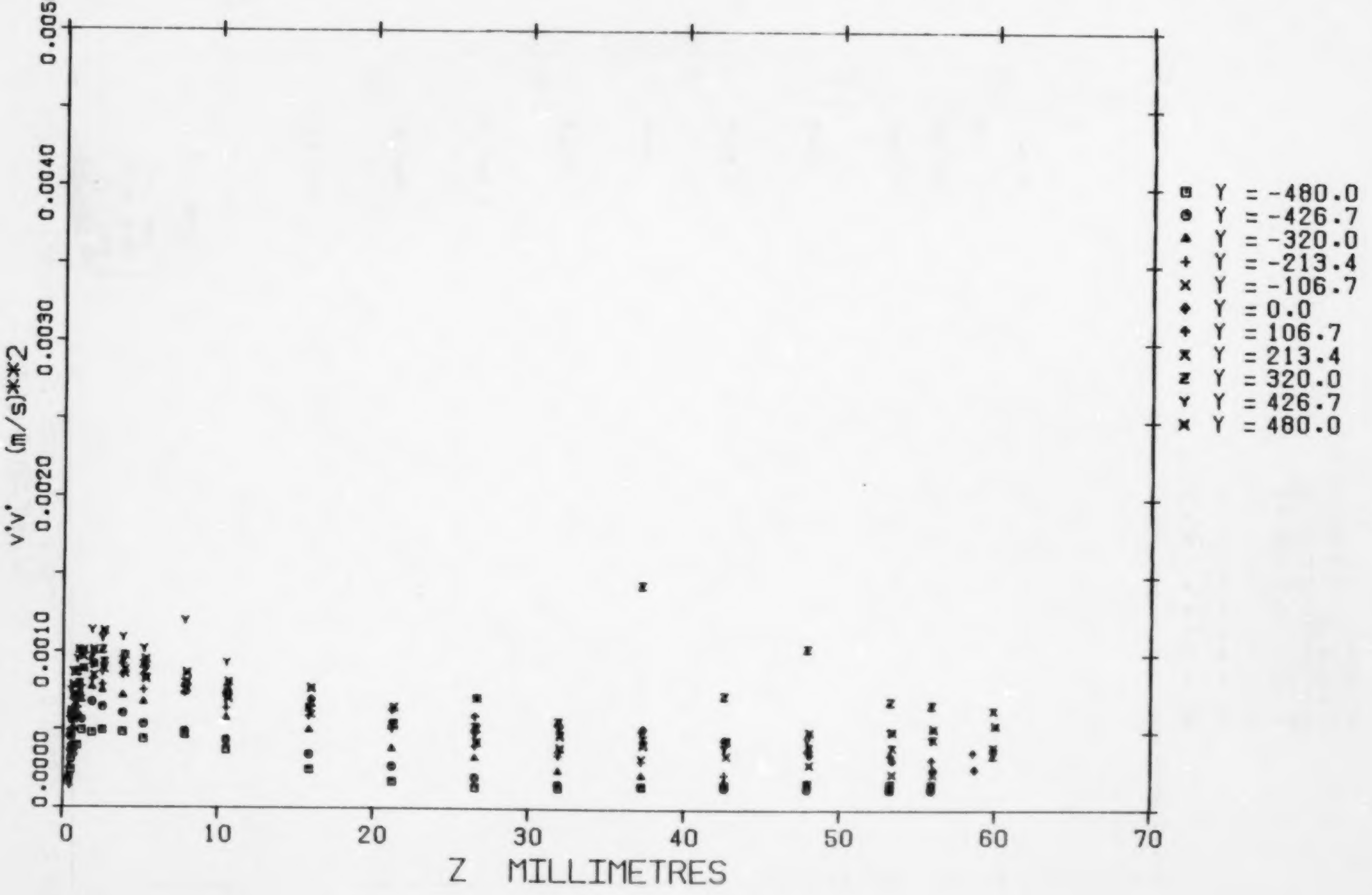

Figure 82. $\overline{v'^2}$ Turbulence Intensity Distribution (x = 9.68 m)

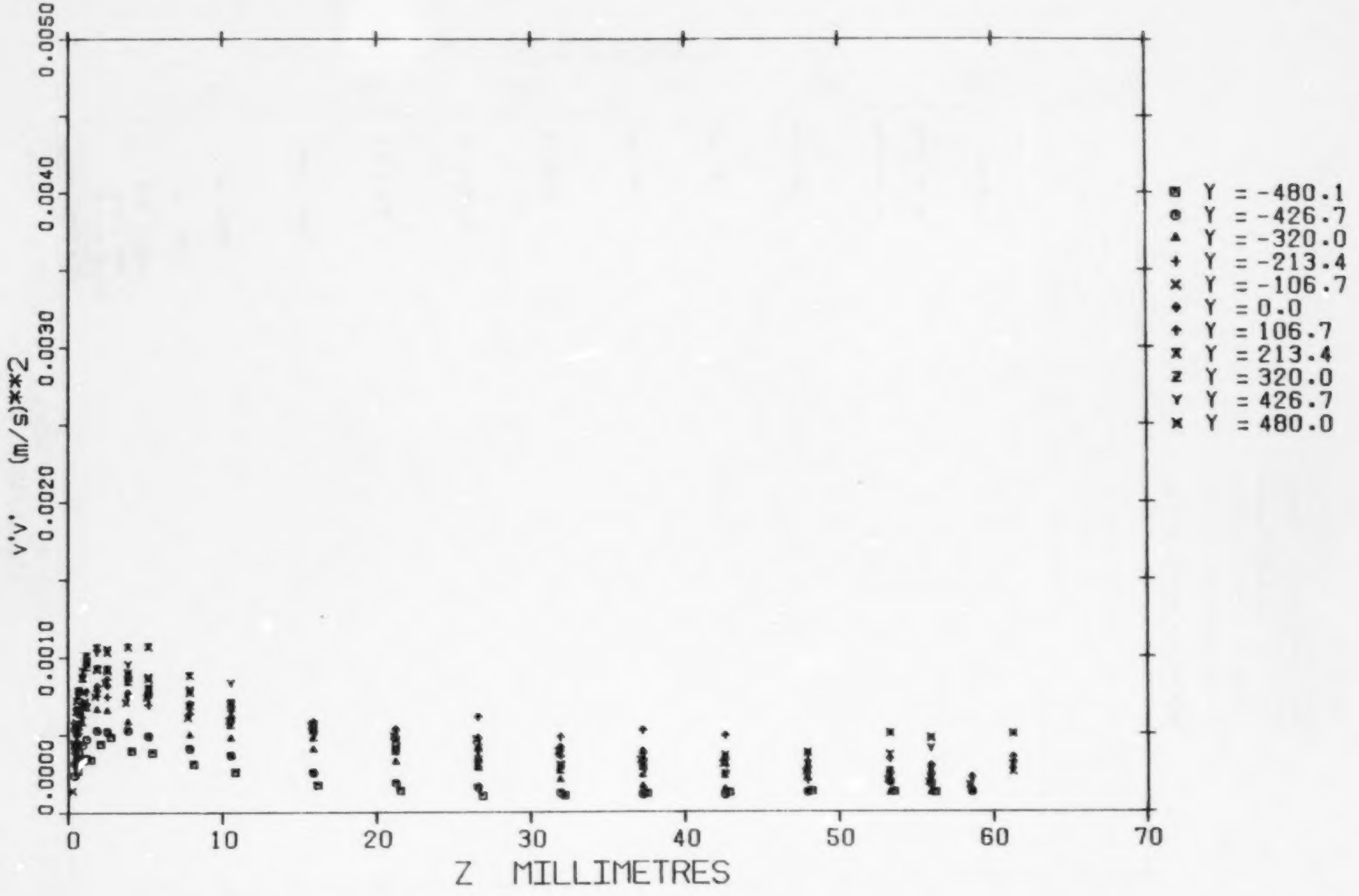

Figure 83. $\overline{v'^2}$ Turbulence Intensity Distribution
(x = 11.49 m)

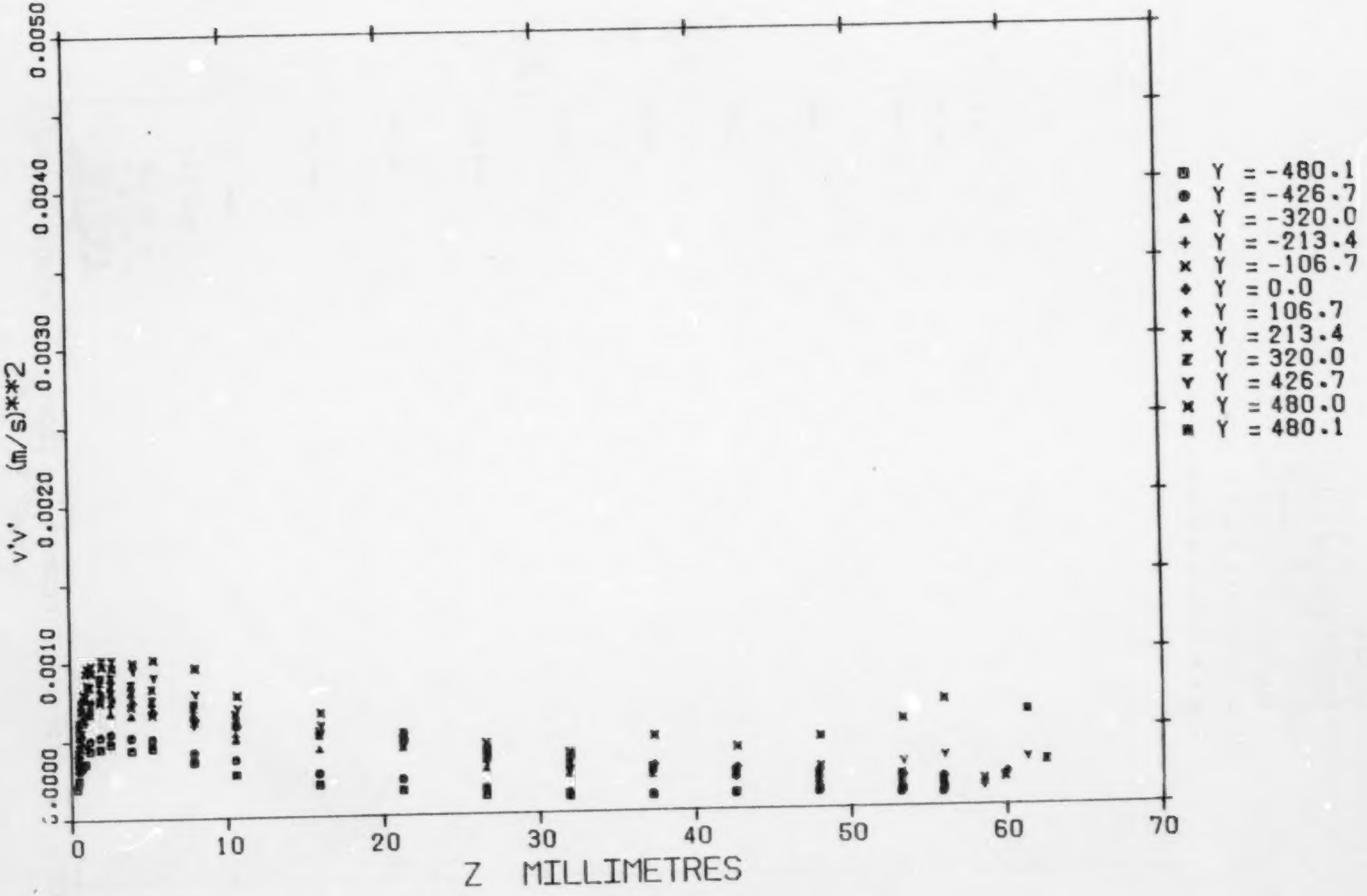

Figure 84. $\overline{v'^2}$ Turbulence Intensity Distribution (x = 13.41 m)

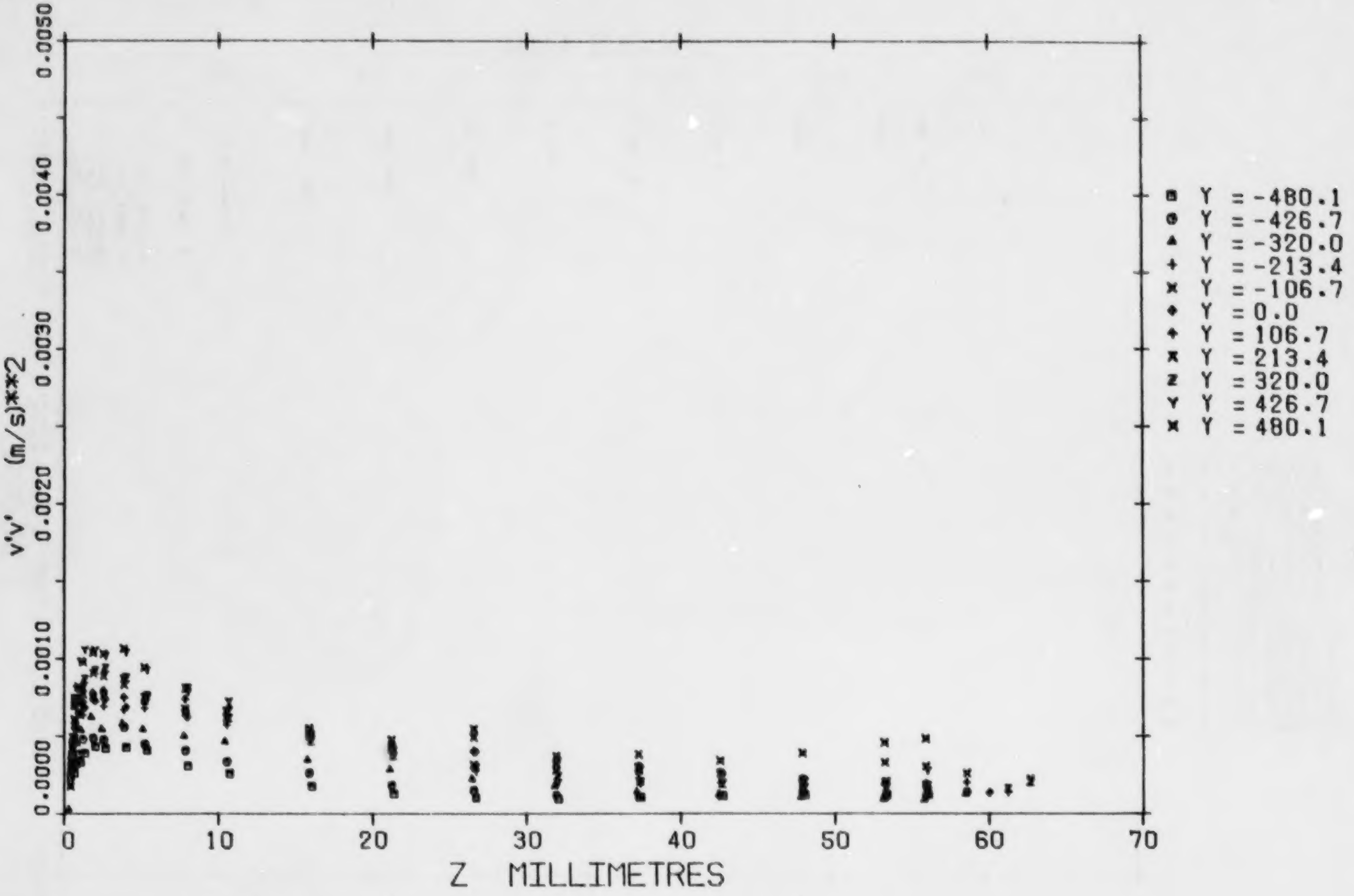

Figure 85. $\overline{v'^2}$ Turbulence Intensity Distribution (x = 16.18 m)

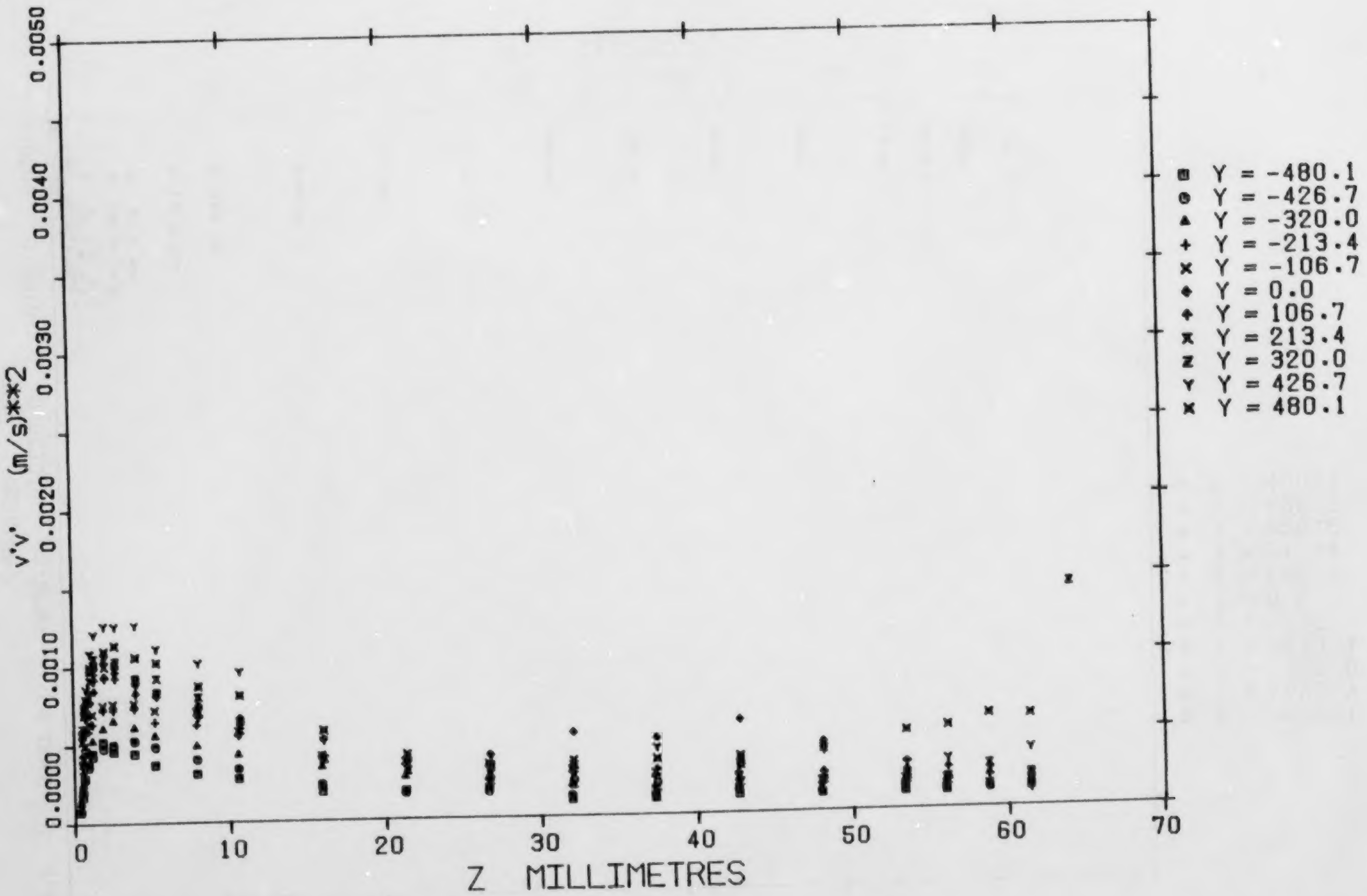

Figure 86. $\overline{v'^2}$ Turbulence Intensity Distribution (x = 17.43 m)

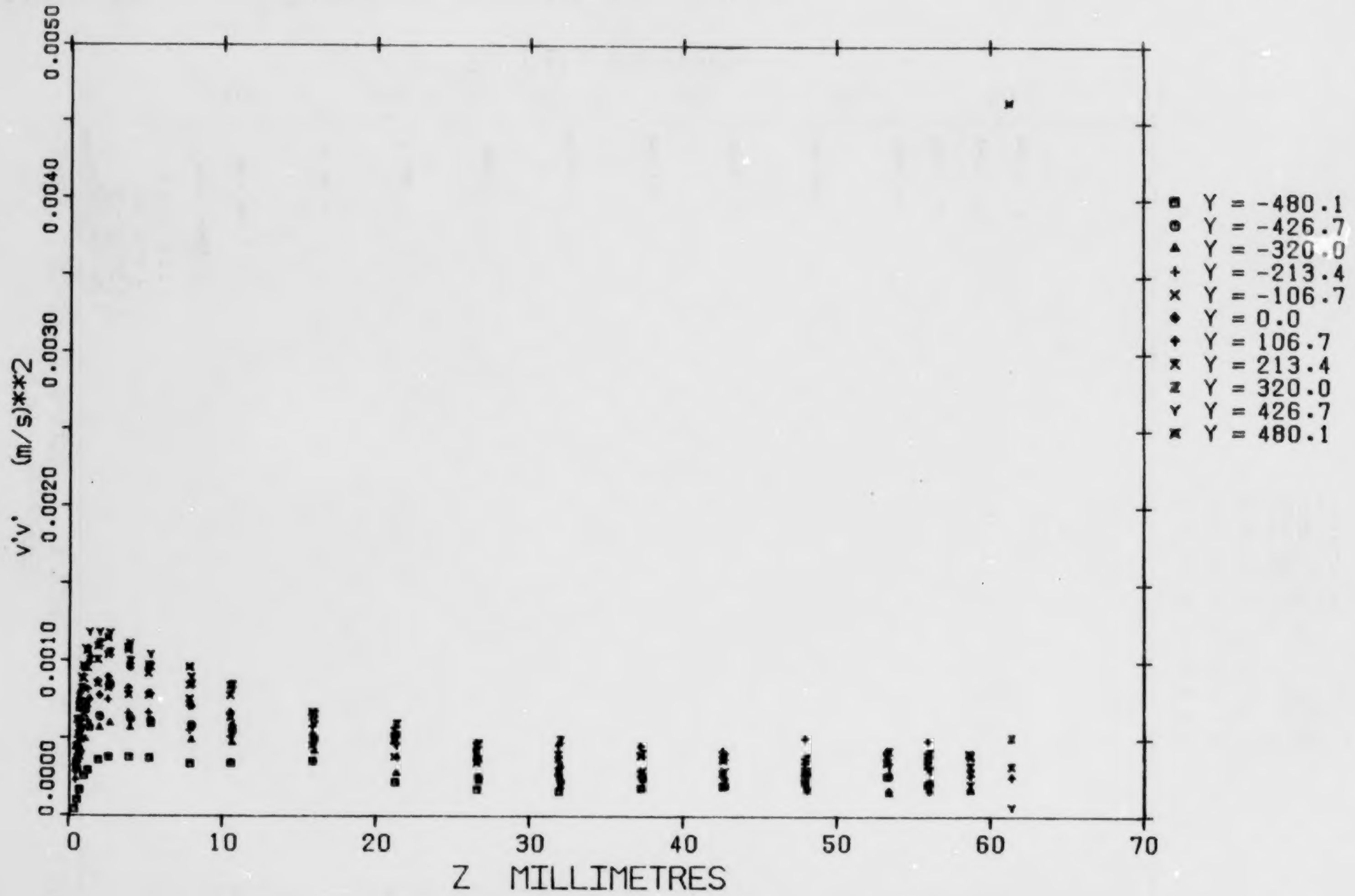

Figure 87. $\overline{v'^2}$ Turbulence Intensity Distribution (x = 18.65 m)

3.4 Analysis of Results

The results of the two experiments were reduced to profile scales to aid in evaluation of the overall trends of the developing flow. The mean longitudinal and lateral velocity for each profile were computed by direct integration. The variation of these quantities would show the redistribution of velocity to the inside of the bend at the beginning and then towards the outside through the rest of the bend.

The longitudinal bed stress was derived by analysis of the u velocity profile. A first estimate of u_* was obtained by fitting a semi-log line through the bottom 10 points of the profile. This estimate was then used to eliminate any points less than 70 ν/u_* from the bed. The regression was done again with the refined set of points until there was no change in u_*.

The total bed stress vector was assumed to be in the same direction as the velocity vector near the bed (Nash and Patel, 1972). Polar plots of velocity (Figure 88, for example) indicated that in many profiles there were several points measured for which this appeared to be true. The bed stress angle was derived by a linear regression of these points. The criteria used for the upper limit was that:

$$\frac{u}{u_*} < 12.0 \qquad (214)$$

as suggested by Nash and Patel (1972). Some profiles in the

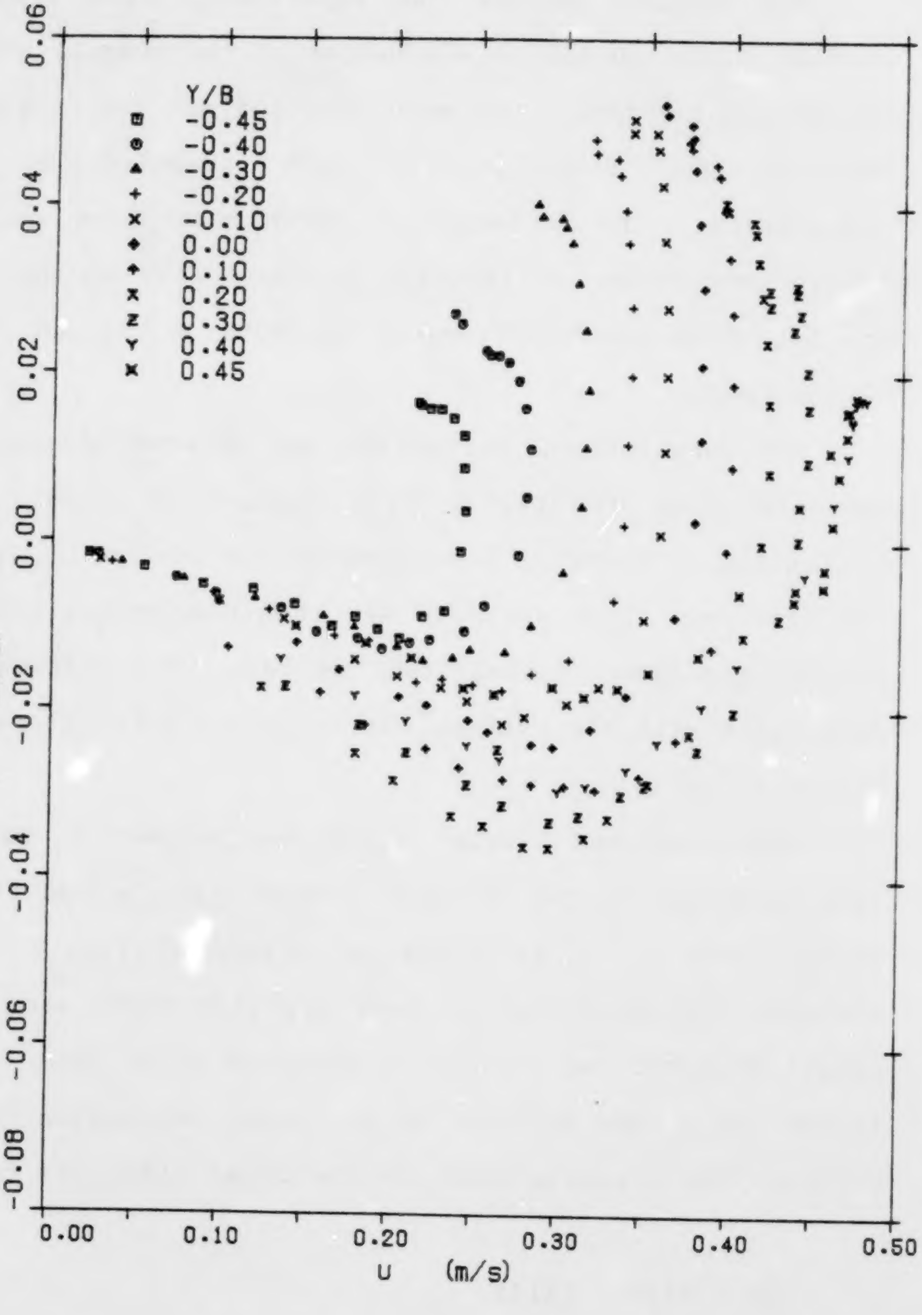

Figure 88. Polar Plot of Velocity Vector
(x = 11.49 m)

second run contained no points in this region and no bed stress angle was computed.

Once the bed stress angle was obtained it was a simple matter to calculate the lateral stress magnitude as:

$$\frac{\tau_{y0}}{\rho} = \tan\phi \, u_*^2 \tag{215}$$

To obtain a measure of the secondary (circulatory) flow the following integral was also calculated:

$$\overline{vz} = \frac{1}{d} \int_0^d z(v - \overline{v}) \, dz \tag{216}$$

This moment of the lateral velocity distribution gives an indiction of the relative strength of (zero depth average) circulation.

All of these quantities were calculated by a computer program which is included in Appendix B for reference. The regression curve fitting subroutine used was from Peterson and Howells (1981).

3.5 DISCUSSION

Figures 89 and 90 show the longitudinal variation of depth averaged longitudinal velocity for the two runs. From a relatively uniform lateral variation before the beginning

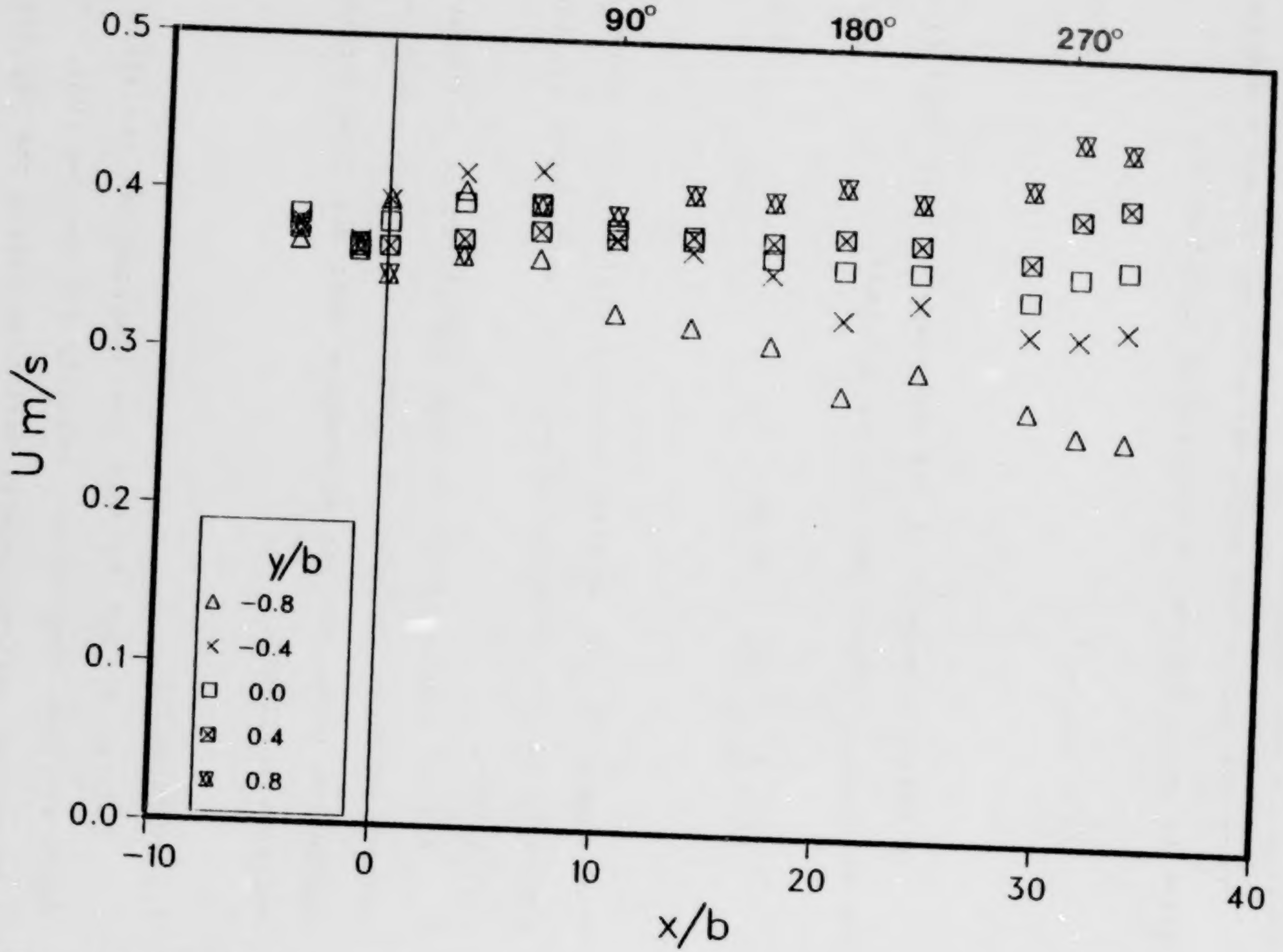

Figure 89. Longitudinal Variation of Depth Averaged Longitudinal Velocity - Run 1

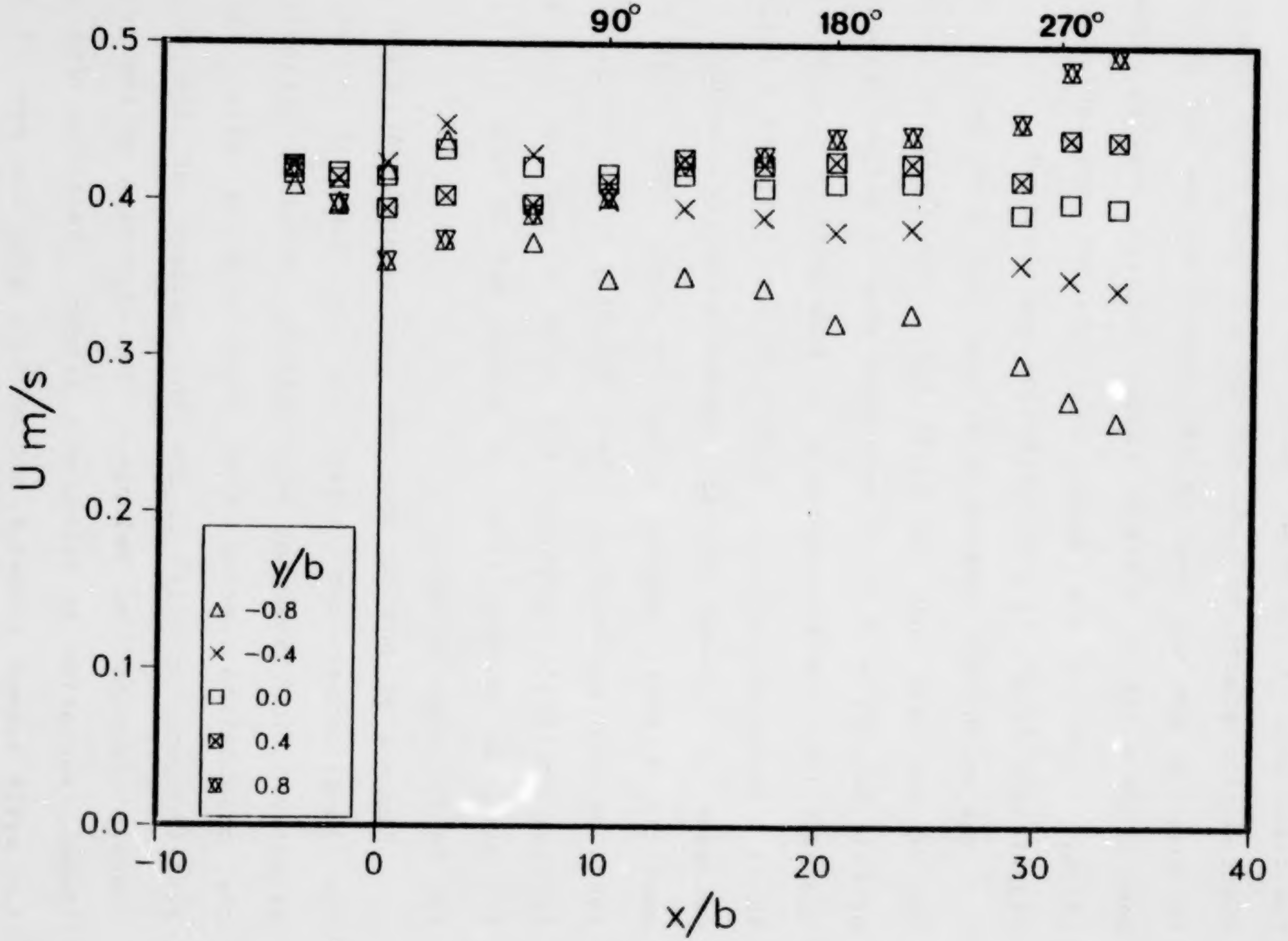

Figure 90. Longitudinal Variation of Depth Averaged Longitudinal Velocity - Run 2

of the bend (x/b = 5) the distribution skews inward for the first part of the bend. After x/b of about 10 the distribution starts to skew outward and this trend appears to continue for the rest of the bend. At the end of the bend (x/b = 32) a further sudden outward skewing takes place. Due to the short exit channel available, no significant return to a distribution was observed.

The second run appears to be even less developed by the end of the bend than the first run. The furthest inside profile (at b/y = -0.8) in both runs shows a larger velocity decrease than the corresponding outside profile (y/b = 0.8) shows a velocity increase. Both runs also indicate a slight decrease in cross-sectional average velocity through the bend but a small rebound after the bend. The ninth and tenth section appeared to behave slightly anomalously, with lateral variation appearing too large at section nine and too small at section ten. An uneven bed in this vicinity may be the explanation.

Figures 91 and 92 show the longitudinal variation of the longitudinal bed stress in the form of a shear velocity. With somewhat more scatter, possibly reflecting the calculation method more than anything else, these distributions basicly follow the pattern of the depth averaged longitudinal velocity. The magnitude of the cross channel variation is relatively larger. Sections nine and ten again appear somewhat out of line with the rest of the sections.

Figures 93 and 94 show the variation of bed stress angle as derived from the polar plots. These distributions show a significant variation across the channel with angles at both y/b = ±0.8 about 60% of the more central profiles. The distributions appear to be approximately constant after x/b ≈ 5 decreasing slightly in magnitude, if anything. The maximum angle for Run 1 ($\tan\phi \approx 0.20$) corresponds to a value of K of about 12 with an average value of about 10 in the central part of the channel through most of the bend. Insufficient profiles meeting the criteria were available to make any comments for run 2.

Figures 95 and 96 show the magnitude of the lateral bed stress as calculated from Equation 215. These variations are similar in general form to the bed stress angle plots but appear to vary more smoothly. The lateral variation is even more pronounced however and the lateral stress at y/b = 0.4 is clearly the largest for the greatest part of the bend.

Figures 97 and 98 show the variation of the depth averaged lateral velocity along the channel. These values are generally small (less than 5 per cent of the mean longitudinal velocity) but show an interesting variation. At the beginning of the bend (x/b = 0) there is a relatively large inward flow, followed almost immediately by a relatively large outward flow. For Run 1, the flow appears outward for most of the channel while for Run 2 the flow appears inward. Since the longitudinal velocity

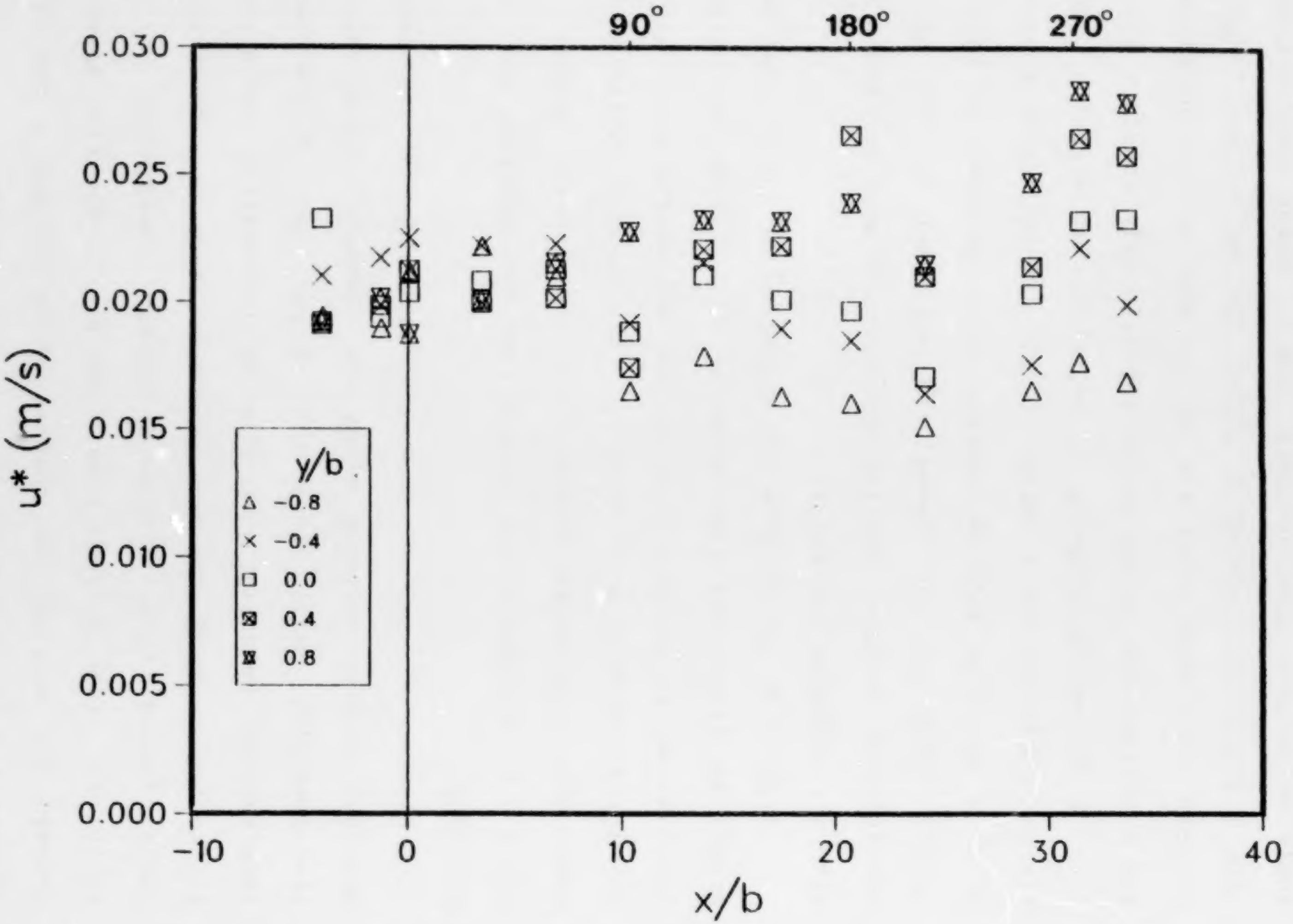

Figure 91. Longitudinal Variation of Longitudinal Shear Velocity - Run 1

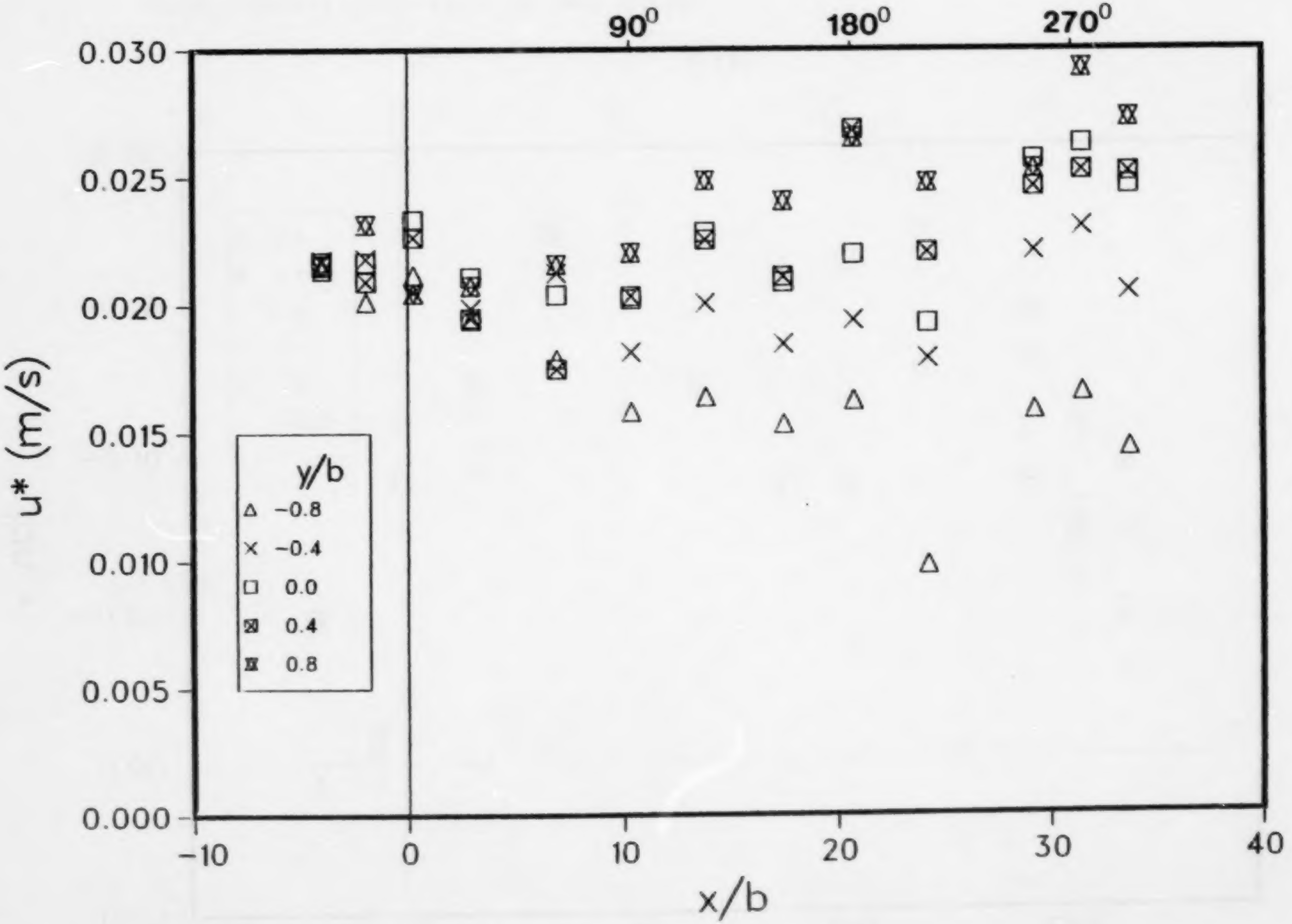

Figure 92. Longitudinal Variation of Longitudinal Shear Velocity - Run 2

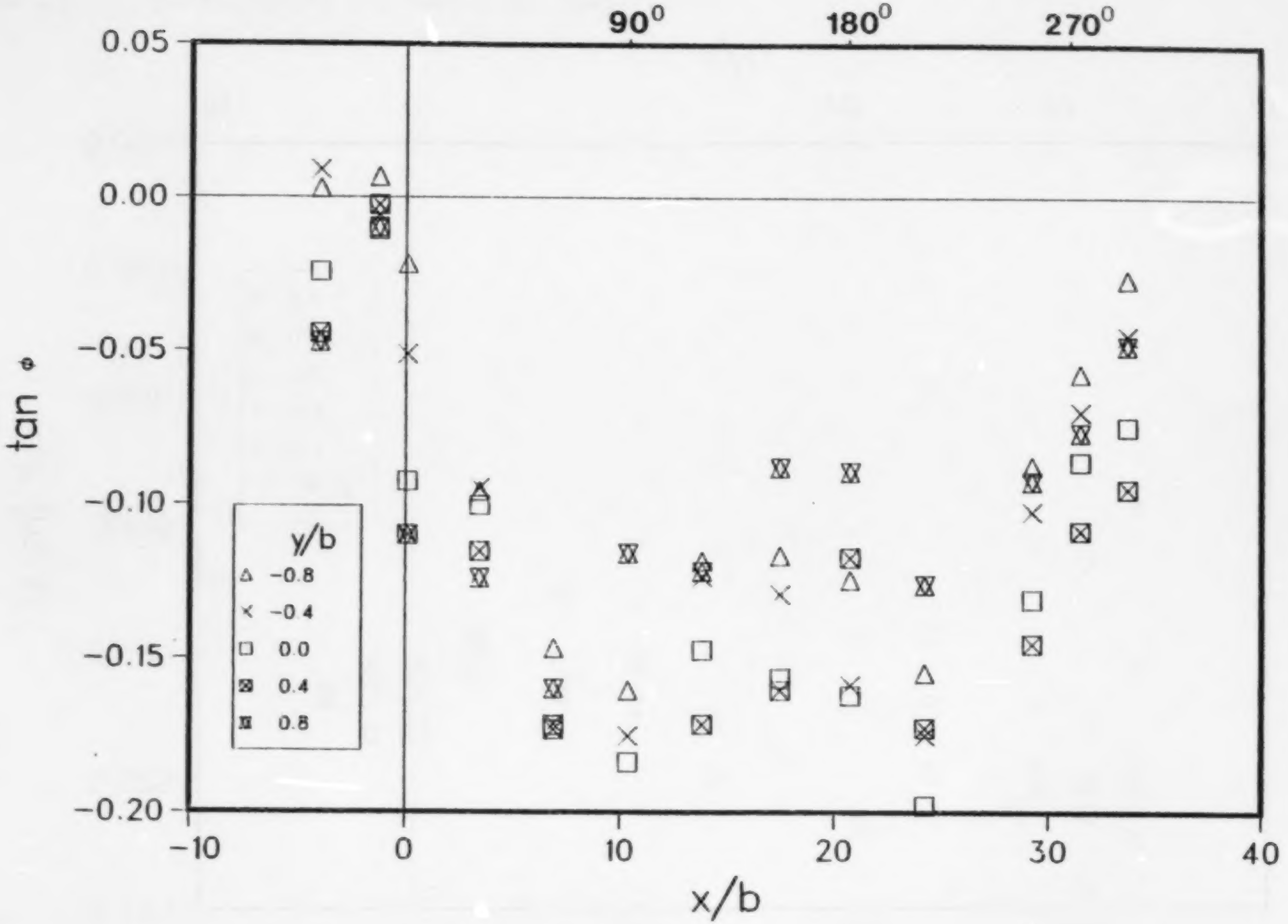

Figure 93. Longitudinal Variation of Bed Stress Angle - Run 1

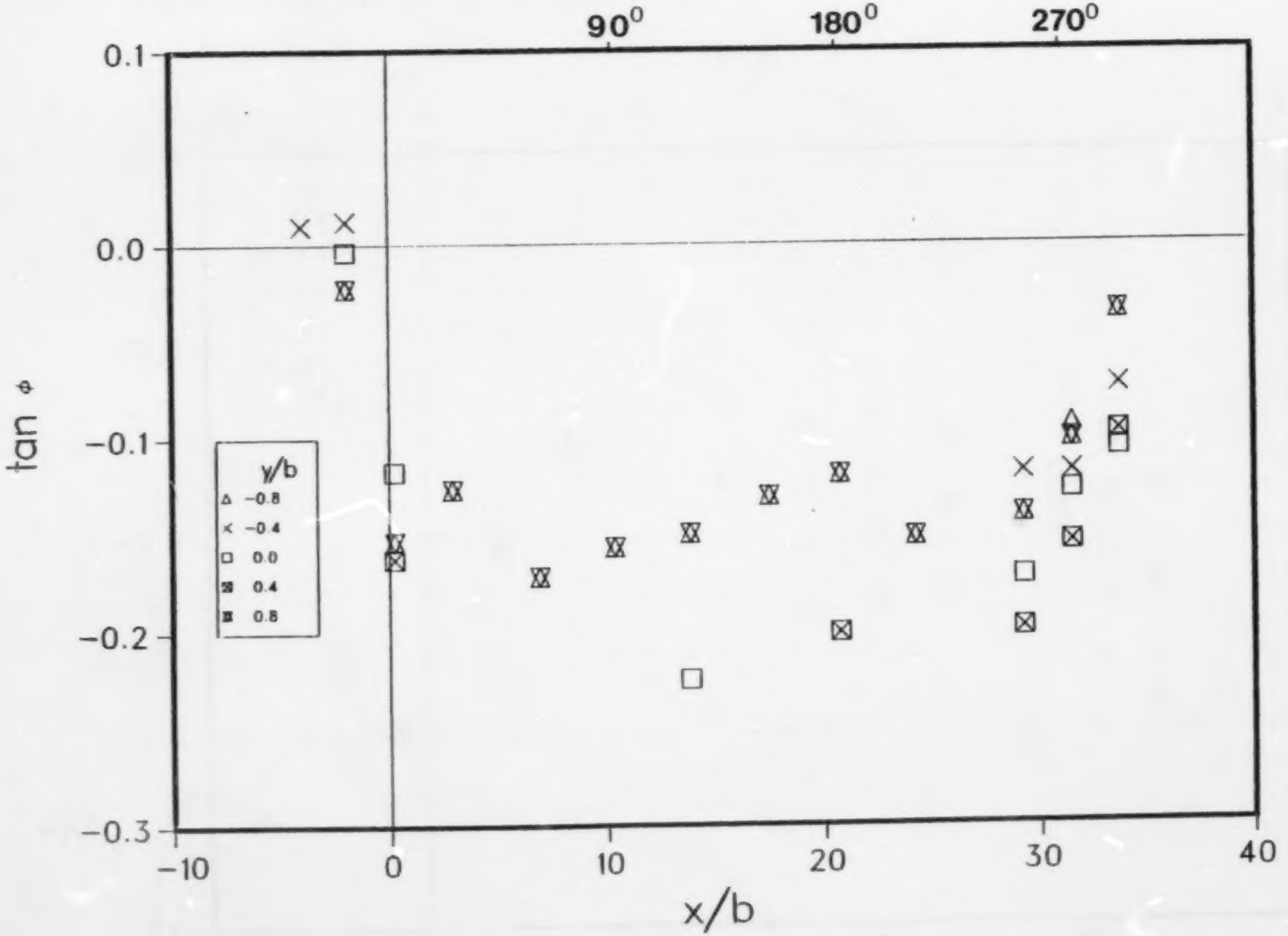

Figure 94. Longitudinal Variation of Bed Stress Angle - Run 2

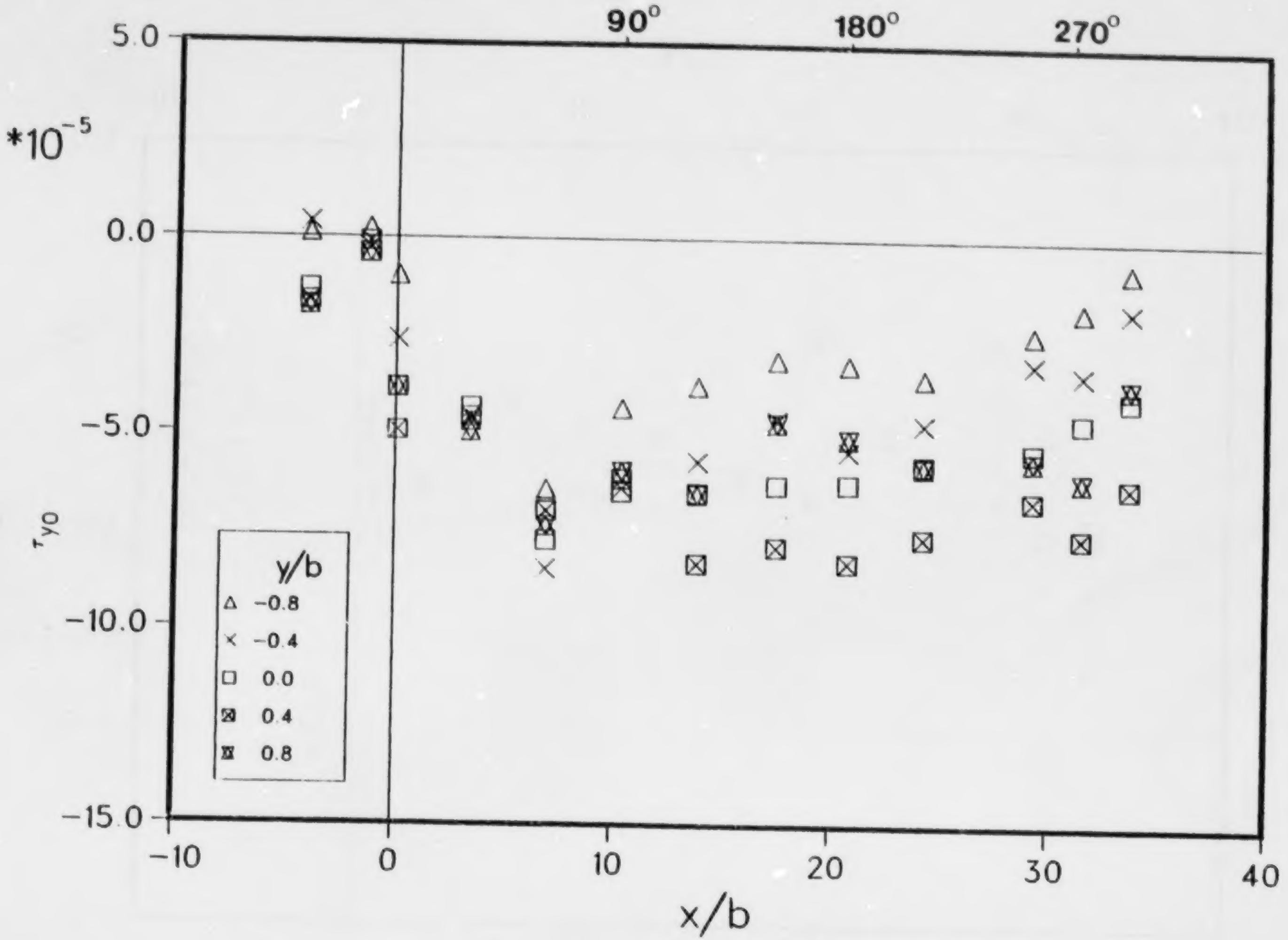

Figure 95. Longitudinal Variation of Lateral Bed Stress - Run 1

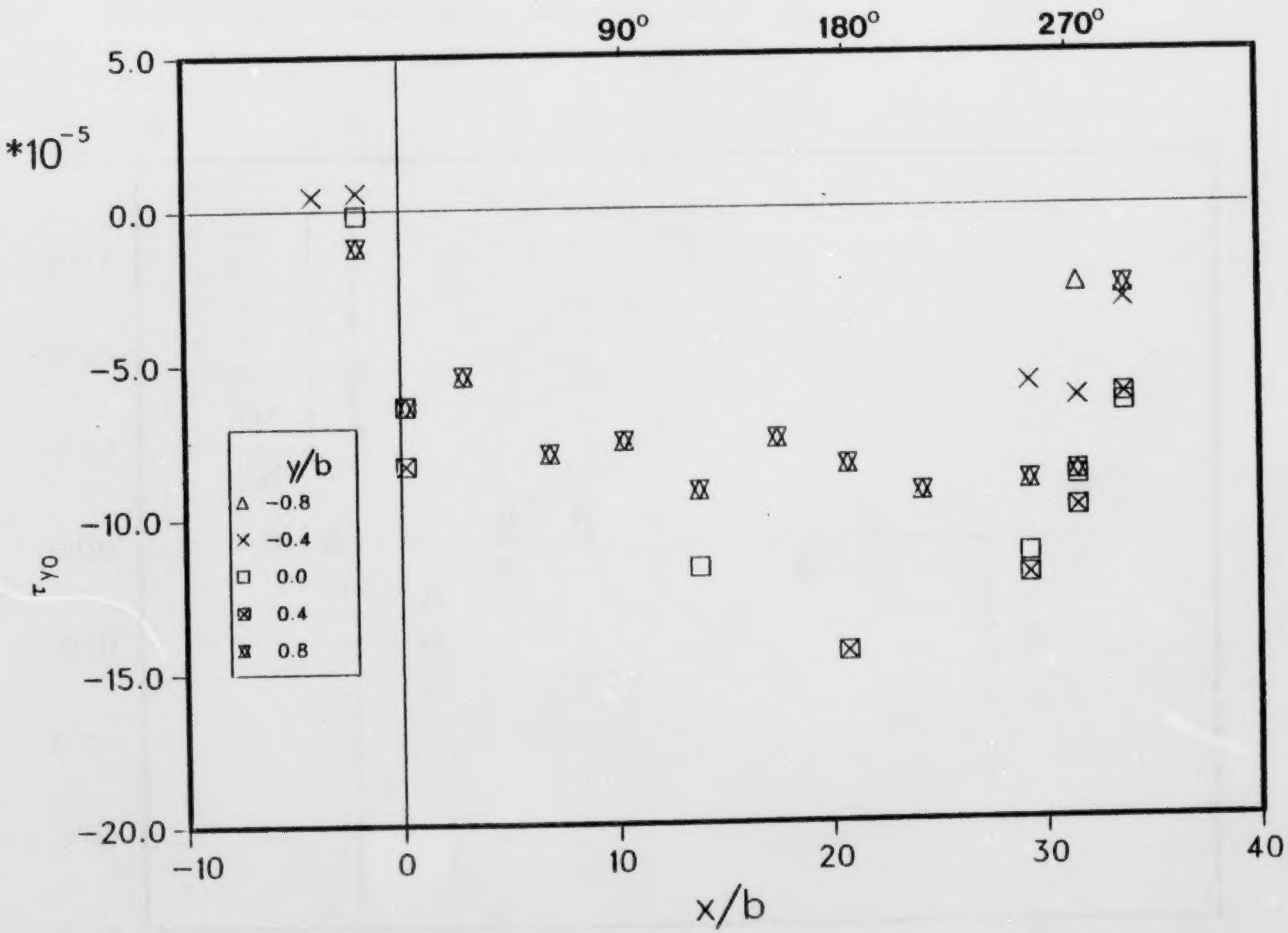

Figure 96. Longitudinal Variation of Lateral Bed Stress - Run 2

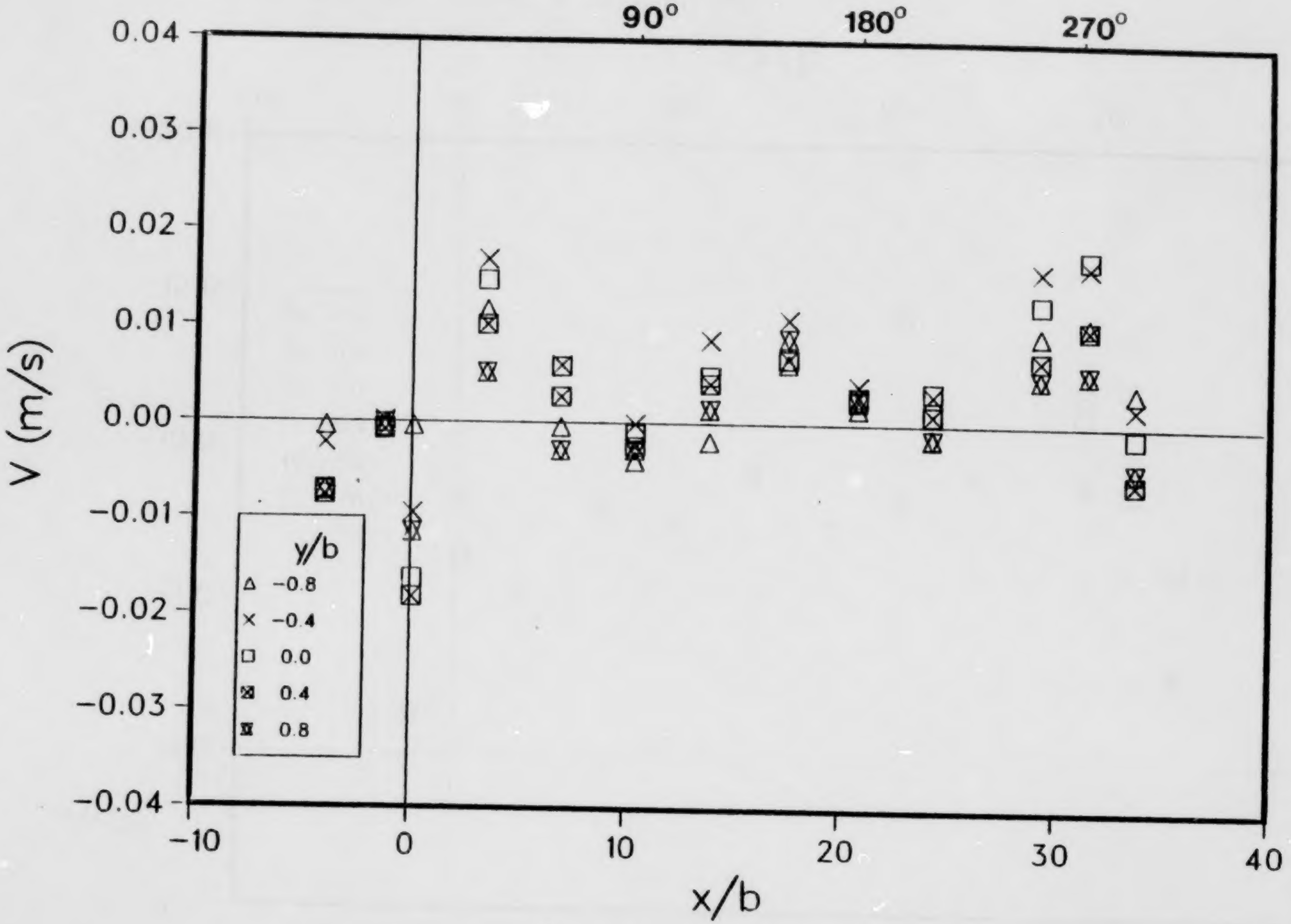

Figure 97. Longitudinal Variation of Depth Averaged Lateral Velocity - Run 1

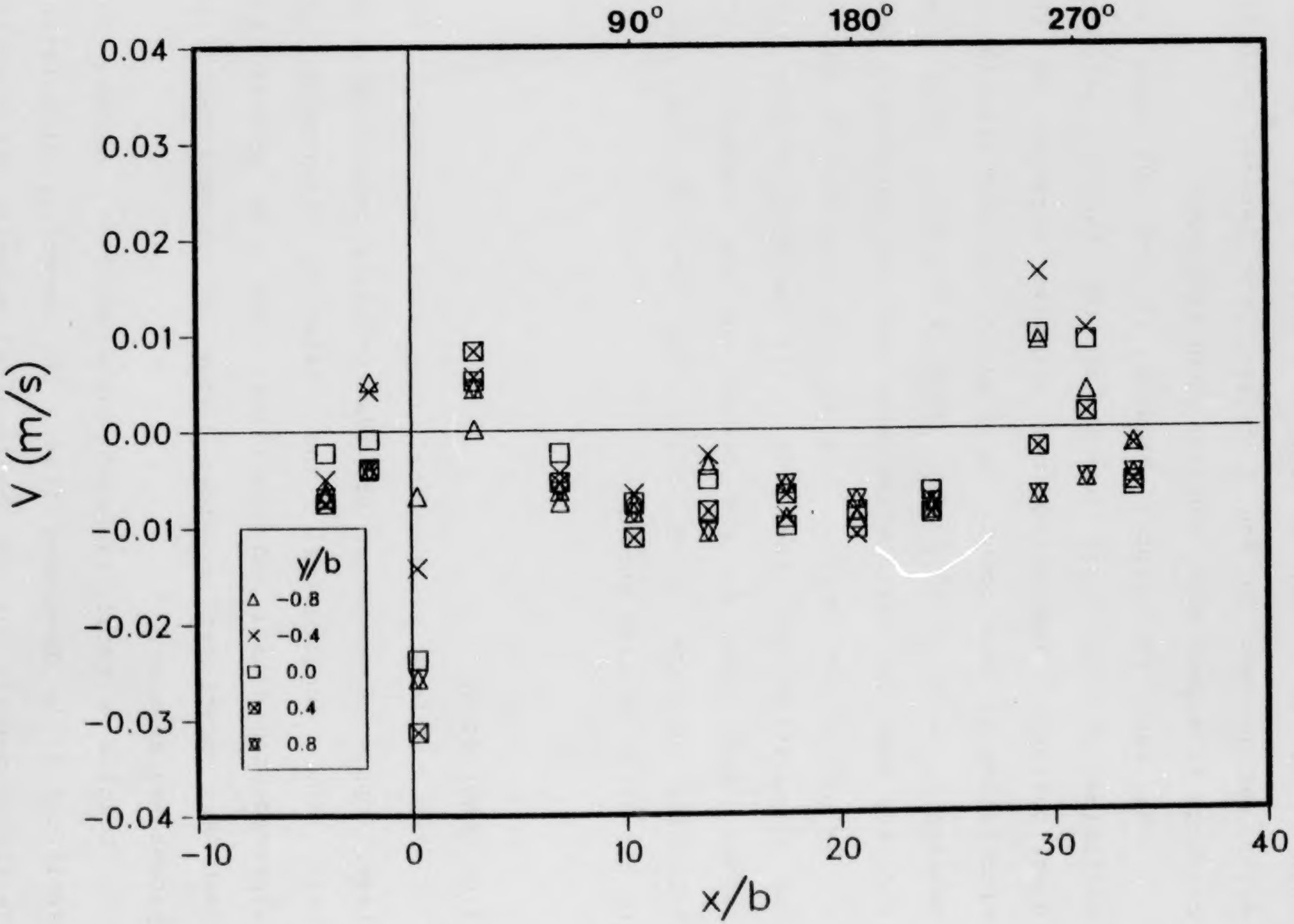

Figure 98. Longitudinal Variation of Depth Averaged Lateral Velocity - Run 2

distribution continued to skew outwards in Run 2 (even more than in Run 1) it may be concluded that a small alignment error was present in Run 2 causing the lateral velocity readings to appear more negative than they were.

The last two plots, Figures 99 and 100 show the variation of the first moment of the lateral velocity distribution. Indicating the relative strength of the circulation at this point, these plots show the circulation developing very quickly (by about x/b = 5). They also indicate that the circulation also declines noticeably over the length of the bend. This is more apparent in Run 2. The circulation near the side walls is considerably less (about half) than in the center of the channel. The beginning of the decay after the end of the curve (y/b = 32.0) is also shown.

3.6 CONCLUSIONS

Two complete experimental runs were performed. The Laser Doppler Anaemometer provided velocity measurements in both the longitudinal and lateral directions of unprecedented detail and precision. The time involved for each run precluded a wider range of geometrical flow parameters however.

Despite a total included angle of 270°, neither run exhibited fully developed flow. The secondary circulation developed quickly but the longitudinal velocity distribution

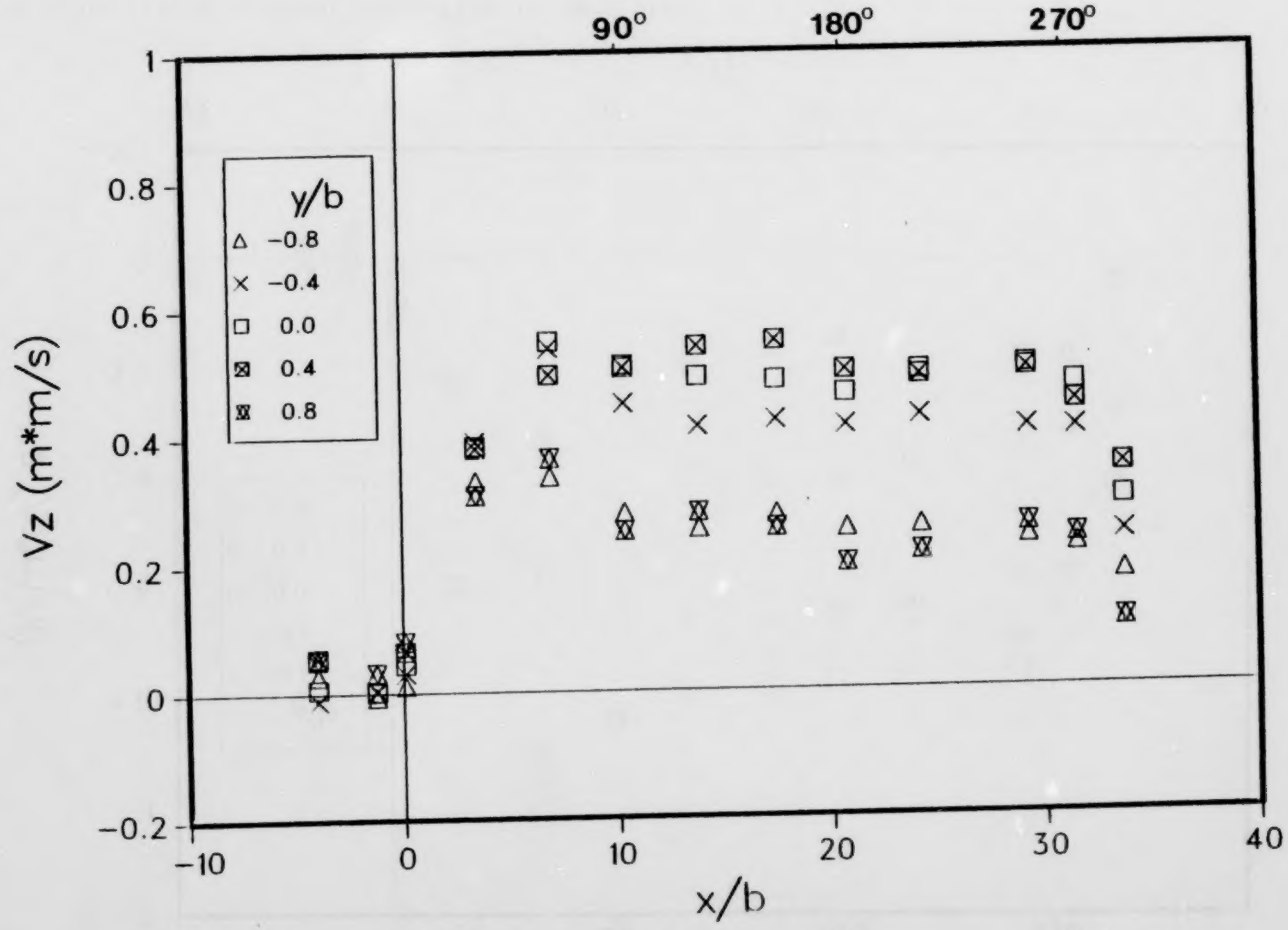

Figure 99. Longitudinal Variation of Secondary Circulation Intensity - Run 1

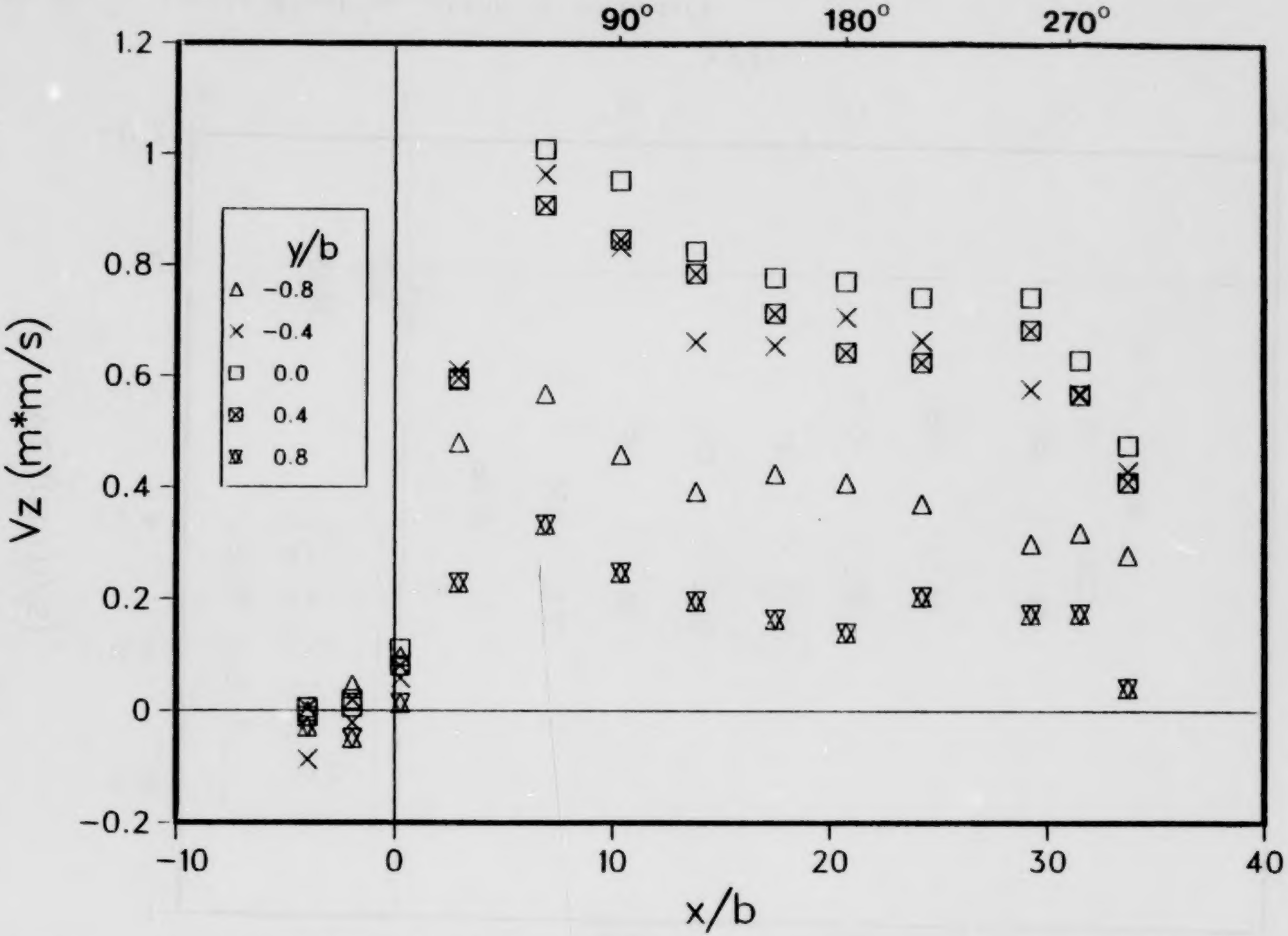

Figure 100. Longitudinal Variation of Secondary Circulation Intensity - Run 2

took far longer.

The longitudinal and lateral velocity profiles were detailed enough near the bed to allow a direct estimate of the velocity vector angle near the bed. This provided a reliable estimate of the bed stress angle and the controversial constant 'K'. It was found that this angle and constant remained approximately constant through the bend but varied considerably across the channel. A typical value of K near the centre of the channel was about 10, which is in close agreement with the assumption of Part One.

The theoretical analysis of Part Two suggests that vertical velocities should be measured, especially in the vicinity of the outside wall and also the lateral turbulent shear stress in this vicinity. The first should be measured because of it's importance in the skewing of the longitudinal velocity profile and second because of it's relation to the lateral eddy viscosity coefficient which also was important in this prediction. These two quantities are very small and would require extreme care even with the best facilities. Only a few sections would be necessary to validate or invalidate the theoretical assumptions made. It would also be desirable to measure the distributions of $\overline{u'w'}$ and $\overline{v'w'}$ directly to provide better stress information that does not rely on assumed velocity distributions. These again would require special facilities and care. The lateral stress $\overline{v'w'}$ especially would be difficult to measure because of geometrical problems.

Finally it would be desirable to make detailed measurements for a wider range of geometrical and flow parameters. The bed and side roughness especially could be changed, although the use of the LDA would be impaired if a clear viewport was not available.

In conclusion, detailed experiments were performed which further illustrate the flow mechanics, provide a reference for comparison with theoretical predictions and add significantly to the body of experimental knowledge. There remains, however, several apsects of problem completely unexplored and a wide range of parameters unmeasured.

CONCLUSION

In this study, the present knowledge was reviewed with the objectives of applying it to practical problems and identifying directions for further research. The lack of prediction methods for the developing and developed longitudinal velocity distribution was identified as the most important gap in the existing knowledge. It was also noted that few detailed experiments had been performed and many important quantities such as lateral bed stress angle and vertical velocity components and turbulence had been measured only indirectly, if at all.

On the positive side, it was found that a good understanding of many aspects of curved channel flow such as superelevation and secondary flow could be applied to practical problems. In particular it is possible to estimate the maximum scour depth in an alluvial channel. The method is still subject to considerable variation but certainly takes better account of the physics of the problem than the existing regime methods.

In an attempt to predict longitudinal velocity variations a perturbation analysis was performed on the governing equations of flow. Using the ratio of channel half width to centreline radius of curvature as the pertubation parameter it was found that a first order (linear) approximation included most of the interesting curved channel effects. The analysis depended on an assumption for the zero order (straight channel) velocity distribution and this may be the greatest weakness in this analysis.

A numerical solution for fully developed flow was run for a range of channel geometries and roughnesses. This provided an estimate of the maximum bank attack velocity likely to be encountered in a given problem. A simplified model of developing flow also gave reasonable agreement to experimental data.

The method appeared to account for all the velocity redistribution factors but is limited to rectangular channels. A useful extension of this work would be to generalize it to arbitrary cross-sectional shapes and also evaluate different initial velocity distribution assumptions. Less important but interesting would be to investigate different turbulence closure assumptions. Calculation of a second order approximation would also be interesting but would involve considerable effort.

An experimental study comprising detailed measurements of longitudinal and lateral velocity components for two flow situations was performed. The intricacies of the flow were revealed by these experiments and the results were used to validate the theoretical predictions. The long bend (270° included angle) covered most of the developing flow region but developed flow was not observed. Bend entrance and exit effects were observed. Measurements of vertical velocities and turbulent shear stresses have yet to be made and it would be desirable to obtain detailed measurements for a wider range of geometrical and flow parameters.

In summary, a detailed literature review, theoretical analysis, and experimental study have been performed on the subject of turbulent flow in curved channels. Although much more research needs to be done, it is felt that the direction taken by this study has provided some valuable results and the potential for further study.

BIBLIOGRAPHY

Ananyan, A.K. 1965. Fluid flow in bends of conduits. Jerusalem. Israel Program for Scientific Translation. 262 pp (translated from Russian).

Bathurst, J.C., C.R. Thorne, and R.D. Hey. 1979. Secondary flow and shear stress at river bends. Journal of the Hydraulics Division, ASCE 105(HY10); 1277-1295.

Bridge, J.S. and J. Jarvis. 1977. Velocity profiles and bed shear stress over various bed configurations in a river bend. Earth Surface Processes 2:281-294.

Buchave, P., W.K. George and J.L. Lumley. 1979. The measurement of turbulence with the Laser Doppler Anaemometer. Annual Review of Fluid Mechanics, 11:443-503.

Choudhary, U.K. and S. Narasimhan. 1977. Flow in 180° open channel rigid boundary bends. Technical note, Journal of the Hydraulics Division, ASCE 103(HY6): 651-657.

Durst, F., A. Melling and J.H. Whitelaw. 1976. Principles and practice of Laser Doppler Anaemometry. New York: Academic Press. 405 pp.

Einstein, H.A. and J.A. Harder. 1954. Velocity distribution and the boundary layer at channel bends. Transactions of the American Geophysical Union 35(1); 114-120.

Engelund, F. 1974. Flow and bed topography in channel bends. Journal of the Hydraulics Division, ASCE 100(HY11): 1631-1648.

Fischer, H.B., E.J. List, R.C.Y. Koh, J. Imberger and N.H. Brooks. 1979. Mixing in inland and coastal waters. New York: Academic Press. 483 pp.

Fox, J.A. and D.J. Ball. 1968. The analysis of secondary flow in open channels. Proceedings, Institution of Civil Engineers 39:467-475.

Francis, J.R.D. and A.F. Asfari. 1971. Velocity distributions in wide curved open-channel flows. Journal of Hydraulic Research, IAHR 9(1): 73-90.

Hinze J.O. 1075. Turbulence (second ed.). New York: McGraw-Hill. 790 pp.

Gerald, C.F. 1978. Applied Numerical Analysis. Second Edition. Reading, Massachusetts: Addison-Wesly Publishing Company. 518 pp.

Hooke, R.L. 1974. Shear stress and sediment distribution in a meander bend. Department of Physical Geography, University of Uppsala, Sweden, Report No. 30, 58 pp.

Ikeda, S., G. Parker and K. Sawai. 1981. Bend theory of river meanders, part 1, linear development. Journal of Fluid Mechanics 112: 363-377.

Ippen, A.T. and P.A. Drinker. 1962. Boundary shear stresses in curved trapezoidal channels. Journal of the Hydraulics Division, ASCE 88(HY5): 143-179.

Kalkwijk, J.P.Th., and H.J. de Vriend. 1980. Computation of the flow in shallow river bends. Journal of Hydraulic Research, IAHR 18(4): 327-341.

Kellerhals, R., C.R. Neill and D.I. Bray. 1972. Hydraulic and geomorphic characteristics of rivers in Alberta. River Engineering and Surface Hydrology Report 72-1. Edmonton Research Council of Alberta 54 pp.

Kamiyama, S. 1966. Two dimensional potential theory on flow through bend of arbitrary profile. Report of the Institute of High Speed Mechanics. Tohuku University, 18(172); 25-42.

Kikkawa, H., S. Ikeda and A. Kitagawa. 1976. Flow and bed topography in curved open channels. Journal of the Hydraulics Division, ASCE 102(HY9); 1327-1342.

Koch, F.G. 1980. Bed level computations for axisymmetric curved channels. Delft Hydraulics Laboratory, TOW Report R657-IX/W308-1, 69 pp.

Koch, F.G. and C. Flokstra. 1981. Bed level computations for curved alluvial channels. Proceedings of the XIX Congress, IAHR, New Delhi, 2(16); 357-364.

Leschizner, M.A. and W. Rodi. 1979. Calculation of strongly curved open channel flow. Journal of the Hydraulics Division, ASCE 105(HY10): 1297-1314.

Lin, C.C. and L.A. Segal. 1974. Mathematics applied to deterministic problems in the natural sciences. New York: Macmillan Publishing Co., Inc. 604 pp.

Nash, J.F. and V.C. Patel. 1972. Three-dimensional turbulent boundary layers. Atlanta. SBC Technical Books. 185 pp.

Nouh, M.A., and R.D. Townsend. 1979. Shear stress distribution in stable channel bends. Journal of the Hydraulics Division, ASCE 105(HY10): 1233-1245.

Nwachukwu, B.A. and C.R. Neill. 1972. Analysis of channel regime, North Saskatchewan River, Edmonton to provincial boundary. Repport REH/72/1. Edmonton: Reserach Council of Alberta. 75pp.

Odgaard, A.J. 1981. Transverse bed slope in alluvial channel bends. Journal of the Hydraulics Division, ASCE 107(HY12): 1677-1694.

Onishi, Y., S.C. Jain and J.F. Kennedy. 1976. Effects of meandering in alluvial streams. Journal of the Hydraulics Division, ASCE 102(HY7): 899-917.

Peterson, A.W. and R.F. Howells. 1981. Users Manual for Hyepol. Department of Civil Engineering, University of Alberta, 192 pp.

Rodi, W. 1980. Turbulence models and their application in hydraulics. State-of-the-Art Paper, IAHR, 104pp.

Rosovskii, I.L. 1961. Flow of water in bends of open channels. Jerusalem: Israel Program for Scientific Translation. 233pp (Translated from Russian).

Schlichting, H. 1979. Boundary-Layer Theory (seventh ed.). New York: McGraw-Hill. 817 pp.

Siebert, W., and W. Gotz. 1975. A study on the deformation of secondary flow in models of rectangular meandering channels. Proceedings of the XVI Congress, IAHR. 1975 July 27 - Aug. 1; Sao Paulo; 2(B-18): 141-149.

Soliman, M.M. and E.R. Tinney. 1968. Flow around 180° bends in open rectangular channels. Journal of the Hydraulics Division, ASCE 94(HY4); 893-908.

Varshney, D.V. and R.J. Garde. 1975. Shear distribution in bends in rectangular channels. Journal of the Hydraulics Division, ASCE 101(HY8): 1053-1066.

de Vriend, H.J. 1976. A mathematical model of steady flow in curved open shallow channels. Communications on Hydraulics, Department of Civil Engineering, Delft University of Technology. Report No. 76-1, 116 pp..

de Vriend, H.J. 1981. Velocity redistribution in curved rectangular channels. Journal of Fluid Mechanics. 107:423-439.

de Vriend, H.J. and H.J. Goldof. 1983. Main flow velocity in short river bends. Journal of Hydraulic Engineering, ASCE 109(7): 991-1011.

Yen, B.C. 1965. Characteristics of subcritical flow in a meandering channel. Institute for Hydraulic Research, University of Iowa. 76 pp.

Yen, C.L. 1970. Bed topography effect on flow in a meander. Journal of the Hydraulics Division, ASCE 969HY1): 57-73.

Yen, C.L. and B.C. Yen. 1971. Water surface configuration in channel bends. Journal of the Hydraulics Division, ASCE 97(HY2): 303-321.

Zimmermann, C. 1977. Roughness effects on the flow direction near curved stream beds. Journal of Hydraulic Research, IAHR 15(1): 73-85.

Zimmermann, C. and J.F. Kennedy. 1978. Transverse bed slopes in curved alluvial streams. Journal of the Hydraulics Division, ASCE 104(HY1): 33-48.

APPENDIX A

WATER SURFACE AT A CHANGE OF CHANNEL CURVATURE

Introduction

The problem of flow in curved open channels is important in hydraulic engineering and has been the subject of much recent research. In most of this work the lateral pressure gradient has been assumed to be an algebraic function of the local channel curvature. Clearly, however, in cases where the curvature changes abruptly, the water surface adjusts continuously. Inspection of experimental water surface profiles indicates that an adjustment length about equal to the channel width is required.

Calculations of developing secondary flow may be quite strongly influenced by the water surface configuration. Rosovskii (1961) and Nouh and Townsend (1979) give a development length (to 90%) for secondary flow as:

$$L \approx 2.0\ HC_f \qquad \text{(A1)}$$

where H is the average depth of flow and C_f is the non-dimensional Chezy coefficient. Therefore many situations will arise where this length is comparable to the development length for the superelevation.

Studies which do account for this phenomenon such as the numerical models of Leschizner and Rodi (1979) and de Vriend (1981) or potential flow solutions such as Kamiyama

(1966) neglect free surface effects and therefore theoretically apply only to situations of small Froude number. It is thus of interest to investigate the effect of Froude number on the water surface configuration.

This paper presents a simple model for the water surface configuration in the vicinity of an abrupt change in channel curvature taking free surface effects into account. The flow is assumed frictionless and the curvature is assumed mild. Preliminary comparisons with experiments are also presented.

Analysis

Referring to Figure A1 we may write the depth averaged Euler and continuity equations for a rectangular channel in a locally cylindrical coordinate system as:

$$\frac{u}{(1 + \frac{y}{R})} \frac{\partial u}{\partial x} + v\frac{\partial u}{\partial y} + \frac{2uv}{R(1 + \frac{y}{R})} = \frac{-g}{(1 + \frac{y}{R})} \frac{\partial h}{\partial x} \qquad \text{(A2)}$$

$$\frac{u}{(1 + \frac{y}{R})} \frac{\partial v}{\partial x} + v\frac{\partial v}{\partial y} + \frac{(v^2 - u^2)}{R(1 + \frac{y}{R})} = -g\frac{\partial h}{\partial y} \qquad \text{(A3)}$$

$$\frac{1}{(1 + \frac{y}{R})} \frac{\partial (uh)}{\partial x} + \frac{\partial (vh)}{\partial y} + \frac{vh}{R(1 + \frac{y}{R})} = 0 \qquad \text{(A4)}$$

wherein the centreline radius of curvature, R, may vary with x.

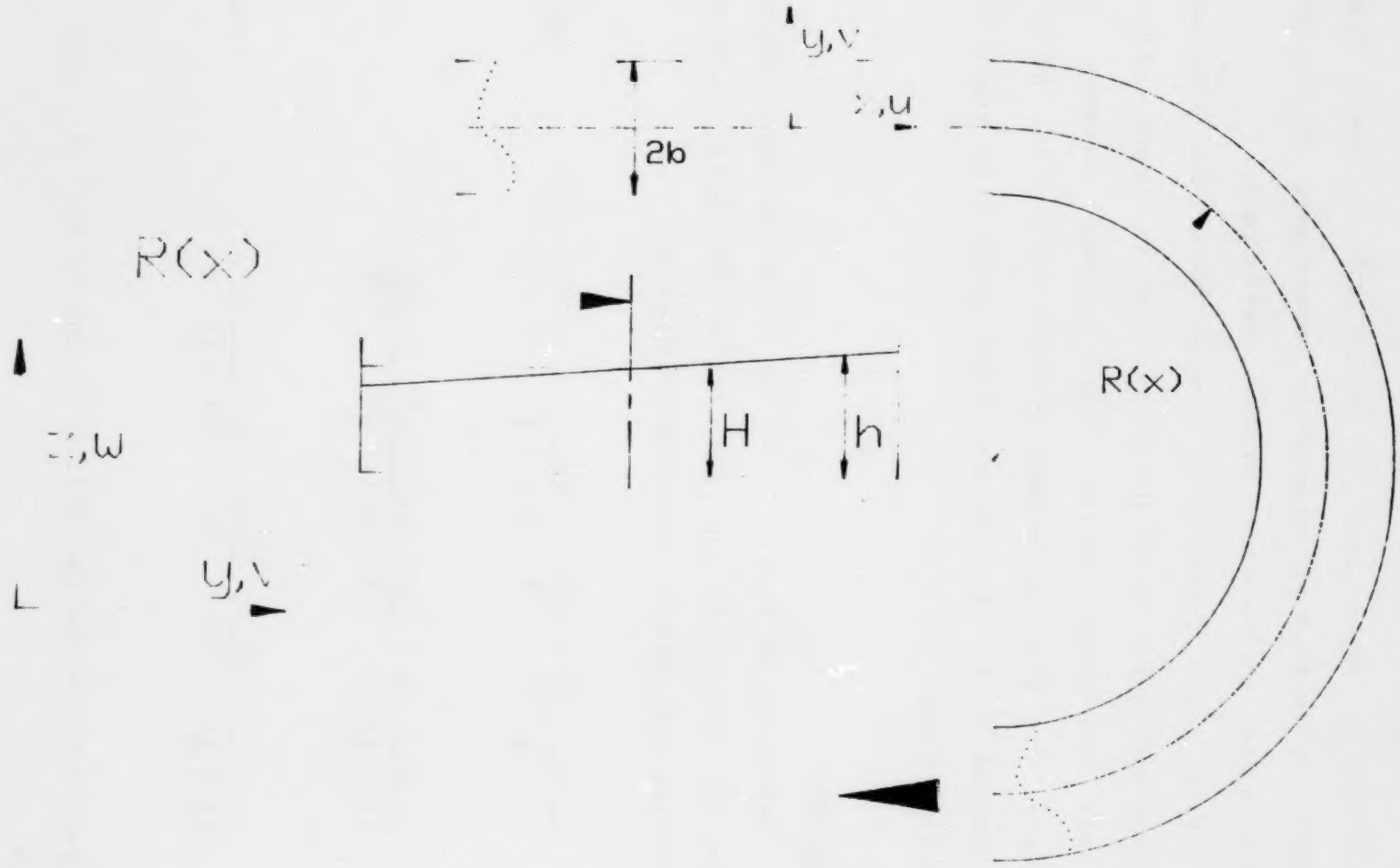
y,v
x,u
2b
R(x)
z,w
y,v
H
h
R(x)

Figure A1. Definition Sketches

The pressure distribution has been assumed hydrostatic and all friction terms have been neglected. The latter assumption is based on the traditional transition assumption of a short length and on the fact that even for fully developed flow in a curved channel, frictional effects on the superelevation are small (Yen and Yen, 1971).

It is useful to non-dimensionalize Equations 2 to 4 using the undisturbed straight channel mean values as scales.

Let:

$$u = Uu_*;\ v = Uv_*;\ h = Hh_* \qquad \text{(A5-A7)}$$

Also let:

$$x = bx_*;\ y = by_*;\ R = R_0R_* \qquad \text{(A8-A10)}$$

where R_0 is the minimum value of R expected.

These may be introduced into Equations 2 to 4 and after some simplification (starred quantities are now represented by their unstarred equivalents) we obtain:

$$\frac{u}{(1 + \frac{\alpha y}{R})} \frac{\partial u}{\partial x} + v\frac{\partial u}{\partial y} + 2\alpha\left(\frac{uv}{R(1 + \frac{\alpha y}{R})}\right) = \frac{-1}{F_R^2\ (1 + \frac{\alpha y}{R})} \frac{\partial h}{\partial y} \qquad \text{(A11)}$$

$$\frac{u}{(1 + \frac{\alpha y}{R})} \frac{\partial v}{\partial x} + v\frac{\partial v}{\partial y} + \frac{\alpha}{R} \left(\frac{v^2 - u^2}{(1 + \frac{\alpha y}{R})}\right) = \frac{-1}{F_R^2} \frac{\partial h}{\partial y} \qquad \text{(A12)}$$

$$\frac{1}{(1 + \frac{\alpha y}{R})} \frac{\partial uh}{\partial x} + \frac{\partial vh}{\partial y} + \frac{\alpha}{R} \frac{vh}{(1 + \frac{\alpha y}{R})} = 0 \qquad \text{(A13)}$$

wherein:

$$\alpha = \frac{b}{R_0} \qquad \text{(A14)}$$

and:

$$F_R^2 = \frac{U^2}{gH} \qquad \text{(A15)}$$

For all but the sharpest bends α is small compared to one. This leads naturally to a solution of the above problem in terms of a power series in α. Thus:

$$u(x,y,F_R,\alpha)+ u_0(x,y,F_R)+ \alpha u_1(x,y,F_R)+ \alpha^2 u_2(x,y,F_R)+\text{etc.} \qquad \text{(A16)}$$

Also:

$$\frac{1}{(1 + \frac{\alpha y}{R})} = 1 - \frac{\alpha y}{R} + \frac{\alpha^2 y^2}{R^2} - \ldots. \qquad \text{(A17)}$$

by binomial expansion.

Equations 16 and 17 may be substituted into 11 through 12 and then grouped by degree of α to be solved separately. The solution to the zero order group is simply:

$$u_0 = 1;\ h_0 = 1;\ v_0 = 0 \qquad \text{(A18-A20)}$$

The first order group with 18-20 substituted becomes:

$$\frac{\partial u_1}{\partial x} = - \frac{1}{F_R^2} \frac{\partial h_1}{\partial x} \quad (A21)$$

$$\frac{\partial v_1}{\partial x} - \frac{1}{R} = - \frac{1}{F_R^2} \frac{\partial h_1}{\partial y} \quad (A22)$$

$$\frac{\partial u_1}{\partial x} + \frac{\partial h_1}{\partial x} + \frac{\partial v_1}{\partial y} = 0 \quad (A23)$$

These equations may be solved for h_1 to give:

$$\frac{\partial^2 h_1}{\partial x^2} + \frac{1}{(1 - F_R^2)} \frac{\partial^2 h_1}{\partial y^2} = 0 \quad (A24)$$

Boundary conditions at $y = \pm 1$ may be obtained from Equation 22:

$$\left(\frac{\partial h_1}{\partial y}\right)_{y = \pm 1} = \frac{1}{R(x)} \quad (A25)$$

At $x = \pm \infty$

$$\left(\frac{\partial h_1}{\partial x}\right)_{x = \pm \infty} = 0 \quad (A26)$$

Similar equations for u_1 and w_1 may also be obtained:

$$\frac{\partial^2 u_1}{\partial x^2} + \frac{1}{(1 - F_R^2)} \frac{\partial^2 u_1}{\partial y^2} = 0 \quad (A27)$$

$$\frac{\partial^2 w_1}{\partial x^2} + \frac{1}{(1 - F_R^2)} \frac{\partial^2 w_1}{\partial y^2} = \frac{d}{dx} \left(\frac{1}{R}\right) \qquad (A28)$$

The boundary conditions for Equation 28 are simply:

$$w_1 = 0 \text{ at } y = \pm 1 \text{ and } x = \pm \infty \qquad (A29)$$

Because of the simple boundary conditions the boundary value problem represented by Equations 28 and 29 will be the one actual solved with u_1 and h_1 given later by Equations 21 and 23.

For the situation of a long straight reach followed by a long curved reach $\frac{1}{R(x)}$ may be specified as follows:

$$\frac{1}{R} = 0\ ; \quad -\infty < x < x_0 \qquad (A30)$$
$$\frac{1}{R} = 1; \quad x_0 < x < \infty$$

where x_0 is the point of curvature change.

It should be noted that Equations 28-29 form a linear system and a solution for arbitrary $\frac{1}{R(x)}$ may be formed by superpositions of the solution for Equation 28.

Equation 28 is elliptic for $F_R < 1$ and hyperbolic for $F_R > 1$. Standing cross channel waves for supercritical flow are correctly predicted (to a linear approximation). In the following only the subcritical case will be considered.

The derivative of the unit step function defined in Equation 30 is the Dirac delta function denoted as D $(x - x_0)$. Letting:

$$a^2 = \frac{1}{(1 - F_R^2)} \tag{A31}$$

Equation 28 becomes:

$$\frac{\partial^2 v_1}{\partial x^2} + a^2 \frac{\partial^2 v_1}{\partial y^2} = D\ (x - x_0) \tag{A32}$$

This boundary value problem may be solved by the Fourier Transform method. Take the Fourier Transform of Equation 32 with respect to $(x - x_0)$

$$-k^2 V - a^2 \frac{d^2 V}{dy^2} = \frac{1}{\sqrt{2\pi}} \tag{A33}$$

where V is the Fourier transform of v_1. Rearrange Equation 33:

$$\frac{d^2 V}{dy^2} - \frac{k^2}{a^2} V = \frac{1}{\overline{\sqrt{2\pi}}\ a^2} \tag{A34}$$

The boundary conditions become:

$$V = 0 \text{ at } y \pm 1 \tag{A35}$$

The general solution of 34 is:

$$V = A\cosh\left(\frac{ky}{a}\right) + B\sinh\left(\frac{ky}{a}\right) + C \qquad (A36)$$

Applying the boundary conditions:

$$0 = A\cosh\left(\frac{k}{a}\right) - B\sinh\left(\frac{k}{a}\right) + C \qquad (A37)$$

$$0 = A\cosh\left(\frac{k}{a}\right) + B\cosh\left(\frac{k}{a}\right) + C \qquad (A38)$$

Solving:

$$B = 0 \qquad (A39)$$

$$A = \frac{1}{k^2 \sqrt{2\pi} \cosh(k/a)} \qquad (A40)$$

$$C = -\frac{1}{k^2 \sqrt{2\pi}} \qquad (A41)$$

Thus:

$$V = \frac{1}{k^2 \sqrt{2\pi}} \left(\frac{\cosh(\frac{ky}{a})}{\cosh(\frac{k}{a})} - 1\right) \qquad (A42)$$

Take the inverse Fourier Transform:

$$v_1 = \frac{1}{2\pi} \int_{-\infty}^{\infty} \frac{1}{k^2} \left(\frac{\cosh(\frac{ky}{a})}{\cosh(\frac{k}{a})} - 1\right) e^{-ik(x-x_0)} dk \qquad (A43)$$

The integral may be evaluated using contour integration in the complex plane. The formula is:

$$\int_C (\ ) = \sum \text{(Residues at singularities enclosed within C)} \tag{A44}$$

The contour used was along the real axis from $-\infty$ to ∞ then along a semicircular arc at $|k| = \infty$ back to $k = -\infty$ (real). The singularities enclosed are simple poles at

$$y = \frac{(2n+1)\ \pi i}{2/a} \tag{A45}$$

The residue at each pole is thus:

$$R_n = \frac{\left(\cosh\left(\frac{(2n+1)\ \pi y i}{2}\right) \exp\left(\frac{(2n+1)\ \pi d(x-x_0))}{2}\right)\right)}{-\left(\frac{(2n+1)^2 a\pi^2}{4}\right) \sinh\left(\frac{(2n+1)\ \pi i}{2}\right)} \tag{A46}$$

Thus:

$$v_1 = \frac{1}{a} \sum_{n=0}^{\infty} \frac{-4\ (-1)^n}{(2n+1)^2\pi^2} \cos\left(\frac{(2n+1)\pi z}{2}\right) \exp\left(\frac{-(2n+1)}{2}\pi a|x-x_0|\right) \tag{A47}$$

This solution may also be verified by direct substitution. The corresponding solutions for u_1 and h_1 are:

$$u_1 = -\sum_{n=0}^{\infty} \frac{4(-1)^n}{(2n+1)^2\pi^2} \sin\left(\frac{(2n+1)\pi y}{2}\right) A \tag{A48}$$

$$h_1 = F^2 \sum_{n=0}^{\infty} \frac{4\,(-1)^n}{(2n+1)^2\pi^2} \sin\left(\frac{(2n+1)\pi y}{2}\right) A \qquad \text{(A49)}$$

where:

$$\begin{aligned} A &= \exp\left(\frac{-(2n+1)}{2}\,\pi a(x_0-x)\right); \quad x < x_0 \\ &= 2-\exp\left(\frac{-(2n+1)}{2}\,\pi a(x_0-x)\right); \quad x > x_0 \end{aligned} \qquad \text{(A50)}$$

and:

$$a = (1-F^2)^{-1/2} \qquad \text{(A51)}$$

A characteristic length may be derived by considering the behaviour of this function at $y = 1$. Define L_s to be the distance between the points where h_1 is 5% and 95% of it's final value. L_s may then be solved from:

$$0.05 = \sum_{n=0}^{\infty} \frac{4}{(2n+1)^2\,\pi^2} \exp\left(\frac{-(2n+1)}{2}\,\pi\left(\frac{aL_s}{2b}\right)\right) \qquad \text{(A52)}$$

Solving numerically:

$$L_s = 2.66b\,(1-F^2)^{1/2} \qquad \text{(A53)}$$

EXPERIMENTS

To provide experimental verification for the preceeding analysis a few preliminary experiments were performed.

Existing experiments were found unsuitable due to lack of detail in the transition region.

The first experiment was done in a flume with a single 270° bend. The average flow depth was 61 mm; the average velocity was 0.38 m/s; the width was 1.07 m and the centerline radius was 3.66 m. The Froude number was therefore equal to 0.495 and α was 0.146.

The water surface elevations were measured with a screwdriver probe and a sloping manometer. Estimated accuracy was ± 0.2 mm.

Figure A2 shows a comparison of Equation 49 and the experimental results. The variable h_* is given by:

$$h_* = \frac{(h - H)}{(U^2 b/gR_0)} = \frac{\alpha h_1}{F_R^2} \tag{A54}$$

The agreement is seen to be reasonable.

The second experiment was performed in an 'S' shaped flume where the curvature was abruptly reversed. In this case $F = 0.50$ and $\alpha = 0.140$. Figure A3 shows a comparison of this experiment with theoretical curves obtained by superposition. Again the agreement is observed to be reasonably good.

CONCLUSIONS

An approximate relation for the water surface configuration at an abrupt change of curvature has been derived for a channel of mild curvature. A simple

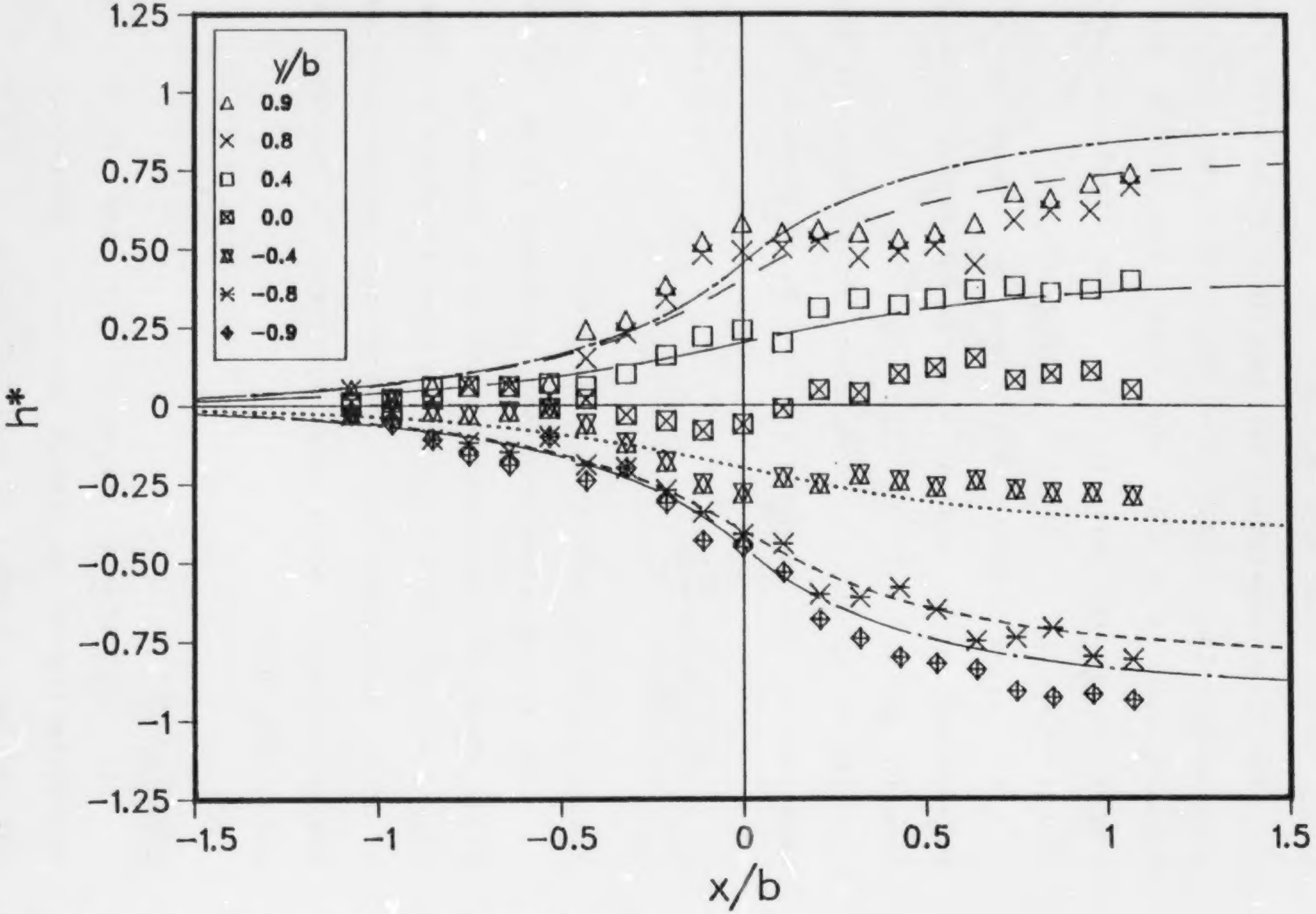

Figure A2. Water Surface at a Transition to a Curved Channel

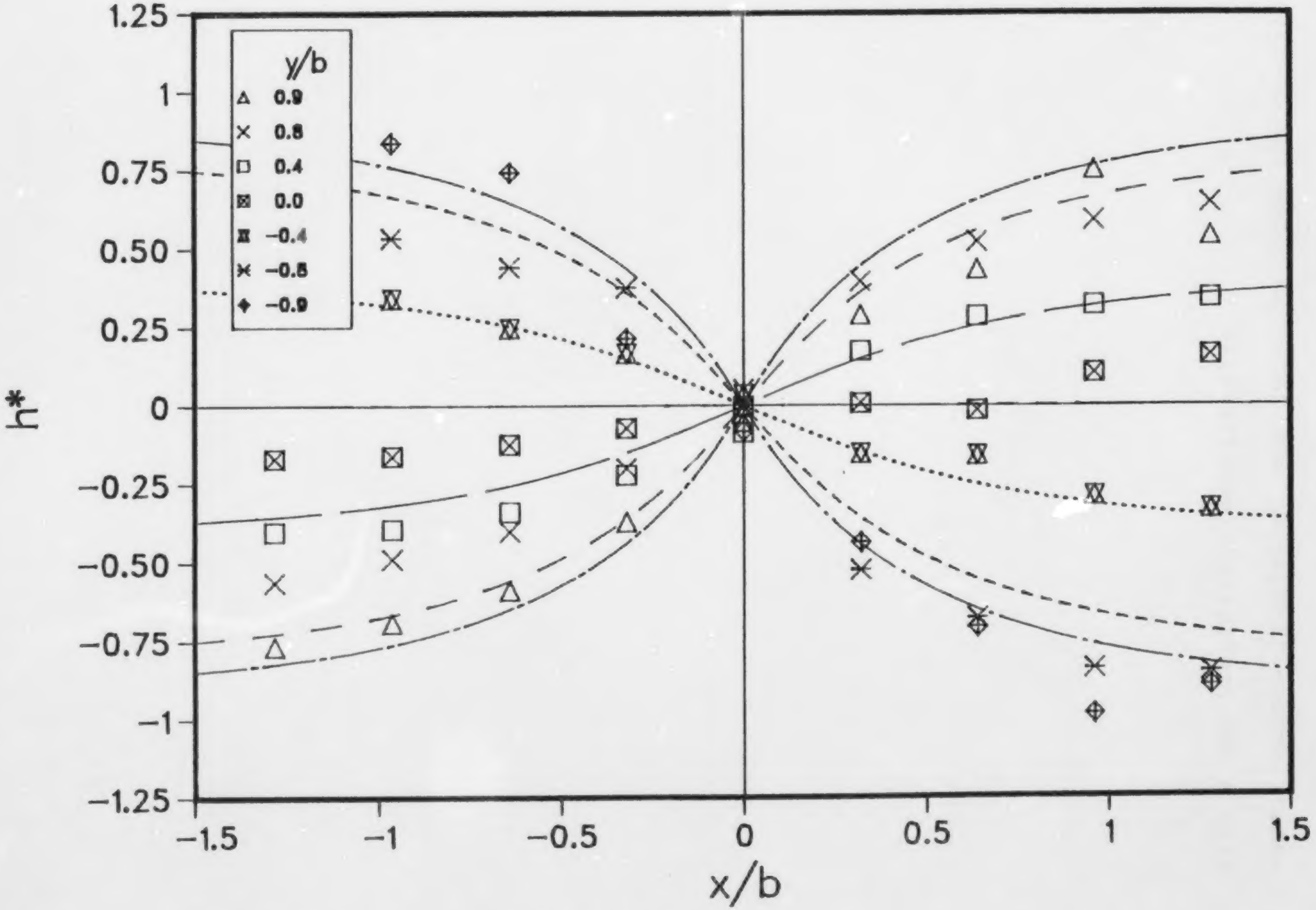

Figure A3. Water Surface at a Sudden Reversal of Channel Curvature

expression for the length of such a transition as a function of Froude number has also been presented. The predicted water surface topography was shown to agree reasonably well with a few preliminary experiments.

APPENDIX B - COMPUTER PROGRAMS

PROGRAM CRVCNL

The computer program CRVCNL is a numerical implementation of the Engelund (1974) method of flow and bed topography calculation for a curved channel. The method has been generalized to allow an arbitrary meander geometry. The channel curvature is calculated from the centreline co-ordinates of the stream plan supplied by the user. The program outputs velocity (longitudinal) corrections and bed depths below the water surface as well as various intermediary calculated quantities.

This program is intended for the demonstration of the Engelund method only. Included are input instructions and a listing of the FORTRAN source code.

INPUT TO CRVCNL

FORTRAN input unit = 5

Card #1 (5F10.4)

1. Average depth of flow for a straight reach (consistent length unit);
2. Average width of stream (consistent length unit);
3. Friction factor of stream defined from:

$$f = \sqrt{\frac{2}{C_f^2}} \qquad \text{(B1)}$$

4. Sediment friction angle (in degrees) (≈ 25 to 30 degrees, may be calibrated);
5. Sediment transport coefficient (≈4.0, may be calibrated).

Card #2 (213,F10.4)

1. Number of longitudinal sections (NSP);
2. Number of calculation points across channel (NNP);
3. Distance between sections (consistent length unit);

Card #3 to Card #(NSP+2) (2F10.4)

1. X co-ordinate of channel plan (consistent length unit);
2. Y co-ordinate of channel plan (consistent length unit).

These co-ordinates are determined by choosing equally spaced points along the channel and referring each point to an arbitary Cartesian co-ordinate system with the positive x-direction corresponding roughly to downstream along the valley axis. All lengths output will be expressed in the same unit used in the data input.

OUTPUT

FORTRAN output unit = 6

The output of the various variables is similar. The longitudinal co-ordinate is printed on the left of the page while the cross channel variation of the variable is printed across the page. The distance between these points is the width divided by (NNP-1).

PROGRAM EXAMPLE

The program is demonstrated on a situation which is an idealization of the North Saskatchewan River near the Mayfair Golf Course in Edmonton. The river is represented as a single 180° bend with a centreline radius of 750 m. Flow conditions are based on the two year flood. All length dimensions are in metres. The input data file is listed on Figure B1, the final bed topography output is shown on Figure B2, and the program source code is listed on Figure B3.

PROGRAMS PERTRB AND DEVFLO

These programs perform the numerical analysis procedures described in Part Two. PERTRB does the developed flow calculations and DEVFLO does the developing flow. These programs are included for reference only and are listed in Figures B4 and B5

PROGRAM ANZDAT

This program analyzes the data as described in part three. It is listed in Figure B6.

```
3.4,170.,0.0050,23.,4.,
 29  7 131.0000
-655.,-750.,
-524.,-750.,
-393.,-750.,
-262.,-750.,
-131.,-750.,
0.,-750.,
130.,-739.,
257.,-705.,
375.,-650.,
482.,-575.,
575.,-482.,
650.,-375.,
705.,-257.,
739.,-130.,
750.,0.,
739.,130.,
705.,257.,
650.,375.,
575.,482.,
482.,575.,
375.,650.,
257.,705.,
130.,739.,
0.,750.,
-131.,750.,
-262.,750.,
-393.,750.,
-524.,750.,
-655.,750.,
End of file
```

Figure B1.   CRVCNL Example Input

```
          CURVED CHANNEL  BED TOPOGRAPHY OUTPUT

      S(M)    BED TOPOGRAPHY

 0.0        0.3400E+01 0.3400E+01 0.3400E+01 0.3400E+01 0.3400E+01 0.3400E+01 0.3400E+01
 0.1310E+03 0.3400E+01 0.3400E+01 0.3400E+01 0.3400E+01 0.3400E+01 0.3400E+01 0.3400E+01
 0.2620E+03 0.3400E+01 0.3400E+01 0.3400E+01 0.3400E+01 0.3400E+01 0.3400E+01 0.3400E+01
 0.3930E+03 0.3400E+01 0.3400E+01 0.3400E+01 0.3400E+01 0.3400E+01 0.3400E+01 0.3400E+01
 0.5240E+03 0.4805E+01 0.4435E+01 0.3903E+01 0.3407E+01 0.2815E+01 0.2357E+01 0.2140E+01
 0.6550E+03 0.4882E+01 0.4888E+01 0.4301E+01 0.3461E+01 0.2561E+01 0.1807E+01 0.1881E+01
 0.7860E+03 0.2788E+01 0.3082E+01 0.3208E+01 0.3324E+01 0.3619E+01 0.3787E+01 0.4177E+01
 0.9170E+03 0.1858E+01 0.1888E+01 0.2544E+01 0.3271E+01 0.4089E+01 0.4895E+01 0.5588E+01
 0.1048E+04 0.1709E+01 0.2047E+01 0.2802E+01 0.3301E+01 0.4085E+01 0.4608E+01 0.5446E+01
 0.1179E+04 0.1742E+01 0.2086E+01 0.2842E+01 0.3323E+01 0.4048E+01 0.4760E+01 0.5356E+01
 0.1310E+04 0.1800E+01 0.2147E+01 0.2888E+01 0.3338E+01 0.4020E+01 0.4878E+01 0.5260E+01
 0.1441E+04 0.1805E+01 0.2157E+01 0.2763E+01 0.3347E+01 0.4018E+01 0.4557E+01 0.5234E+01
 0.1572E+04 0.1850E+01 0.2203E+01 0.2727E+01 0.3358E+01 0.3983E+01 0.4805E+01 0.5188E+01
 0.1703E+04 0.1852E+01 0.2208E+01 0.2744E+01 0.3386E+01 0.3989E+01 0.4888E+01 0.5188E+01
 0.1834E+04 0.1830E+01 0.2190E+01 0.2739E+01 0.3384E+01 0.4000E+01 0.4804E+01 0.5170E+01
 0.1965E+04 0.1806E+01 0.2171E+01 0.2723E+01 0.3368E+01 0.4011E+01 0.4823E+01 0.5186E+01
 0.2096E+04 0.1851E+01 0.2213E+01 0.2758E+01 0.3372E+01 0.3990E+01 0.4578E+01 0.5126E+01
 0.2227E+04 0.1878E+01 0.2236E+01 0.2773E+01 0.3374E+01 0.3877E+01 0.4585E+01 0.5088E+01
 0.2358E+04 0.1885E+01 0.2248E+01 0.2780E+01 0.3378E+01 0.3873E+01 0.4544E+01 0.5060E+01
 0.2489E+04 0.1925E+01 0.2261E+01 0.2801E+01 0.3376E+01 0.3853E+01 0.4508E+01 0.5035E+01
 0.2620E+04 0.1908E+01 0.2268E+01 0.2786E+01 0.3378E+01 0.3860E+01 0.4520E+01 0.5052E+01
 0.2751E+04 0.1940E+01 0.2298E+01 0.2611E+01 0.3377E+01 0.3848E+01 0.4453E+01 0.5017E+01
 0.2882E+04 0.5888E+00 0.1048E+01 0.2182E+01 0.3423E+01 0.4636E+01 0.5550E+01 0.6443E+01
 0.3013E+04 0.8587E-01 0.5700E+00 0.2041E+01 0.3664E+01 0.4814E+01 0.5921E+01 0.6485E+01
 0.3144E+04 0.2573E+01 0.2709E+01 0.3038E+01 0.3431E+01 0.3786E+01 0.4060E+01 0.4158E+01
 0.3275E+04 0.3824E+01 0.3410E+01 0.3888E+01 0.3328E+01 0.3157E+01 0.3061E+01 0.3031E+01
 0.3406E+04 0.3810E+01 0.3727E+01 0.3541E+01 0.3353E+01 0.3207E+01 0.3121E+01 0.3083E+01
 0.3537E+04 0.3728E+01 0.3683E+01 0.3520E+01 0.3388E+01 0.3245E+01 0.3169E+01 0.3144E+01
 0.3668E+04 0.3680E+01 0.3612E+01 0.3501E+01 0.3378E+01 0.3276E+01 0.3208E+01 0.3187E+01
```

Figure B2.   CRVCNL Example Output

```
C
C       CRVCNL
C
C
C  PROGRAM TO CALCULATE BED TOPOGRAPHY OF A MEANDERING RIVER.
C   USES METHOD OF ENGLEUND(1974) GENERALIZED TO ALLOW
C    ARBITRARY MEANDER GEOMETRY.
C
C
        IMPLICIT REAL*8 (A-H, O-Z)
        DIMENSION XM(100),YM(100),C(100),DC(100)
        DIMENSION DEP1(101,21),U(101,21),DU(101,21)
        DIMENSION V(101,21),DUI(101,21),DEPC(101,21),DEP2(101,21)
C
C   INPUT DATA
C
        READ(5,100)D,B,F,PHI,P
  100   FORMAT(5D10.4)
        TPHI=7.*DTAN(PHI*3.14159/180.)
        READ(5,101)NSP,NRP,DS
  101   FORMAT(2I3,D10.4)
        DO10 I=1,NSP
        READ(5,102)XM(I),YM(I)
  102   FORMAT(2D10.4)
   10   CONTINUE
C
C     CALCULATE CURVATURES
C
        NSP1=NSP-1
        DO 20 I=2,NSP1
        C(I)=DATAN((YM(I+1)-YM(I))/(XM(I+1)-XM(I)))
     *       -DATAN((YM(I)-YM(I-1))/(XM(I)-XM(I-1)))
        C(I)=C(I)/DS
        IF(XM(I).GE.XM(I-1).AND.XM(I).GE.XM(I+1))C(I)=C(I-1)
        IF(XM(I).LE.XM(I-1).AND.XM(I).LE.XM(I+1))C(I)=C(I-1)
   20    CONTINUE
        DC(1)=0.
        DC(NSP)=0.
        C(1)=C(2)
        C(NSP)=C(NSP1)
        DO 30 I=2,NSP1
   30   DC(I)=(C(I+1)-C(I-1))/2./DS
C
        CALL OUTPUT(NSP,DS,1,'CURVATURE',9,C)
        CALL OUTPUT(NSP,DS,1,'DERIVATIVE OF CURVATURE',23,DC)
C
C       CALCULATE FIRST APPROXIMATION TO BED TOPOGRAPHY
C
        DR=B/(NRP-1)
        RO=-B/2.
        DO31 I=1,NSP
        DO 31 J=1,NRP
   31   DEP1(I,J)=(1.+((J-1)*DR+RO)*C(I))**TPHI
C
        CALL OUTPUT(NSP,DS,NRP,'FIRST DEPTH APPROXIMATION',25,DEP1)
C
C     CALCULATE LONGITUDINAL VELOCITY CORRECTION
C
        DO 32 J=1,NRP
        R=(J-1)*DR+RO
```

Figure B3.   CRVCNL Program Listing

```
      U(1,J)=R*TPHI*C(1)/2.
      DU(1,J)=0.
      DO32 I=2,NSP
      UK1=DS*(R*(-DC(I-1)+TPHI*F/D/2.*C(I-1))-F/D*U(I-1,J))
      DU(I-1,J)=UK1/DS
      UK2=DS*(R*((-DC(I-1)-DC(I))/2.+TPHI*F/D/4.*(C(I-1)+C(I)))-F/D
     **(U(I-1,J)+UK1/2.))
      UK3=DS*(R*((-DC(I-1)-DC(I))/2.+TPHI*F/D/4.*(C(I-1)+C(I)))-F/D
     **(U(I-1,J)+UK2/2.))
      UK4=DS*(R*(-DC(I)+TPHI*F/D/2.*C(I))-F/D*(U(I-1,J)+UK3))
      U(I,J)=U(I-1,J)+(UK1+2.*UK2+2.*UK3+UK4)/6.
   32 CONTINUE
C
      CALL OUTPUT(NSP,DS,NRP,'LONGITUDINAL VELOCITY CORRECTION',32,U)
C
C      CALCULATE LATERAL VELOCITY
C
      DO33 I=1,NSP
      TE=(-1.+TPHI)*DC(I)+TPHI*F/2./D*C(I)-F/B/D*U(I,NRP)
      TI=-DC(I)+TPHI*F/2./D*C(I)-F/B/D*U(I,NRP)
      DO 33 J=1,NRP
      R=(J-1)*DR+RO
      V(I,J)=TE/2./DEP1(I,J)/(1.+C(I)*R)*(RO*RO-R*R)
      DUI(I,J)=TI*(R*R-RO*RO)/2.
   33 CONTINUE
C
      CALL OUTPUT(NSP,DS,NRP,'LATERAL INTEGRAL OF DU/DS',25,DUI)
      CALL OUTPUT(NSP,DS,NRP,'LATERAL VELOCITY',16,V)
```

Figure B3 Continued

```
C    CALCULATE SECOND APPROXIMATION TO DEPTH
C
      DO 34 I=1,NSP
      TO=0.
      DEPC(I,1)=0.
      DO 35 J=2,NRP
      R=(J-1)*DR+RO
      T1=(1./DEP1(I,J)*(-1)*(V(I,J)+P/(1.+U(I,J))**P/(1.+R*C(I))
     **DUI(I,J)))
      DEPC(I,J)=(T1+TO)/2.*DR*TPHI/7./D+DEPC(I,J-1)
   35 TO=T1
      NRP1=NRP-1
      DEPK=0.5*(DEP1(I,1)*DEPC(I,1)+DEP1(I,NRP)*DEPC(I,NRP))
      DO 36 J=2,NRP1
   36 DEPK=DEPK+DEP1(I,J)*DEPC(I,J)
      DEPK=(-1)*DEPK/NRP1
      DEP1A=0.5*(DEP1(I,1)+DEP1(I,NRP))
      DO38 J=2,NRP1
   38 DEP1A=DEP1A+DEP1(I,J)
      DEP1A=DEP1A/NRP1
      DEPK=DEPK/DEP1A
      DEPK2=1.-DEP1A
      DO 37 J=1,NRP
   37 DEP2(I,J)=(DEP1(I,J)*(1.+DEPC(I,J)+DEPK)+DEPK2)*D
   34 CONTINUE
C
      CALL OUTPUT(NSP,DS,NRP,'DEPTH CORRECTION',16,DEPC)
      CALL OUTPUT(NSP,DS,NRP,'BED TOPOGRAPHY',14,DEP2)
C
      STOP
      END
C
C
      SUBROUTINE OUTPUT(NSP,DS,NSI,TITLE,LT,VAR)
      IMPLICIT REAL*8 (A-H, O-Z)
      LOGICAL*1 TITLE(LT)
      DIMENSION VAR(101,21)
      WRITE(6,100)
  100 FORMAT('1',5X,'   CURVED CHANNEL  BED TOPOGRAPHY OUTPUT'/)
      WRITE(6,101)(TITLE(I),I=1,LT)
  101 FORMAT(/5X,'S(M)',3X,80A1//)
      WRITE(6,105)
  105 FORMAT(10X)
      DO 10 I=1,NSP
      S=DS*(I-1)
      WRITE(6,102)S,(VAR(I,J),J=1,NSI)
  102 FORMAT(/12D11.4/11X,11D11.4)
   10 CONTINUE
      RETURN
      END
End of file
```

Figure B3 Continued

```
C
      PROGRAM PERTRB
      IMPLICIT DOUBLE PRECISION (A-H, O-Z)
      DIMENSION VOR(51,51),C(3,51),RHS(51,51),PSI(51,51), C1(3,51)
      DIMENSION V(51,51),W(51,51),U(51,51),ETA(51,51)
      DIMENSION DWDY(51,51), DWDZ(51,51), UAV(51,51), D2UODY(51,51)
      DIMENSION UO(51,51),DUODY(51,51),DUODZ(51,51),DUODYZ(51,51)
      DIMENSION C2(3,51), UFINAL(101,51), RHS2(51,51)
      N=51
      M=51
      MO=5
      NO=5
      MAXIT=200
      OPEN(UNIT=4, FILE='DEVDAT', STATUS='OLD')
      OPEN(UNIT=7, FILE='OUTPUT', STATUS='NEW')
      CALL INITA(VOR,M,N,0.0)
      CALL INITA(PSI,M,N,0.0)
      CALL INITA(ETA,M,N,0.0)
    1 READ(4,*)EDDY, ELAT, CF,BETA,SOR,UOBC,ALPHA
      IF(EDDY.LT.0.0)STOP
      WRITE(7,'(''1'')')
      WRITE(7,*)  'EDDY VISCOSITY COEFFICENT = ',EDDY
      WRITE(7,*)  'LATERAL EDDY VISCOSITY MULTIPLIER = ',ELAT
      WRITE(7,*) 'FRICTION COEFFICENT = ', CF
      WRITE(7,*) 'ASPECT RATIO = ', BETA
      WRITE(7,*) 'SUCCESIVE OVER-RELAXATION FACTOR = ', SOR
      WRITE(7,*) 'SIDE BOUNDARY CONSTANT = ',UOBC
      WRITE(7,*) 'WIDTH TO RADIUS RATIO = ',ALPHA
      CALL INITA(UO,M,N,0.0)
      SOR=SOR/(1.0+1.0/BETA*ELAT)
      UBB=1.0-1.0/3.0/CF/EDDY
      UBS=1.0+1.0/6.0/CF/EDDY
      UORHS=-1.0/EDDY/CF
      CALL INITA(RHS,M,N,UORHS)
      DO 33 I=1,M
      C(1,I)=1
      C1(1,I)=1
      C1(2,I)=1.0/EDDY/CF/UBB*BETA/ELAT*UOBC
      C1(3,I)=0.0
      C2(1,I)=1
      C2(2,I)=1.0/EDDY/CF/UBB*BETA/ELAT
      C2(3,I)=0.0
      C(2,I)=-1.0/EDDY/CF/UBB
   33 C(3,I)=0.0
      CALL ITERA(UO,M,N,1,1,2,2,0.00001,C1,C,SOR,BETA,RHS,ELAT)
      CALL DINTEG(UO,M,N,RHS,2,1.0)
      CALL DINTEG(RHS,M,N,UAV,1,1.0)
      DO 15 I=1, M
      DO 15 J=1, N
   15 UAV(I,J)=UO(I,J)/UAV(M,N)
      CALL OUTA(UAV,M,N,MO,NO,'INITIAL VELOCITY DISTRIBUTION',29)
      CALL DERIVA(UAV,M,N,DUODZ,1,2,1.0)
      CALL DERIVA(UAV,M,N,DUODY,1,1,1.0)
      CALL DERIVA(UAV,M,N,D2UODY,2,1,1.0)
      CALL DERIVA(DUODY,M,N,DUODYZ,1,1,1.0)
      DO 10 J=1,N
      DO 10 I=1,M
   10 RHS(I,J)=CF/EDDY*2.*UAV(I,J)*DUODZ(I,J)
   21 CALL ITERA(VOR,N,N,1,0,0,0,0.00001,C1,C,SOR,BETA,RHS,ELAT)
      DO 22 J=1,N
```

Figure B4.   PERTRB Program Listing

```
      DO 22 I=1,M
   22 RHS2(I,J)=-VOR(I,J)/BETA/BETA
      CALL ITERA(PSI,N,N,1,0,0,0,0.00001,C1,C,SOR,BETA,RHS2,1.0)
      VC=BETA
      CALL DERIVA(PSI,N,N,V,1,2,VC)
      CALL DERIVA(PSI,N,N,W,1,1,-1.0)
      IF(ABS(V(1,1)-VO).LT.0.001)GOTO 31
      VO=V(1,1)
      DO 30 I=1,M-1
   30 VOR(I,1)=-BETA/EDDY/CF*V(I,1)/UBB
      DO 32 J=2,N
   32 VOR(M,J)=-W(M,J)/EDDY/CF/UBB*BETA
      GOTO 21
   31 CONTINUE
      CALL OUTA(V,M,N,MO,NO,'LATERAL VELOCITY DISTRIBUTION',29)
      CALL OUTA(W,M,N,MO,NO,'VERTICAL VELOCITY DISTRIBUTION',30)
      CALL DINTEG(W,M,N,RHS2,2,1.0)
      CALL OUTA(RHS2,M,N,MO,NO,'DEPTH AVG VERTICAL VELOCITY',27)
      CALL DERIVA(PSI,M,N,DWDY,2,1,-1.0)
      CALL DERIVA(W,M,N,DWDZ,1,2,1.0)
      DO 40 I=1,M
      DO 40 J=1,N
      RHS(I,J)=-(V(I,J)*BETA*CF/EDDY+1)*D2UODY(I,J)/BETA/BETA
      RHS(I,J)=RHS(I,J)-CF/EDDY*(DWDY(I,J)*DUODZ(I,J)
     * -DWDZ(I,J)*DUODY(I,J)+W(I,J)*DUODYZ(I,J)+1.0/CF/CF)
   40 CONTINUE
      IT=0
      USO=-9999.9
   42 IT=IT+1
C     IF(IT.GT.MAXIT)GOTO 43
      CALL ITERA(ETA,M,N,1,1,0,2,0.0001,C1,C,SOR,BETA,RHS,ELAT)
      CALL DINTEG(ETA,M,N,U,1,-1.0)
      IF(ABS(U(M,N)-USO).LT.0.002)GOTO 50
      USO=U(M,N)
      WRITE(*,*) ' USO = ', USO
      DO 51 J=1,N
   51 ETA(M,J)=U(M,J)/EDDY/CF/UBB*BETA/ELAT*UOBC
      GOTO 42
   50 CONTINUE
      CALL OUTA(U,M,N,MO,NO,'LONGITUDINAL VELOCITY DISTRIBUTION',34)
      CALL DINTEG(U,M,N,RHS,2,1.0)
      CALL OUTA(RHS,M,N,MO,NO,'DEPTH-AVERAGED LONG. VELOCITY',29)
      DO 61 I=1,N
      UFINAL(M,I)=UAV(1,I)+ALPHA*U(1,I)
      DO 61 J=1,M-1
      JP=M+J
      JM=M-J
      UFINAL(JP,I)=UAV(J+1,I)+ALPHA*U(J+1,I)
      UFINAL(JM,I)=UAV(J+1,I)-ALPHA*U(J+1,I)
   61 CONTINUE
      MF=2*M-1
      CALL OUTA(UFINAL,MF,N,MO,NO,'TOTAL VELOCITY DISTRIBUTION',27)
      GOTO 1
C  43 WRITE(7,*) ' MAXIMUM NUMBER OF SIDE BOUNDARY ITERATIONS'
C     GOTO 1
      END
C
C
      SUBROUTINE ITERA(A,M,N,NBC1,NBC2,NBC3,NBC4,TOL,C2,C,W,B,RHS,E)
      IMPLICIT DOUBLE PRECISION (A-H, O-Z)
```

Figure B4 Continued

```
      DIMENSION A(M,N),C(3,*),RHS(M,N),CO(3,200),C1(3,200),C2(3,200)
      AO=-999999.999
      A1=AO
      MAXIT=6000
      IT=1
      M2=(M-1)/2
      N2=(N-1)/2
      H=1.0/B/B*E
      DXDY=1.0/(M-1)/(N-1)
      R=0.25*W
      CC1=1.0-2.0*R*H-2.0*R
      CC2=R*H
      CC3=R
      CC4=-R*DXDY
      DO 20 I=1,M
      CO(1,I)=1.0
      CO(2,I)=0.0
   20 CO(3,I)=0.0
      DO 21 I=1,N
      C1(1,I)=1.0
      C1(2,I)=0.0
   21 C1(3,I)=0.0
   10 CALL AASOR(A,M,N,W,B,RHS,E)
      IF(NBC1.EQ.2)CALL BCSOR(A,M,N,1,W,B,RHS,C,E)
      IF(NBC1.EQ.1)CALL BCSOR(A,M,N,1,W,B,RHS,C1,E)
      IF(NBC2.EQ.2)CALL BCSOR(A,M,N,2,W,B,RHS,C,E)
      IF(NBC2.EQ.1)CALL BCSOR(A,M,N,2,W,B,RHS,CO,E)
      IF(NBC3.EQ.2)CALL BCSOR(A,M,N,3,W,B,RHS,C2,E)
      IF(NBC3.EQ.1)CALL BCSOR(A,M,N,3,W,B,RHS,C1,E)
      IF(NBC4.EQ.2)CALL BCSOR(A,M,N,4,W,B,RHS,C,E)
      IF(NBC4.EQ.1)CALL BCSOR(A,M,N,4,W,B,RHS,CO,E)
      IF(NBC3.EQ.2.AND.NBC4.EQ.2)THEN
        AI=A(M-1,1)-C2(2,1)*A(M,1)*2.0/(M-1)
        AJ=A(M,2)+C(2,M)*A(M,1)*2.0/(N-1)
        A(M,1)=CC1*A(M,1)+CC2*(AI+A(M-1,1))+CC3*(AJ+A(M,2))
     *  +CC4*RHS(M,1)
      ENDIF
      IT=IT+1
      IF(IT.GT.MAXIT)GOTO 31
      IF(ABS((A(M2,N2)-AO)/AO).LT.TOL)GOTO 32
      AO=A(M2,N2)
      GOTO 10
C  30 IF(ABS((A(M-1,N-1)-A1)/A1).LT.TOL)GOTO 32
C     A1=A(M-1,N-1)
C     GOTO 10
   31 WRITE(*,*) ' MAXIMUM NUMBER OF ITERATIONS REACHED'
   32 RETURN
      END
C
C
      SUBROUTINE INITA(A,M,N,C)
      IMPLICIT DOUBLE PRECISION (A-H, O-Z)
      DIMENSION A(M,N)
      DO 10 I=1,N
      DO 10 J=1,M
   10 A(J,I)=C
      RETURN
      END
C
C
```

Figure B4 Continued

```
      SUBROUTINE AASOR(A,M,N,W,B,RHS,E)
      IMPLICIT DOUBLE PRECISION (A-H, O-Z)
      DIMENSION A(M,N),RHS(M,N)
      H=1.0/B/B*E
      DXDY=1.0/(M-1)/(M-1)
      R=0.25*W
      C1=1.0-2.0*R*H-2.0*R
      C2=R*H
      C3=R
      C4=-R*DXDY
      DO 10 J=2,M-1
      DO 10 K=2,N-1
   10 A(J,K)=C1*A(J,K)+C2*(A(J-1,K)+A(J+1,K))+C3*(A(J,K-1)+A(J,K+1))
     *+C4*RHS(J,K)
      RETURN
      END
C
C
      SUBROUTINE BCSOR(A,M,N,NB,W,B,RHS,C,E)
      IMPLICIT DOUBLE PRECISION (A-H, O-Z)
      DIMENSION A(M,N),RHS(M,N),C(3,*)
      H=1.0/B/B*E
      DXDY=1.0/(M-1)/(N-1)
      R=0.25*W
      C1=1.0-2.0*R*H-2.0*R
      C2=R*H
      C3=R
      C4=-R*DXDY
      IF(NB.EQ.1)THEN
        DO 10 I=2,N-1
        AI=A(2,I)-2.0*(-C(2,I)*A(1,I)+C(3,I))/C(1,I)/(M-1)
   10   A(1,I)=C1*A(1,I)+C2*(AI+A(2,I))+C3*(A(1,I-1)+A(1,I+1))
     *  +C4*RHS(1,I)
      ELSEIF(NB.EQ.2)THEN
        AI=A(1,N-1)+2.0*(-C(2,1)*A(1,N)+C(3,1))/C(1,1)/(N-1)
        A(1,N)=C1*A(1,N)+C3*(AI+A(1,N-1))+C2*(A(2,N)+A(2,N))
     *  +C4*RHS(1,N)
        DO 20 I=2,M-1
        AI=A(I,N-1)+2.0*(-C(2,I)*A(I,N)+C(3,I))/C(1,I)/(N-1)
   20   A(I,N)=C1*A(I,N)+C3*(AI+A(I,N-1))+C2*(A(I-1,N)+A(I+1,N))
     *  +C4*RHS(I,N)
      ELSEIF(NB.EQ.3)THEN
        DO 30 I=2,N-1
        AI=A(M-1,I)+2.0*(-C(2,I)*A(M,I)+C(3,I))/C(1,I)/(M-1)
   30   A(M,I)=C1*A(M,I)+C2*(AI+A(M-1,I))+C3*(A(M,I-1)+A(M,I+1))
     *  +C4*RHS(M,I)
        AI=A(M-1,N)+2.0*(-C(2,N)*A(M,N)+C(3,N))/C(1,N)/(M-1)
        A(M,N)=C1*A(M,N)+C2*(AI+A(M-1,N))+C3*(A(M,N-1)+A(M,N-1))
     *  +C4*RHS(M,N)
      ELSEIF(NB.EQ.4)THEN
        AI=A(1,2)-2.0*(-C(2,1)*A(1,1)+C(3,1))/C(1,1)/(M-1)
        A(1,1)=C1*A(1,1)+C2*(A(2,1)+A(2,1))+C3*(AI+A(1,2))
     *  +C4*RHS(1,1)
        DO 40 I=2,M-1
        AI=A(I,2)-2.0*(-C(2,I)*A(I,1)+C(3,I))/C(1,I)/(M-1)
   40   A(I,1)=C1*A(I,1)+C2*(A(I-1,1)+A(I+1,1))+C3*(AI+A(I,2))
     *  +C4*RHS(I,1)
      ELSE
        WRITE(*,200)NB
  200   FORMAT(5X,'THE VALUE OF NB IS INCORRECT   ',I3/)
```

Figure B4 Continued

```
      ENDIF
      RETURN
      END
C
C
      SUBROUTINE OUTA(A,M,N,NX,NY,TITLE,NCT)
      IMPLICIT DOUBLE PRECISION (A-H, O-Z)
      DIMENSION A(M,N),TOP(21)
      CHARACTER TITLE(NCT)
      WRITE(7,200)(TITLE(I),I=1,NCT)
  200 FORMAT('O',80A1//)
      DX=1.0/(M-1)
      DY=1.0/(N-1)
      NO=(N-2)/NY
      MO=(M-2)/NX
      DO 10 I=1,MO
   10 TOP(I)=I*NX*DX
      TOP(MO+1)=1.0
      WRITE(7,201)(TOP(I),I=1,MO+1)
  201 FORMAT('O',10X,'     0.0    ',21F10.4)
      DO 20 J=N,NY+1,-NY
      K=0
      DO 30 I=1,M-NX,NX
      K=K+1
   30 TOP(K)=A(I;J)
      Y=(J-1)*DY
   20 WRITE(7,202)Y,(TOP(K),K=1,MO+1),A(M,J)
  202 FORMAT(1X,22F10.4)
      K=0
      DO 40 I=1,M-NX,NX
      K=K+1
   40 TOP(K)=A(I,1)
      Y=0.0
      WRITE(7,202)Y,(TOP(K),K=1,MO+1),A(M,1)
      RETURN
      END
C
C
      SUBROUTINE ADUMP(A,M,N)
      IMPLICIT DOUBLE PRECISION (A-H, O-Z)
      DIMENSION A(M,N), OUTV(13)
      MR=M
      MIN=1
      MAX=13
      WRITE(7,*) ' MATRIX DUMP'
   30 MO=MR
      IF(MR.GT.MAX)MO=MAX
      DO 10 I=1,N
      DO 11 J=1,MO
   11 OUTV(J)=A(MIN+J-1,I)
      WRITE(7,200)(OUTV(J),J=1,MO)
  200 FORMAT(1X,13F10.4)
   10 CONTINUE
      IF(MO.EQ.MR)GOTO 20
      MR=MR-MAX
      MIN=MAX+MIN
      WRITE(7,*)' MATRIX CONTINUATION'
      GOTO 30
   20 RETURN
      END
```

Figure B4 Continued

```
C
C
      SUBROUTINE DERIVA(A,M,N,D,ND,NYZ,C)
      IMPLICIT DOUBLE PRECISION (A-H, O-Z)
      DIMENSION A(M,N), D(M,N)
      DX=1.0/(M-1)
      DY=1.0/(N-1)
      IF(ND.EQ.1) THEN
        IF(NYZ.EQ.1) THEN
          DO 10 I=1,N
          D(1,I)=(A(2,I)-A(1,I))/DX
          DO 11 J=2,M-1
   11     D(J,I)=(A(J+1,I)-A(J-1,I))/2./DX
   10     D(M,I)=(A(M,I)-A(M-1,I))/DX
        ELSEIF(NYZ.EQ.2)THEN
          DO 20 I=1,M
          D(I,1)=(A(I,2)-A(I,1))/DY
          DO 21 J=2,N-1
   21     D(I,J)=(A(I,J+1)-A(I,J-1))/2./DY
   20     D(I,N)=(A(I,N)-A(I,N-1))/DY
        ELSE
          WRITE(*,'('' THE VALUE OF ND IS OK BUT NOT NXY'')')
        ENDIF
      ELSEIF(ND.EQ.2) THEN
        IF(NYZ.EQ.1) THEN
          DO 30 I=1,N
          D(1,I)=(2.*A(2,I)-2.*A(1,I))/DX/DX
          DO 31 J=2,M-1
   31     D(J,I)=(A(J+1,I)-2.*A(J,I)+A(J-1,I))/DX/DX
   30     D(M,I)=(2.*A(M,I)-5.*A(M-1,I)+4.*A(M-2,I)-A(M-3,I))/DX/DX
        ELSEIF(NYZ.EQ.2)THEN
          DO 40 I=1,M
          D(I,1)=(2.*A(I,2)-2.*A(I,1))/DY/DY
          DO 41 J=2,N-1
   41     D(I,J)=(A(I,J+1)-2.*A(I,J)+A(I,J-1))/DY/DY
   40     D(I,N)=(2.*A(I,N)-5.*A(I,N-1)+4.*A(I,N-2)-A(I,N-3))/DY/DY
        ELSE
          WRITE(*,'('' THE VALUE OF ND IS OK BUT NOT NXY'')')
        ENDIF
      ELSE
        WRITE(*,'('' THE VALUE OF ND IS INCORRECT'')')
      ENDIF
      DO 50 I=1,N
      DO 50 J=1,M
   50 D(J,I)=C*D(J,I)
      RETURN
      END
C
C
      SUBROUTINE DINTEG(A,M,N,DIN,NYZ,C)
      IMPLICIT DOUBLE PRECISION (A-H, O-Z)
      DIMENSION A(M,N), DIN(M,N)
      DX=1.0/(M-1)
      DY=1.0/(N-1)
      CALL INITA(DIN,M,N,0.0)
      IF(NYZ.EQ.1) THEN
        DO 10 J=1,N
        DO 10 I=2,M
   10   DIN(I,J)=DIN(I-1,J)+0.5*(A(I-1,J)+A(I,J))*DX*C
      ELSEIF(NYZ.EQ.2) THEN
```

Figure B4 Continued

```
        DO 20 I=1,M
        DO 20 J=2,N
 20     DIN(I,J)=DIN(I,J-1)+0.5*DY*(A(I,J-1)+A(I,J))*C
      ELSE
        WRITE(*,*) ' THE VALUE OF NXY IS INVALID '
      ENDIF
      RETURN
      END
End of file
```

Figure B4 Continued

```
C
      PROGRAM DEVFLO
      IMPLICIT DOUBLE PRECISION (A-H, O-Z)
      DIMENSION VOR(21,21),C(3,21),RHS(21,21),PSI(21,21), C1(3,21)
      DIMENSION V(21,21),W(21,21),U(21,21),ETA(21,21),ETAT(21,21)
      DIMENSION DWDY(21,21), DWDZ(21,21), UAV(21,21), D2UODY(21,21)
      DIMENSION UO(21,21),DUODY(21,21),DUODZ(21,21),DUODYZ(21,21)
      DIMENSION C2(3,21), UFINAL(101,21), RHS2(21,21), CDO(3,21)
      N=21
      M=21
      MD=2
      ND=2
      MAXIT=200
      OPEN(UNIT=4, FILE='DEVDAT', STATUS='OLD')
      OPEN(UNIT=7, FILE='OUTPUT', STATUS='NEW')
      CALL INITA(VOR,M,N,0.0)
      CALL INITA(PSI,M,N,0.0)
      CALL INITA(ETA,M,N,0.0)
    1 READ(4,*)EDDY, ELAT, CF,BETA,SOR,UOBC,ALPHA
      IF(EDDY.LT.0.0)STOP
      WRITE(7,'(''1'')')
      WRITE(7,*)  'EDDY VISCOSITY COEFFICENT = ',EDDY
      WRITE(7,*)  'LATERAL EDDY VISCOSITY MULTIPLIER = ',ELAT
      WRITE(7,*) 'FRICTION COEFFICENT = ', CF
      WRITE(7,*) 'ASPECT RATIO = ', BETA
      WRITE(7,*) 'SUCCESIVE OVER-RELAXATION FACTOR = ', SOR
      WRITE(7,*) 'SIDE BOUNDARY CONSTANT = ',UOBC
      WRITE(7,*) 'WIDTH TO RADIUS RATIO = ',ALPHA
      CALL INITA(UO,M,N,0.0)
      SOR=SOR/(1.0+1.0/BETA*ELAT)
      UBB=1.0-1.0/3.0/CF/EDDY
      UBS=1.0+1.0/6.0/CF/EDDY
      UORHS=-1.0/EDDY/CF
      CALL INITA(RHS,M,N,UORHS)
      DO 33 I=1,M
      C(1,I)=1.0
      C1(1,I)=1.0
      C1(2,I)=1.0/EDDY/CF/UBB*BETA/ELAT*UOBC
      C1(3,I)=0.0
      C2(1,I)=1.0
      C2(2,I)=1.0/EDDY/CF/UBB*BETA/ELAT
      C2(3,I)=0.0
      CDO(1,I)=1.0
      CDO(2,I)=0.0
      CDO(3,I)=0.0
      C(2,I)=-1.0/EDDY/CF/UBB
   33 C(3,I)=0.0
      CALL ITERA(UO,M,N,1,1,2,2,0.00001,C1,C,SOR,BETA,RHS,ELAT)
      CALL DINTEG(UO,M,N,RHS,2,1.0)
      CALL DINTEG(RHS,M,N,UAV,1,1.0)
      DO 15 I=1, M
      DO 15 J=1, N
   15 UAV(I,J)=UO(I,J)/UAV(M,N)
      CALL OUTA(UAV,M,N,MD,ND,'INITIAL VELOCITY DISTRIBUTION',29)
      CALL DERIVA(UAV,M,N,DUODZ,1,2,1.0)
      CALL DERIVA(UAV,M,N,DUODY,1,1,1.0)
      CALL DERIVA(UAV,M,N,D2UODY,2,1,1.0)
      CALL DERIVA(DUODY,M,N,DUODYZ,1,1,1.0)
      DO 10 J=1,N
      DO 10 I=1,M
```

Figure B5.   DEVFLO Program Listing

```
   10 RHS(I,J)=CF/EDDY*2.*UAV(I,J)*DUODZ(I,J)
   21 CALL ITERA(VOR,N,N,1,0,0,0,0.00001,C1,C,SOR,BETA,RHS,ELAT)
      DO 22 J=1,N
      DO 22 I=1,M
   22 RHS2(I,J)=-VOR(I,J)/BETA/BETA
      CALL ITERA(PSI,N,N,1,0,0,0,0.00001,C1,C,SOR,BETA,RHS2,1.0)
      VC=BETA
      CALL DERIVA(PSI,N,N,V,1,2,VC)
      CALL DERIVA(PSI,N,N,W,1,1,-1.0)
      IF(ABS(V(1,1)-VO).LT.0.001)GOTO 31
      VO=V(1,1)
      DO 30 I=1,M-1
   30 VOR(I,1)=-BETA/EDDY/CF*V(I,1)/UBB
      DO 32 J=2,N
   32 VOR(M,J)=-W(M,J)/EDDY/CF/UBB*BETA
      GOTO 21
   31 CONTINUE
      CALL OUTA(V,M,N,MD,ND,'LATERAL VELOCITY DISTRIBUTION',29)
      CALL OUTA(W,M,N,MD,ND,'VERTICAL VELOCITY DISTRIBUTION',30)
      CALL DINTEG(W,M,N,RHS2,2,1.0)
      CALL OUTA(RHS2,M,N,MD,ND,'DEPTH AVG VERTICAL VELOCITY',27)
      CALL DERIVA(PSI,M,N,DWDY,2,1,-1.0)
      CALL DERIVA(W,M,N,DWDZ,1,2,1.0)
      DX=0.25*CF/BETA/EDDY/(M-1)/(M-1)
      XL=0.1*CF/BETA
      XE=32.313
      X=-5.0
      NSTEP=0
   35 X=X+DX
      DO 40 I=1,M
      DO 40 J=1,N
      RHS(I,J)=-(V(I,J))*D2UODY(I,J)
      RHS(I,J)=RHS(I,J)-BETA*(DWDY(I,J)*DUODZ(I,J)
     * -DWDZ(I,J)*DUODY(I,J)+W(I,J)*DUODYZ(I,J))
      RHS(I,J)=RHS(I,J)*SECF(X,XE,XL)-SUPF(X,XE)
     *-RFUNC(X,XE)*BETA/CF/CF
   40 CONTINUE
      CALL AAEXP(ETA,ETAT,M,N,1.0,BETA,RHS,ELAT,DX)
      CALL BCEXP(ETA,ETAT,M,N,1,1.0,BETA,RHS,CDO,ELAT,DX)
      CALL BCEXP(ETA,ETAT,M,N,2,1.0,BETA,RHS,CDO,ELAT,DX)
      CALL BCEXP(ETA,ETAT,M,N,4,1.0,BETA,RHS,C,ELAT,DX)
      NSTEP=NSTEP+1
      IF(NSTEP.EQ.10)GOTO 50
      GOTO 35
   50 CONTINUE
      CALL DINTEG(ETA,M,N,U,1,-1.0)
      CALL DINTEG(U,M,N,RHS,2,1.0)
      WRITE(7,121)X,RHS(17,N),RHS(19,N),RHS(21,N)
  121 FORMAT(5X,4F15.5)
      NSTEP=0
      IF(X.GT.40.0)GOTO71
      GOTO 35
   71 GOTO 1
      END
C
C
      SUBROUTINE ITERA(A,M,N,NBC1,NBC2,NBC3,NBC4,TOL,C2,C,W,B,RHS,E)
      IMPLICIT DOUBLE PRECISION (A-H, O-Z)
      DIMENSION A(M,N),C(3,*),RHS(M,N),CO(3,200),C1(3,200),C2(3,200)
      AO=-999999.999
```

Figure B5 Continued

```
      A1=A0
      MAXIT=6000
      IT=1
      M2=(M-1)/2
      N2=(N-1)/2
      H=1.0/B/B*E
      DXDY=1.0/(M-1)/(N-1)
      R=0.25*W
      CC1=1.0-2.0*R*H-2.0*R
      CC2=R*H
      CC3=R
      CC4=-R*DXDY
      DO 20 I=1,M
      C0(1,I)=1.0
      C0(2,I)=0.0
   20 C0(3,I)=0.0
      DO 21 I=1,N
      C1(1,I)=1.0
      C1(2,I)=0.0
   21 C1(3,I)=0.0
   10 CALL AASOR(A,M,N,W,B,RHS,E)
      IF(NBC1.EQ.2)CALL BCSOR(A,M,N,1,W,B,RHS,C,E)
      IF(NBC1.EQ.1)CALL BCSOR(A,M,N,1,W,B,RHS,C1,E)
      IF(NBC2.EQ.2)CALL BCSOR(A,M,N,2,W,B,RHS,C,E)
      IF(NBC2.EQ.1)CALL BCSOR(A,M,N,2,W,B,RHS,C0,E)
      IF(NBC3.EQ.2)CALL BCSOR(A,M,N,3,W,B,RHS,C2,E)
      IF(NBC3.EQ.1)CALL BCSOR(A,M,N,3,W,B,RHS,C1,E)
      IF(NBC4.EQ.2)CALL BCSOR(A,M,N,4,W,B,RHS,C,E)
      IF(NBC4.EQ.1)CALL BCSOR(A,M,N,4,W,B,RHS,C0,E)
      IF(NBC3.EQ.2.AND.NBC4.EQ.2)THEN
        AI=A(M-1,1)-C2(2,1)*A(M,1)*2.0/(M-1)
        AJ=A(M,2)+C(2,M)*A(M,1)*2.0/(N-1)
        A(M,1)=CC1*A(M,1)+CC2*(AI+A(M-1,1))+CC3*(AJ+A(M,2))
     *  +CC4*RHS(M,1)
      ENDIF
      IT=IT+1
      IF(IT.GT.MAXIT)GOTO 31
      IF(ABS((A(M2,N2)-A0)/A0).LT.TOL)GOTO 32
      A0=A(M2,N2)
      GOTO 10
C  30 IF(ABS((A(M-1,N-1)-A1)/A1).LT.TOL)GOTO 32
C     A1=A(M-1,N-1)
C     GOTO 10
   31 WRITE(*,*) ' MAXIMUM NUMBER OF ITERATIONS REACHED'
   32 RETURN
      END
C
C
      SUBROUTINE INITA(A,M,N,C)
      IMPLICIT DOUBLE PRECISION (A-H, O-Z)
      DIMENSION A(M,N)
      DO 10 I=1,N
      DO 10 J=1,M
   10 A(J,I)=C
      RETURN
      END
C
C
      SUBROUTINE AASOR(A,M,N,W,B,RHS,E)
      IMPLICIT DOUBLE PRECISION (A-H, O-Z)
```

Figure B5 Continued

```
       DIMENSION A(M,N),RHS(M,N)
      H=1.0/B/B*E
      DXDY=1.0/(M-1)/(M-1)
      R=0.25*W
      C1=1.0-2.0*R*H-2.0*R
      C2=R*H
      C3=R
      C4=-R*DXDY
      DO 10 J=2,M-1
      DO 10 K=2,N-1
   10 A(J,K)=C1*A(J,K)+C2*(A(J-1,K)+A(J+1,K))+C3*(A(J,K-1)+A(J,K+1))
     *+C4*RHS(J,K)
      RETURN
      END
C
C
      SUBROUTINE BCSOR(A,M,N,NB,W,B,RHS,C,E)
      IMPLICIT DOUBLE PRECISION (A-H, O-Z)
      DIMENSION A(M,N),RHS(M,N),C(3,*)
      H=1.0/B/B*E
      DXDY=1.0/(M-1)/(N-1)
      R=0.25*W
      C1=1.0-2.0*R*H-2.0*R
      C2=R*H
      C3=R
      C4=-R*DXDY
      IF(NB.EQ.1)THEN
        DO 10 I=2,N-1
        AI=A(2,I)-2.0*(-C(2,I)*A(1,I)+C(3,I))/C(1,I)/(M-1)
   10   A(1,I)=C1*A(1,I)+C2*(AI+A(2,I))+C3*(A(1,I-1)+A(1,I+1))
     *  +C4*RHS(1,I)
      ELSEIF(NB.EQ.2)THEN
        AI=A(1,N-1)+2.0*(-C(2,1)*A(1,N)+C(3,1))/C(1,1)/(N-1)
        A(1,N)=C1*A(1,N)+C3*(AI+A(1,N-1))+C2*(A(2,N)+A(2,N))
     *  +C4*RHS(1,N)
        DO 20 I=2,M-1
        AI=A(I,N-1)+2.0*(-C(2,I)*A(I,N)+C(3,I))/C(1,I)/(N-1)
   20   A(I,N)=C1*A(I,N)+C3*(AI+A(I,N-1))+C2*(A(I-1,N)+A(I+1,N))
     *  +C4*RHS(I,N)
      ELSEIF(NB.EQ.3)THEN
        DO 30 I=2,N-1
        AI=A(M-1,I)+2.0*(-C(2,I)*A(M,I)+C(3,I))/C(1,I)/(M-1)
   30   A(M,I)=C1*A(M,I)+C2*(AI+A(M-1,I))+C3*(A(M,I-1)+A(M,I+1))
     *  +C4*RHS(M,I)
        AI=A(M-1,N)+2.0*(-C(2,N)*A(M,N)+C(3,N))/C(1,N)/(M-1)
        A(M,N)=C1*A(M,N)+C2*(AI+A(M-1,N))+C3*(A(M,N-1)+A(M,N-1))
     *  +C4*RHS(M,N)
      ELSEIF(NB.EQ.4)THEN
        AI=A(1,2)-2.0*(-C(2,1)*A(1,1)+C(3,1))/C(1,1)/(M-1)
        A(1,1)=C1*A(1,1)+C2*(A(2,1)+A(2,1))+C3*(AI+A(1,2))
     *  +C4*RHS(1,1)
        DO 40 I=2,M-1
        AI=A(I,2)-2.0*(-C(2,I)*A(I,1)+C(3,I))/C(1,I)/(M-1)
   40   A(I,1)=C1*A(I,1)+C2*(A(I-1,1)+A(I+1,1))+C3*(AI+A(I,2))
     *  +C4*RHS(I,1)
      ELSE
        WRITE(*,200)NB
  200   FORMAT(5X,'THE VALUE OF NB IS INCORRECT    ',I3/)
      ENDIF
      RETURN
```

Figure B5 Continued

```
      END
C
C
      SUBROUTINE OUTA(A,M,N,NX,NY,TITLE,NCT)
      IMPLICIT DOUBLE PRECISION (A-H, O-Z)
      DIMENSION A(M,N),TOP(21)
      CHARACTER TITLE(NCT)
      WRITE(7,200)(TITLE(I),I=1,NCT)
  200 FORMAT('0',80A1//)
      DX=1.0/(M-1)
      DY=1.0/(N-1)
      ND=(N-2)/NY
      MD=(M-2)/NX
      DO 10 I=1,MD
   10 TOP(I)=I*NX*DX
      TOP(MD+1)=1.0
      WRITE(7,201)(TOP(I),I=1,MD+1)
  201 FORMAT('0',10X,'    0.0    ',21F10.4)
      DO 20 J=N,NY+1,-NY
      K=0
      DO 30 I=1,M-NX,NX
      K=K+1
   30 TOP(K)=A(I,J)
      Y=(J-1)*DY
   20 WRITE(7,202)Y,(TOP(K),K=1,MD+1),A(M,J)
  202 FORMAT(1X,22F10.4)
      K=0
      DO 40 I=1,M-NX,NX
      K=K+1
   40 TOP(K)=A(I,1)
      Y=0.0
      WRITE(7,202)Y,(TOP(K),K=1,MD+1),A(M,1)
      RETURN
      END
C
C
      SUBROUTINE ADUMP(A,M,N)
      IMPLICIT DOUBLE PRECISION (A-H, O-Z)
      DIMENSION A(M,N), OUTV(13)
      MR=M
      MIN=1
      MAX=13
      WRITE(7,*) ' MATRIX DUMP'
   30 MD=MR
      IF(MR.GT.MAX)MD=MAX
      DO 10 I=1,N
      DO 11 J=1,MD
   11 OUTV(J)=A(MIN+J-1,I)
      WRITE(7,200)(OUTV(J),J=1,MD)
  200 FORMAT(1X,13F10.4)
   10 CONTINUE
      IF(MD.EQ.MR)GOTO 20
      MR=MR-MAX
      MIN=MAX+MIN
      WRITE(7,*)' MATRIX CONTINUATION'
      GOTO 30
   20 RETURN
      END
C
C
```

Figure B5 Continued

```
      SUBROUTINE DERIVA(A,M,N,D,ND,NYZ,C)
      IMPLICIT DOUBLE PRECISION (A-H, O-Z)
      DIMENSION A(M,N), D(M,N)
      DX=1.0/(M-1)
      DY=1.0/(N-1)
      IF(ND.EQ.1) THEN
        IF(NYZ.EQ.1) THEN
          DO 10 I=1,N
          D(1,I)=(A(2,I)-A(1,I))/DX
          DO 11 J=2,M-1
   11     D(J,I)=(A(J+1,I)-A(J-1,I))/2./DX
   10     D(M,I)=(A(M,I)-A(M-1,I))/DX
        ELSEIF(NYZ.EQ.2)THEN
          DO 20 I=1,M
          D(I,1)=(A(I,2)-A(I,1))/DY
          DO 21 J=2,N-1
   21     D(I,J)=(A(I,J+1)-A(I,J-1))/2./DY
   20     D(I,N)=(A(I,N)-A(I,N-1))/DY
        ELSE
          WRITE(*,'('' THE VALUE OF ND IS OK BUT NOT NXY'')')
        ENDIF
      ELSEIF(ND.EQ.2) THEN
        IF(NYZ.EQ.1) THEN
          DO 30 I=1,N
          D(1,I)=(2.*A(2,I)-2.*A(1,I))/DX/DX
          DO 31 J=2,M-1
   31     D(J,I)=(A(J+1,I)-2.*A(J,I)+A(J-1,I))/DX/DX
   30     D(M,I)=(2.*A(M,I)-5.*A(M-1,I)+4.*A(M-2,I)-A(M-3,I))/DX/DX
        ELSEIF(NYZ.EQ.2)THEN
          DO 40 I=1,M
          D(I,1)=(2.*A(I,2)-2.*A(I,1))/DY/DY
          DO 41 J=2,N-1
   41     D(I,J)=(A(I,J+1)-2.*A(I,J)+A(I,J-1))/DY/DY
   40     D(I,N)=(2.*A(I,N)-5.*A(I,N-1)+4.*A(I,N-2)-A(I,N-3))/DY/DY
        ELSE
          WRITE(*,'('' THE VALUE OF ND IS OK BUT NOT NXY'')')
        ENDIF
      ELSE
        WRITE(*,'('' THE VALUE OF ND IS INCORRECT'')')
      ENDIF
      DO 50 I=1,N
      DO 50 J=1,M
   50 D(J,I)=C*D(J,I)
      RETURN
      END
C
C
      SUBROUTINE DINTEG(A,M,N,DIN,NYZ,C)
      IMPLICIT DOUBLE PRECISION (A-H, O-Z)
      DIMENSION A(M,N), DIN(M,N)
      DX=1.0/(M-1)
      DY=1.0/(N-1)
      CALL INITA(DIN,M,N,0.0)
      IF(NYZ.EQ.1) THEN
        DO 10 J=1,N
        DO 10 I=2,M
   10   DIN(I,J)=DIN(I-1,J)+0.5*(A(I-1,J)+A(I,J))*DX*C
      ELSEIF(NYZ.EQ.2) THEN
        DO 20 I=1,M
        DO 20 J=2,N
```

Figure B5 Continued

```
   20   DIN(I,J)=DIN(I,J-1)+0.5*DY*(A(I,J-1)+A(I,J))*C
      ELSE
        WRITE(*,*) ' THE VALUE OF NXY IS INVALID '
      ENDIF
      RETURN
      END
C
C
      SUBROUTINE AAEXP(A,AT,M,N,W,B,RHS,E,DX)
      IMPLICIT DOUBLE PRECISION (A-H, O-Z)
      DIMENSION A(M,N),RHS(M,N),AT(M,N)
      DO 20 I=1,M
      DO 20 J=1,N
   20 AT(I,J)=A(I,J)
      H=1.0/B/B*E
      DXDY=1.0/(M-1)/(M-1)
      R=0.25*W
      C1=1.0-2.0*R*H-2.0*R
      C2=R*H
      C3=R
      C4=-DX
      DO 10 J=2,M-1
      DO 10 K=2,N-1
   10 A(J,K)=C1*AT(J,K)+C2*(AT(J-1,K)+AT(J+1,K))+C3*(AT(J,K-1)+
     *AT(J,K+1))+C4*RHS(J,K)
      RETURN
      END
C
C
      SUBROUTINE BCEXP(A,AT,M,N,NB,W,B,RHS,C,E,DX)
      IMPLICIT DOUBLE PRECISION (A-H, O-Z)
      DIMENSION A(M,N),RHS(M,N),C(3,*),AT(M,N)
      H=1.0/B/B*E
      DXDY=1.0/(M-1)/(N-1)
      R=0.25*W
      C1=1.0-2.0*R*H-2.0*R
      C2=R*H
      C3=R
      C4=-DX
      IF(NB.EQ.1)THEN
        DO 10 I=2,N-1
        AI=AT(2,I)-2.0*(-C(2,I)*AT(1,I)+C(3,I))/C(1,I)/(M-1)
   10   A(1,I)=C1*AT(1,I)+C2*(AI+AT(2,I))+C3*(AT(1,I-1)+AT(1,I+1))
     *  +C4*RHS(1,I)
      ELSEIF(NB.EQ.2)THEN
        AI=AT(1,N-1)+2.0*(-C(2,1)*AT(1,N)+C(3,1))/C(1,1)/(N-1)
        A(1,N)=C1*AT(1,N)+C3*(AI+AT(1,N-1))+C2*(AT(2,N)+AT(2,N))
     *  +C4*RHS(1,N)
        DO 20 I=2,M-1
        AI=AT(I,N-1)+2.0*(-C(2,I)*AT(I,N)+C(3,I))/C(1,I)/(N-1)
   20   A(I,N)=C1*AT(I,N)+C3*(AI+AT(I,N-1))+C2*(AT(I-1,N)+AT(I+1,N))
     *  +C4*RHS(I,N)
      ELSEIF(NB.EQ.3)THEN
        DO 30 I=2,N-1
        AI=AT(M-1,I)+2.0*(-C(2,I)*AT(M,I)+C(3,I))/C(1,I)/(M-1)
   30   A(M,I)=C1*AT(M,I)+C2*(AI+AT(M-1,I))+C3*(AT(M,I-1)+AT(M,I+1))
     *  +C4*RHS(M,I)
        AI=AT(M-1,N)+2.0*(-C(2,N)*AT(M,N)+C(3,N))/C(1,N)/(M-1)
        A(M,N)=C1*AT(M,N)+C2*(AI+AT(M-1,N))+C3*(AT(M,N-1)+AT(M,N-1))
     *  +C4*RHS(M,N)
```

Figure B5 Continued

```
        ELSEIF(NB.EQ.4)THEN
          AI=AT(1,2)-2.0*(-C(2,1)*AT(1,1)+C(3,1))/C(1,1)/(M-1)
          A(1,1)=C1*AT(1,1)+C2*(AT(2,1)+AT(2,1))+C3*(AI+AT(1,2))
     *    +C4*RHS(1,1)
          DO 40 I=2,M-1
          AI=AT(I,2)-2.0*(-C(2,I)*AT(1,1)+C(3,I))/C(1,I)/(M-1)
   40     A(I,1)=C1*AT(I,1)+C2*(AT(I-1,1)+AT(I+1,1))+C3*(AI+AT(I,2))
     *    +C4*RHS(I,1)
        ELSE
          WRITE(*,200)NB
  200     FORMAT(5X,'THE VALUE OF NB IS INCORRECT   ',I3/)
        ENDIF
        RETURN
        END
C
C
        FUNCTION RFUNC(X,XE)
        IMPLICIT DOUBLE PRECISION (A-H, O-Z)
        IF(X.LT.0.0.OR.X.GT.XE)THEN
          TEMP=0.0
        ELSE
          TEMP=1.0
        ENDIF
        RFUNC=TEMP
        RETURN
        END
C
C
        FUNCTION SECF(X,XE,XL)
        IMPLICIT DOUBLE PRECISION (A-H, O-Z)
        IF(X.LT.0.0)THEN
          TEMP=0.0
        ELSEIF(X.LT.XL)THEN
          TEMP=X/XL
        ELSEIF(X.LT.XE)THEN
          TEMP=1.0
        ELSEIF(X.LT.(XL+XE))THEN
          TEMP=1.0-(X-XE)/(XL)
        ELSE
          TEMP=0.0
        ENDIF
        SECF=TEMP
        RETURN
        END
C
C
        FUNCTION SUPF(X,XE)
        IMPLICIT DOUBLE PRECISION (A-H, O-Z)
        IF(X.LT.-1.0)THEN
          TEMP=0
        ELSEIF(X.LT.0.0)THEN
          TEMP=1.0+X
        ELSEIF(X.LT.1.0)THEN
          TEMP=1.0-X
        ELSEIF(X.LT.(XE-1.0))THEN
          TEMP=0.0
        ELSEIF(X.LT.XE)THEN
          TEMP=-1+XE-X
        ELSEIF(X.LT.(XE+1.0))THEN
          TEMP=-1+X-XE
```

Figure B5 Continued

```
      ELSE
        TEMP=0.0
      ENDIF
      SUPF=TEMP
      RETURN
      END
End of file
```

Figure B5 Continued

```
C
      PROGRAM ANZDAT
C
      DIMENSION X(5000),Y(5000),Z(5000),U(5000),V(5000)
      DIMENSION U2(5000),V2(5000),UV(5000)
      DIMENSION ZO(150),ZT(50),UT(50),VT(50),U2T(50),V2T(50),ZS(150)
C
      NT=0
   10 NT=NT+1
      READ(5,100,END=12)X(NT),Y(NT),Z(NT),U(NT),V(NT),U2(NT),V2(NT),
     *UV(NT)
      GOTO 10
   12 NT=NT-1
  100 FORMAT(8E11.4)
C
      I=0
   20 I=I+1
      READ(4,101,END=21)ZO(I),ZS(I)
      GOTO 20
   21 NP=I-1
  101 FORMAT(2F10.4)
C
      NPROFL=0
      NPOINT=1
   30 NPROFL=NPROFL+1
      YPICK=Y(NPOINT)
      N=0
      IF(NPOINT.GT.NT)STOP
   31 I=NPOINT+N
      IF(I.GT.NT)GOTO 32
      IF(ABS(Y(I)-YPICK).GT.1.0)GOTO 32
      N=N+1
      ZT(N)=Z(I)
      UT(N)=U(I)
      VT(N)=V(I)
      U2T(N)=U2(I)
      V2T(N)=V2(I)
      GOTO 31
   32 CONTINUE
C
      DO 40 J=1,N
      ZT(J)=ZT(J)-ZO(NPROFL)
   40 CONTINUE
      ZS(NPROFL)=ZS(NPROFL)-ZO(NPROFL)
C
      NTIMES=0
      NFST=3
      USO=0.0
   45 CALL LOGREG(ZT,UT,NFST,12,50,A,B)
      NTIMES=NTIMES+1
      US=A/5.75
      IF(NTIMES.GT.20)THEN
        US=0.5*(US+USO)
        GOTO 47
      ENDIF
      IF(ABS(US-USO).LT.0.001)GO TO 47
      USO=US
      ZMIN=70.0*0.001/US
      NFST=0
   46 NFST=NFST+1
```

Figure B6.   ANZDAT Program listing

```
      IF(ZT(NFST).GT.ZMIN) GOTO 45
      GOTO 46
   47 CONTINUE
C
      NA=0
   50 NA=NA+1
      IF(UT(NA)/US.GT.12.0)GOTO 51
      IF(NA.EQ.N)GOTO 51
      GOTO 50
   51 NA=NA-1
      CALL LREGRS(UT,VT,1,NA,50,A,B)
      TPHI=A
      TAUL=US*US*TPHI
C
      CALL DEPAVG(ZT,UT,50,ZS(NPROFL),0,N,UB)
      CALL DEPAVG(ZT,VT,50,ZS(NPROFL),0,N,VB)
      DO 60, I=1, N
   60 VT(I)=VT(I)-VB
      CALL DEPAVG(ZT,VT,50,ZS(NPROFL),1,N,VZB)
C
      WRITE(6,200)X(NPOINT),Y(NPOINT),US,TPHI,TAUL,UB,VB,VZB
  200 FORMAT(8E11.4)
      NPOINT=NPOINT+N
      GOTO 30
C
      END
C
C
      SUBROUTINE LREGRS(X,Y,N1,N2,NDIM,A,B)
      DIMENSION X(NDIM),Y(NDIM),XR(50),YR(50)
      XR(1)=0.0
      YR(1)=0.0
      N=N2-N1+2
      DO 10 I=2,N
      XR(I)=X(N1+I-1)
   10 YR(I)=Y(N1+I-1)
      A=1.0
      CALL CRVFIT(N,XR,YR,A,B,R,7)
      RETURN
      END
C
C
      SUBROUTINE LOGREG(X,Y,N1,N2,NDIM,A,B)
      DIMENSION X(NDIM),Y(NDIM),XR(50),YR(50)
      N=N2-N1+1
      DO 10 I=1,N
      XR(I)=ALOG10(X(N1+I-1))
   10 YR(I)=Y(N1+I-1)
      A=1.0
      CALL CRVFIT(N,XR,YR,A,B,R,7)
      RETURN
      END
C
C
      SUBROUTINE DEPAVG(Z,U,NDIM,ZMAX,NM,N,UB)
      DIMENSION Z(NDIM),U(NDIM)
      SUM=(0.5*U(1)*Z(1)+0.5*U(1)*(Z(2)-Z(1)))*Z(1)**NM
      DO 10 I=2,N-1
   10 SUM=SUM+0.5*U(I)*(Z(I+1)-Z(I-1))*Z(I)**NM
      SUM=SUM+U(N)*(ZMAX-0.5*(Z(N)+Z(N-1)))*Z(I)**NM
```

Figure B6 Continued

```
      UB=SUM/ZMAX
      RETURN
      END
End of file
```

Figure B6 Continued